Resilient Operation of Microgrids: Optimisation Models for Steady-State and Transiently Secure Operation

Agnes Marjorie Nakiganda

Submitted in accordance with the requirements for the degree of

Doctor of Philosophy

UNIVERSITY OF LEEDS

School of Electronic and Electrical Engineering

University of Leeds

June 2022

Declaration

The candidate confirms that the work submitted is their own, except where work which has formed part of jointly authored publications has been included. The contribution of the candidate and the other authors to this work has been explicitly indicated below. The candidate confirms that appropriate credit has been given within the thesis where reference has been made to the work of others.

- The work in Chapter 3 of the thesis has appeared in the following publications:

  A. M. Nakiganda, S Dehghan, P Aristidou, "Comparison of AC Optimal Power Flow Methods in Low-Voltage Distribution Networks," *2021 IEEE PES Innovative Smart Grid Technologies Europe (ISGT Europe)*, 2021, pp. 1-5.

  – As the lead author, the candidate the candidate performed all the conceptualisation, methodology derivation, software formulation, investigation, writing - original draft and visualisation.

  – Dr. Shahab Dehghan helped with supervision and writing - review and editing.

  – Dr. Petros Aristidou supervised the work, helped with writing - review and editing and provided different resources to support the paper.

- The work in Chapter 4 of the thesis has appeared in the following publications:

  S. Dehghan , **A. M. Nakiganda**, J. Lancaster, P. Aristidou, "Towards a Sustainable Microgrid on Alderney Island Using a Python-based Energy Planning Tool" in *The 12th Mediterranean Conference on Power Generation, Transmission, Distribution and Energy Conversion (MEDPOWER 2020)*, 2021, pp. 196 – 201.

  – As the second author, the candidate performed the software formulation, investigation, visualisations and writing - review and editing.

  – Dr. Shahab Dehghan provided a methodology, software, performed the writing

- original draft and visualisation.

  – J. Lancaster, was the industry partner and provided resources and reviewed the paper.

  – Dr. Petros Aristidou supervised the work, helped with writing - review and editing and provided different resources to support the paper.

- The work in Chapter 6 of the thesis has appeared in the following publications:

  A. M. Nakiganda, Shahab Dehghan, Uros Markovic, Gabriela Hug, and Petros Aristidou. "A Stochastic-Robust Approach for Resilient Microgrid Investment Planning Under Static and Transient Islanding Security Constraints". *IEEE Transactions on Smart Grid*, 2022.

  – As the lead author, the candidate the candidate performed all the conceptualisation, methodology derivation, software formulation, investigation, writing - original draft and visualisation.

  – Dr. Shahab Dehghan helped with the methodology, software and writing - review and editing.

  – Dr. Uros Markovic helped with the writing - review and editing.

  – Prof. Gabriela Hug helped with the writing - review and editing.

  – Dr. Petros Aristidou supervised the work, helped with writing - review and editing and provided resources to support the paper.

  A. M. Nakiganda, S Dehghan, P Aristidou, "Enhancing Microgrid Resilience and Survivability under Static and Dynamic Islanding Constraints" in *2020 IEEE PES Innovative Smart Grid Technologies Europe (ISGT-Europe)*, 2020, pp. 539-543.

  – As the lead author, the candidate the candidate performed all the conceptualisation, methodology derivation, software formulation, investigation, writing - original draft and visualisation.

  – Dr. Shahab Dehghan helped with the software and writing - review and editing.

  – Dr. Petros Aristidou supervised the work, helped with writing - review and editing and provided resources to support the paper.

- The work in Chapter 8 of the thesis has appeared in the following publications:

A. M. Nakiganda, T Van Cutsem, P Aristidou, "Microgrid Operational Optimization with Dynamic Voltage Security Constraints" *2021 IEEE Madrid PowerTech*, 2021, pp. 1-6.

- As the lead author, the candidate the candidate performed all the conceptualisation, methodology derivation, software formulation, investigation, writing - original draft and visualisation.
- Prof. Thierry Van Cutsem helped with the methodology and writing - review and editing.
- Dr. Petros Aristidou supervised the work, helped with writing - review and editing and provided resources to support the paper.

Abstract

Recent years have seen electric power systems transitioned to become more sustainable through the incorporation of Renewable Energy Resources (RES), such as wind and solar. RESs interfaced to the grid via fast-acting Power Electronic (PE) converters are therefore gradually replacing conventional generators. Unlike Synchronous Generators (SGs) that have well-defined mechanisms for frequency and voltage support provision, Converter-Interfaced Generators (CIGs) lack these support features inherently. This leads to more volatile system dynamic response when faced with contingencies due to the lack of reactive power support and the low inertia levels. The large excursions in frequency and voltage during such events affect the operational stability and security, potentially resulting in cascading failures and total system collapse. Therefore, there is a great necessity for mechanisms to increase the resilience of power systems.

In this respect, Microgrids (MGs) present a revolutionary step in the electric power system infrastructure and operation due to their ability to split from the bulk network and form self-sufficient islands. MGs can enhance the system resilience by forming islands during extreme conditions in the bulk grid, thus ensuring power supply continuity to customers. However, this can only be achieved if MG security is ensured before, during and after an islanding event. The MG should be able to survive the system transients, preventing generator disconnections due to action of device protection systems – a scenario that can result in cascading disconnections.

This thesis proposes a set of optimisation-based algorithms for investment and operation planning of MGs that ensure the security in grid-connected mode, islanded mode, as well as the transitions between the two. The first part of the thesis investigates various formulations of Optimal Power Flow-based (OPF) planning models for MGs. Convex relaxations, restrictions and approximations are investigated for tractability and their applicability to MG networks is assessed. Moreover, the issues of uncertainty due RES and load demand variations are analysed and tackled using two proposed methods, a stochas-

tic approach incorporating machine learning clustering techniques and a distributionally robust technique using linear decision rules. Finally, the proposed MG optimisation models are then enhanced to include security requirements for both steady-state operation as well as transient frequency and voltage response during islanding.

Using an analytical formulation for the transient frequency response metrics, an iterative bound-tightening strategy is first proposed to solve a MG planning model consisting of both static and transient security metrics. The same problem is also tackled with a decomposition-based approach using dual cutting planes and sensitivities to frequency support parameters of the different generators. Finally, a dynamic optimisation approach with sequential transient constraint transcription based on time-domain simulations of the MG operation is proposed, incorporating security constraints for both frequency and voltage transient operation in an operational planning problem. All three algorithms investigate both infrastructural enhancement and operational flexibility mechanisms that can be adopted to enhance system performance. Moreover, the algorithms developed ensure cost effective and secure operation of the MG in the pre-islanding, post-islanding and during the event-triggered unscheduled transition to islanded state.

The proposed algorithms are tested on MG networks with both CIGs and SGs. The computations and simulations are performed on benchmark low-voltage and medium-voltage distribution networks, as well as the real MG network of Alderney Island.

Acknowledgement

The success of this journey has been a result of many people to whom I wish to convey my utmost gratitude.

First and foremost, I would like to express my deepest gratitude to my supervisor Dr. Petros Aristidou, for the unlimited support provided to me during my PhD studies. I am forever grateful for the patience, generosity and time he devoted to guide me through my research. More especially for his experience, inspiration and encouragement through all the challenges along the way. I am indeed forever indebted.

My deepest gratitude also goes to Dr. Shahab Dehghan for his immense support during my PhD. For the discussions and countless hours he dedicated to review my work. His intelligence, enthusiasm and eye for perfection provided great encouragement. Of course, the food ideas and witty humour made even the most complex discussions a walk in the park. I will always value his professionalism and friendship awarded to me.

Special thanks go to my second supervisor Prof. Kang Li for the valuable comments on my research work. I have also had the great fortune to fruitfully collaborate with different researchers along this journey. I would especially like to thank Prof. Jon Lovett for giving me the opportunity to contribute to the CRESUM-HYRES project. I benefited greatly from the discussions with the team as and the field work done both in the UK and abroad. Another special thanks go to my co-authors Prof. Thierry Van Cutsem, Prof. Gabriela Hug and Dr. Uros Markovic for the valuable discussions and comments on my work that helped me improve the quality of my research.

I would like to thank the University of Leeds for financially supporting my PhD studies during the three years of my research. Many thanks to the Funds for Women Graduates for the support towards the completion of my thesis.

Even though the pandemic robbed me of many great moments with my colleagues, I still enjoyed the time we had together at office. I would like to thank my group-mates and

colleagues with whom I shared an office for the great discussions and support.

Thanks to all my friends in both in Uganda and the United Kingdom for being there and sharing many memorable moments with me. In particular, I want to thank Paul for his constant support in many ways especially during my final year. Mike, our brief coffee sessions were always packed with loads of wisdom to share. Ambreen, thanks for always sharing your kindness with me, we have literally walked this journey together from the start. And to Regina, Wilson and Brenda, for our very long phone calls and chats that were always filled with loads of laughter.

Finally, my deep appreciation goes to my family for their constant encouragement and inspiring me to live, serve and for making my life worthwhile. My siblings, Rachel, Angela, Ann, Grace, Peter, Jim and Harriet, you have been my rock through this journey. Last but not least, I thank my mother, Geraldine Nansamba Ssemwezi, I am who I am because the strong person she is.

To my father James and brother Jim, in loving memory.

Contents

List of Acronyms

ADN	Active Distribution Network
AEL	Alderney Electricity Limited
AHC	Agglomerative Hierarchical Clustering
AVR	Automatic Voltage Regulator
BFM	Branch Flow Model
BIM	Bus Injection Model
CF	Capacity Factor
CIG	Converter Interfaced Generators
CoI	Center-of-Inertia
CRF	Capital Recovery Factor
DAD	Differential-Algebraic-Discrete
DER	Distributed Energy Resources
DN	Distribution Networks
DRO	Distributionally Robust Optimisation
DSA	Dynamic Security Analysis
ENTSO-E	European Network of Transmission System Operators
ES	Energy Storage
FRT	Fault Ride-Through
HFRT	High-Frequency Ride Through

HILF High-Impact Low-Frequency

HVRT High-Voltage Ride Through

IR Inertia Response

LCOE Levelized Cost of Energy

LDRs Linear Decision Rules

LFRT Low-Frequency Ride Through

LIHF Low-Impact High-Frequency

LV Low Voltage

LVRT Low-Voltage Ride Through

MGs Microgrids

MILP Mixed-Integer Linear Programming

MINLP Mixed-Integer Non Linear Programming

MISOCP Mixed-Integer Second-Order Cone Programming

MV Medium Voltage

NLP Non-Linear Programming

NP Non-deterministic Polynomial-time

OPF Optimal Power Flow

PCC Point-of-Common-Coupling

PFC Primary Frequency Control

PSS Power System Stabiliser

PV Photo-Voltaic

PWL Piece-Wise Linearisation

RES Renewable Energy Sources

RO Robust Optimisation

RoCoF Rate-of-change of frequency

SFC Secondary Frequency Control

SG Synchronous Generator

SO Stochastic Optimisation

SoC State-of-Charge

SOCP Second-Order Cone Programming

SSA Static Security Analysis

TFC Tertiary Frequency Control

UC Unit Commitment

VSM Virtual Synchronous Machine

List of Figures

List of Tables

Chapter 1

Introduction

1.1 Background and Motivation

1.1.1 Motivation

The electric power system has for the last decades seen a transformation of generation systems, transmission and distribution networks facilitated by the invent and maturity of new technologies as well as diversification of primary energy supply sources. Current energy systems have seen a proliferation of several distributed generation units located much closer to load demand. Distributed Energy Resources (DER) are majorly powered by renewable energy sources and interfaced to the network through fast-acting power electronic devices that bring with them numerous grid support capabilities. DERs greatly increase the flexibility of the grid providing power reserves, ancillary services and in cases attenuating the heavy financial requirement needed in grid expansion programmes. This flexibility is vital in ensuring system adequacy, security and resilience during the various operation scenarios.

One of the most important engineering challenges of the century is the design of resilient infrastructure that can survive extreme events and continue to provide services during critical outages. The resilience of an energy system entails its capacity to tolerate disturbances and continue to deliver affordable energy services to consumers [5]. A resilient system is able to downgrade its functionality as well as alter its structure in an agile manner without collapsing. System operators normally perform *'N-1'* or *'N-k'* security analyses to ensure that the system is able to survive all possible credible contingencies.

However, catastrophic events for example major grid faults, extreme weather conditions and cyber attacks are less predictable and can result in wide-scale disruptions, cascading failures and system black-outs. Such disturbances do not usually qualify for the '*N-k*' security analyses. This necessitates the adoption of robust and adaptive solutions rethinking either operational measures or network infrastructure reinforcement measures to enhance resilience of the electricity grid and ensure survivability during major contingencies. In power system infrastructural planning, operators may opt to upgrade existing equipment and adopt more robust designs and materials that are less vulnerable to a specified set of contingencies. During system operation however, the solution requires the design and adoption of control measures that can ensure adaptability, flexibility and fast recovery of power supply to the load demand in the event of a major contingency.

One of the key technologies proposed to enhance the resilience of the electricity grid is the use of Microgrids (MGs). A MG, as defined in [6], refers to "*a group of interconnected loads and distributed energy resources with clearly defined electrical boundaries that acts as a single controllable entity with respect to the grid and can connect and disconnect from the grid to enable it to operate in both grid-connected or island modes*". They are able to concurrently provide both infrastructural and operational measures as they split from the grid into self-sufficient islands ensuring continuity of supply [7]. Moreover, their inherent DERs ensure increased flexibility in the grid that can be leveraged in the design of operational measures for increased resilience [8, 9].

However, the influx of Converter-Interfaced Generators (CIGs) in MGs has resulted in radical changes in both the dynamic and operational characteristics i.e. static and transient performance of the electricity network [10]. Impacts such as reduced inertia levels and variability of supply can affect the MG performance especially during major contingencies such as those resulting in the abrupt islanding of the MG. Events such as these are characterised by large excursions in both frequency and voltage [11, 12] affecting system survivability. Therefore, to ensure operational stability and security during emergency conditions, it is necessary that any limitations the system may present in response to such conditions are mitigated. This can be ensured by leveraging the grid-supporting capabilities of the DERs and other operational measures to enhance system survivability. Survivability includes the non-activation of generator protective devices during major contigencies, as this would otherwise result in the onset of generator disconnections and cascading failures in the network. During the design of MGs, the decision normally incorporates the capacity factors of units to be adopted, investment costs and the operation costs of the units in addition to the required system adequacy and loading requirements.

However, for a system to be both statically and dynamically secure and hence resilient, the static and dynamic control capability and the effect of various levels of disruption need to be put into consideration.

The goal of this dissertation is to improve system preparedness by enhancing traditional MG planning models to incorporate the nature and effect of DERs, through the inclusion of both static and dynamic operation security aspects for reliable and resilient operation. Chapters 2, 3, 4 and 5 focus on modelling the grid-supporting capabilities of DERs, power flows in MGs and present techniques to handle the uncertainties inherent in MG operation. While Chapters 6, 7 and 8 present various methods to efficiently incorporate static and transient frequency and voltage security into network planning models ensuring security, survivability and optimality of the network.

1.1.2 Microgrid

A MG illustrated in Fig. 1.1 is conceptually considered as an independent power distribution network, capable of operating in both grid connected and autonomous mode or in either modes. It is composed of DERs, energy storage devices, and a cluster of loads that operate in coordination to reliably supply electricity connected to the host power system at a single point of connection refered to as the Point-of-Common-Coupling (PCC) [13,14].

Reference [15] further details that a MG has the following attributes:

- It is connected to either the low voltage distribution network or medium voltage transmission network through the PCC.
- It has the capacity to supply its loads especially the critical load autonomously during a pre-defined period of time.
- In islanded operation mode, it should maintain balance between generation and consumption, while satisfying certain reliability, power quality, and adequacy standards.
- In grid-connected mode, MGs may behave as a single controllable unit i.e., controllable source or controllable load from the viewpoint of the rest of the power grid.
- In the islanded mode, it has the capability to actively control frequency, voltage and power flow.

In grid-connected mode of operation, voltage and frequency are imposed by the main grid. The microgrid is operated as a power source providing/consuming a specified amount of power to/from the grid based on the power dispatch references provided by a higher level

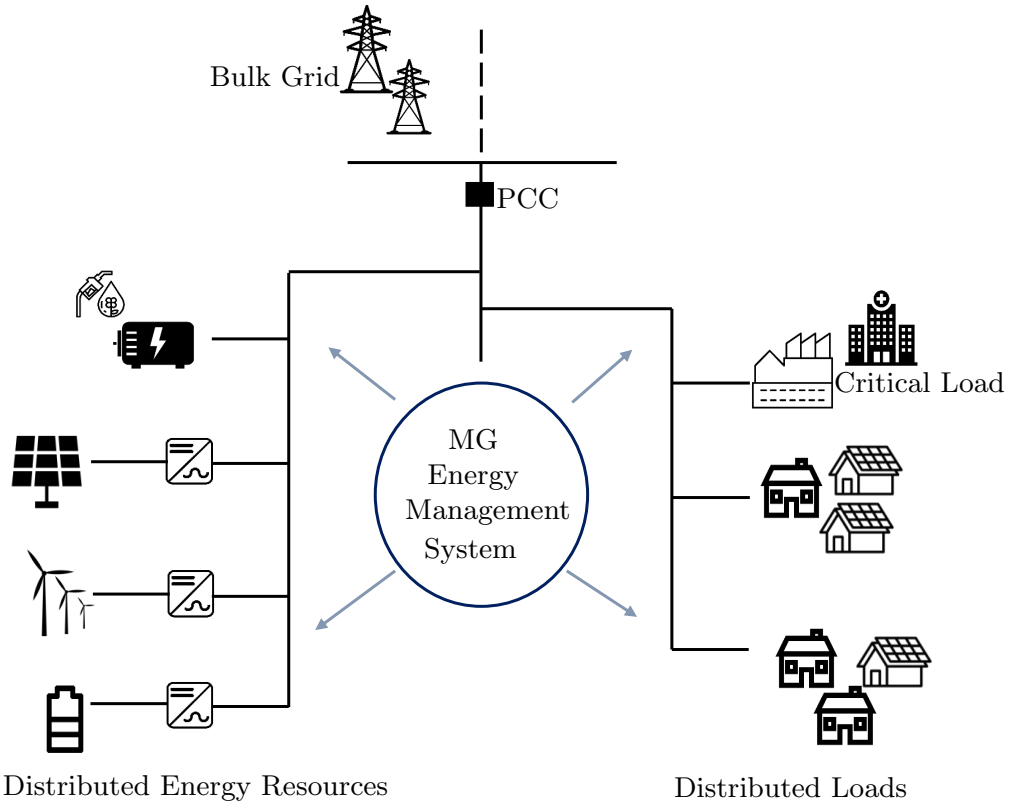

Figure 1.1: Illustration of a microgrid network.

control. The MG's role is then limited to providing ancillary services when called upon by the grid operator. On the contrary, in islanded mode, the system voltage and frequency are no longer imposed by the main grid, and the different DERs in the MG must maintain these states within acceptable ranges. During the transition between operation modes, a thorough transient security and stability analysis is required to ensure seamless switching.

In a MG, generation units are either directly coupled to the network through AC rotating machines, i.e. Synchronous Generator (SG) or interfaced through power electronic converters, i.e. Converter Interfaced Generators (CIG). Due to the operational and control flexibility they offer, e.g. power conditioning ability and their fast acting nature, power electronic converters are widely adopted technologies. A MG can be composed of purely CIGs, purely SGs, or a combination of the two; herein referred to as a hybrid MG.

1.1.3 Overview Security and Resilience of Power Systems

1.1.3.1 Definition of Key Terms

The security and resilience of a power system given the occurrence of an event can be described by different metrics. These are dependant on whether or not it can maintain a

pre-determined level of functionality despite the occurrence of either Low-Impact High-Frequency (LIHF) or High-Impact Low-Frequency (HILF) contingencies.

LIHF contingencies relates to such events that have a high probability of occurrence in the day-to-day operation of the power system (such as the loss of a line, loss of a generator etc.,) but with a minor impact to the operation of the system. On-the-other-hand, HILF contingencies rarely occur, however, they are more detrimental to the system's ability to continue operation and are usually associated with cascading failures and black-outs if not adequately managed. These include: extreme weather events such as floods, hurricanes and earthquakes; man-made events including cyber attacks and technical errors; and, equipment failures [4, 16, 17].

Table 1.1 presents the definitions for system security, resilience, reliability and adequacy adopted in this thesis.

Table 1.1: Description of key terms in power system operation.

Term	Description
Security	Operational security relates to the ability of the power system to operate within defined boundaries and tolerances while ensuring continuity of supply in the event of contingencies.
Resilience	Power system resilience, generally includes its ability to anticipate, absorb, adapt and rapidly recover from HILF events subjected to the network internally or externally [9]. The UK Energy Research Centre defines resilience as [5]: *"Resilience is the capacity of an energy system to tolerate disturbance and to continue to deliver affordable energy services to consumers. A resilient energy system can speedily recover from shocks and can provide alternative means of satisfying energy service needs in the event of changed external circumstances."* A resilient system is able to downgrade its functionality as well as alter its structure in an agile manner without collapsing.

Reliability	Reliability of a power system is the probability of satisfactory operation, i.e. delivering power to customers with acceptable standards and in the amount desired, over a pre-defined period of time and with few interruptions [18]. Reliability entails both system adequacy and system security.
Adequacy	System adequacy relates to the ability of a power system to supply the load demand, taking into account uncertainties in the generation availability and load level, and scheduled and unscheduled outages of system components.
Stability	"*Power system stability is the ability of an electric power system, for a given initial operating condition, to regain a state of operating equilibrium after being subjected to a physical disturbance, with most system variables bounded so that practically the entire system remains intact*" [18].
Survivability	Survivability is the ability of the system to maintain adequate functionality during and after a contingency. It entails all actions that allow the system to internally adjust to adverse situations so as to minimise performance degradation.
Cascading failure	The uncontrolled successive loss of various elements in a network triggered usually by a major contingency.

It is noteworthy to mention that system security generally encompasses resilience and stability. A secure network is generally resilient to a given disturbance, however network resilience does not always imply network security. Additionally, network resilience is usually defined for HILF events while security thresholds should be adhered to during both LIHF and HILF events.

1.1.3.2 Leveraging microgrids for power grid resilience support

HILP events are characterized by unpredictability in their occurrence and duration with their temporal progression associated with multiple disruptions and failures in both the transmission and distribution systems. This calls for diversity in power supply resources,

operation, and control measures in addition to grid robustness to mitigate the associated negative effects. Such measures are more suited to actively adapt to the conditions during and after an event. Resources that can be leveraged to improve the system resilience include utility-owned distributed generation, energy storage, MGs, and demand response [19, 20].

In [14, 21–23] the capabilities of MGs and their associated distributed energy resources that facilitate reliability and enhancement of the grid in both grid-connected and islanding modes have been studied. MGs are able to provide local power support, voltage and frequency secondary control reserves, frequency and voltage regulation (to maintain operational bounds), fault ride-through capabilities, and restoration services in case of black-start capabilities.

Frequency and voltage control reserves

MG energy resources can be controlled either with fixed active (P) and reactive (Q) power output, i.e. PQ control, or with the ability to provide both frequency and voltage references and regulation, i.e with droop control or dynamic frequency and/or voltage support. With frequency droop control, generating units are able to participate in mitigating mismatch in demand and supply as well as provide synthetic or virtual inertia (VI). Similarly, voltage support provided by the MG composite units can mitigate the effects of voltage dips and spikes and unbalanced voltage conditions especially in LV networks. Frequency and voltage support offered by CIGs are subject to the different grid standards stipulated in a given locality. A more detailed analysis of the control strategies will be given in the following chapters.

Fault ride-through capability

High/low-voltage and/or high/low-frequency ride through (H/LVRT and H/LFRT) functionalities refer to the ability of DERs to remain connected to the grid during instances of major disturbances causing critical frequency and voltage bounds violations. The acceptable minimum voltage and frequency levels are set by grid code. This is done to prevent further system degradation due to the cascaded disconnection of DERs. During these instances, the MG may also be called on to further offer active power, inertia, and reactive power reserves to allow for faster network restoration.

Black-start capability

The black-start capability of a generating unit refers to its ability to start delivering power without relying on the network. This implies that the unit has the capability to define

both the voltage magnitude and frequency as well as to provide the required real and reactive power to energize the network. MG generation units with black-start capability can enable the restoration of power to a section of the distribution network. Reference [24] proposes a sequence of control actions to adopt in energizingthe distribution grid through coordination and synchronization of several MGs.

Islanded operation

MGs have the ability to operate autonomously serving local load demand for a given period of time. The islanding process may be initiated as an intentional disconnection from the grid (during grid maintenance) or from a forced disconnection (due to a fault in the network).

This ability is however affected by two major issues. First, unlike traditional grids which have large synchronous machines with the required rotational inertia to balance the imbalance in demand and supply, MGs are usually supplied by electronically interfaced generators that lack the inertia required to balance the system. Second, a large share of the MG power is supplied by intermittent renewable energy resources with their inherent uncertainty in the available power. Both these aspects need to be carefully considered during MG operation and when assessing the MG potential to provide support to the grid in islanded mode.

The disruptions caused by HILP events may lead to two general forms of disruptions:

- Highly degraded levels of service leading to instances of reduced power quality levels such as voltage sags/spikes, congestion in distribution systems, and over/under-frequency in the power system.
- In extreme cases, loss of major generation units, transmission lines, or substation equipment cause either localized or global system blackouts.

In the first case, MGS can be leveraged to provide emergency reserve services, e.g in distribution systems during voltage sag and in transmission systems requiring frequency support. The control flexibility of the different distributed generating units and loads that compose the MG is key in achieving the required response. In the latter case, the MG capability to form islands can serve to ensure continuity of power supply to the critical loads, as shown in [17], while the system restoration process commences. The work in this thesis focuses on the processes and techniques necessary to support MG resilience in the latter case.

1.2 Problem Description

In power system infrastructural planning, operators may opt to upgrade existing equipment and adopt more robust designs and materials that are less vulnerable to a set of contingencies usually caused by the natural elements. In system operation, the solution requires the design and adoption of control measures that can ensure adaptability, flexibility, and fast recovery of power supply to the load demand in the event of a major contingency. The MG can be viewed by the grid as a controllable entity whose capabilities depend on the aggregated control capabilities of the constituent generators and loads. These can be leveraged to provide support to the power system in case of major disturbances through ancillary service provision or islanded operation to serve local demand.

However, investigations currently are geared to either static ("snap-shot") analysis of pre-event and post-event states of the system through security-constrained optimal power flow and unit commitment formulations or the design of robust real-time control frameworks with inherent ability to adapt to uncertainty in system operation. The "snap-shot" analysis assumes that any dynamic changes during and after event progression are automatically handled by the controllers and the system is able to reach a steady state securely. Therefore, the main operational challenges presented to the system are to guarantee resilience in the event of HILP contingencies by application of a system-wide optimal solution is obtained.

This thesis designs solutions to enhance the resilient operation of the microgrid thereby providing answers to the following questions:

1. How can the MG survive the initial transients associated with high-impact events, ensuring that excursions in node voltages, line currents and system frequency are maintained within the required operating standards thus preventing further failures?

2. How can the system be able to maintain a balance of demand and supply for a defined period of time thus ensuring sufficient energy content for local demand given the occurrence of a major contingency?

3. How can the MG operate robustly given the uncertainties emanating from renewable sources, load profile changes, and grid faults?

Question one deals with the ability of the MG to retain dynamic security and stability during a network emergency. Question two deals with the adequacy of generation re-

sources in the MG to meet demand, this factor is crucial in determining the successful microgrid operation given defined system objectives. This can be tested through operational planning problems such as optimal power flow, dispatch, and unit commitment. Question three deals with the ability of the MG to remain physically intact and operationally flexible given the different uncertainties that may be presented during system operation.

In answering these questions, this thesis proposes an integrated robust decision-making framework that incorporates aspects of the dynamic performance of the MG into the investment and operational planning problems to provide system operators with a more realistic solution that can be adopted to enhance secure and resilient grid operation. This solution facilitates the effective identification of system vulnerabilities and thus necessary modifications in system control can be determined. In finding solutions to the questions defined above, the techniques and applications proposed in this thesis realised the following benefits:

- Enhancement of the system preparedness and survivability given the occurrence of potentially detrimental events thus preventing further disconnections and cascading failures from propagating into the MG network.
- The inclusion of system dynamics in the investment and operational planning problem to provide operators with a more realistic solution and clear origins on the cause of potential inadequacies and vulnerabilities in system control and operation.
- Preventive control solutions provided by the planning solutions that are usually a lot cheaper than the corrective control required during real-time emergency conditions.

1.3 Research Contributions

The main contributions of this thesis are the following:

- A stochastic-robust centralised investment and operational planning model that includes static and transient frequency security considerations utilising an iterative bounds-tightening approach to ensure MG resilience during instances of abrupt islanding from the main.
- A decomposition-based, inertia-aware MG investment planning algorithm that applies dual-cutting planes to tractably include inertial constraints.
- A multi-level algorithm that uses time-domain analysis to formulate dynamic fre-

quency and voltage security constraints transcribed into the operational planning optimisation problem to enhance system security and survivability in the case of emergency islanding.

- A tractable data-driven distributionally robust algorithm that handles uncertainties in MG investment planning models using multi-period linear decision rules while respecting the non-anticipativity nature of the short-term operational decisions.
- A two-stage stochastic investment planning model that characterises correlated uncertainties of load demand and renewable energy production using risk-seeker, risk-neutral and risk-averse scenarios generated by a clustering technique.

1.4 Publications List

The work presented in this thesis has been reported in the following journal (**J***), and conference (**C***) publications and technical report (**R***):

[**J1**]. **A. M. Nakiganda** and Petros Aristidou, "Resilient Microgrid Scheduling Ensuring Secure Frequency and Voltage Transient Response". *Submitted to IEEE Transactions on Power Systems (2022)* (under review).

[**C1**]. **A. M. Nakiganda**, S Dehghan, P Aristidou, "A Data-Driven Optimization Model for Designing Islanded Microgrids". *2022 International Conference on Probabilistic Methods Applied to Power Systems (PMAPS)* **(Best Paper Award)**.

[**J2**]. **A. M. Nakiganda**, Shahab Dehghan, Uros Markovic, Gabriela Hug, and Petros Aristidou. "A Stochastic-Robust Approach for Resilient Microgrid Investment Planning Under Static and Transient Islanding Security Constraints". *IEEE Transactions on Smart Grid*, 2022.

[**C2**]. **A. M. Nakiganda**, S Dehghan, P Aristidou, "Comparison of AC Optimal Power Flow Methods in Low-Voltage Distribution Networks," *2021 IEEE PES Innovative Smart Grid Technologies Europe (ISGT Europe)*, 2021, pp. 1-5. **(Best Paper Award)**

[**C3**]. **A. M. Nakiganda**, T Van Cutsem, P Aristidou, "Microgrid Operational Optimization with Dynamic Voltage Security Constraints" *2021 IEEE Madrid PowerTech*, 2021, pp. 1-6. **(Best Paper Award)**

[**C4**]. **A. M. Nakiganda**, S Dehghan, P Aristidou, "Enhancing Microgrid Resilience and Survivability under Static and Dynamic Islanding Constraints" in *2020 IEEE PES*

Innovative Smart Grid Technologies Europe (ISGT-Europe), 2020, pp. 539-543.

[**C5**]. S. Dehghan , **A. M. Nakiganda**, J. Lancaster, P. Aristidou, "Towards a Sustainable Microgrid on Alderney Island Using a Python-based Energy Planning Tool" in *The 12th Mediterranean Conference on Power Generation, Transmission, Distribution and Energy Conversion (MEDPOWER 2020)*, 2021, pp. 196 – 201.

[**C6**]. S Dehghan, **A. M. Nakiganda**, P Aristidou, "A Data-Driven Two-Stage Distributionally Robust Planning Tool for Sustainable Microgrids" in *2020 IEEE Power & Energy Society General Meeting (PESGM)*, 2020, pp. 1-5.

[**R1**]. S Dehghan, **A. M. Nakiganda**, P Aristidou, "Resilient and Sustainable Microgrid Planning on Alderney Island", June 2020.

1.5 Thesis Organisation

This thesis is organised as follows.

- **Chapter 2** presents an overview of security and resilient mechanisms in microgrids with an emphasis on systems with higher penetration levels of converter-based generators. The different grid requirements and guidelines to be adhered to by DERs are presented. Control algorithms required for the support of the system in both steady-state and transient conditions are discussed at device- and system-level. Finally, this chapter presents the control approaches that are utilised in the rest of the thesis.

- **Chapter 3** presents the general mathematical formulation for an Optimal Power Flow-based (OPF) planning problem in microgrids and the technical challenges associated with modelling such systems. This chapter further investigates four commonly adopted approximations and convexifications aimed at tackling the tractability of the general OPF model in Distribution Networks (DN). Simulation results compare their performance and suitability for adoption in active distribution networks and MG planning problems using different metrics.

- **Chapter 4** presents methods that deal with uncertainty in MG planning problems especially due to forecasting errors in load and generation. Furthermore, a two-stage stochastic investment planning model is presented characterising the uncertainties of load and renewable generation using risk-seeker, risk-neutral, and risk-averse representative operational scenarios. The different operational scenarios are generated by the agglomerative hierarchical clustering method. In the simulation results, the

optimal solutions under the three risk levels is assessed for the real MG of Alderney Island to ensure sustainability given various types of investment candidates. Furthermore, the trade-offs with respect to the application of carbon emissions limitations and number of operational scenarios considered during planning is analysed to ensure optimality and robustness of the solutions.

- **Chapter 5** proposes a robust data-driven approach for dealing with the challenge of uncertainty in MG operational planning problems. Using available historical data, a data-driven distributionally robust model to tackle the system uncertainties is presented. The model proposed uses data-driven ambiguity sets to model the uncertain parameters and a three-stage approach to transform the model into a computationally tractable form. Simulation results compare the data-driven robust approach and stochastic approach presented in Chapter 4 against their expected cost and computational efficiency.

- **Chapter 6** proposes a novel three-level iterative investment and operational planning algorithm that includes both steady-state and transient frequency-related constraints, thus enhancing MG survivability during unplanned islanding events. The first level solves a multi-period, stochastic investment and operational planning problem. The second level sequentially tests the feasibility of the first level solution against analytically formulated security metrics of the frequency transients while the third level utilises a bound-tightening approach to constrict grid power imports/exports in the first level problem. Simulation results show that the proposed method ensures system preparedness and survivability during emergency operational scenarios by applying both operational measures and/or the installation of new units.

- **Chapter 7** proposes an alternative strategy for solving MG investment and operational planning problems with non-linear transient and static frequency security constraints using a decomposition-based approach. The algorithm tackles issues of the impact of information exchange between different stages of the methodology and convergence rate presented by techniques in Chapter 6. The strategy, based on dual-cutting planes, ensures bidirectional information exchange between the different levels of the algorithm providing a solution that not only considers cost but also available frequency support from the different candidate units. Simulation results demonstrate the superiority and versatility of the decomposition-based approach over the bound-tightening approach of Chapter 6.

- Critical events during system operation will cause excursions in both frequency and voltage affecting system integrity. While in the previous chapters only transient frequency-related constraints were considered, in **Chapter 8**, the operational planning problem is modified to include both transient frequency and transient voltage security constraints to ensure system preparedness and survivability. Unlike the case of frequency transient criteria where a closed form of security metrics is easily obtainable, a relatively simple model capturing the transient voltage response at local nodes is unavailable. A novel algorithm based on a dynamic optimisation technique using sequential constraint transcription is proposed. It uses sensitives based on time-domain simulations to transcribe the transient frequency constraints onto the operational planning problem formulated as resilience cuts. Simulation results demonstrate the efficacy of the model given the abrupt islanding of a MG under various operating scenarios.

Finally, **Chapter 9** summarises the key findings of this thesis and suggests directions for future work.

Figure 1.2 depicts the contents and organisation of the thesis highlighting applications and methods utilised in blue.

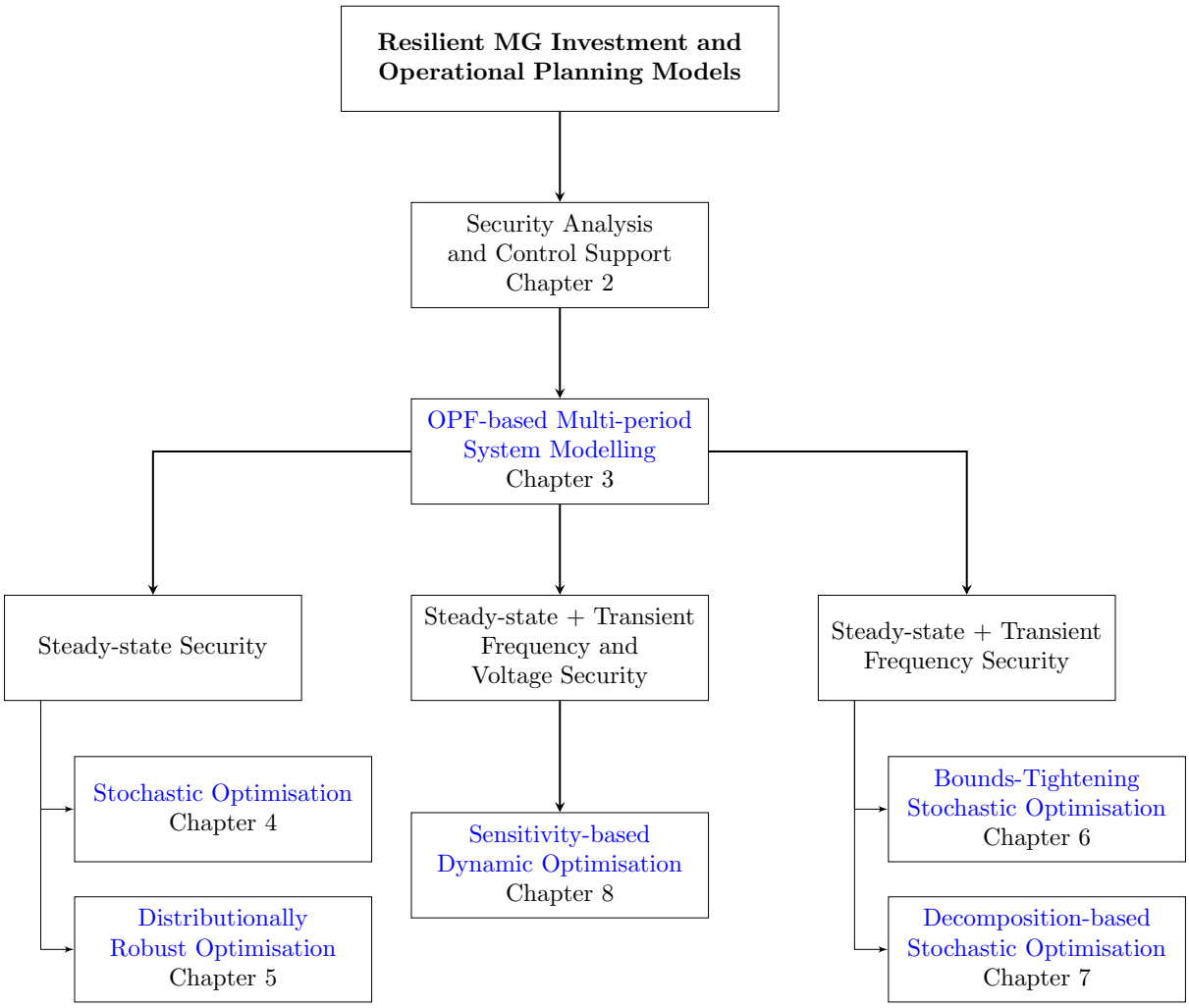

Figure 1.2: Thesis organisation.

Part I

Microgrid Modelling, Control and Security

Chapter 2

Microgrid Security Analysis and Control Support

2.1 Introduction

Distributed Energy Resources (DER) have existed in traditional power systems for decades providing power supply to remotely located communities that lack access to national grids. These were traditionally composed of diesel/hydro generators with trends shifting towards renewable energy powered generators including wind, bio-gas/fuel and photo-voltaics in recent years. With the maturity of renewable energy technologies, DERs are now widely integrated into both Low Voltage (LV) and Medium Voltage (MV) systems to provide power reserves or support critical loads such as hospitals, schools and production facilitates. However, if not properly controlled and coordinated their integration may cause power quality and reliability issues diminishing their benefits. Microgrids (MG) can be employed to coordinate the integration of DERs into the grid and maximise their potential. MGs present various benefits including the enhancement of the resilience of the power grid. However, adequate coordination and control of the various components is necessary to ensure the resilient and secure operation required during instances of system disruption.

This preliminary chapter introduces the security and resilience concepts in relation to microgrid network operations. Moreover, the grid requirements and control support models for the DERs used in this thesis are presented and discussed.

This chapter is organised as follows: Section 2.2 discusses the framework used in the analysis, evaluation and enhancement of security in power systems. Then, Section 2.3 presents the different grid requirements for secure operation of systems with DERs and different support structures that can be adopted to enhance secure and resilient operation. Finally, Section 2.4 summarises the chapter.

2.2 Framework for Security Analysis

Security analysis involves the evaluation of operating points and system trajectories to ensure operation within acceptable operating limits and secure regions given the occurrence of predefined contingencies. It can also include the derivation of remedial actions where required to move the system to a secure state or region. The secure operating region is defined by boundaries that include static security criteria and dynamic security criteria.

Static security criteria related to the pre- and post-contingency steady-state operation include:

- node under and over voltage limits
- voltage angle limits between successive nodes
- transformer thermal limits and transmission line current and thermal limits
- generator power operating limits
- steady-state frequency limits

The most commonly used dynamic security criteria between pre- and post-contingency states include thresholds on:

- levels and time duration of transient voltage excursions, i.e., under/over voltages
- levels and duration of transient frequency excursions, i.e. under/over frequency and rate-of-change
- system stability forms including transient angle stability, voltage stability, small signal stability and damping levels

Traditionally, security assessment has been classified into Static Security Analysis (SSA) and Dynamic Security Analysis (DSA) where the former deals with the steady-state criteria while the later is concerned with the transient criteria.

2.2.1 System Modelling

The quality of the models utilised in security analysis is essential to the accurate representation of system behaviour during various operating conditions. During system modelling, the model accuracy, i.e., accurate representation of the physical phenomena and model completeness, is the main focus. The modelling requirements vary based on the type of assessment being performed i.e., SSA or DSA. During SSA, a power flow model consisting of a detailed network representation along with the steady-state response model of the various units can suffice. However, during DSA, an accurate representation of system dynamics, unit controls and protections is crucial. The key aspects in system modelling include the network model, components model and the contingency model.

Network Model

The network model can be described by either a set of differential equations modelling the Π-circuit line model between nodes or by utilising algebraic equations when the phasor approximation is considered [25]. These equations, also referred to as power flow equations are comprised of highly non-linear relations describing the operating state of the entire power system, using nodal voltage magnitudes and angles, line currents, active and reactive power flows and injected active and reactive power at each node.

During SSA, network-constrained optimisation problems employing power flow models provide a tool to analyse system performance and ensure security thresholds are not violated [26]. However, due to the inherent features of the power flow model, no closed form solution can be obtained requiring approximations or iterations to solve. Therefore, to ensure model tractability, several approximations and relations have been proposed in literature [27]. It also is noteworthy to mention that the suitability of a solution algorithm also depends on the topological characteristics of the network, for example distribution system tend to have a radial structure hence can be represented as a unidirectional graph which is not the case for mesh networks.

Component Model

For DSA, time-domain simulations studies require the dynamic model of the different components connected to the network. These include but are not limited to synchronous machine models, excitation systems, governors, power system loads and converter models. In some cases due to the high dimension and size of the models, dynamic equivalents through model-order reduction techniques can be adopted [28]. Moreover, where

model parameters and structure are unknown, system identification methods can be adopted [29].

Contingency Model

The contingency model identifies the components that have failed or have been affected by the disturbance in the network including the spatial and temporal effect. These can include transformer disconnections, loss of a generator or load, unbalanced fault at different locations of a line, or adjustment of generation or load consumption.

2.2.2 System Response and Evaluation

The network response during contingencies can be analysed analytically using power flow solutions or through time-domain solutions. Traditionally, power-flow solutions have been used to evaluate SSA, while both power-flow and dynamic simulations are performed during DSA. A power flow solution provides a pre- and post-fault snapshot of system operation assuming steady-stage stability during and after the disturbance. This provides an assessment of system adequacy to satisfy demand while neglecting the transient and dynamic processes associated with the event trajectory.

Subsequent to a disturbance, the system may either settle down to a new normal state i.e., with all technical operational and load constraints satisfied, of may successively enter:
Emergency state: The power system is intact and able to fulfil load constraints but severe violations exist in the technical operating constraints.
In extremis state: The system collapses due to major violations exists in the technical constraints resulting in the tripping of generators, disconnection of load supply and cascading failures.
Restorative state: Technical operational constraints have been satisfied and load reconnection ensues. Based on the state of operation from system evaluation, different measures may be adopted to improve the system resilience and security.

2.2.3 Performance Enhancement

Various actions can be taken to enhance the system performance depending on its operating state, thus aiding the return to a normal operation. Preventive measures are applied during the pre-contingency normal operation with the aim of ensuring system preparedness in the event of a disturbance. These include generator rescheduling, and

voltage and frequency reserve scheduling. Alternatively, corrective measures taken in the aftermath of a disturbance include actions to drive the system from an emergency state to a normal state. Typical actions include load shedding, switching operations, application of fast spinning reserves and generation re-dispatch.

2.3 Secure and Resilient Microgrid Operation

High-Impact Low-Frequency (HILF) events in the power network are usually associated with multiple disruptions, failures and in some cases total system collapse. A resilient operation thus implies that as system is able to mitigate the associated negative effects of HILF events and restore normal functionality within the prescribed time period [2, 9].

The measures to improve the resilience of the power network can be summarised into:

- Infrastructural reinforcement (hardening): that include all activities aimed at improving component designs and constructions with the aim of preserving functionality and minimising damage. These measures include actions that involve long term structural and topology reinforcements which usually result in a more robust (i.e. strength and resistance) power system. These are usually incorporated into the grid expansion plan and their performance analysed based on different operating scenarios [30–32]. Hardening measures include upgrading of equipment, investment in underground versus overhead cables that are more robust in the event of extreme weather conditions, utilising stronger and more weather resistant materials for poles and lines, enhance system redundancy by installing backup generation e.g. distributed generation [24, 33–35], network reconfiguration through installation of automatic switches for controlled islanding and transmission switching [36, 37] e.t.c. Such measures are however known to be static as they do not consider the temporal dynamics of the event and can be less effective to some hazards as compared to others [2, 9, 33].

- Operational measures: aimed at improving the observability, control capability and operational flexibility by ensuring low levels of performance degradation and rapid action to allow the system return to a normal state i.e. 'bend rather than break the system'. They include both preventive (pre-disturbance) and corrective actions (during and post-disturbance). Examples of such measures include improved system state estimation, monitoring tools, adaptive and robust control schemes, demand-side management, generator rescheduling, adaptive wide-area protective schemes e.g. defensive islanding and advanced weather forecasting [2].

Table 2.1: Comparison between operational and infrastructural resilience measures. [2–4]

Hardening	Operational Measures
Make the system more resistant to disturbances by preserving individual component functionalities.	Ensure lower performance degradation and additionally rapid restoration to the normal operating levels.
Embedded into the system design or architecture hence promoting utilization of assets that are more robust in terms of physical strength and durability.	Integrated into the system's operational behavior like its control system, therefore, promoting enhanced flexibility, adaptability, agility, and quality of service.
Defined against specific threats to the system e.g. high temperatures or floods, but may be fragile when faced with a different set of events i.e. extreme robustness conjures fragility.	Can adapt to any event based on the availability of resources.
Passive approach aimed to increase system security.	Active approach with real-time reactions to disturbances.
Can only be adapted to isolated network components and hence requires stronger coupling between network components.	Boosts inter-dependency between system components e.g. securing alternative paths to re-route supply to ensure demand is met in the event of a disaster.

The survivability and timely recovery of the network during and after high impact events, can be ensured by either one or a combination of both measures. Table 2.1 presents a comparative analysis between operational and infrastructural.

2.3.1 Resilient Microgrid Operation

MGs have the ability to operate autonomously serving local load demand for a given period of time. The islanding process may be initiated as an intentional disconnection from the grid (during grid maintenance) or from a forced disconnection (due to a fault in the network). The latter is referred to as unplanned or abrupt islanding. The resilient operation of the MG requires the successful transition to islanded state i.e., its survivability during islanding and the continuance of power supply to the critical loads in the network.

The abrupt islanding of the MG leads to a sudden power imbalance for both active and reactive power in the system. In return, this leads to frequency and voltage transients at different nodes that can result in disconnections if device security thresholds are violated.

In traditional grids, kinetic energy stored in the rotating masses of the synchronous machines provides physical inertia to the system ensuring lower and less frequent frequency deviations. MGs have a high percentage of power electronic-interfaced renewable energy generators that inherently lack this feature resulting in larger frequency deviations. This is similarly true with regards to the excitation systems physically present in synchronous generators to provide voltage support but absent with electronically interfaced units. This results in larger excursions in frequency and voltage during transitions to islanded mode.

Moreover, the problem is exacerbated by the intermittent power generation from renewable energy resources. The variation in power output from renewable units implies supply irregularity affecting both the adequacy of the network as well as the level of support CIGs can provide to the network. This support is vital in ensuring that power mismatches during emergency conditions and islanding scenarios are mitigated. Therefore, to ensure the resilient operation of MGs, different grid-supporting controls and capabilities are vital.

The work in this thesis focuses on operational measures that enhance MG survivability during high-impact events in the main grid that lead to abrupt/unscheduled islanding. These include the application of frequency control and voltage control capabilities of the MG units and the adoption of flexibility mechanisms. With an aim of enhancing network support during critical events, and the prevention of system collapse various guidelines and standards have been set out for DERs to follow. The next section presents such guidelines and approaches that can be taken to enhance system survivability.

2.3.2 Grid Performance Requirements

The large-scale penetration of renewable-based CIG has affected the operation and tolerance levels of the power grid resulting in reliability issues in the network. This has led to the updated grid interconnection standards, especially with regards to DERs, to include frequency and voltage support in addition to the implementation of Fault Ride-Through (FRT) requirements. The European Network of Transmission System Operators (ENTSO-E) Requirements for Generators [38] and IEEE Standard 1547 [39] include requirements relating to the steady state behaviour and dynamic requirements relating to the transient behaviour during fault conditions (i.e. FRT). In the case of FRT capabilities, the goal is to mitigate against security deterioration in case of large frequency and voltage deviations during critical grid events.

2.3.2.1 Fault Ride-Through Capability

During instances of major disturbances causing critical frequency and voltage excursion, the DERs may be required to temporarily (for a pre-defined time duration) stay connected to the grid. This requirement is defined by the High-Voltage Ride Through (HVRT)/Low-Voltage Ride Through (LVRT) and/or High-Frequency Ride Through (HFRT)/Low-Frequency Ride Through (LFRT) functionalities. In addition, frequency and voltage support in form of active and/or reactive power boosts can be required both during the fault and in the post-fault dynamic periods to aid in the quick recovery of the system. Grid codes define the performance requirements, based on the size and capability of the generators, in terms of voltage and frequency versus time curves to reflect the conditions/regions within which the DERs should not trip, further enhancing system reliability. These criteria are typically applied to the associated frequency and voltage relay settings to ensure the action of generator protection to prevent equipment damage.

2.3.2.2 Frequency Requirement

Figure. 2.1 presents the main frequency criteria to be obeyed by DERs during a frequency event and the regions where frequency support can be provided by the DERs. The requirements during the transient response include: Rate-of-change of frequency (RoCoF), $\dot{f}$; frequency nadir, $f_{\min}$; frequency zenith, $f_{\max}$; and, the post-transient response requirement for frequency deviation in the quasi-steady-state, Δf_{qss}.

The reduced system inertia in MGs can compromise the frequency performance especially with regards to the registered levels of RoCoF. To prevent the activation of over/under frequency relays and RoCoF relays, active power should be critically managed. The ENTSO-E standards describe four stages for frequency support in a network i.e. Inertia

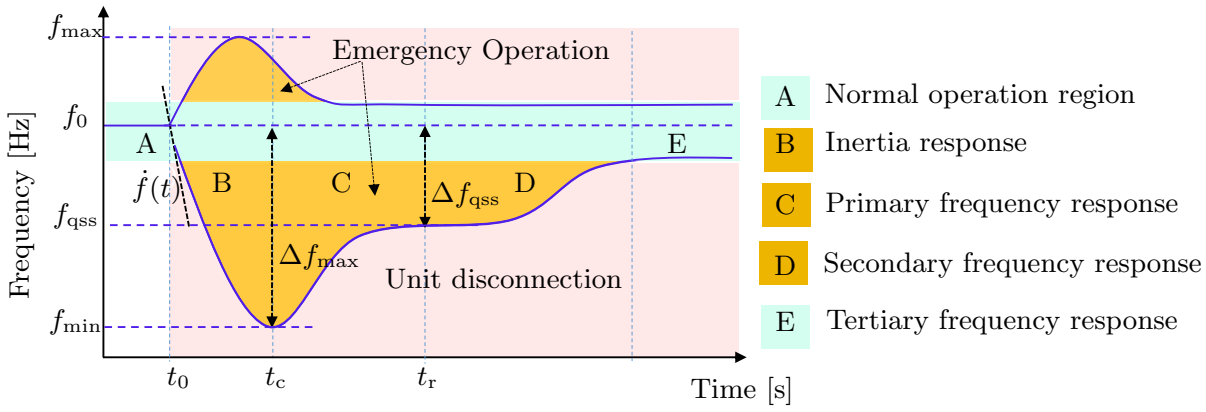

Figure 2.1: Frequency ride-through profile and regions for frequency support from DERs.

Table 2.2: ENTSO-E recommended parameters for frequency ride-through of DERs for the synchronous zone of continental Europe .

Frequency		Clearing Time [s]	
$\dot{f}(t)$	0.5 - 3 Hz/s	-	-
$f_{\min}$	47.5 Hz	t_c	≤ 0.16
$f_{\max}$	51.5 Hz	t_c	≤ 0.16
$\underline{f}_{qss}$	49.8-49 Hz	t_r	≤ 4.5
$\overline{f}_{qss}$	50.2 -51 Hz	t_r	≤ 2.5

Response (IR), Primary Frequency Control (PFC), Secondary Frequency Control (SFC) and Tertiary Frequency Control (TFC), illustrated in Fig. 2.1.

At each level, different operating reserves have to be present in the network to arrest further deterioration of system frequency. IR, activated within the first few seconds after a significant frequency drop, depends on the rotor inertia of a synchronous generator or the virtual inertia in case of Converter-Interfaced Generators (CIG), as well as the generation demand imbalance. This ensures that the RoCoF levels are kept within secure levels preventing the activation of RoCoF protection. PFC is activated within 2 s up to 30 s of frequency decay/rise to arrest the activation of under/over frequency protection and subsequently ensure the non-violation of the defined quasi steady state frequency levels. Further deviations that may exist in the frequency away from the normal operation range up to 15 min to 30 min are corrected with the SFC corrects the deviations in frequency at quasi steady state levels back to nominal values. This includes the adjustment of generator set points to ensure frequency levels return to the nominal values. TFC is applied to correct any further deviations from the nominal frequency (f_0) that may exist in the long term. Guidelines provided by the ENTSO-E for frequency ride-through are indicated in Table. 2.2.

2.3.2.3 Voltage Requirement

The FRT capability relating to the voltage requirements is shown in Fig. 2.2. Here the requirements relate to the thresholds towards the LVRT, HVRT and post-transient recovery voltage levels indicated by $V_{\min}$, $V_{\max}$, $\overline{V}_{rec}$ and $\underline{V}_{rec}$, respectively. Units are required to remain connected to the network given that nodal voltage levels remain within the acceptable LVRT and HVRT for the associated time periods. Sample thresholds for voltage FRT levels and fault clearance time period requirements by the IEEE Standard 1547-2018 are provided in Table. 2.3 [39].

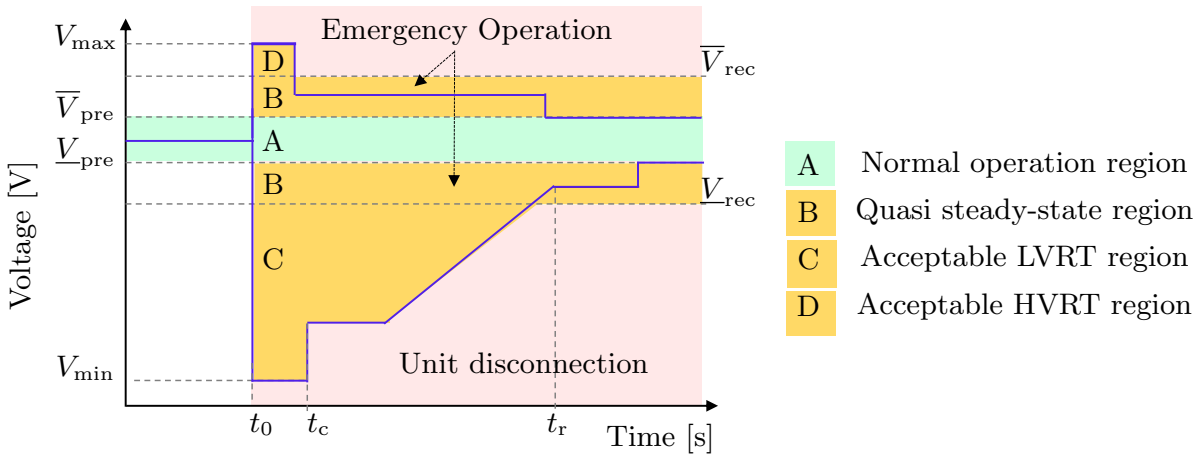

Figure 2.2: Voltage ride-through profile and regions for voltage support from DERs.

Table 2.3: IEEE Standard 1547 recommended parameters for voltage ride-through of DERs.

Voltage [p.u]		Clearing Time [s]	
V_{min}	0.45 - 0.50	t_c	≤ 0.16
V_{max}	1.2	t_c	≤ 0.16
$\underline{V}_{rec}$	0.70 - 0.88	t_r	≤ 2
$\overline{V}_{rec}$	1.10	t_r	≤ 2

FRT requirements further denote that where possible DERs should provide reactive power support i.e, absorb or inject reactive current (regions C and D in Fig. 2.2) in the short term, to immunise against voltage degradation during fault conditions [40, 41]. Unlike conventional networks composed mainly of SGs with under/over excitation limiters providing momentary voltage support, this feature is absent in CIGs which can result in further degradation [11, 12].

The following sections present approaches for voltage and frequency support for both SG and CIG units in a MG. The different support mechanisms, implemented at the device level, are essential in enhancing the security and resilience of the system during both steady-state and transient operation. While conformance to grid requirements prevents the loss of generation, control support reduces the level of frequency and voltage degradation further reducing the risk of system blackout.

2.3.3 Frequency Support

2.3.3.1 Frequency Control in Synchronous Generators

During network disturbances, the SG rotor can accelerate or decelerate due to the unbalance in the machine's mechanical and electrical torques. This behaviour is described by the the "swing equation" [42]:

$$\omega_i = \dot{\theta}_i \tag{2.1a}$$

$$M_i\dot{\omega}_i = -D_i\omega_i - P_i + P_{\mathrm{m}_i} \tag{2.1b}$$

where ω_i is electrical angular velocity, θ_i is the rotor angle, M_i is the moment of inertia of the rotor shaft, D_i is the damping coefficient, P_i is the generated electrical power and P_{m_i} the mechanical power.

SG units are equipped with a governor to regulate the machine speed and provide frequency support to the network. The turbine provides the mechanical power to the generator rotor while the governor adjusts the turbine valve position such that the generator output power changes based on the system frequency. Figure 2.3 represents a turbine-governor model [43] for a reheat turbine adopted for frequency response. Additionally, a Woodward diesel governor model [44, 45] sketched in Fig. 2.4 is used in this thesis. Parameters of the reheat turbine and DEGOV models are described in Table 2.4.

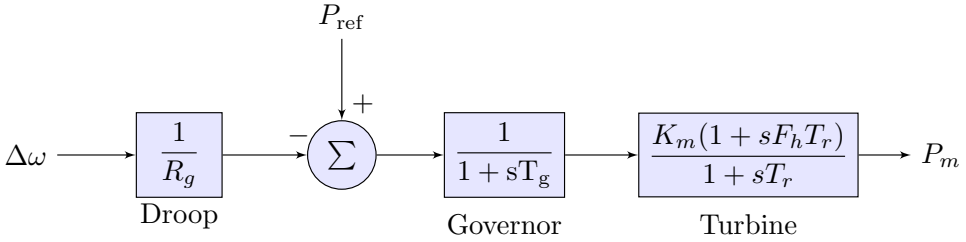

Figure 2.3: Block diagram of a reheat turbine governor model for a synchronous generator.

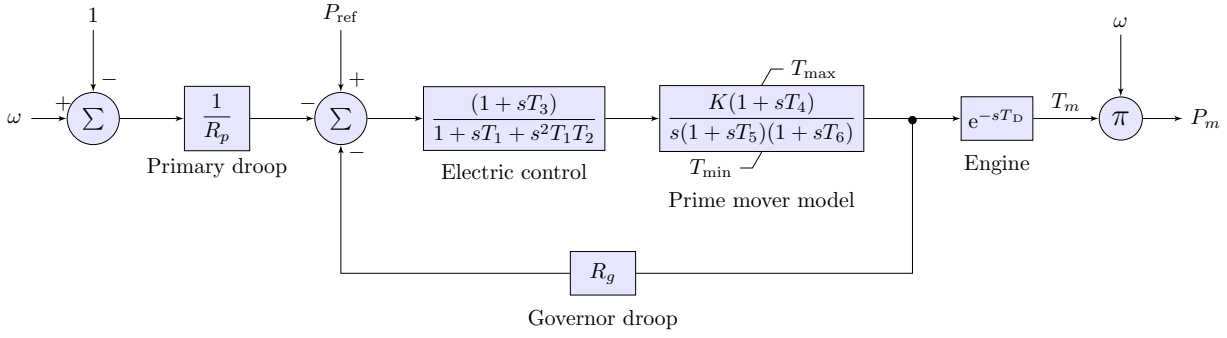

Figure 2.4: Modified diesel generator governor (DEGOV) model.

Table 2.4: Turbine-governor model parameters

Name	Unit	Description	Value
Reheat Turbine parameters			
R_g	p.u	Droop control gain	0.03
T_g	s	Governor time constant	0.5
K_m	p.u	Mechanical power gain factor	1
F_h	p.u	Fraction of the total power generated by the turbine	0.35
T_r	s	Reheat time constant	10
DEGOV Parameters			
T_1	s	Control box time constant	0.01
T_2	s	Control box time constant	0.02
T_3	s	Control box time constant	0.2
K	p.u	Actuator gain	18
T_4	s	Actuator time constant	0.25
T_5	s	Actuator time constant	0.009
T_6	s	Actuator time constant	0.0384
$T_{\min}$	p.u	Minimum actuator torque	0
$T_{\max}$	p.u	Maximum actuator torque	1.1
T_{D}	s	Engine firing delay time	0.024
R_g	p.u	Feedback gain (Droop)	0.04

2.3.3.2 Frequency Control in Converter-Interfaced Generators

The CIG units in the MG can be classified into either *grid-feeding* i.e., delivering only predefined active and reactive power to the network and providing no contribution to frequency and voltage control, or *grid-supporting* i.e., able to regulate frequency and/or voltage of the network by adjusting their active and reactive power injection to the network [46].

The type of support offered by a CIG will depend on the region of operation (see Fig. 2.1). During normal operation and post-transient operation regions i.e., PFC, SFC and TFC, smaller deviations exist between the measured frequency at the device terminal and the nominal frequency. Droop control [42], derived from traditional systems with SGs - where a reduction frequency results in an increase in the active power production and vice-versa can be applied. For the droop control at unit i, $P-\omega$ control loops are defined as follows:

$$\omega_i = \omega_i^* - K_p^{\mathrm{D}} \left(P_i^* - P_i\right) \tag{2.2}$$

where P_i and ω_i and V_i are the measured values of active power and angular speed, respectively, and superscript * is used to denote reference values that are provided at a system level. K_p^{D} is the proportional droop numerically defined by $K_p = \dfrac{\Delta\omega}{P_{max}}$.

The frequency droop in (2.2) provides frequency regulation to the MG during smaller frequency excursions but cannot provide dynamic support in case of large deviations. The lower inertia in CIGs results in faster RoCoF speeds and larger deviations in case of a major event which may lead to the activation of under/over-frequency protection if not appropriately arrested. This is very vital especially in the case of islanded operation. In order to mitigate such adverse effects, the CIG can be controlled to emulate the rotating inertia of a SG by adding a virtual inertia control loop to improve frequency response to system transients as well as stabilise the system.

Different control formulations for virtual inertia presented in literature are based on the replication of the synchronous machine model (synchronverters), droop control, and the swing equation [47–52]. A general formulation for virtual inertia thus takes the form:

$$P_i^* - P_i = K^{\mathrm{Dmp}}\left(\omega_i - \omega_i^*\right) + K^{\mathrm{VI}}\dot{\omega}_i \tag{2.3}$$

where the gains K^{Dmp} and K^{VI} have an equivalence to the damping coefficient and inertia constant respectively in the swing equation (2.1). The virtual inertia support will become operational given the RoCoF exceeds a defined minimum threshold. The parameters in (2.3) should be efficiently tuned to enhance the dynamic response of the system.

The overall frequency support provided by CIGs with *grid-supporting* capability is formulated in (2.4) and illustrated in Fig. 2.5.

$$P_{\mathrm{IR}}(t) = -K^{\mathrm{VI}}\dot{\omega}_i \tag{2.4a}$$

$$\Delta\omega(t) = \left(\omega_i^* - \omega_i\right) \tag{2.4b}$$

$$P_{\mathrm{PFC}}(t) = \begin{cases} K^{\mathrm{D_{UF}}}\Delta\omega(t), & \text{if } -\underline{\Delta}\omega \leq \Delta\omega(t) \\ 0, & \text{if } -\underline{\Delta}\omega_{\mathrm{db}} < \Delta\omega(t) < \overline{\Delta}\omega_{\mathrm{db}} \\ K^{\mathrm{D_{OF}}}\Delta\omega(t), & \text{if } \Delta\omega(t) \geq \overline{\Delta}\omega \end{cases} \tag{2.4c}$$

$$P(t) = P_{\mathrm{pre}} + P_{\mathrm{PFC}}(t) + P_{\mathrm{IR}}(t) = P_{\mathrm{pre}} + P_{\mathrm{DFS}}(t) \tag{2.4d}$$

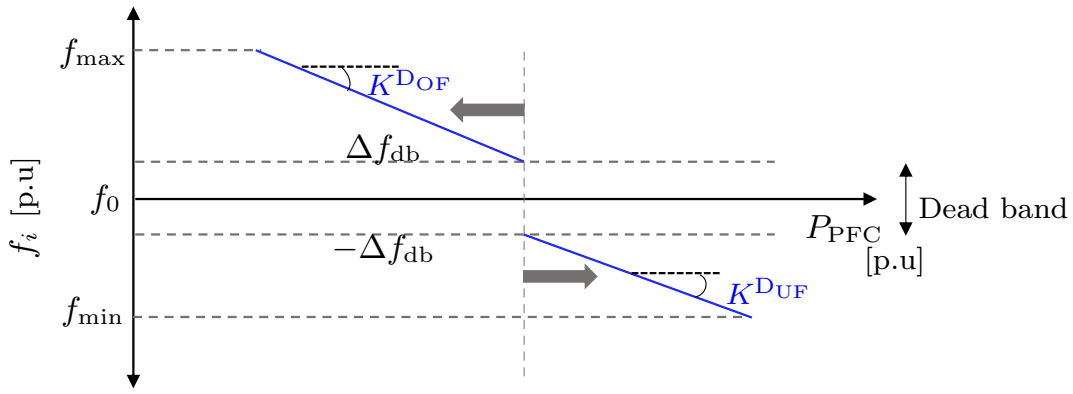

Figure 2.5: Active power support requirement during primary frequency response.

where $K^{\mathrm{D_{UF}}}$ and $K^{\mathrm{D_{OF}}}$ are droop parameters (see Fig. 2.5) applied during under-frequency and over-frequency operating conditions. Variable $P_{\mathrm{DFS}}(t)$ represents the Dynamic Frequency Support (DFS) provided by the CBG during the IR and PFC periods.

2.3.4 Voltage Support

Similar to the frequency support, voltage support from DERs in the MG will vary based on the region of operation indicated in Fig. 2.2. Standards and guidelines require DERs to contribute to the steady-state and post-fault quasi-steady state voltage support of the network. This is constrained by the relation of the required reactive power and the generated active power as illustrated by the P-Q capability diagram in Fig. 2.6 [53]. The different upper and lower limits to reactive power generated by the DERs are defined as:

- Triangular: Here reactive power generation is limited to the minimum power factor

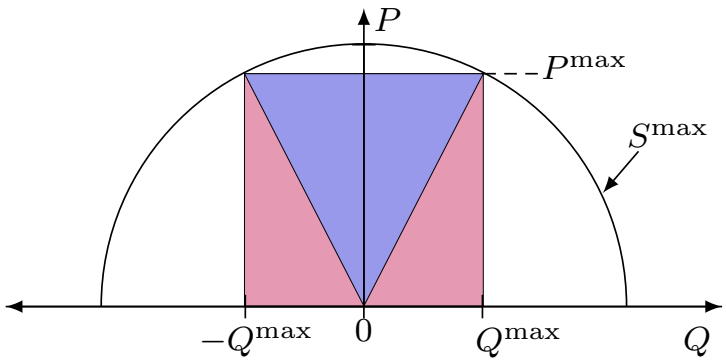

Figure 2.6: P-Q capability diagrams for steady-state voltage support

during operation based on the active power injection i.e.:

$$-\tan\phi_{\max} \cdot P \leq Q \leq \tan\phi_{\max} \cdot P \tag{2.5}$$

- Semicircular: No limitations are imposed on the power factor during operation and the DERs can fully utilise their nominal apparent power at all active power levels, this is defined by:

$$Q \leq \sqrt{(S^{\max})^2 - (P^{\max})^2} \tag{2.6}$$

- Rectangular: This standard is more flexible than the fixed reactive power requirement using the triangular limitation. It allows for reactive power generation at the maximum level, $Q^{\max}$ even at instances with low active power injection i.e.:

$$-\tan\phi_{\max} \cdot P^{\max} \leq Q \leq \tan\phi_{\max} \cdot P^{\max} \tag{2.7}$$

CIGs can be oversized to allow for reactive power support during instances of maximum active power production.

2.3.4.1 Voltage Control in Synchronous Generators

An exciter system fitted with an Automatic Voltage Regulator (AVR) is the primary voltage controller for SG units. The exciter can rapidly adjust the excitation levels i.e., field current of an SG unit such that terminal voltage is kept within specified limits during disturbances. SG units have adjusted over-/underexcitation capability to ensure momentary reactive power support during over/under voltage conditions. Figure. 2.7 illustrates a simple exciter and AVR system for voltage control in SG units. V is the

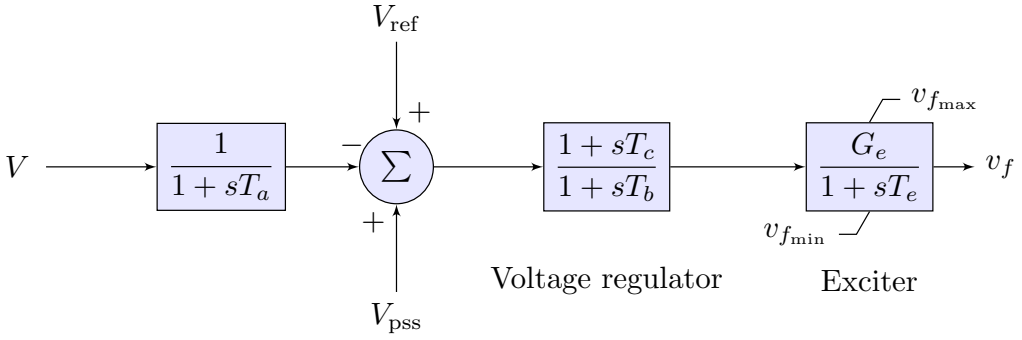

Figure 2.7: Block diagram of an exciter and AVR model of a synchronous generator.

terminal voltage of the generator, V_{ref} is its reference, v_f is the field voltage, while V_{pss} denotes the signal from the a Power System Stabiliser (PSS) if incorporated into the SG model. Parameter T_a is the filter time constant, T_b and T_c are voltage regulator time constants, G_e and T_e are exciter control gain and time constant respectively while $v_{f_{\max}}$ and $v_{f_{\min}}$ denote the exciter field voltage limits. In this work, we use the standard IEEE AC1A [54] exciter model to regulate the voltage in the SG units.

2.3.4.2 Dynamic Voltage Support in Converter-Interfaced Generators

Dynamic Voltage Support (DVS) is aimed at reinforcing the network voltage in the event of high levels of voltage dips or rise. DVS capability is composed of two stages i.e., first, DERs should not disconnect from the network given the voltage FRT requirements are not violated (see Fig. 2.2). Second, DERs should support the network voltage where possible by injecting or absorbing reactive current [38,39,55]. In LVRT and HVRT regions C and D in Fig. 2.2, additional reactive power support is required to arrest the deteriorating voltages.

In [56, 57], a voltage supporting strategy have been presented for CIG units. Therein, when voltage levels enter regions C and D (Fig. 2.2), priority is given to reactive power injection or absorption based on the strategy shown in Fig. 2.8. The DVS capability is achieved based on a discrete control strategy as:

$$Q_{\text{DVS}}(t) = \begin{cases} K^{\text{I}} \cdot i_{\text{Q,max}} \cdot (\underline{V}_{\text{pre}} - V(t)) & \text{if } V(t) < \underline{V}_{\text{pre}} \\ K^{\text{A}} \cdot i_{\text{Q,max}} \cdot (\overline{V}_{\text{pre}} - V(t)) & \text{if } V(t) > \overline{V}_{\text{pre}} \\ 0 & \text{otherwise} \end{cases} \tag{2.8a}$$

$$Q(t) = Q_{\text{pre}} + Q_{\text{DVS}}(t) \tag{2.8b}$$

where parameters K^{I} and K^{A} define the respective dynamic rate of change of reactive power injection and absorption with respect to a change in voltage.

The output of the CIG is limited by its rated current i_{nom}. During DVS, the unit prioritises reactive current injection to active current. It is however necessary that the nominal current limits are not exceeded. This is ensured by a limit updating current

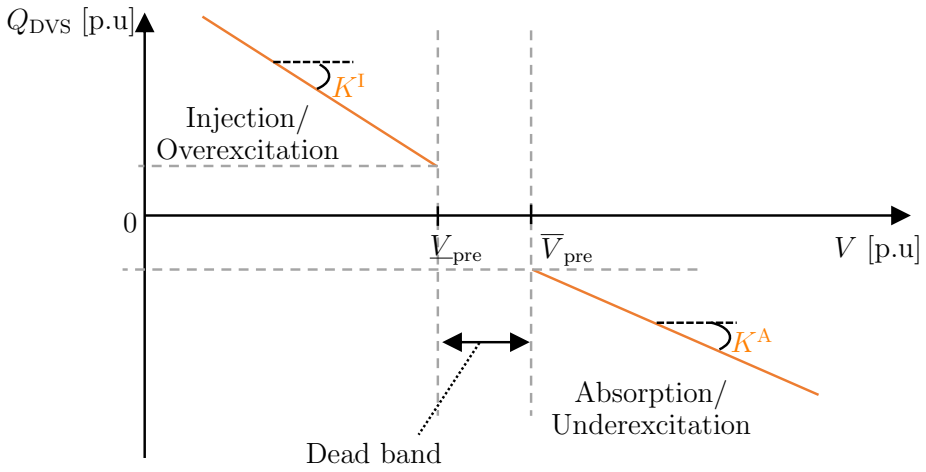

Figure 2.8: Voltage support regions during fault ride-through conditions

allocation logic described as:

$$\begin{aligned} i_{\text{P,max}} &= F_{\text{PQ}} i_{\text{nom}} + \left(1 - F_{\text{PQ}}\right) \sqrt{i_{\text{nom}}^2 - i_{\text{Q}}^2} \\ i_{\text{Q,max}} &= F_{\text{PQ}} \sqrt{i_{\text{nom}}^2 - i_{\text{P}}^2} + \left(1 - F_{\text{PQ}}\right) i_{\text{nom}} \end{aligned} \tag{2.9}$$

where binary flag (0/1) F_{PQ} is used to indicate whether active or reactive current injection has priority.

When voltage levels are within the normal voltage operating range, illustrated by the dead band region in Fig. 2.8 priority is given to active current and the variable F_{PQ} is set at one. The maximum value of reactive current in this case will depend on the active current reference i_{P} and set based on limitations defined in Fig. 2.6. When DVS capability is required fron the CIG i.e., voltages falling outside the normal ranges $\underline{V}_{\text{pre}} \leq V \leq \overline{V}_{\text{pre}}$ (see Fig. 2.8), the flag F_{PQ} is switched to zero. The priority is given to reactive current and the maximum active current will depend on the reactive current reference i_{Q} set based on (2.8).

The rate at which active power output is to be recovered to the pre-fault value is usually prescribed by the grid standards. A comparison for different jurisdictions is given in reference [58].

2.3.5 Converter Based Generator Model

A block diagram representing the different controls implemented for the CIG is shown in Fig. 2.9. It has been modified from [59] to include droop control and virtual inertia based on RoCoF measurements. The model is implemented in PyRAMSES [60] that adopts a

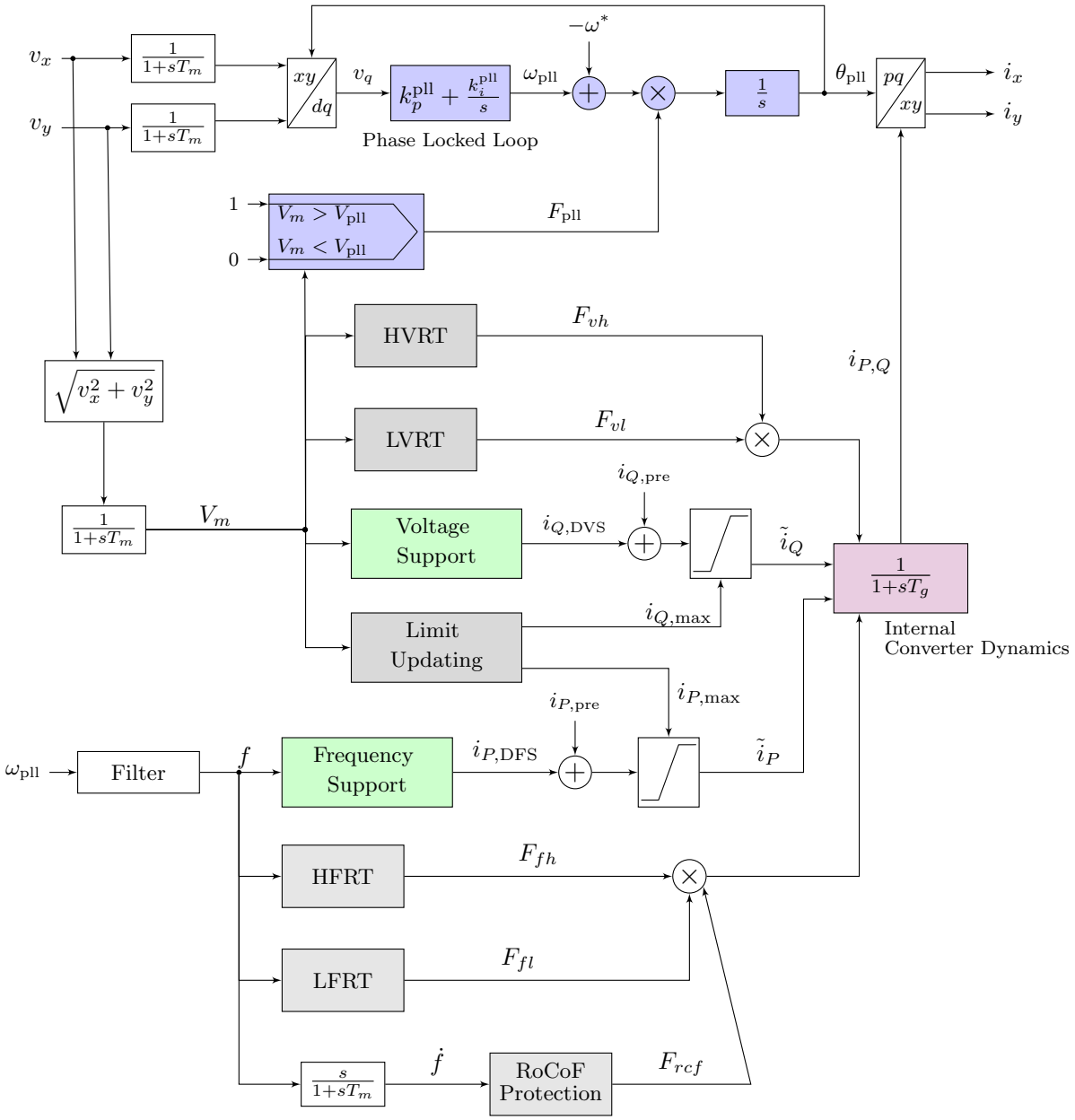

Figure 2.9: Converter Interfaced Generator model.

phasor approximation representing the network using algebraic equations.

The voltage and frequency controllers (green blocks) have been described in in Section 2.3.4.2 and Section 2.3.3.2, respectively. The ride-through conditions described in Fig. 2.2 and Fig. 2.1 are set in the HVRT, LVRT, HFRT and LFRT blocks. However, if the frequency or voltage is outside of the predefined operating range, the unit is tripped by activating the respective frequency or voltage flag to protect it from any damage. Voltage protections are set in the HVRT and LVRT blocks where the respective flags i.e., either F_{vh} or F_{vl} are set to zero if the measures voltage violates maximum or minimum voltages,

respectively.

$$F_{vh} = \begin{cases} 1 & \text{if } V_m < V_{\max} \\ 0 & \text{if } V_m > V_{\max} \end{cases} \tag{2.10}$$

$$F_{vl} = \begin{cases} 1 & \text{if } V_m > V_{\min} \\ 0 & \text{if } V_m < V_{\min} \end{cases} \tag{2.11}$$

Similarly, if frequency thresholds are violated frequency protections including HFRT, LFRT and RoCof protections are set using on flags F_{fh}, F_{fl} and F_{rcf}, respectively.

$$F_{fh} = \begin{cases} 1 & \text{if } f < f_{\max} \\ 0 & \text{if } f > f_{\max} \end{cases} \tag{2.12}$$

$$F_{fl} = \begin{cases} 1 & \text{if } f > \underline{f}_{\min} \\ 0 & \text{if } f < \overline{f}_{\min} \end{cases} \tag{2.13}$$

$$F_{rcf} = \begin{cases} 1 & \text{if } \underline{\dot{f}} < f < \overline{\dot{f}} \\ 0 & \text{otherwise} \end{cases} \tag{2.14}$$

Only the outer loop controls are considered in detail with inner converter current controls approximated and fast switching dynamics ignored [59]. The emphasis is to capture variations of injected current with the terminal voltage and frequency, assuming good tracking performance of the current control and neglecting the internal fast dynamics (pink block).

The Phase-Locked Loop (PLL) (blue block) sets the reference frame of the converter providing an estimate of the voltage angle θ. During instances of voltage drops below the threshold V_{pll}, the action of the PLL is temporarily suspended to prevent instability using the flag F_{pll}. Table 2.5 provides a description of the different parameters and variables presented in Fig. 2.9.

2.3.6 Operational Planning

Sections 2.3.3 and 2.3.4 presented device-level controls based on local measurements at the unit terminals. These operate independently reacting instantaneously to events in a pre-defined manner. Such controls if adopted by the generators in the MG can enhance system resilience during critical events. However, preventive measures can also

Table 2.5: CIG model parameters

Name	Unit	Description	Value
T_m	s	Measurement delay	0.02
T_g	s	Current controller time constant	0.01 - 0.03
V^{pll}	p.u	Voltage below which the PLL is frozen	0.5
$K_p^{\text{pll}}, K_i^{\text{pll}}$	p.u	PI control parameters	

be taken in the pre-disturbance state to enhance system preparedness in the event of a disturbance. Optimal generator scheduling can provide secure operational set points or reference points with the goal of ensuring system-wide adequacy and security as well as global controllability.

Operational planning is concerned with utilisation of the existing generation capacity and flexibility mechanisms in the best possible manner. This is achieved while ensuring that the network operates securely and optimally under different potential scenarios and loading conditions. The objective is to ensure power balance i.e., reliable operation that can accommodate sudden power imbalances with minimal security limits violations, as well as economical operation of the MG. Problems investigated during operational planning include Optimal Power Flow (OPF), Unit Commitment (UC) and Economic Dispatch (ED) of the available DERs. The set points determined during planning aid in the coordination of the power injections by the different local controllers.

Traditionally, security constrained OPF, UC or ED problems take into account operation given a set of *N-1* or *N-k* postulated *credible* contingencies based on a snap-shot of system operation have been utilised to analyse system security. The assumption taken is that the system will endure system transients with no violations and will reach steady-state in the post-disturbance operational state. The validity of this assumption is rather optimistic given that system transient performance is not usually modelled in the problem formulation. The situation can be further aggravated in the case of HILF events with large excursions. Such events are normally not accounted for during system planning. As a result solutions are sub-optimal and present an undetected risk of insecurity and system collapse. An extension to the system-wide planning approaches to support secure and resilient operation during HILF events is to include model transient-aware planning approaches that include security constraints applied to system trajectories in the transient state. This thesis presents different solution approaches that can adopted to enhance MG security and resilience during HILF events.

2.4 Conclusion

The survivability of a MG when in the event of high impact events such as those leading to unplanned MG islanding will depend on the available levels of support both at a device level and system level. By ensuring a secure operation during system disturbance, we enhance the MG survivability and resilience to critical disturbances in the network. In this chapter, the key aspects of system security have been presented. Furthermore, the grid requirements and guidelines to be adopted by systems with higher penetration of CIGs have been discussed. A description on the control structures adopted in this thesis for frequency and voltage support from CIG units have been presented. While these enhance the capability of the unit to survive critical events, system-wide control is vital to enhance network survivability.

The following chapters present formulations for transient-aware MG planning models with the objective of enhancing their security and resilience. Moreover aspects of uncertainty due to renewable units and loads, as well as model tractability due to the inherent nonlineriaties of power flow solutions are accounted for. More importantly the practical applicability and relevance to current challenges in MG operation is showcased.

Chapter 3

Power Flow Models in Active Distribution Networks

In the past, distribution grids were modelled as either passive elements or aggregated loads, due to their lack of participation in power, frequency and voltage control. This has however changed in recent years due to the major transformations in the design and operation of Low Voltage (LV) and Medium Voltage (MV) Distribution Networks (DNs). Changes include the proliferation of Distributed Energy Resources (DERs), mainly consisting of Renewable Energy Sources (RES), and the requirement for them to provide active support to the grid thus the term Active Distribution Network (ADN).

Optimisation-based investment and operation planning problems can be used to optimise the operation of ADNs, minimise costs and enhance system security. In order to incorporate security constraints stemming from the network, network-constrained formulations that allow for the inclusion of congestion limits, frequency limits, voltage limits, e.t.c. are employed. However, due to the non-linear nature of the network model, the tractability of network-constrained optimisation problems can be challenging. The redistribution of power flows during various events in the network can be modelled using various formulations including those based on complex network theory, electrical properties such as Kirchhoff's law or a combination of both [61]. The most common and accurate mathematical model used to introduce network constraints is the Alternating Current (AC) Power Flow-based (PF) model. At their core, different investment and operation planning problems for ADNs employ the Optimal Power Flow (OPF) problem, that includes the AC PF model to provide optimal solution subject to stipulated security constraints.

To tackle the model tractability, various reformulations based on approximations, linearisations, convexifications, e.t.c have been proposed in research. This chapter presents and compares five multi-period OPF formulations (including the basic non-linear and non-convex one), with different linearizations/convexifications for the AC PF equations. Different metrics are employed to analyse their accuracy and suitability in capturing the operational features of ADNs and Microgrids (MGs). The models are implemented on the IEEE 34-bus test system and their modeling accuracy and computational complexity are compared and discussed. The work in this chapter is presented in publication [C2].

3.1 Introduction

The energy management and decision making framework in MGs is majorly composed of three major stages i.e., network design and expansion planning (months - years), operational planning (monthly – near real-time) and real time control. The planning stages depend usually on large-scale optimisation problems solved repeatedly depending on the planning stage timescale. The decisions at each stage include:

- Expansion planning: where to build new power lines, technologies selection, capacity requirements and technology sizing, upgrades, installation of control devices e.t.c.
- Operational planning: generators to be committed, outage management, generator schedules, preventive and corrective control actions, interactions with energy markets, adjustment of control set-points e.t.c.
- Real-time control: Adjustment of control variables based on measured data to ensure the secure operation and stability of the system in real time.

During operational planning the aim is to optimally utilise the existing capacity while also ensuring that an electric power network operates securely and efficiently under different potential scenarios and loading conditions. The most fundamental problems solved at this stage include Unit Commitment (UC), energy resource scheduling and OPF [62]. The operational planning of a MG determines its interaction with the main grid, the decision to switch between grid-connected and islanded modes, and optimal allocation and operation of local resources while ensuring technical and operational constraints and load demand are satisfied [63]. Investment problems on the other hand are aimed at identification of the optimal type, capacity, and location of different generation, lines, and distribution technologies to meet the long term demand specifications.

Planning problems in MGs however present various challenges that render them in-

tractable i.e.:

1. The non-linear, non-convex nature of the power flow equations that describe the physical laws of the network. This results in a Non-deterministic Polynomial-time (NP) hard problem given the absence of an analytical solution to the power flow problem.

2. The uncertainties affecting the system operation making deterministic analyses inconclusive and inaccurate.

This chapter discusses potential solutions to the first challenge while the second challenge is handled and discussed in Chapters 4 and 5.

At the core of the different planning problems are the AC power flow equations of a network that ensure satisfaction of the physical laws governing system operation. Power flow solutions describes the operating state of the entire system, by calculating some quantities such as the complex voltage at each bus, line flows and power injections at each bus. The model consisting of the full AC power flow equations is however a non-convex and NP-hard problem. This has prompted researchers to propose approximations and relaxations of the power flow equations to ensure that globally optimal solutions are obtained. However, these have an inherent risk of not always obtaining physically meaningful solutions i.e solutions that are not practically applicable [64, 65]. Additionally, relaxations/approximations applicable to mesh networks at transmission level that present low resistance (R) and high reactance (X) i.e., low R/X ratio transmission networks, may not perform well in the high R/X ratio radial distribution networks which are further characterised by reverse power flows from DERs.

The optimisation problems defined in MGs are generally complex to solve due to the non-linearities described and as such different optimisation algorithms have been proposed to aid in finding optimal solutions. In this research, emphasis is on techniques that seek global optima. These can be classified into the heuristic-based and the numerical/mathematical convex optimisation methods. Meta-heuristic methods e.g. Genetic algorithms (GA), Particle swarm optimization, Parallel simulated annealing (PSA), and Tabu search, provide global solutions with minimal computational effort and have been widely adopted in research [66–68]. These methods, sometimes referred to as 'black-box' methods do not exploit system structure and are evaluated based on simulations, thus lacking guarantees on the quality of the solutions returned [69]. Unlike heuristic approaches, in mathematical programming methods, the upper and lower bounds of the solution can be qualitatively proved. In addition, these methods benefit from mature al-

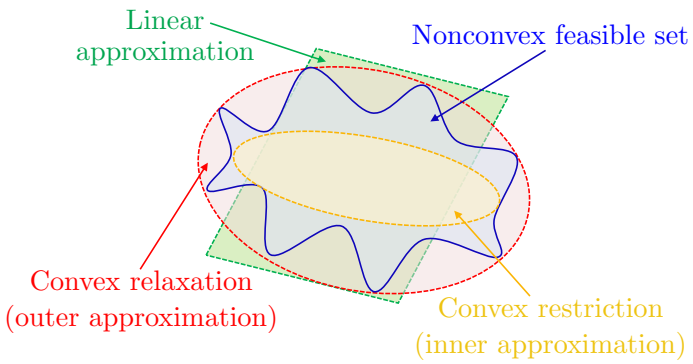

Figure 3.1: Illustration of a linear approximation (green area), convex relaxation (red area) and convex restriction (yellow area) for a non-convex space (blue area).

gorithms and different solvers that are continually being improved e.g. CPLEX, Gurobi, and MOSEK [70]. Mathematical programming approaches are used to solve operational and investment planning problems in this thesis can be classified as either approximations or relaxations based on their representation of the power flow equations. These approaches leverage available mathematical programming solvers e.g. linear, quadratic, second-order cone and semi-definite programming solvers in obtaining optimal solutions to a given problem.

The OPF problem at the core of the different planning problems aims at obtaining a feasible and optimal operating point that satisfies operational and physical constraints at the minimum cost. In finding a solution to the first challenge, models that ensure AC feasibility (i.e., exactness), global optimality, and computational efficiency are required.

In the past, different optimisation techniques with various linearisations, convexifications, and approximations have been proposed to obtain locally or globally optimal solutions of the OPF problem under specific assumptions [27]. Figure 3.1 illustrates the different approximations that can be applied to the non-convex solution space. In general, non-linear and non-convex techniques converge to locally optimal solutions with no guarantees of global optimality, while their optimal solutions exactly satisfy the original power flow equations. In contrast, convex relaxations provide a lower bound on the objective, yield a global optimum, can certify the existence of problem infeasibility, and tend to be tractable [27, 64, 71]. However, the solution obtained is not always physically meaningful and thus can be inapplicable practically [64, 65].

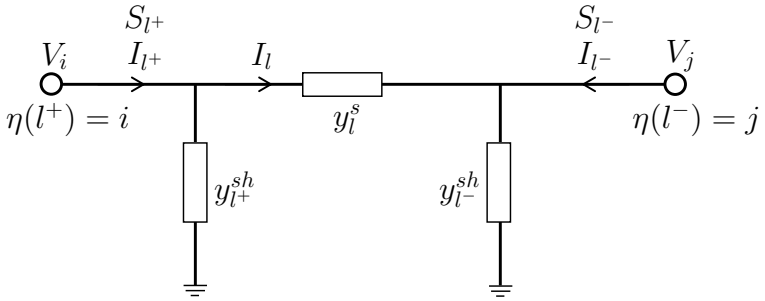

Figure 3.2: The Π model of the line and notation used in OPF formulation.

Contributions

The contributions of this chapter are as follows.
First, an analyssis and comparison of five different widely adopted OPF formulations for ADNs and MGs under different performance metrics. These include basic Non-Linear OPF [72], DistFlow (DF) [73, 74], Linearised DistFlow (LinDF) without line shunts [75], Extended DistFlow (ExDF) with line shunts [73], and Extended Augmented DistFlow (ExAgDF) including line shunts [74].

Secondly, the models are presented under a unified mathematical structure and their performance in practical situations analysed based on metrics defining the optimality gap, normalised distance to a local AC feasible solution and normalised constraint violation.

Finally, the computational performance of each model is evaluated in a multi-period optimisation problem with varying load and generation profiles. In this regard, the IEEE 34-bus test system is adopted to analyse their applicability for adoption in distribution networks.

The rest of the chapter is organised as follows. In Section 3.2, the mathematical formulations of the five AC OPF models mentioned above are presented. Section 3.3 presents the metrics used to compare the different formulations. In Section 3.4, the proposed OPF models are implemented on the IEEE 34-bus test system and their performances are evaluated and discussed. Finally, in Section 3.5, the main conclusions of the chapter are summarised.

3.2 Formulations of the Optimal Power Flow Problem

3.2.1 Notations

Let $\mathbf{j} = \sqrt{-1}$, $|\bullet|$ denote the magnitude, $\bullet^*$ complex conjugate while $\underline{\bullet}/\overline{\bullet}$ represent lower/upper bounds of the quantity $\bullet$. We assume a balanced radial balanced network represented by a connected graph $\mathcal{G}(\mathcal{N}, \mathcal{L})$, with $\mathcal{N} \coloneqq \{1, \ldots, N\}$ denoting the set of network nodes with index 1 defined as the Point of Common Coupling (PCC) to the transmission network. Set $\mathcal{L} \subseteq \mathcal{N} \times \mathcal{N}$ designates the set of network branches. The ADN hosts a number of generators and loads, where $\mathcal{G} \subseteq \mathcal{N}$ indicates the subset of nodes with DERs, and $\mathcal{D} \subseteq \mathcal{N}$ the subset of nodes with load demand.

The active and reactive power injections at each bus i are defined by $s_i = p_i + \mathbf{j}q_i$. The power injections are of the bulk grid import (export), DERs, and loads defined by: s^{imp} (s^{exp}), $s_g : g \in \mathcal{G}$ and $s_i^{\text{d}} \in \mathcal{D}$, respectively. Set $\mathcal{G}^i$ represents all generators connected to node i. The voltage at each bus is defined by $V_i = |V_i|\angle\theta_i$ with the square of voltage magnitude denoted by $v_i = |V_i|^2$. Bus voltage at the PCC node is fixed at $V_1 = 1\angle 0^\circ$ pu. Each branch $l \in \mathcal{L}$ is represented by a Π model (Fig. 3.2) with the sending and receiving ends denoted by l^+ and l^-, respectively, connected by two adjacent nodes $\eta(l^+) = i$ and $\eta(l^-) = j$. Set $\mathcal{L}^{\eta(l^+)}$ includes all lines connecting from downstream of a node/line in the *from* direction indexed by m, while $\mathcal{L}^{\eta(l^-)}$ includes all lines connecting from upstream in the *to* direction indexed by n. y_l^s is the series admittance given by $y_l^s = g_l + \mathbf{j}b_l = 1/(r_l + \mathbf{j}x_l) = 1/z_l$ while $y_{l^+}^{sh} = \mathbf{j}b_{l^+}^{sh}$ and $y_{l^-}^{sh} = \mathbf{j}b_{l^+}^{sh}$ are the shunt admittances at the sending and receiving ends, respectively ($y_{l^+}^{sh} = y_{l^-}^{sh} = \mathbf{j}b_l^{sh}/2$). The active and reactive power flows into the line at the sending (receiving) end are denoted by $S_{l^+} = P_{l^+} + \mathbf{j}Q_{l^+}$ ($S_{l^-} = P_{l^-} + \mathbf{j}Q_{l^-}$). $I_{l^+} = |I_{l^+}|\angle\vartheta_{l^+}$ ($I_{l^-} = |I_{l^-}|\angle\vartheta_{l^-}$) is the current flowing into the line from sending (receiving) nodes while I_l is the current in the longitudinal section. The square of current flow is denoted by $f_{l^+} = |I_{l^+}|^2$, $f_{l^-} = |I_{l^-}|^2$, and $f_l = |I_l|^2$ in each case. Each time step in the planning horizon T is indexed by $t \in \mathcal{T}$.

3.2.2 Non-Convex Extended AC Optimal Power Flow

The compact formulation of the AC OPF problem can be defined as:

$$\underset{\chi}{\textbf{minimize}} : \ \Theta(\chi) \tag{3.1a}$$

$$\textbf{subject to} : \ h_k(\chi) = 0, \ \ k = 1, \ldots, n, \tag{3.1b}$$

$$g_k(\chi) \leq 0, \;\; k = 1, \ldots, m \tag{3.1c}$$

The operational decision variables are represented by χ include power in-feed of different generators and power consumption in the network. The objective is defined in (3.1a), (3.1b) represents the AC power flow equations while the operational limits on the control variables are defined in (3.1c).

Depending on the goal of the optimisation problem, the objective (3.1a) can be aimed at minimising active and reactive power generation costs, minimising active power losses, minimising costs of power import from the grid and maximisation of profits in the case of exports, minimising load shedding penalties, e.t.c. For an investment planning problem, the objective will take the form of reduction of the total capital investment costs given the investment candidates that can include both generating units and transmission lines.

The objective function is defined by:

$$\Theta = \min_{\chi} \left(\sum_{t \in \mathcal{T}} \left(C^{\text{imp}} p_t^{\text{imp}} - C^{\text{exp}} p_t^{\text{exp}} \right) + \sum_{t \in \mathcal{T}} \sum_{g \in \mathcal{G}} C^{\text{g}} p_{gt} + \sum_{t \in \mathcal{T}} \sum_{l \in \mathcal{L}} C^{\text{loss}} p_{lt}^{\text{loss}} \right) \tag{3.2}$$

where χ defines the decision variables while $p^{\text{imp/exp}}$ denotes the active power import/export, p_g is the active power generation by the different units, and p^{loss} is the active power loss function. The objective is to minimise the respective costs incurred due to power import/export from/to the grid, unit power generation costs and the real power losses in the network.

3.2.2.1 Generic AC Power Flow Model

The representation of the power flow equations in (3.1b) at each node can vary based on the topology of the network i.e. radial or mesh network. The Branch Flow Model (BFM) considers the power network as a directed graph. This model formulates the power flow equations in terms of active and reactive power flows, squared current magnitude flows and squared voltage magnitude at each node as indicated in [76]. On the other hand the, Bus Injection Model (BIM) defines the network as an undirected graph. Therein, the power flow equations are given in terms of voltages, current injections, and power injection variables. The BFM is suited to a tree topology i.e. radial networks while the BIM is widely adapted to the meshed topology of transmission networks.

In **Model 1** the complex form of the non-linear AC OPF formulation is presented taking into account the line shunts. Equation (3.3a) enforces the power balance at each node in

Model 1 : Generic AC Optimal Power Flow [72]

$$s^{\mathrm{d}}_{it} - s^{\mathrm{imp}}_{t|i=1} + s^{\mathrm{exp}}_{t|i=1} - \sum_{g\in\mathcal{G}^i} s_{gt} = \sum_{\eta(l^+)=i} S_{l^+} + \sum_{\eta(l^-)=i} S_{l^-} \qquad \forall i,t \qquad (3.3a)$$

$$S_{l^+} = V_{\eta(l^+)t}(I_{l^+})^*, \qquad S_{l^-} = V_{\eta(l^-)t}(I_{l^-})^*, \qquad \forall l,t \qquad (3.3b)$$

$$I_{l^+} = y^s_l(V_{\eta(l^+)} - V_{\eta(l^-)}) + y^{sh}_l V_{\eta(l^+)}, \qquad \forall l,t \qquad (3.3c)$$

$$I_{l^-} = y^s_l(V_{\eta(l^-)} - V_{\eta(l^+)}) + y^{sh}_l V_{\eta(l^-)}, \qquad \forall l,t \qquad (3.3d)$$

the network while (3.3b)-(3.3d) define the active and reactive power flows at both ends of each line.

As a result of the non-linearity of the power flow equations in (3.3b), this non-convex model can only be solved through the adoption of Non-Linear Programming (NLP) techniques. Given that the model converges, the solution is locally optimal with no guarantees on global optimality.

3.2.2.2 Technical Constraints

The constraints (3.1c) applied to the planning model define the technical operating boundaries within which the problem is to be solved and can vary based on the aim of the optimisation problem. The constraints enforced in this study are defined as follows:

Constraints on transmission line loading limits

The thermal limits on the transmission lines can be imposed either by limiting the branch current magnitudes or the apparent power flow in the line. These are defined using a quadratic constraint as:

$$|S_{l^+}| \le \overline{S}_l \quad \text{or} \quad |I_{l^+}| \le \overline{I}_l, \qquad \forall l,t \qquad (3.4a)$$

$$|S_{l^-}| \le \overline{S}_l \quad \text{or} \quad |I_{l^-}| \le \overline{I}_l, \qquad \forall l,t \qquad (3.4b)$$

where $\overline{I}_l$ and $\overline{S}_l$ denote the maximum admissible line current and power loading, respectively, for branch l.

Constraints on the nodal voltage limits

The secure operating limits for steady state operation within the MG are defined in (3.4c), at the PCC i.e., node $\eta(l) = 1$, with the grid the voltage reference is set to the nominal

network voltage i.e, 1 p.u:

$$\underline{V} \leq |V_{\eta(l)t}| \leq \overline{V}, \qquad |V_{t|\eta(l)=1}| = 1, \quad \theta_{t|\eta(l)=1} = 0, \qquad \forall i, t \tag{3.4c}$$

Constraints on the power exchange with the grid

Thresholds on active and reactive power imported from and exported to the grid are applied by:

$$0 \leq p_t^{\text{imp}} \leq \overline{p}_t^{\text{imp}}, \qquad 0 \leq p_t^{\text{exp}} \leq \overline{p}_t^{\text{exp}}, \qquad \forall i, t \tag{3.4d}$$

$$0 \leq q_t^{\text{imp}} \leq \overline{q}_t^{\text{imp}}, \qquad 0 \leq q_t^{\text{exp}} \leq \overline{q}_t^{\text{exp}}, \qquad \forall i, t \tag{3.4e}$$

Constraints on the power generated by DERs

Generator operation should not violate the capacity limits on the active and reactive power of the unit, this is ensured by:

$$\underline{p}_{gt} \leq p_{gt} \leq \overline{p}_{gt}, \qquad \underline{q}_{gt} \leq q_{gt} \leq \overline{q}_{gt}, \qquad \forall g, t \tag{3.4f}$$

3.2.3 Convex Reformulations of the AC Power Flow Problem

Convex relations yield global optimal bounds to the original non-convex AC OPF. The exactness of the relaxation will depend on the tightness of the envelope and defined sufficient conditions thus providing a lower bound on the objective at the least. In practical applications, however, sufficient conditions may not always be entirely satisfied [77]. In this work, the focus is on formulations that adopt the BFM due to its desirable numerical characteristics in relation to radial networks [76], which generally characterise the configuration of ADNs.

At the core of the BFM relaxations based on Second-Order Cone Programming (SOCP), two relaxation steps are followed [76]:

i. Elimination of the voltage and current angles from Model 1. This is performed by the separation of the complex real and imaginary parts.

ii. Convexification of the non-convex hyperbolic constraint (3.3b), this is achieved by relaxing the equality using SOCP to an inequality.

3.2.3.1 Adapted DistFlow Relaxation

The DistFlow (DF) model [73, 74] is presented in **Model 2** where the AC power flows are described by constraints (3.5a)-(3.5e). Constraint (3.5d) defines the SOCP relaxation applied to the equality constraint (3.3b) in **Model 1** thus resulting in the convexification of the model. Model 2 can be used with either zero line shunts (hereinafter denoted as DF) i.e., line parameter $b_l^{sh} = 0$, or with non-zero line shunts (hereinafter denoted as $\text{DF}_{w/s}$) i.e., line parameter $b_l^{sh} > 0$. The sufficient conditions for the exactness of this model are defined in [77–79] for the case of zero line shunts and include:

- A load over-satisfaction assumption i.e., rather than have both fixed upper and lower limits on load demand, only upper limits are defined and no lower limits are ensured [27, 80]. This implies that active power injections at a node can increase beyond specified demands. This is especially unrealistic in case flexible loads and ZIP load models are utilised.
- In radial networks, reverse power flows should consist of either only active power or only reactive power or no reverse power should exist [78]. In ADNs with distributed generation, scenarios of reverse power flow consisting of both active and reactive power are imminent, especially during periods of high resource availability. This renders the technique inaccurate and inapplicable in such scenarios.
- Optimal power injections lie in a region where the upper bounds on voltage are non-binding [79].

3.2.3.2 Modified Lin-DistFlow Relaxation

A modified linear approximation of the DistFlow formulation in **Model 2**, defined as LinDistFlow, is presented in **Model 3**. Here, the power flow equations are defined as in (3.6a)-(3.6b) with the assumption that line losses indicated by the square of current flow are negligible in comparison with the active and reactive power flows (i.e., $f_{lt} << S_{tl} \ \therefore f_{lt} \simeq 0$) [75]. We apply the modification to the initial model in [75] to include line flow limits using constraints (3.6c)-(3.6f). Here, in order to maintain the linear nature of the problem, the quadratic line flow constraint (3.5d) is linearised using a convex polygon defined by inner approximations of the thermal loading circle [81, 82]. Thus, constraint (3.5d) is replaced by its piece-wise approximation as defined in (3.6c)-(3.6f) where parameter $a_d = \sqrt{2}-1$ is the derivative of the lines constructing the eight segments of the convex approximation. This model provides an upper bound on voltage and lower bound on power flows in the network [75].

Model 2 : Adapted DistFlow Relaxation ($\text{DF}_{w/s}$) [73, 74]

$$S_{tl^+} = s^{\text{d}}_{t\eta(l^-)} - s^{\text{imp}}_{t|\eta(l^-)=1} + s^{\text{exp}}_{t|\eta(l^-)=1} - \sum_{g\in\mathcal{G}^{\eta(l^-)}} s_{gt} + \sum_{m\in\mathcal{L}^{\eta(l^+)}} S_{tl^+_m} + z_l f_{lt} - \mathbf{j}(v_{\eta(l^+)t} + v_{\eta(l^-)t})\frac{b^{sh}_l}{2}, \quad \forall l,t \quad (3.5a)$$

$$S_{tl^+} = s^{\text{d}}_{t\eta(l^-)} - s^{\text{imp}}_{t|\eta(l^-)=1} + s^{\text{exp}}_{t|\eta(l^-)=1} - \sum_{g\in\mathcal{G}^{\eta(l^-)}} s_{gt} + \sum_{m\in\mathcal{L}^{\eta(l^+)}} S_{tl^+_m}, \quad \forall l,t \quad (3.5b)$$

$$v_{\eta(l^-)t} = v_{\eta(l^+)t} + |z_l|^2 f_{lt} - 2\,\text{Re}\left(z^*_l\left(S_{tl^+} + \mathbf{j}v_{\eta(l^+)t}\frac{b^{sh}_l}{2}\right)\right), \quad \forall l,t \quad (3.5c)$$

$$f_{lt} \geq \frac{|S_{tl^+} + \mathbf{j}v_{\eta(l^+)t}\frac{b^{sh}_l}{2}|^2}{v_{\eta(l^+)t}} \text{ or } \frac{|S_{tl^-} - \mathbf{j}v_{\eta(l^-)t}\frac{b^{sh}_l}{2}|^2}{v_{\eta(l^-)t}}, \quad \forall l,t \quad (3.5d)$$

$$\overline{f}_l v_{\eta(l^+)t} \geq |S_{tl^+}|^2, \quad \overline{f}_l v_{\eta(l^-)t} \geq |S_{tl^-}|^2, \quad \forall l,t \quad (3.5e)$$

$$|S_{tl^+}| \leq \overline{S}_l, \quad |S_{tl^-}| \leq \overline{S}_l, \quad \forall l,t \quad (3.5f)$$

$$\underline{v} \leq v_{\eta(l)t} \leq \overline{v}, \quad v_{t\eta(l)=1} = 1, \quad \forall l,t \quad (3.5g)$$

(3.4d) – (3.4f) (3.5h)

Model 3 : Modified Lin-DistFlow Relaxation (LinDF) [75]

$$S_{tl^+} + s_{t\eta(l^-)} = \sum_{m\in\mathcal{L}^{\eta(l^+)}} S_{tl^+_m}, \quad \forall l,t \quad (3.6a)$$

$$v_{\eta(l^-)t} = v_{\eta(l^+)t} - 2\left(r_l P_{tl^+} + x_l Q_{tl^+}\right), \quad \forall l,t \quad (3.6b)$$

$$-\overline{S}_l \leq P_{tl^+} + a_d Q_{tl^+} \leq \overline{S}_l, \quad \forall l,t \quad (3.6c)$$

$$-\overline{S}_l \leq P_{tl^+} - a_d Q_{tl^+} \leq \overline{S}_l, \quad \forall l,t \quad (3.6d)$$

$$-\overline{S}_l \leq a_d P_{tl^+} + Q_{tl^+} \leq \overline{S}_l, \quad \forall l,t \quad (3.6e)$$

$$-\overline{S}_l \leq a_d P_{tl^+} - Q_{tl^+} \leq \overline{S}_l, \quad \forall l,t \quad (3.6f)$$

(3.4c) – (3.4f) (3.6g)

3.2.3.3 Extended DistFlow Relaxation with Line Shunts

Model 4 presents a variant of the BFM relaxation for the AC power flows considering non-zero line shunts [73]. Unlike **Model 2** where current flow is only defined in the longitudinal section of the Π model in Fig. 3.2, the current and power flows here are defined at both ends of the line. This enhances the non-violation of the line ampacity limits in the physical network [72]. Here, (3.7a)-(3.7e) define the power flow equations while the line flows are constrained by (3.7f). Parameter α_{l^+} is defined as $\alpha_{l^+} = 1 +$

Model 4 : Extended DistFlow Relaxation with Line Shunts (ExDF) [73]

$$s_{it} = \sum_{\eta(l^+)=i} S_{l^+} + \sum_{\eta(l^-)=i} S_{l^-} \qquad \forall i,t \qquad (3.7a)$$

$$f_{tl^+} v_{t\eta(l^+)} \geq |S_{tl^+}|^2 \text{ or } f_{tl^-} v_{t\eta(l^-)} \geq |S_{tl^-}|^2, \qquad \forall l,t \qquad (3.7b)$$

$$|\alpha_{l^+}|^2 v_{t\eta(l^+)} - v_{t\eta(l^-)} = 2\,\mathrm{Re}(\alpha_{l^+} z_l^* S_{tl^+}) - |z_l|^2 f_{tl^+}, \qquad \forall l,t \qquad (3.7c)$$

$$|\alpha_{l^-}|^2 v_{t\eta(l^-)} - v_{t\eta(l^+)} = 2\,\mathrm{Re}(\alpha_{l^-} z_l^* S_{tl^-}) - |z_l|^2 f_{tl^-}, \qquad \forall l,t \qquad (3.7d)$$

$$\alpha_{l^+}^* v_{t\eta(l^+)} - z_l^* S_{tl^+} = \left(\alpha_{l^-}^* v_{t\eta(l^-)} - z_l^* S_{tl^-}\right)^*, \qquad \forall l,t \qquad (3.7e)$$

$$0 \leq f_{l^+} \leq (\overline{f}_l), \quad 0 \leq f_{l^-} \leq (\overline{f}_l), \qquad \forall l,t \qquad (3.7f)$$

$$\underline{v} \leq v_{\eta(l)t} \leq \overline{v}, \quad v_{t\eta(l)=1} = 1, \qquad \forall l,t \qquad (3.7g)$$

$$(3.4d) - (3.4f) \qquad (3.7h)$$

$z_l y_{l^+}^{sh}$. Similar to **Model 2**, constraint (3.7b) has been relaxed from an equality (3.3b) to inequality thus obtaining an SOCP relaxation of the non-convex power flow. Sufficient conditions for the exact SOCP relation of this model are detailed in [73] and include:

- There exist no lower bounds on active and reactive power injections i.e. load over-satisfaction.
- Parameter α_{l^+} is strictly positive. As shunt admittances are usually much smaller than the series admittances in practice, this generally holds.

3.2.3.4 Augmented DistFlow with Line Shunts

The formulation in **Model 5** enhances **Model 2** by adding a new set of constraints i.e. "augmentations", defined by (3.8c)-(3.8m) with conditions on its sufficient operation defined in [74]. The augmentations create inner approximations (restrictions) for the feasible space of the problem that ensure a tighter envelope for the original relaxation in **Model 2**. This is achieved by introducing auxiliary variables on the lines and node voltages that apply security constraints on these variables. In **Model 5**, auxiliary variables defined by superscripts $\hat{\bullet}/\check{\bullet}$ indicate the lower/upper bound on the associated variable. However, while the set of security constraints improves the feasibility of the model, it creates a larger set of optimisation variables that widens the solution space. Sufficient conditions for exactness of Model 5 include requirement for strictly increasing cost function for active power in the objective and various conditions on the network parameters defined in [74].

Model 5 : Augmented DistFlow with Line Shunts (ExAgDF) [74]

$$(3.5a) - (3.5e) \tag{3.8a}$$

$$(3.4d) - (3.4f) \tag{3.8b}$$

$$\hat{S}_{tl^+} + s_{t\eta(l^-)} = \sum_{m \in \mathcal{L}^{\eta(l^+)}} \hat{S}_{tl_m^+} - \mathbf{j}\left(\check{v}_{\eta(l^+)t} + \check{v}_{\eta(l^-)t}\right)\frac{b_l^{sh}}{2}, \qquad \forall l,t \tag{3.8c}$$

$$\hat{S}_{tl^-} + s_{t\eta(l^-)} = \sum_{m \in \mathcal{L}^{\eta(l^+)}} \hat{S}_{tl_m^+}, \qquad \forall l,t \tag{3.8d}$$

$$\check{v}_{\eta(l^-)t} = \check{v}_{\eta(l^+)t} - 2\,\mathrm{Re}\left(z_l^*\left(S_{tl^+} + \mathbf{j}\check{v}_{\eta(l^+)t}\frac{b_l^{sh}}{2}\right)\right), \qquad \forall l,t \tag{3.8e}$$

$$\check{S}_{tl^+} + s_{t\eta(l^-)} = \sum_{m \in \mathcal{L}^{\eta(l^+)}} \check{S}_{tl_m^+} + z_l\check{f}_{lt} - \mathbf{j}(v_{\eta(l^+)t} + v_{\eta(l^-)t})\frac{b_l^{sh}}{2}, \qquad \forall l,t \tag{3.8f}$$

$$\check{S}_{tl^-} + s_{t\eta(l^-)} = \sum_{m \in \mathcal{L}^{\eta(l^+)}} \check{S}_{tl_m^+}, \qquad \forall l,t \tag{3.8g}$$

$$\begin{aligned}\check{f}_l v_{\eta(l^+)t} \geq \max\left(\left|\hat{P}_{tl^+}\right|^2, \left|\check{P}_{tl^+}\right|^2\right) + \\ \max\left(\left|\hat{Q}_{tl^+} + \check{v}_{\eta(l^+)t}\frac{b_l^{sh}}{2}\right|^2, \left|\check{Q}_{tl^+} + v_{\eta(l^+)t}\frac{b_l^{sh}}{2}\right|^2\right),\end{aligned} \qquad \forall l,t \tag{3.8h}$$

$$\begin{aligned}\check{f}_l v_{\eta(l^-)t} \geq \max\left(\left|\hat{P}_{tl^-}\right|^2, \left|\check{P}_{tl^-}\right|^2\right) + \\ \max\left(\left|\hat{Q}_{tl^-} - \check{v}_{\eta(l^-)t}\frac{b_l^{sh}}{2}\right|^2, \left|\check{Q}_{tl^-} - v_{\eta(l^-)t}\frac{b_l^{sh}}{2}\right|^2\right),\end{aligned} \qquad \forall l,t \tag{3.8i}$$

$$\overline{f}_l v_{\eta(l^+)t} \geq \max\left(\left|\hat{P}_{tl^+}\right|^2, \left|\check{P}_{tl^+}\right|^2\right) + \max\left(\left|\hat{Q}_{tl^+}\right|^2, \left|\check{Q}_{tl^+}\right|^2\right), \qquad \forall l,t \tag{3.8j}$$

$$\overline{f}_l v_{\eta(l^-)t} \geq \max\left(\left|\hat{P}_{tl^-}\right|^2, \left|\check{P}_{tl^-}\right|^2\right) + \max\left(\left|\hat{Q}_{tl^-}\right|^2, \left|\check{Q}_{tl^-}\right|^2\right), \qquad \forall l,t \tag{3.8k}$$

$$\underline{v} \leq v_{it}, \qquad \check{v}_{\eta(l^-)t} \leq \overline{v}, \qquad v_{t|n=1} = 1, \qquad \forall l,t \tag{3.8l}$$

$$\hat{P}_{tl^+} \leq \check{P}_{tl^+} \leq \overline{P}_{l^+}, \qquad \hat{Q}_{tl^+} \leq \check{Q}_{tl^+} \leq \overline{Q}_{l^+}, \qquad \forall l,t \tag{3.8m}$$

3.3 Model Feasibility Assessment

A relaxed OPF model is "exact" if its optimal solution satisfies the original non-convex AC power flow equations. Each model is evaluated based on optimality, tractablity, and exactness of its solution to the OPF problem. The metrics used in assessment of a model performance therefore include the optimality gap, normalised deviation and constraint

violation as discussed below.

3.3.1 Optimality gap

This metric compares the quality of the optimal solution for approximated/relaxed models (Θ^{relax}) w.r.t the optimal solution of the basic non-convex NLP-based OPF model (Θ^{NLP}). It is defined as:

$$\text{OG}^{\text{relax}} = \left| \frac{\Theta^{\text{NLP}} - \Theta^{\text{relax}}}{\Theta^{\text{NLP}}} \right| \tag{3.9}$$

3.3.2 Average normalised deviation from NLP

This metric compares the divergence of the optimal value of decision variable $\chi_{\bullet}^{\text{relax}}$ obtained for the approximated/relaxed models w.r.t. the optimal solution $\chi_{\bullet}^{\text{NLP}}$ obtained from the NLP model. It provides an indication of the AC feasibility of the solutions of the approximations/relaxations for each of the variables and is defined as follows:

$$\delta_{\chi}^{\text{relax}} = \frac{1}{|\mathcal{T}| \cdot |\Omega|} \sum_{t \in \mathcal{T}} \sum_{n \in \Omega} \left| \frac{\chi_{nt}^{\text{NLP}} - \chi_{nt}^{\text{relax}}}{\chi_{nt}^{\text{NLP}}} \right| \tag{3.10}$$

The sets $\mathcal{T}$ and Ω are the corresponding sets where variable $\chi_{\bullet} \equiv \chi_{nt}$ lies.

3.3.3 Normalized constraint violation

The variables derived (χ_n^{LF}) are assessed for violation of the prescribed maximum and minimum limits as indicated in (3.11). The violation relates to the largest positive difference between a variable and their upper bound or lower bound. This metric tests the feasibility of the different relaxations against the engineering constraints for different operating conditions. It is defined as:

$$\text{CV}^{\text{relax}} = \max \left(\frac{\chi_{nt}^{\text{LF}} - \overline{\chi}_{nt}}{\overline{\chi}_{nt}}, \frac{\underline{\chi}_{nt} - \chi_{nt}^{\text{LF}}}{\underline{\chi}_{nt}}, 0 \right) \tag{3.11}$$

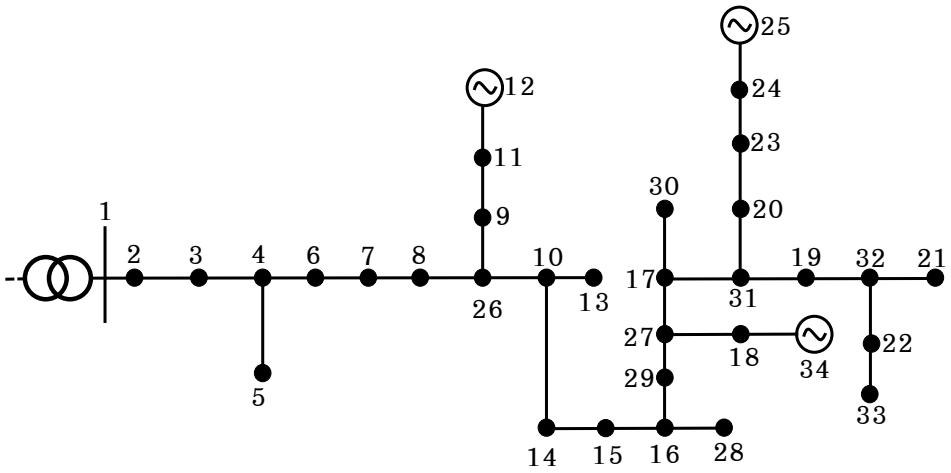

Figure 3.3: Modified IEEE 34 bus network

3.4 Case Study

3.4.1 System Setup

The aforementioned five OPF models are evaluated on a modified version of the IEEE 34-bus network [83] shown in Fig. 3.3. The original system in [83] is adjusted to a balanced three-phase network and includes three distributed Photo-Voltaic (PV) units at nodes 12, 25, 34. The parameters for the network are indicated in Appendix A.4, where all loads are modified as balanced three-phase ones and all transformers are modelled as lines with series resistance and inductance. The base values of apparent power and voltage magnitude are assumed to be 1 MVA and 24.9 kV, respectively. The load and PV generation profiles adopted from [84] in Texas during 2016 using an average single day 24-hour period. The optimization model was implemented in PYOMO [85] and GUROBI [86] was employed as the convex solver while IPOPT [87] was adopted for the NLP problem.

3.4.2 Optimality gap

In Fig. 3.4, the quality of the objective value based on the metric $\mathrm{OG}^{\mathbf{relax}}$ in (3.9) is presented. While a larger gap of over 10% is recorded in the models that do not consider shunt parameters (DF and LinDF), a near to zero gap is obtained in the case of the more accurate models (ExDF and ExAgDF). Although both the 25th and 75th percentiles of the LinDF are closer to AC optimality as compared to DF, this may not necessarily be an indication to AC feasibility of the solution. This will be highlighted in the the following section where the deviations of each of the variables to the local solution provided by the AC NLP model are analysed.

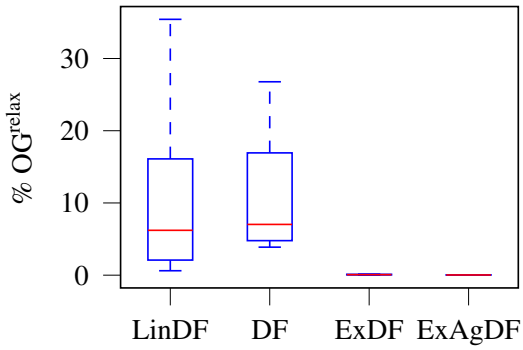

Figure 3.4: Optimality gap of each model w.r.t the total operational cost of the AC NLP solution.

3.4.3 Deviations from local optimality

Furthermore, we studied the solutions provided by each model using the metric defining deviations from the solutions offered by the NLP model, Model 1, defined in (3.10). Recall that the solution of Model 1 is always feasible but provides no guarantees on global optimality. The deviations in nodal voltages for the different models are indicated in Fig. 3.5. Average deviations are obtained at 0.52%, 0.57%, 0.005% and 0.003% for the LinDF, DF, ExDF and ExAgDF models, respectively, when compared to the solution in Model 1. The LinDF model marginally outperforms the DF model as its is known to provide an upper bound on voltage. This however is not the the case with regards to the line flow deviations presented in Fig. 3.6. It should be noted that as the LinDF model neglects line losses, it provides an optimistic solution for active power flow. The 75th percentile of the active power flow in the DF model is much lower than that of the LinDF model. The average deviations for active power line flows are obtained as 6.69%, 4.23%, 0.20% and 0.03% for the LinDF, DF, ExDF and ExAgDF models, respectively. However, as both models neglect the shunt parameters, both their reactive power flows are shown to have large discrepancies. The 75th percentile of the ExDF and ExAgDF models exhibit negligible deviations in both case. A similar trend is observed in Fig. 3.7 with regards to power injection deviations.

It is noteworthy to mention that ignoring the line charging of the shunt elements in the OPF formulation may result in significant deviations in the reactive powers of the network. Hence, in both Fig. 3.6 and Fig. 3.7, higher deviations in reactive power flows as compared to active power flows are obtained for the models neglecting line shunts (i.e., LinDF and DF). For reactive power injections, average deviations of 14.14%, 14.53%, 0.19% and 0.16% for the LinDF, DF, ExDF and ExAgDF models, respectively are obtained. The average deviations for different variables are summarised in Table 3.1. It should be

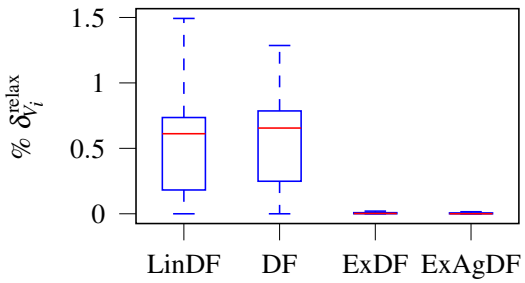

Figure 3.5: Voltage deviations of the different relaxations to the local solution of the NLP model.

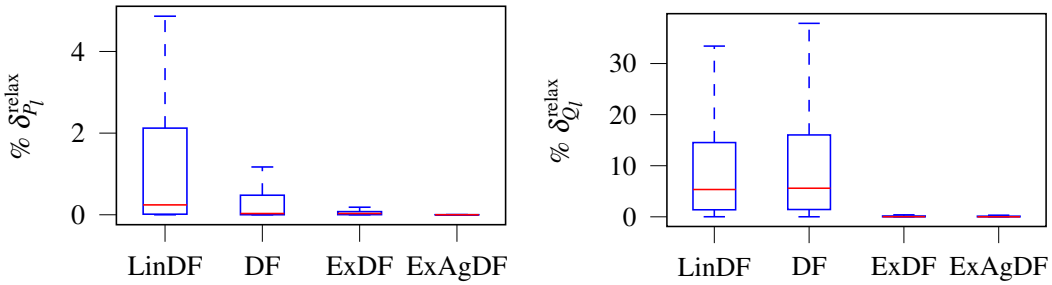

Figure 3.6: Power flow deviations of the different relaxations to the local solution of the NLP model.

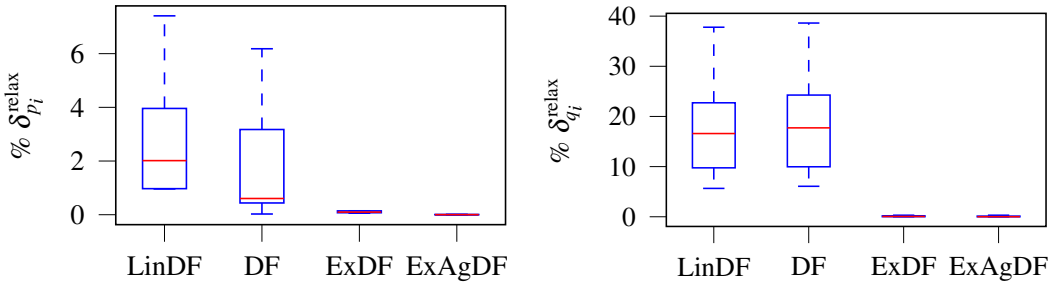

Figure 3.7: Power injection deviations of the different relaxations to the local solution of the NLP model.

emphasised that the inaccurate modelling of the lines can present major effects to the reactive power control of the network.

3.4.4 Constraint Violation

Convex relaxations using the SOCP have been applied to (3.3b) in the DF, ExDF and ExAgDF models to ensure global optimality as well as tractability of the NLP. This implies that for a model to be feasible i.e. physically meaningful, the relaxation should remain within the bound defined by the product of nodal voltage and line current flows shown in (3.5f) and (3.7b). Figure 3.8 presents the percentage normalised violation in each of the SOCP models. The tight restrictions defined for the ExDF model ensure that negligible violations exists implying that a physically meaningful solution can be

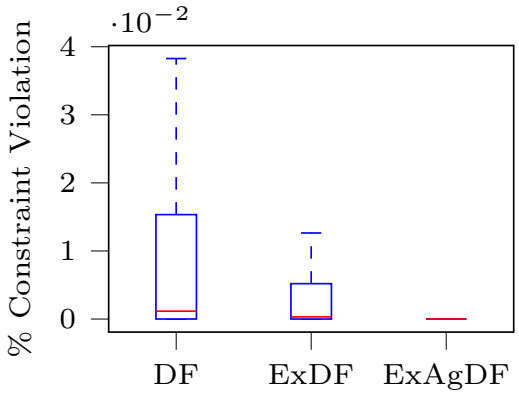

Figure 3.8: Violations in the hyperbolic SOCP constraint (3.3b) for the convex relations DF, ExDF and ExAgDF for all the lines and time periods.

obtained with a high percentage. Average percentage violations of 0.011%, 0.094% and 0.476% were obtained for the ExAgDF, ExDF and DF models, respectively.

In this study, all models indicated no constraint violation for the voltage and line thermal limits. The different approximations and relaxations were thus able to provide an AC feasible solution in each case. However, uncertainties and variations in operational conditions may lead to deviations from reported results.

3.4.5 Computational Performance

In Table 3.1, the operational costs and computational times of the different models are compared. The LinDF model as a linear approximation of the AC power flow indicated the fastest time and a low cost. Note however that this model provides an optimistic solution for the OPF problem. The ExAgDF provided the lowest optimal cost but the solution time in comparison with the other relaxations is relatively high. It is worthwhile to mention that the auxiliary variables used for the augmentations in this model aimed at ensuring AC feasibility and greater accuracy, result in a larger solution space that increases the computational time of the model. The NLP model guarantees AC feasibility but only provides a locally optimum solution. However, as detailed in Table 3.1, this model suffers from a large computational time in comparison with the approximated and relaxed models and can fail to converge in some instances. The choice between accuracy in network modelling and computation performance will thus dictate the end application of the model. For larger networks, the computational performance of the LinDF model can provide a faster solution at a cost of lower accuracy and optimality.

Table 3.1: Computation time, optimal cost and average variations of the different algorithms

	NLP	LinDF	DF	ExDF	ExAgDF
Computation Time [s]	727.34	0.18	2.04	2.86	171.52
Total Cost [$]	38133	39088	41155	38122	38080
% $\delta_{V_i}^{\text{relax}}$	-	0.52	0.57	0.005	0.003
% $\delta_{p_i}^{\text{relax}}$	-	7.54	3.19	0.24	0.03
% $\delta_{q_i}^{\text{relax}}$	-	23.60	23.65	0.33	0.31
% $\delta_{P_l}^{\text{relax}}$	-	6.69	4.23	0.20	0.03
% $\delta_{Q_l}^{\text{relax}}$	-	14.14	14.58	0.19	0.16

3.5 Conclusion

In this Chapter, the non-linear OPF model and five of its approximations and relaxations suited to ADNs and MGs have been presented. The OPF solution provides a fundamental result for network analysis and the different approximations are used in the rest of this thesis for the power flow and power balance models. A comparison is made between the different models based on the optimality gap, variable deviations from the NLP solution, and the constraints violation measures. The optimality gap while providing an indication of the quality of the objective value may not provide a detailed indication of the feasibility of a linearization or relaxation. Using average deviations of different OPF variables, the divergence of each variable from local optimality and an indication of the AC feasibility of the approximation/relaxation can be obtained. The normalised constraint violation metric further ensures the practical applicability of a model by testing it against physical technical limits. The effect of accurate network modeling to the OPF solution is further investigated by analysing the results of approximations and relaxations with/without line shunts. The results of approximated/relaxed models highlight significant effects of ignoring shunt elements to reactive power control. Finally, the computational performance of each model is analysed to evaluate its scalability for the larger networks.

Accurate modeling of the network is vital in ensuring that power flows, voltages, and generation states are correctly captured during system operation. This ensures that any existing security violations that exist during the steady-state operation are observed in time and mitigation processes are put in place to ensure secure operation. In MGs, the operator is always presented with the choice and compromise between techniques that offer practical AC feasibility and those that present computational efficiency. Moreover, there is an added complexity due to the intermittency of renewable energy units and

loads. In the next Chapters, 4 and 5, the OPF problem is enhanced to handle uncertain variations in the network using stochastic and robust reformulations to ensure holistic modeling of the network.

Part II

Steady-State Security and Uncertainty Handling

Chapter 4

A Stochastic Investment Planning Model for Designing Sustainable Island Microgrids

In practice, Microgrids (MGs) have traditionally been operated by fossil-fueled producers with competitive total investment/operation costs in comparison with renewable producers. However, Renewable Energy Resources (RES) are currently a high-priority option for designing and creating MGs due to serious concerns about global warming and climate change in addition to rapid evolution of sustainable energy resources with reasonable investment and operation costs [88]. However, these sources add to the uncertainty in power system operation due to their intermittent nature. This is in addition to the variations present in load consumption during real-time operation. Therefore, during the optimal design and operation of MG systems, the handling of the different uncertainties is key to the secure and resilient operation. In this chapter, a two-stage stochastic approach is employed to deal the uncertain generation from RES and load demand in MGs. The variations in load demands and solar/wind power productions are captured using three types of scenarios i.e. risk-seeker (best), risk-neutral (nominal), and risk-averse (worst) representative days, generated by the agglomerative hierarchical clustering technique. Additionally, to enhance computational tractability, Model 2 i.e., DF model as presented in Chapter 3 is adopted. The performance of the proposed Mixed-Integer Second-Order Cone Programming (MISOCP) formulation is tested on a real MG network on Alderney Island (the third largest of the Channel Islands) to design a sustainable network through

optimal investment in battery, solar, and wind units. The work in this chapter is partially presented in publication [C5].

4.1 Dealing with Uncertainty in Microgrid Planning

Technically, the variations in load profiles and generation output especially for renewable energy sources as well as large variations in power injections caused by contingencies affect the optimal planning of the network. The deregulation of the power network in different localities has also brought about uncertainties due to price volatility in the energy markets and flexibility of the demand consumption.

The system state x_{t+1} at a future time period can be defined as:

$$x_{t+1} = f(x_t, \tilde{u}_t) \tag{4.1}$$

where u_t represents the exogenous disturbance process making the trajectory of the system uncertain i.e. the uncontrollable or random parameters. In decision making under uncertainty in power systems, the state x_t denotes to the decision variable that can represent a control variable, operation variable or design variable. The goal of the decision making process is to determine the optimal decision variable that will minimise a defined cost function given the realisation of the uncertain parameters. Generally, the approaches that have been adopted in power systems to deal with uncertainty can be characterised into: Stochastic Optimisation (SO), Robust Optimisation (RO) and Distributionally Robust Optimisation (DRO) techniques [71]. Their characteristic features and general model formulations are discussed below.

4.1.1 Stochastic Optimisation

SO assumes that complete knowledge of the probability distribution of the uncertain parameters exists. The SO model is defined as:

$$\min_{\boldsymbol{x}\in\chi} \left(\mathbb{E}_{\mathbb{P}} \left\{ h\big(\boldsymbol{x}, \tilde{\boldsymbol{u}}\big) \right\} \right) \tag{4.2}$$

where $\boldsymbol{x}$ is a vector of decision variables, χ is the feasible set of the decision variables, $\mathbb{P}$ is the probability distribution of the uncertain parameters and h is the cost function. The objective in SO minimises the expected-value $\mathbb{E}$ of the cost over all scenarios of the uncertain parameters in the probability distribution space. The probability distribution is normally inferred from historical data or expert opinions. In cases where a known

probability distribution function of the uncertain parameters does not exist, an empirical distribution function can be built from Monte Carlo simulations [89]. It is evident that this approach requires large amounts of data to model the different operational scenarios and this can result in computational problems.

4.1.2 Robust Optimisation

Unlike SO that considers finite sets of pre-selected scenarios of the uncertain parameters or injections, the uncertainty in RO is modelled using a compact deterministic uncertainty set ($\mathcal{D}$) that takes into account all future uncertainties. The uncertainty set is constructed assuming no distributional knowledge about the underlying uncertainty, except for its support e.g. mean and/or co-variance. RO aims at finding decision variables that maximises the uncertainty for the minimum possible objective function value i.e., minimise the worst-case scenario [90–92]. In so doing the approach immunises against all realisations of uncertain data within the uncertainty set, minimising the worst-case cost. The RO model is defined as:

$$\min_{\boldsymbol{x}\in\chi} \left(\max_{\tilde{\boldsymbol{u}}\in\mathcal{V}} \left\{ h\big(\boldsymbol{x}, \tilde{\boldsymbol{u}}\big) \right\} \right) \tag{4.3}$$

where $\mathcal{V}$ denotes the uncertainty set of the random parameters $\tilde{u}$. A solution to (4.3) is feasible iff it satisfies all constraints for all possible realisations of the uncertain parameters in $\mathcal{V}$. The uncertainty set can take the form of bound intervals, polytopes and other convex sets.

The benefits presented by RO include its requirement of only moderate information about the uncertainty e.g. mean, range of uncertainty, but yet it includes the flexibility to incorporate more probabilistic information as and when it is available. However, RO suffers from "conservativeness", an attribute that renders it imperative to the analysis of HILP events but can result in instances of impracticability. The conservatism of RO can be controlled by a flexible design of the uncertainty set and the proper choice of the optimisation structure for example a static one-stage formulation versus a multi-stage formulation [71, 93]. In one-stage strategies, all decisions are made at once and it is not possible to adjust the the solution before the result of the uncertain process is known. In two/multi-stage approaches, similar in concept to the separable problems, it is possible to observe and adjust the plan before the final outcome i.e the goal is to minimise the cost of the first stage decision in addition to an overall/average cost of the second stage decisions which are based on the different scenarios to which the problem is applied.

4.1.3 Distributionally Robust Optimisation

On a practical level, it is almost impossible to obtain a distinct Probability Distribution Function (PDF) about a given uncertain parameter to be used in the stochastic model. The DRO approach assumes that the underlying PDF of the uncertain parameters is unknown but belongs to an ambiguity set of probability distributions that are close to the true distribution [94]. The parameters of the ambiguity set are specified based on available distribution information in terms of empirical mean, variances, co-variances, distance from a known distribution etc., hence the solution is robust against the inaccuracies in the probability data. The DRO model is defined as:

$$\min_{\boldsymbol{x}\in\chi}\left(\max_{\mathbb{P}\in\mathcal{U}}\left(\mathbb{E}_{\mathbb{P}}\left\{h\big(\boldsymbol{x},\tilde{\boldsymbol{u}}\big)\right\}\right)\right) \tag{4.4}$$

where $\mathcal{U}$ defines the ambiguity set of PDFs. The DRO approach minimises the the worst-case expected cost over a family of possible PDFs characterising the uncertain parameters in the ambiguity set instead of assuming a single probability distribution function [95, 96]. If compared with the uncertainty set used in RO, an ambiguity set is a set of probability distributions (measures) while uncertainty set is a set of possible realisations of the random variable. Moreover, DRO considers the worst-case distribution in the ambiguity set while RO considers the worst-case realisation in the uncertainty set. DRO therefore provides an intermediate solution between RO and SO and therefore can provide a more practical solution that is less dependant on available data and less conservative.

The choice of uncertainty handling approach to adopt in MG planning problems can depend on the planning horizon i.e., long-term for investment problems to short-term for operation problems, size of the network i.e., small scale MG to large-scale MG and the optimisation goal e.g., resilient operation, secure operation, unit commitment, economic dispatch e.t.c. The tractability of the final optimisation problem will depend both on the uncertainty handling approach and level of detail included in the problem. In the following, a MG investment and operational planning problem considering the uncertainties in the load demand and renewable generation are presented.

The rest of the chapter is organised as follows: Section 4.2 outlines the modelling preliminaries adopted throughout this chapter. Section 4.3 presents the proposed stochastic modelling approach to MG design, the approach is applied to the study of the Alderney Island electricity network in Section 4.4. Finally, conclusions are drawn in Section 4.5.

4.2 Related Works and Contributions

Related Works

Various non-deterministic optimisation models have been introduced in the literature for MG investment planning including SO [97–102] and RO [103–110]. In reference [103], a robust technique that decomposes the problem into investment planning in the master problem and an optimality checking operational planning sub-problem is proposed to handle the different uncertainties in the network. A tri-level decomposition algorithm using both primal and dual cutting planes is proposed in [105] for an active distribution expansion planning problem. A robust approach transformed into a single-level model by duality gap theory is proposed in [111] for robust MG design under severe uncertainty. A scenario-based deterministic iterative algorithm is presented in [98] to ensure the reliability of the network in a joint expansion planning of distribution network assets and generation. Furthermore, the stochastic approach in [100] uses a Monte Carlo stochastic programming-based approach for optimal sizing of MGs with wind and battery energy systems. While a meta-heuristic optimisation approach has been presented in [112] for efficient planning considering both AC and DC microgrids in remote isolated communities using virtual scenarios generated from Monte Carlo. In [113] particle swarm optimisation and genetic algorithm-based optimisation techniques are proposed for optimal sizing and siting of distributed generation resources in an existing distribution network to convert it into sustainable autonomous MG. The approach in [102] solves the stochastic model proposed for optimal investment in distribution networks under different disastrous events characterised by a set of scenarios, with Bender's Decomposition coupled with heuristic approaches. A scenario-based stochastic programming framework is proposed to model the correlated uncertainty using probability trees to represent the dynamics of the random parameters and the non-anticipativity of the decisions in [99]. The approach in [114] proposes a *Markovitz* i.e., mean-variance objective function to minimise the risk in the operation of the MG with an SO model formulated as a two-stage model.

However, the stochastic MG planning frameworks reported in the aforementioned literature do not present guarantees on the robustness of the scenarios incorporated into the problem i.e., risk-neutral scenarios considering mean values are utilised. Moreover, the use of multi-level frameworks increases the complexity of the solution approaches. As well, the large data requirement can result in intractability in large systems. On the other hand the over-conservatism in RO-based approaches can result in unaffordable MG designs, particularly in areas with lack of sufficient financial budgets. Additionally, incor-

porating the basic non-linear and non-convex AC power flow equations into the proposed model further complicates the problem.

Contributions

In this Chapter, a stochastic model is formulated with data based on previous historical realisations. A clustering technique is adopted to reduce the data requirement of the model creating representative days. Furthermore, to improve guarantees on reliability and robustness of the solution, decision-making under risk seeker and risk averse scenarios at each representative day are analysed. Furthermore, as discussed in Chapter 3, directly incorporating the basic non-linear and non-convex AC power flow equations into the proposed model may result in intractability. Accordingly, a second-order cone convexification of the AC power flow equations is employed to obtain a tractable optimisation model as a Mixed-Integer Second-Order Cone Programming (MISOCP) problem. The contributions in this chapter are threefold.

- First, the uncertainties of correlated load demands and solar/wind power productions are characterised with risk-seeker (best), risk-neutral (nominal), and risk-averse (worst) representative days generated by the agglomerative hierarchical clustering.
- Secondly, a two-stage stochastic investment planning model is proposed, formulated as an MISOCP optimisation problem.
- The stochastic formulation is applied for optimal investment into battery, solar, and wind units under the uncertainty of load demands and solar/wind power productions for a real network for Alderney Island.

4.3 Formulation of Stochastic Planning Model

4.3.1 Modelling Preliminaries

Throughout this chapter, bold letters are used to indicate vectors while entries of vectors are denoted by regular letters. The MG is considered to be a radial balanced network represented by a connected graph $\mathcal{G}(\mathcal{N}, \mathcal{L})$, with $\mathcal{N} \coloneqq \{0, 1, \ldots, N\}$ denoting the set of network nodes including the substation node 0, and $\mathcal{L} \subseteq \mathcal{N} \times \mathcal{N}$ designating the set of network branches. A distribution network hosts a number of Distributed Energy Resources (DERs) and loads, where $\mathcal{S} \subseteq \mathcal{N}$ indicates the subset of nodes with conventional generators, $\mathcal{R} \subseteq \mathcal{N}$ the subset of nodes with Renewable Energy Sources (RESs), $\mathcal{B} \subseteq \mathcal{N}$ the subset of nodes with Battery Energy Storage Sources (BESSs), $\mathcal{D} \subseteq \mathcal{N}$ the subset of

nodes with load demand.The set of nodes with DERs is thus obtained by the following set union $\mathcal{M} \coloneqq \mathcal{S} \cup \mathcal{R} \cup \mathcal{B}$. The set of respective units at node $i \in \mathcal{N}$ are given by $\mathcal{S}^i \subseteq \mathcal{S}$, $\mathcal{R}^i \subseteq \mathcal{R}$, $\mathcal{B}^i \subseteq \mathcal{B}$, and $\mathcal{D}^i \subseteq \mathcal{D}$. Cardinallity of the previously defined sets is denoted by: $n_d \coloneqq |\mathcal{D}|$, $n_s \coloneqq |\mathcal{S}|$, $n_b \coloneqq |\mathcal{B}|$, $n_l \coloneqq |\mathcal{L}|$, $n_c \coloneqq |\mathcal{C}|$, $n_r \coloneqq |\mathcal{R}|$.

For each DER $g \in \mathcal{S} \cup \mathcal{R} \cup \mathcal{B}$, variables p_{gto} and q_{gto} represent active and reactive power injections at time period $t \in \mathcal{T}$ and operating condition i.e., representative day $o \in \mathcal{O}$; and, the upper/lower limits are represented by -/_. The active and reactive power flows in each line $l \in \mathcal{L}$ are defined as P_l and Q_l respectively with l^{i^+} and l^{i^-} denoting the upstream and downstream lines connected to node $i \in \mathcal{N}$. Moreover, the square of current magnitude flowing through a line is denoted by f_l.

4.3.2 A Data Clustering Technique

In investment planning, it can be assumed that the patterns of load demands and RES power productions remain unchanged during a one-year period. Due to tractability issues, it may not be practical to consider the entire yearly patterns of uncertain load demands and RES power productions in the model. Accordingly, the model considers a sufficient number of representative daily patterns (i.e., representative days) instead of the yearly patterns for correlated load demands and RES power productions through appropriate data clustering techniques to characterise their increasing/decreasing variations during the planning horizon proficiently.

In general, data clustering techniques offer a means for grouping patterns exhibiting consistent behaviour, and thus, allowing for a reduced number of scenarios to be utilised instead of the entire input data-set. Different clustering techniques fall into two common groups, i.e., hierarchical and partitional algorithms [115]. In this chapter, the Agglomerative Hierarchical Clustering (AHC) technique [115, 116] is adopted to generate risk-seeker (best), risk-neutral (nominal), and risk-averse (worst) scenarios (i.e., representative days) characterising the uncertainty of correlated load demands and RES power productions during the entire planning horizon. This technique merges data based on a proximity (similarity) measure using a bottom-up approach, i.e., aggregating from individual points to the most high-level cluster [116]. In this case, the data clustering procedure groups daily patterns consisting of 72 distinct entries corresponding to the 24 hourly values each of normalised load demand, solar power production, and wind power production for all 365 days. In other words, the input data-set is a (365×72)-dimensional matrix wherein each row of the matrix pertains to daily profiles of load demands, solar power productions, and wind power productions during a specific day of the planning

horizon. All data is normalised using the system base power thus taking on values between '0' and '1'. In summary, the AHC algorithm takes the following major steps:

1. Calculate the proximity matrix for the initial clusters consisting of each daily pattern of load demands, solar power productions, and wind power productions as a separate cluster,
2. Merge the pair of nodes with the smallest distance in the proximity matrix into one unique cluster,
3. Update the proximity matrix to reflect the merge operation of Step 2 by calculating the distances between the new cluster and the other clusters,
4. Repeat Step 2 and Step 3 until a single cluster remains or a pre-defined number of clusters is reached,
5. Report the representative days for the obtained clusters.

In this study, the euclidean distance is used as a proximity measure to merge clusters at each iteration [115, 116]. Unlike the partitional clustering algorithms, e.g., k-means clustering technique, the hierarchical clustering algorithm do not require a predefined number of clusters as an input parameter and provide a deterministic approach where the same hierarchy is always obtained for the same input data-set. Additionally, data structures created by the AHC hierarchies are more informative than the unstructured clusters resulting from partitional clustering.

After clustering all historical observations, the model incorporates the best (risk-seeker), nominal (risk-neutral), and worst (risk-averse) representative days [117] for each data cluster. The α-quantile of the empirical cumulative probability distribution of each cluster represent the best representative day, while the $(1 - \alpha)$-quantile of the empirical cumulative probability distribution of each cluster represent the worst representative day. Without loss of generality, it is assumed that $\alpha = 0.01$. Moreover, the nominal representative day is similar to $\alpha = 0.50$.

4.3.3 Problem Model Formulation

This section presents the mathematical formulation of the investment and operational planning mode. A single-year planning horizon under a specific number of scenarios, i.e., representative days, is considered to ensure a compromise between accuracy and computational tractability of the model. Each representative day is described by distinct

patterns for load demands and RES power generations. In the following, a description of the objective and technical constraints considered is presented.

In the proposed model, the first-stage investment variables are *here-and-now* decisions and not a function of uncertain parameters, while the second-stage operation variables are *wait-and-see* and a function of uncertain parameters.

4.3.3.1 Objective Function

The objective function (4.5a) simultaneously minimises the total investment ($\mathbf{\Theta}^{\text{inv}}$) and total operational ($\mathbf{\Theta}^{\text{opr}}$) costs. It is defined as:

$$\min \left(\mathbf{\Theta}^{\text{inv}} + \mathbf{\Theta}^{\text{opr}} \right) \tag{4.5a}$$

$$\mathbf{\Theta}^{\text{inv}} = \sum_{b \in \mathcal{B}} (ic_b \cdot z_b) + \sum_{g \in \mathcal{R}} (ic_g \cdot z_g) \tag{4.5b}$$

$$\begin{aligned} \mathbf{\Theta}^{\text{opr}} = & \sum_{o \in \mathcal{O}} \sum_{t \in \mathcal{T}} \sum_{g \in \{\mathcal{S},\mathcal{R}\}} (\tau_o \cdot mc_g \cdot p_{gto}) + \sum_{o \in \mathcal{O}} \sum_{t \in \mathcal{T}} \sum_{d \in \mathcal{D}} (\tau_o \cdot pc_d \cdot p_{dto} \cdot (1 - y_{dto})) \\ & + \sum_{o \in \mathcal{O}} \sum_{t \in \mathcal{T}} \sum_{g \in \mathcal{R}} \left(\tau_o \cdot pc_g \cdot \left(p^{\text{AV}}_{gto} - p_{gto} \right) \right) \end{aligned} \tag{4.5c}$$

where z_b and z_g denote the investment status of the BESS and RESs respectively. Costs ic_b and ic_g and mc_b denote the annualised investment costs each BESS unit, RES unit and marginal cost of each generator, respectively, while pc_d defines the penalty costs for curtailment of load, while and pc_g is the penalty for RES power generation curtailment from the maximum power available p^{AV}_{gto} at each hour and representative day. Binary variable y_{dto} denotes the curtailment status of load demand at a node i.e., 1/0 implies not-curtailed/curtailed. Parameter τ_o is the weighting factor of representative day o.

$\mathbf{\Theta}^{\text{inv}}$ defined in (4.5b) calculates the total investment costs of the battery and RES units, while $\mathbf{\Theta}^{\text{opr}}$ in (4.5c) includes the operational costs for the micro-turbine/diesel, load shedding costs and the curtailment costs for the RES power generations, respectively.

4.3.3.2 Operational Constraints

The constraints taken into account to indicate the operational limitations of the network include the following:

Network Constraints

In this study, the DistFlow model [76] defined as Model 2 (DF) in Chapter 3 is selected to represent the network constraints. The large number of operational scenarios, i.e.

representative days, and the existence of integer variables from the investment candidates make the problem large and complex. Hence the DF technique was adopted as opposed to the ExDF and ExAgDF techniques that provide better approximations as indicated in Section 3.4. Note that computational efficiency exponentially increases with the size of the optimisation problem. The active and reactive nodal power balances for each hour of every representative day are re-defined in (4.6a) and (4.6b). The battery charging power and discharging power are distinguished by superscripts 'ch' and 'dch' while the node voltages and line flows are as defined in Model 2 (see Chapter 3).

$$P_{l^{i+}to} + \sum_{g\in\{\mathcal{R}^i,\mathcal{S}^i\}} p_{gto} + \sum_{b\in\mathcal{B}^i}\left(p^{\text{dch}}_{bto} - p^{\text{ch}}_{bto}\right) = \sum_{l^{i-}\in\mathcal{L}^i} P_{l^{i-}to} + \sum_{d\in\mathcal{D}^i}\left(\bar{p}_{dto}\cdot y_{dto}\right), \qquad \forall i,t,o \quad (4.6a)$$

$$Q_{l^{i+}to} + \sum_{g\in\{\mathcal{R}^i,\mathcal{S}^i\}} q_{gto} = \sum_{l^{i-}\in\mathcal{L}^i} Q_{l^{i-}to} + \sum_{d\in\mathcal{D}^i}\left(\bar{q}_{dto}\cdot y_{dto}\right), \qquad \forall i,t,o \quad (4.6b)$$

$$v_{i^-to} = v_{ito} + 2\cdot\left(r_{l^{i-}}\cdot P_{l^{i-}to} + x_{l^{i-}}\cdot Q_{l^{i-}to}\right) + \left(r^2_{l^{i-}} + x^2_{l^{i-}}\right)\cdot f_{l^{i-}}, \qquad \forall i,t,o \quad (4.6c)$$

$$v_{i^-to}\cdot f_{l^{i-}} = \left(p^2_{l^{i-}} + q^2_{l^{i-}}\right), \qquad \forall i,t,o \quad (4.6d)$$

Technical Constraints

The minimum and maximum bounds on nodal voltages are set by (4.7a) while (4.7b) sets the voltage at the power station to 1 p.u. Additionally, (4.7c) bounds the active and reactive power flows between two connected nodes within the thermal limitations of the connecting line.

$$\underline{v} \le v_{ito} \le \overline{v}, \qquad \forall i,t,o \quad (4.7a)$$

$$v_{1to} = 1, \qquad \forall t,o \quad (4.7b)$$

$$P^2_{lto} + Q^2_{lto} \le \overline{S}_l, \qquad \forall l,t,o \quad (4.7c)$$

Constraints (4.7d) and (4.7e) ensure the limits on active and reactive power generation for existing units in the network, respectively, while constraints (4.7f) and (4.7g) ensure the limits of active power generation for the candidate conventional and RES units.

$$0 \le p_{gto} \le \overline{p}_g, \qquad \forall g\in\{\mathcal{S},\mathcal{R}\},t,o \quad (4.7d)$$

$$\underline{q}_g \le q_{gto} \le \overline{q}_g, \qquad \forall g\in\{\mathcal{S},\mathcal{R}\},t,o \quad (4.7e)$$

$$0 \le p_{gto} \le \overline{p}_{gto}\cdot z_g, \qquad \forall g\in\{\mathcal{S},\mathcal{R}\},t,o \quad (4.7f)$$

$$\underline{q}_g\cdot z_g \le q_{gto} \le \overline{q}_g\cdot z_g, \qquad \forall g\in\{\mathcal{S},\mathcal{R}\},t,o \quad (4.7g)$$

The battery dynamics are defined in (4.7h)-(4.7l). Constraint (4.7h) ensures that the stored energy of each battery unit at every hour of each of the representative days is within the state-of-charge limits. The battery initial charge e_{bo}^{ini} for each day should be maintained at the same level at the end of the day, this is ensured by constraint (4.7i). The maximum charging and discharging levels are ensured by constraints (4.7j) and (4.7k), respectively. Moreover, constraint (4.7l) ensures that the battery does not simultaneously charge and discharge at each hour in all representative days.

$$\underline{e}_b \cdot z_b \leq e_{bo}^{\text{ini}} + \sum_{\tau=1}^{t} \left(\eta_b^{\text{ch}} \cdot p_{b\tau o}^{\text{ch}} - \frac{1}{\eta_b^{\text{dch}}} \cdot p_{b\tau o}^{\text{dch}} \right) \leq \overline{e}_b \cdot z_b, \qquad \forall b, t, o \qquad (4.7\text{h})$$

$$\sum_{\tau=1}^{T} \left(\eta_b^{\text{ch}} \cdot p_{b\tau o}^{\text{ch}} - \frac{1}{\eta^{\text{dch}}} \cdot p_{b\tau o}^{\text{dch}} \right) = 0, \qquad \forall b, t, o \qquad (4.7\text{i})$$

$$0 \leq p_{bto}^{\text{c}} \leq p^{\text{max,ch}} \cdot z_b^{\text{ch}}, \qquad \forall b, t, o \qquad (4.7\text{j})$$

$$0 \leq p_{bto}^{\text{d}} \leq p^{\text{max,dch}} \cdot z_b^{\text{dch}}, \qquad \forall b, t, o \qquad (4.7\text{k})$$

$$z_b^{\text{ch}} + z_b^{\text{dch}} \leq z_b, \qquad \forall b, t, o \qquad (4.7\text{l})$$

Carbon Emission Limits

An emission factor ef_g gram/kWh is applied to the conventional units for each kilo watt of power generated. A maximum intensity $ef^{\max}$ is then set for each of these generators for each representative to limit its carbon emissions. The non-violation of this limit is ensured by (4.8).

$$\sum_{t \in \Omega^T} \sum_{g \in \Omega^{Mn}} ef_g \cdot p_{gto} \leq ef^{\max} \cdot \sum_{t \in \Omega^T} \sum_{s \in \Omega^S} p_{dto}, \qquad \forall g \in \mathcal{S}, t, o \qquad (4.8)$$

The two-stage stochastic optimisation model described in (4.5)-(4.8) is a Mixed Integer Second Order Cone Programming (MISOCP) problem that is tractable and can be easily solved by off-the-shelf optimisation packages.

4.4 Case Study-Results

4.4.1 System Description

Alderney island has a closed energy system fully fed by imported fuel oil for electricity, heat, and transportation. The Alderney network consists of both the 11 kV primary distribution network, and the 415 V secondary distribution network. It consists of four

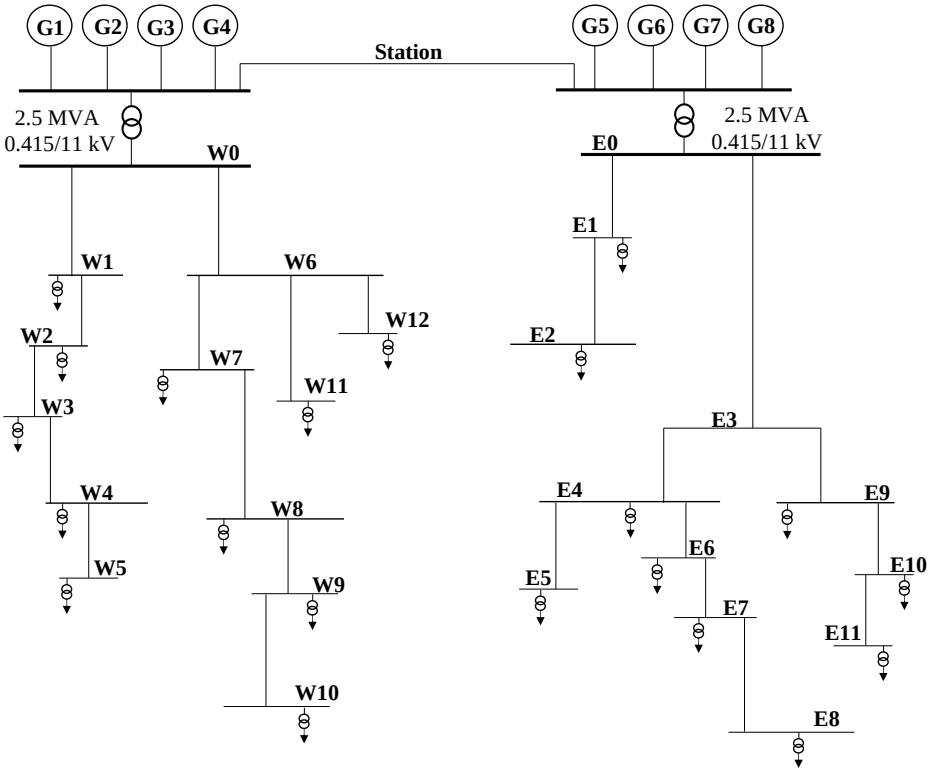

Figure 4.1: The AEL network one-line diagram.

radial feeders with 26 buses as depicted in Fig. 4.1. The existing infrastructure constitutes of electric power generated solely at the centrally located power station by the 8×450 kW diesel units. The power station is connected to the 11 kV primary distribution network via two 2500 kVA transformers and the 11 kV primary distribution network is connected to the 415 V secondary distribution network by 500 kVA transformers at different substations. The network parameters are as defined in Appendix A.1. Both primary and secondary networks are connected by an underground cable network. A sole operator Alderney Electricity Limited (AEL) manages the Alderney network.

Although investment into sustainable energy resources obviates the full reliance of the Alderney island MG network on fossil-fueled energy resources, the power productions of renewable technologies are highly intermittent. In other words, designing a sustainable MG without characterising the uncertainty and volatility in power productions of renewable technologies may result in significant non-supplied energy demand under specific operational scenarios. Therefore, it is vital to develop and utilise uncertainty-aware practical planning tools ensuring the adequacy of the MG design under different uncertainty sources (e.g., load demand and solar/wind power production). The stochastic MISOCP model described above is therefore applied to design a sustainable solution for the Alderney network.

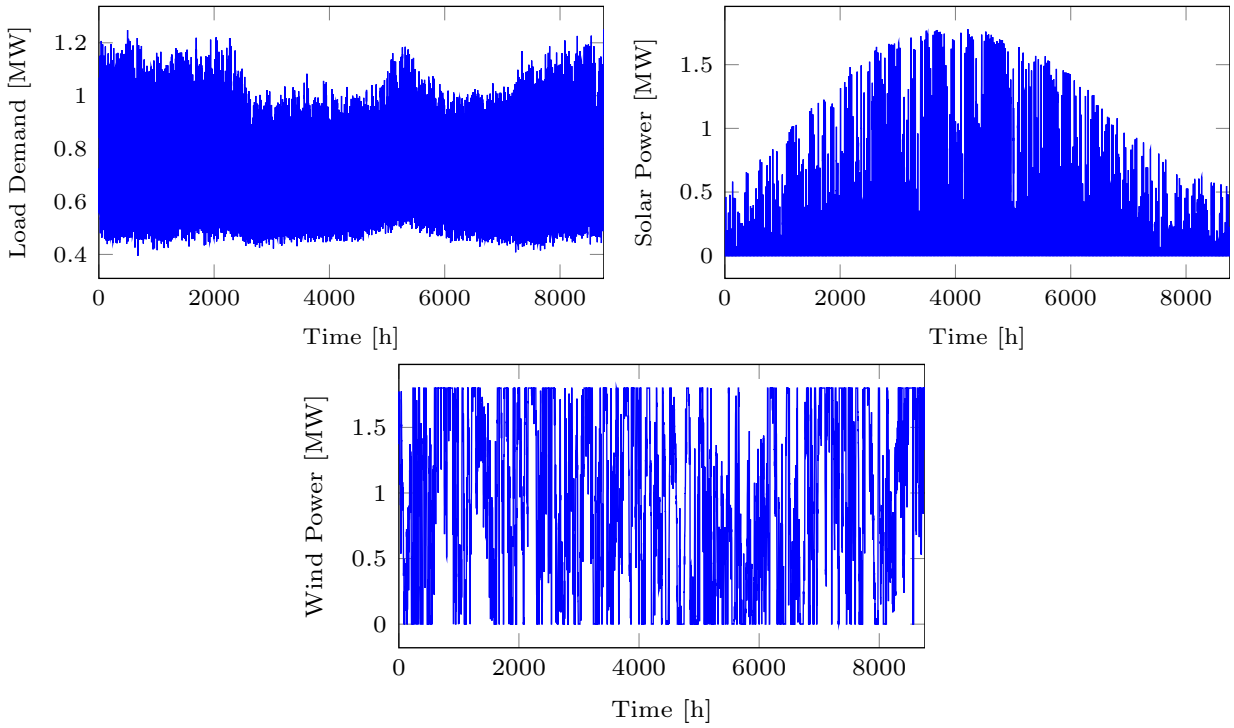

Figure 4.2: Yearly profiles of load demands and solar/wind power generations on Alderney island in 2013.

4.4.2 Input Data

The peak load for the island was equal to 1.252 MW in 2013. In addition, the solar irradiation and wind speed on Alderney island in 2013 are taken from [118]. It is assumed that the efficiency of candidate solar panels/modules in solar farm is equal to 10% [119] and the cut-in speed, rated speed, and cut-out speed of candidate wind turbines (i.e., Vestas V90 1.8 MW) are equal to 4 m/s, 12 m/s, and 25 m/s, respectively. In addition, the hub height of each wind turbine is equal to 80 m. Given a 1.8 MW solar farm with a 2-hectare land used to construct this power plant and a 1.8 MW wind farm, the yearly profiles of load demands, solar power generations, and wind power generations in 2013 are depicted in Fig. 4.2. The AHC technique is used to obtain representative days using the yearly profiles of load demands and RES power generations on Alderney island in 2013. For each cluster, three scenarios, i.e., risk-seeker, risk-neutral, and risk-averse representative days, are obtained as illustrated in Fig. 4.3 for the case of one representative day. Risk-seeker, risk-neutral, and risk-averse options are defined by the 0.99-, 0.50-, and 0.01-quantile of the respective clusters, respectively.

The investment candidates considered include battery, solar and wind generation units. Data profiles for the year 2013 were applied for load demand, solar and wind generation as depicted in Fig. 4.2 and Table 4.1 indicates a comparison of the costs and capacity

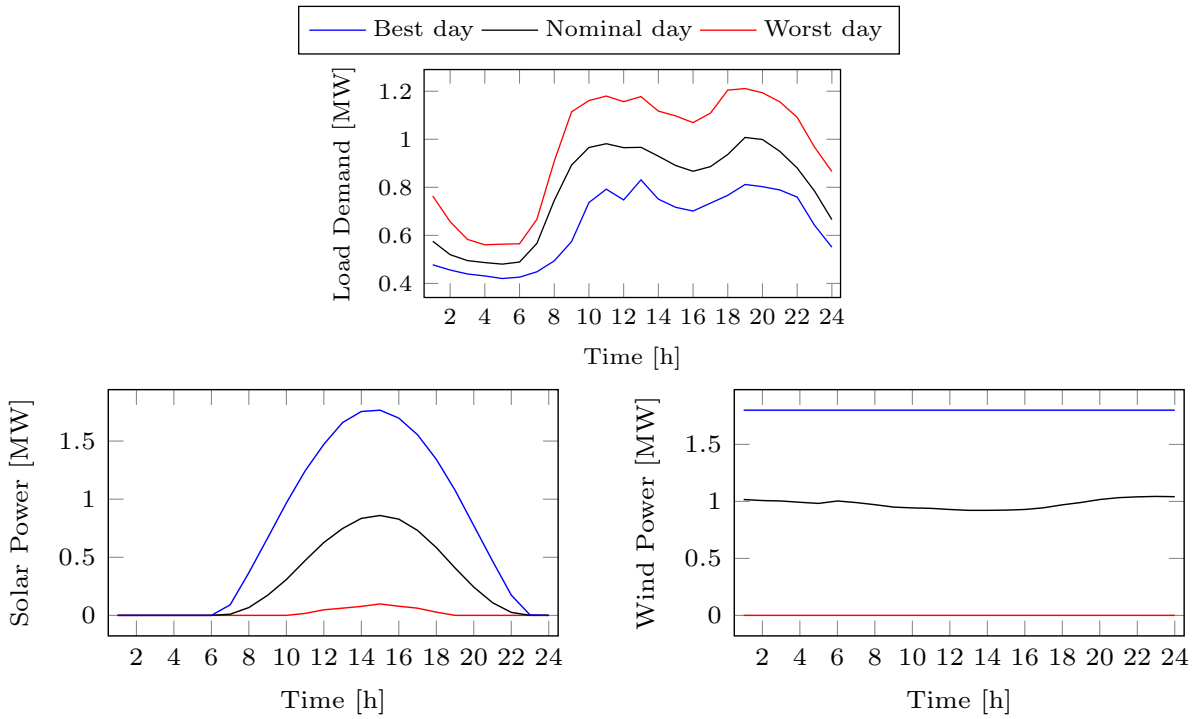

Figure 4.3: Best, nominal, and worst representative days for load demand, solar and renewable power generation on Alderney island considering one representative day.

factors for the different units. The investment costs of different technologies are taken from https://atb.nrel.gov. In order to calculate the annualised costs the Capital Recovery Factor (CRF) is employed which is defined as:

$$\text{CRF} = \frac{i \cdot (1+i)^y}{(1+i)^y - 1} \tag{4.9}$$

where i is the interest rate and y is the lifetime of the generation unit. It is assumed that the interest rate (i.e., i) is equal to 0.053, while the life time (i.e., y) of battery, solar, and wind units is equal 15, 30, and 30, respectively. Accordingly, the CRF used to calculate the annualised costs for battery, solar, and wind units is equal to 0.098, 0.067, and 0.067, respectively.

From Table 4.1, the Capacity Factor (CF) for wind technology is significantly higher than that of the solar technology, however the former has higher annualized costs. Battery technologies however have the highest annualized costs given their short life cycles. Furthermore, it is assumed that operational costs of battery, solar, and wind units are equal to zero while the operational cost of diesel units is equal to 196.2 £/MWh [120] on Alderney island based on prices at the time of writing. The penalty cost of curtailing load demand is set to 1962 £/MWh. The cost is set 10× higher than the highest operational

Table 4.1: Investment costs of different technologies

Technology	Battery (B)	Solar (S)	Wind (W)
Investment Cost [M£/MW]	0.98	0.84	1.21
Annualized Investment Cost [£/MW]	96040	56280	81070
Capacity Factor [%] (at 1.8MW capacity)	-	16.27	54.39

cost to ensure load curtailment is only applied as a last resort.

4.4.3 Simulation Results and Analysis

In order to ensure that an optimal technology mix is obtained to adequately and sustainably supply the electricity demand at Alderney, six cases defining alternative network configurations with varying investment candidates are considered as follows:

Case 1 (C1): 10×1.8 MW solar and 10×1.8 MW battery units;

Case 2 (C2): 10×1.8 MW wind and 10×1.8 MW battery units;

Case 3 (C3): 10×1.8 MW solar, 10×1.8 MW wind and 10×1.8 MW battery units;

Case 4 (C4): 10×1.8 MW solar, 10×1.8 MW battery units and existing diesel units;

Case 5 (C5): 10×1.8 MW wind, 10×1.8 MW battery units and existing diesel units;

Case 6 (C6): 10×1.8 MW solar, 10×1.8 MW wind, 10×1.8 MW battery units and existing diesel units.

Cases 1 to 3 consider an entirely RES supplied AEL network while Cases 4 to 6 are hybrid options that consider a mix of renewable sources as investment candidates and the existing diesel generators to meet the Alderney load demand. All simulations are carried out using PyEPLAN [121] with Gurobi [86] used as an optimisation solver.

4.4.3.1 Costs Analysis of the Investment Alternatives under Different Risk Levels

In Fig. 4.4, the total investment and operational costs are presented for the different cases considering five representative days. The risk-seeker, risk-neutral and risk-averse scenarios allude to the best, nominal and worst representative days. Figure 4.4 shows that in all scenarios, higher costs are recorded in the case of the purely renewable investment plans as opposed to the hybrid cases that consider the existing AEL diesel units in addition to the RES units. With regards to a 100% renewable AEL network, it is indicated that wind units provide a more economical solution as compared to solar units. This

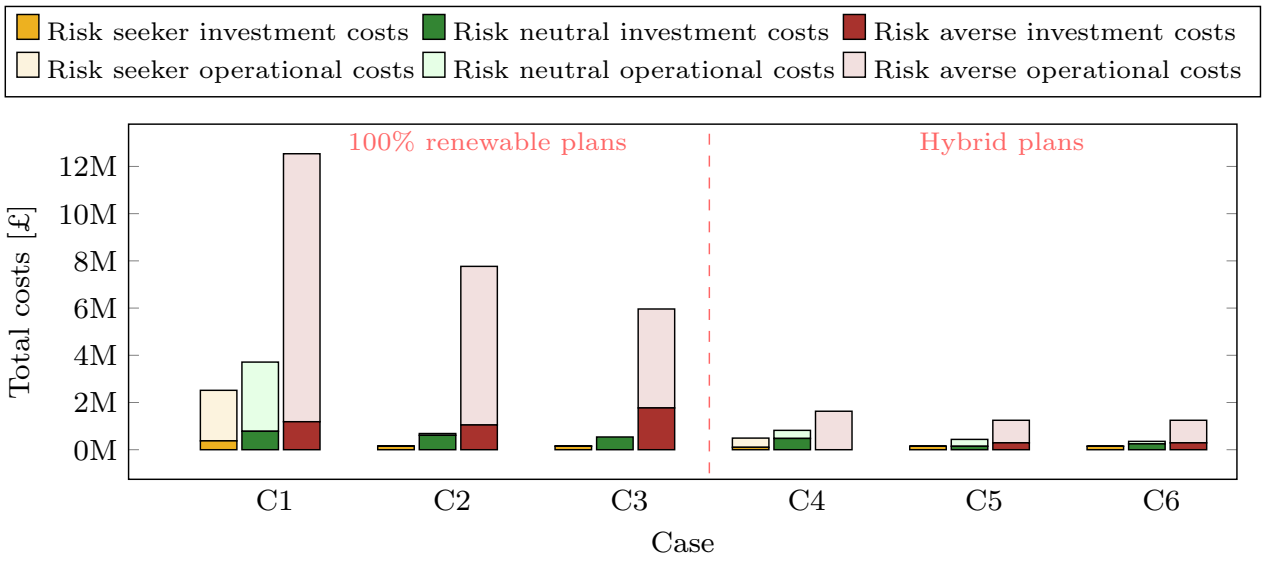

Figure 4.4: Total costs for all cases considering best, nominal and worst representative days i.e., risk-seeker, risk-neutral and risk-averse planning scenarios respectively.

Table 4.2: Investment decisions and LCOE values for all case studies with the best, worst and nominal representative days.

	Best Representative Day (Risk-Seeker)			Nominal Representative Day (Risk-Neutral)			Worst Representative Day (Risk-Averse)		
	Investment Decisions	LCOE [£/kWh]	Adequacy [%]	Investment Decisions	LCOE [£/kWh]	Adequacy [%]	Investment Decisions	LCOE [£/kWh]	Adequacy [%]
C1	1×B, 2×S	0.546	80.9	1×B, 6×S	0.686	78.4	1×B, 10×S	4.855	31.1
C2	1×W	0.028	100	1×B, 3×W	0.100	99.4	1×B, 6×W	1.593	58.8
C3	1×W	0.028	100	1×S, 3×W	0.078	100	1×B, 10×S, 4×W	0.967	74.2
C4	1×S	0.086	100	1×B, 3×S	0.119	100	-	0.196	100
C5	1×W	0.026	100	1×W	0.063	100	2×W	0.150	100
C6	1×W	0.026	100	1×S, 1×W	0.051	100	2×W	0.150	100

is further observed in Case C3 where both solar and wind units in addition to battery units are considered as investment options. From Table 4.2, it is indicated that solar units are only installed during risk-averse scenarios that are characterised by low load and high generation. These units while having a much lower investment costs per unit, are associated with a much lower capacity factor resulting in much lower generation levels throughout the year. Furthermore, in Cases C1, C2 and C3, operational costs are related to load demand curtailment penalties. This is further clarified in Table 4.2 which indicates a less than 100% adequacy level for the purely renewable investment plans.

In the hybrid planning options, while all cases indicate 100% adequacy (Table 4.2), Case C6 indicates the lowest total costs in all planning scenarios. For the case of 100% adequacy

levels, all operational cost are attributed to the operational costs of the existing diesel units in the AEL network. Note that with most hybrid planning options, the system flexibility provided by battery units fo the case of a fully renewable-supplied network, is replaced with the flexibility from the dispatchable diesel units. This can also be attributed to the high investment costs associated with battery units making them the least preferred investment candidate. Additionally, the renewable energy units do not generate excessive surplus levels of power given the low capacity factors to make battery units a viable candidate. Table 4.2 further shows the variation of the Levelized Cost of Energy (LCOE) values for the panning options under different scenarios. Similarly, Case C6 indicates the lowest LCOE while the highest values are recorded by Case C1. The low values indicated with the risk-seeker scenarios are attributed to the low load and high generation, the reverse is true for the risk-averse scenarios. For the AEL network, maximum, minimum and average values are observed as 4.855 £/kWh (C1) , 0.026 £/kWh (C6) and 0.541 £/kWh. The hybrid investment plan C6 in this case is shown to provide the most viable option to support a sustainable AEL network and as well supporting the transition to a more renewable network.

4.4.3.2 Sensitivity of Investment Decisions to Carbon Emission Limits

The UK government has set an emissions intensity target of 50-100 gCO_2/kWh to be achieved by power generation by 2030 [122]. In Fig. 4.5 the sensitivity of the total costs to the consideration of carbon emissions target limits (CL) is presented. The comparison is made considering the risk neutral investment scenario for the hybrid cases. The CL constraint when applied to the power generated by diesel generators as the most dominant

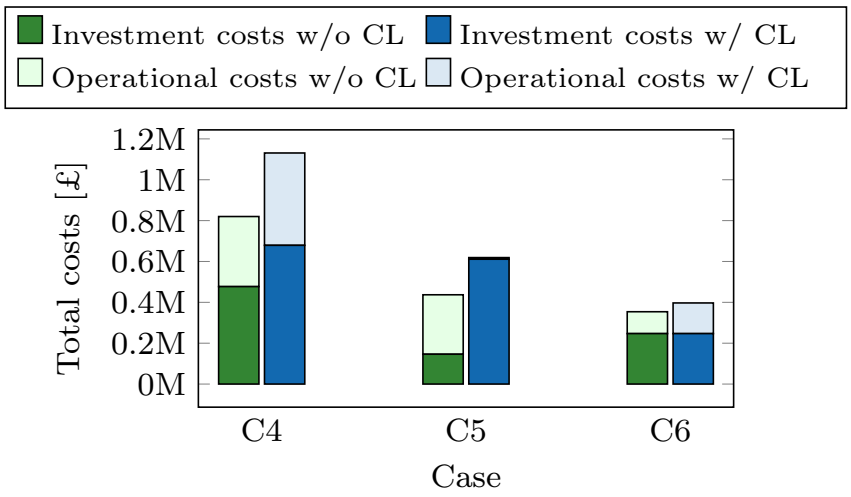

Figure 4.5: Sensitivity of total costs for hybrid Cases C4, C5, and C6 to the inclusion of carbon emission limits of the diesel generators.

Table 4.3: Investment plans and LCOE values considering carbon emission limits for Cases C4, C5 and C6.

	w/o CL		w/ CL	
	Investment Decisions	LCOE [£/kWh]	Investment Decisions	LCOE [£/kWh]
C4	1XB, 3XS	0.119	1XB, 5XS	0.166
C5	1XW	0.063	1XB, 3XW	0.089
C6	1XS, 1XW	0.051	1XS, 1XW	0.058

carbon emission producers results in a reduction in their total usage. In Case C4, both investment and operational costs show an increase with the application of the CO_2 targets while the result in Case C5 shows an increase in investment and no operational costs. The increased operational costs in this case are attributed to demand curtailment penalties while increased investment costs are related to the adoption of more RES units as shown in Table 4.3. The investment plan provided by Case C6 only indicates a slight variation in operational costs. Furthermore, as indicated in Table 4.3, the LCOE values are shown to be slightly higher when CO_2 targets are considered, this is attributed to the higher investment costs due to the adoption of more cleaner energy sources and/or the shedding of load demand to meet pre-defined targets. While Case C6 remains the most economical, Case C4 and C5 ensures that load demand is adequately served in all scenarios.

4.4.3.3 Sensitivity of Investment Decisions to Number of Representative Days

The accuracy of the proposed solution is enhanced by increasing the number of representative days considered as indicated in Fig. 4.6 for Case C6. As load demand and RES

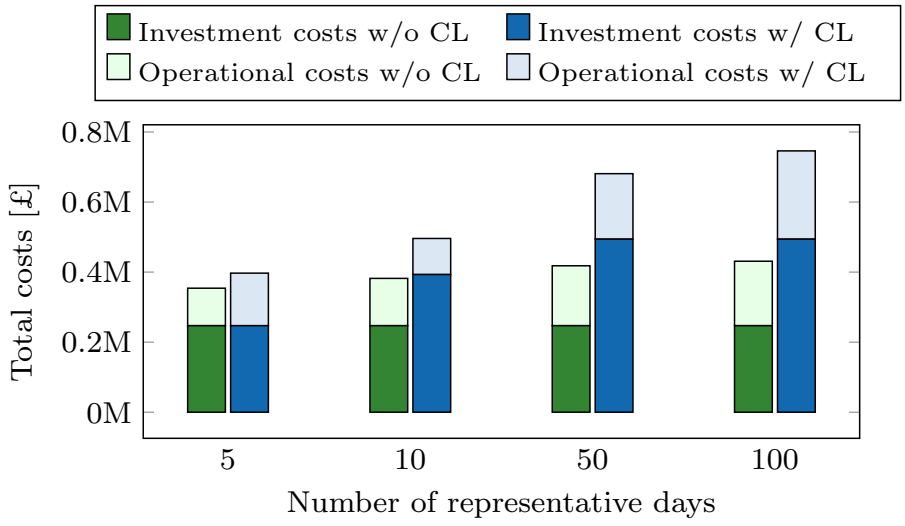

Figure 4.6: Sensitivity of total costs for Case C6 to the number of representative days.

Table 4.4: Comparison of Case C6 investment plans under different representative days.

	w/o CL		w/ CL	
No. of representative days	Investment Decisions	LCOE [£/kWh]	Investment Decisions	LCOE [£/kWh]
5	1XS, 1XW	0.051	1XS, 1XW	0.058
10	1XS, 1XW	0.055	1XS, 2XW	0.072
50	1XS, 1XW	0.061	2XS, 2XW	0.100
100	1XS, 1xW	0.062	2XS, 2XW	0.109

units are characterized by varying profiles over the planning profiles, it is necessary to adequately represent the yearly patterns accurately while considering the computational performance. The AHC technique adopted is used to jointly characterize the load demand and RES generation patterns into 5, 10, 50 and 100 correlated representative daily patterns. It is shown that investment costs when CO_2 targets are ignored remain the same while operational costs show an upward trend. On the contrary, both investment and additionally operational costs indicate an upward trend with the application of CO_2 limits. In Table 4.4 a larger increase in LCOE values is observed with CO_2 targets considered. However, both simulation scenarios plateau after 50 representative days. It is however noteworthy to mention that an increase in the number of representative days increases the solution space of the optimisation problem thus requiring a higher computation effort. In this case, 50 representative days provide a good trade-off between results accuracy and computational burden.

Therefore, in order to ensure the security of the MG networks, system designs that remain robust to the possible adverse impacts of uncertainty are crucial.

4.5 Conclusion

It is crucial that MG systems remain robust to the uncertain real-time variations in power injections and absorption from demand and generation. As a first potential approach to dealing with such variations, a two-stage stochastic MISOCP planning model considering a generation mix of low-carbon investments has been presented in this chapter. The inherent uncertainties of load demand and RES power production was handled using the AHC technique and a sensitivity analysis provided when various number of scenarios (representative days) are considered. The planning accuracy is enhanced by adopting a second-order conic convexification of the power flow equations of the network. Additionally, carbon emission limits are applied to case studies with diesel units to provide

a solution that is not only optimal but in line with the UK CO_2 emission targets. The planning model is applied to the practical network of the Alderney island demonstrating a variety of potential investment solutions when considering a 100% renewable and hybrid renewable system.

In this chapter, the planning decisions against the risk seeker, risk neutral and risk averse operation scenarios are analysed to compare the robustness of the proposed designs. Moreover, it is shown that the optimal solution is heavily dependant on the number of operational scenarios (representative days) considered during planning. In the next chapter, to enhance the robust operation of the network, a data-driven robust approach that reduces this dependency and provides guarantees on the robustness of the optimal solution obtained is proposed.

Chapter 5

A Data-Driven Optimisation Model for Designing Islanded Microgrids

The sustainability of islanded networks is normally ensured by the utilisation of various Renewable Energy Sources (RES). It is crucial that system designs remain robust to the possible adverse impacts of uncertainty to ensure the security of these networks. This chapter proposes a model for designing sustainable Microgrids (MGs) using the notion of Distributionally Robust Optimisation (DRO) to handle the uncertainties arising from forecast data. Wherein the non-convex AC power flow equations are reformulated into convex constraints. Furthermore, a three-step approach is introduced to recast the tri-level DRO-based model into a tractable single-stage Mixed-Integer Linear Programming (MILP) problem. The proposed approach is tested on a modified Europrean CIGRE 18-bus test network and its performance is compared with the stochastic optimisation approach. The work in this chapter is presented in publication [C1].

5.1 Introduction

MGs have enabled off-grid communities to economically access electricity without the requirement for potentially high-cost long-distance energy infrastructure. Such systems have globally enhanced the electrification efforts and resilience of energy supply. The sustainability of islanded networks is normally ensured by the utilisation of various RESs. However, the intermittent power production of RESs is inherently adding to the level of uncertainty in the network. To ensure the security of the islanded MGs, system de-

signs that remain robust to the possible adverse impacts of uncertainty are crucial. The power quality during system operation should be upheld concerning the technical limits on under/over voltage and maximum line flows. The cost-effective design of islanded MGs involves the solution of optimisation models for investment or reinforcement planning. Therefore, the handling of different uncertainties is key to the secure and resilient operation of MGs.

Related Works

As discussed in Chapter 4, Stochastic Optimisation (SO) based models obtain a solution that is optimal on average for all scenarios capturing the uncertainty spectrum [98–101]. The quality of the optimal solution in SO-based models is largely dependant on the number of available scenarios or historical data. On the contrary, Robust Optimisation (RO) based models obtain a solution that is optimal for the worst scenario of a bounded uncertainty set capturing all realisations of uncertain parameters [106–108, 123, 124]. In DRO, the optimal solution is obtained as the worst-case expected cost over a family of possible Probability Distribution Functions (PDF) characterising the uncertain parameters in an ambiguity set instead of assuming a single probability distribution function [95, 96]. As compared to SO and RO optimisation methods, it provides an intermediate and more practical solution that is less dependant on available data and less conservative than the former and latter respectively. The recourse decisions made in a DRO problem should adapt to all uncertain outcomes in the ambiguity set making the problem generally NP hard. The nature of the ambiguity set is key in facilitating the tractable reformulations that can be solved by available numerical solvers.

The uncertainty of renewable generation can result in power imbalance during MG operation. It is therefore vital that proposed system designs and energy management tasks handle these uncertainties to mitigate any inadequacy and security related risks. Reference [125] deals with this problem using a two-stage SO technique coupled with a receding horizon approach to capture the inter-temporal variations for the time-coupling constraints. In [126] a chance-constrained problem reformulated using DRO is proposed for energy management of islanded microgrids. A box-type ambiguity set that assumes the moments to lie in a box region specified by upper and lower bounds is adopted to capture the uncertain moment information.

The distributionally robust chance-constrained generation expansion optimisation problem presented in [127] uses a moment-based ambiguity set including second-order moment information from empirical data. The problem is then reformulated using linear decision

rules considering only active power to obtain a tractable Mixed-Integer Second-Order Cone Program (MISOCP). The authors in [128] further incorporate additional distribution information, such as mean absolute deviations and the asymmetry of distribution functions, in the moment-based ambiguity set to better describe the possible pattern of distributions. The joint energy and reserve dispatch problem solved in [129] similarly uses a moment-based ambiguity set but adopts a delayed constraint generation decomposition algorithm to solve the tri-level optimisation problem in a tractable manner. A multi-level dispatch DRO problem for a combined power and heat network in [130] a confidence set including norm-1 (absolute deviation summation constraints) and norm-inf (absolute deviation maximum constraints) is adopted and the multi-level problem solved using the column and constraint generation decomposition algorithm. A novel ambiguity set, based on a non-parametric confidence band of the cumulative distribution function of the uncertainties, is built-in [131]. The problem is then reformulated with an affine policy and distributionally robust chance constraints and recast into a mixed-integer linear programming problem.

In [C6], a data-driven Wasserstein metric-based ambiguity set is presented to characterise the uncertainty of load and power generation of RES for an investment planning problem for MGs. Metric-based ambiguity sets contain all distributions that are close to the true distribution and use a probability metric, such as the Wasserstein Metric detailed in [132]. The empirical distributions of historical data are considered as the center of the Wasserstein ball and the conservatism of the optimal solution is adjusted by means of the confidence level of the Wasserstein ambiguity set in [C6]. The problem is reformulated using duality theory to obtain a tractable counterpart.

This chapter proposes a DRO based technique for investment and reinforcement planning in islanded or off-grid MGs. A moment-based ambiguity set is employed due to its tractability in comparison to other techniques [132]. Differing from the existing literature, the distributional data in the ambiguity set is inferred from historical data of load demand and renewable profiles and scenarios reduced using a machine learning data clustering approach. The moment applied is the empirical mean of the load and renewable generation forecasts. Moreover, the problem is reformulated using an enhanced linear decision rule that incorporates the non-anticipativity aspects to improve the solution quality and reduce on the conservativeness of the approach. Additionally, unlike exisiting literature, decision rules for both active and reactive power are adopted to capture the whole spectrum of operational scenarios in MGs.

Contributions

The main contributions of this chapter are three-fold:

1. A novel DRO-based investment planning model is proposed for islanded MGs in remote areas aimed at immunising the optimal investment plan against uncertainties in forecast loads and renewable generations. In the proposed approach, temporal variations of loads and renewable generations during the entire planning horizon are modelled by a sufficient number of representative days where these representative days are extracted by the agglomerative hierarchical clustering [116]. Furthermore, a data-driven ambiguity set is presented in this paper to characterise the unknown PDFs pertaining to representative loads and renewable generations.
2. The duality theory and multi-period Linear Decision Rules (LDRs) are employed, respecting the non-anticipativity nature of the short-term operational decisions, to recast the proposed DRO-based model into a tractable MILP.
3. The algorithm performance is bench-marked against a SO-based model using the CIGRE 18-bus test network. Indices concerning computational efficiency, investment costs, and expected operational costs, are presented.

The rest of the chapter is organised as follows: Section 5.2 presents the mathematical formulation for the proposed DRO-based planning model and the definition of the ambiguity set. Section 5.3 presents the three-step approach proposed to obtain a tractable robust reformulation of model. The numerical results assessing the performance of the proposed algorithm are presented in Section 5.4, while conclusions are drawn in Section 5.5.

5.2 Distributionally Robust Planning Model

5.2.1 Modeling Preliminaries

The uncertain power injection $\tilde{u}_{\{r/d\}to}$ of RES $r \in \mathcal{R}$ or load $d \in \mathcal{D}$ at timestep $t \in \mathcal{T}$ and operating condition $o \in \mathcal{O}$ is expressed as:

$$\begin{aligned} \tilde{u}_{\{r/d\}to} &= u^{\mathrm{N}}_{\{r/d\}to} + \Delta\tilde{u}_{\{r/d\}to} \\ \Delta\tilde{u}_{\{r/d\}to} &= \hat{u}_{\{r/d\}to} - \check{u}_{\{r/d\}to} \end{aligned} \tag{5.1}$$

where $u^{\mathrm{N}}_{\{r/d\}to}$ denotes the expected/forecasted value of the power while $\Delta\tilde{u}_{\{r/d\}to}$ is the forecast error where $\hat{u}_{\{r/d\}to}/\check{u}_{\{r/d\}to}$ denotes the upward/downward deviation from

the forecast value. As both load and generation uncertainties are considered, $\tilde{u}_{\{r/d\}to}$ is defined as:

$$\tilde{u}_{to} = \left\{ \begin{array}{ll} \tilde{p}_{dto} = p^{\mathrm{N}}_{dto} + \hat{p}_{dto} - \check{p}_{dto}, & \forall d \\ \tilde{p}_{rto} = p^{\mathrm{N}}_{rto} + \hat{p}_{rto} - \check{p}_{rto}, & \forall r \end{array} \right\}, \quad \forall t, o \tag{5.2}$$

where $\tilde{p}_{dto}$ relates to the uncertain load demand and $\tilde{p}_{rto}$ relates to the uncertain renewable power generation.

In this work, it is assumed that a constant load power factor is maintained during load variations i.e., the uncertain power injections result from large appliances with a constant power factor [133], given as: $\cos\theta_{dto} = \frac{p^{\mathrm{N}}_{dto}}{\sqrt{(p^{\mathrm{N}}_{dto})^2+(q^{\mathrm{N}}_{dto})^2}}$. Therefore, forecast errors for the reactive power load injections are defined as: $\tilde{q}_{dto} = tan\theta_{dto} \cdot \tilde{p}_{dto}$.
Similarly, a constant power factor control for the renewable units is adopted (see Fig. 2.6),

$$-\tan\overline{\phi}_r \cdot \tilde{p}_{rto} \leq g^{\mathrm{Q}}_{rto} \leq \tan\overline{\phi}_r \cdot \tilde{p}_{rto} \tag{5.3}$$

where parameter $\cos\overline{\phi}_r$ is the minimum power factor set by the grid operator. The reactive power forecast error is therefore defined as: $\tilde{q}_{rto} = \tan\overline{\phi}_r \cdot \tilde{p}_{rto}$. Both uncertain reactive power injections (load and RES) are a function of the uncertain active power and not defined explicitly.

Bold letters are used to indicate vectors while entries of vectors are denoted by regular letters. The transpose of a matrix is denoted by $'$. This work considers a radial balanced network represented by a connected graph $\mathcal{G}(\mathcal{N}, \mathcal{E})$, with $\mathcal{N} \coloneqq \{0, 1, \ldots, N\}$ denoting the set of network nodes including the substation node 0, and $\mathcal{E} \subseteq \mathcal{N} \times \mathcal{N}$ designating the set of network branches. The distribution network hosts a number of DERs and loads, where $\mathcal{S} \subseteq \mathcal{N}$ indicates the subset of nodes with conventional generators, $\mathcal{R} \subseteq \mathcal{N}$ the subset of nodes with RESs, $\mathcal{B} \subseteq \mathcal{N}$ the subset of nodes with BESSs, $\mathcal{D} \subseteq \mathcal{N}$ the subset of nodes with loads. The set of nodes with DERs is thus obtained by the following set union $\mathcal{M} \coloneqq \mathcal{S} \cup \mathcal{R} \cup \mathcal{B}$. The set of respective units at node $i \in \mathcal{N}$ are given by $\mathcal{S}^i \subseteq \mathcal{S}$, $\mathcal{R}^i \subseteq \mathcal{R}$, $\mathcal{B}^i \subseteq \mathcal{B}$, and $\mathcal{D}^i \subseteq \mathcal{D}$. Cardinallity of the previously defined sets is denoted by: $n_d \coloneqq |\mathcal{D}|$, $n_s \coloneqq |\mathcal{S}|$, $n_b \coloneqq |\mathcal{B}|$, $n_l \coloneqq |\mathcal{L}|$, $n_r \coloneqq |\mathcal{R}|$. Indices d, s, b and r are associated with load demand, diesel generators, battery units and RESs.

For each DER $n \in \mathcal{M}$, variables p_{nto} and q_{nto} represent active and reactive power injections; superscript $^{\mathrm{N}}$ denotes the non-adjustable/adjustable terms decisions based on forecasted parameters while superscript $^{\mathrm{A}}$ relates to the adjustable decisions due to realisation of the forecast errors. Each node $i \in \mathcal{N}$ is connected to an upstream/downstream

node i^+/i^- by a branch with resistance r_{ii^-} and reactance x_{ii^-}, while $\mathcal{N}^{i^-}$ is a set of nodes connected downstream to node i. P_{ii^-} and Q_{ii^-} denote the active and reactive power flows in branch $ii^- \in \mathcal{E}$ while S is the apparent power flow. The upper/lower limits for a variable/parameter $\bullet$ are represented by $\overline{\bullet}/\underline{\bullet}$.

5.2.2 Ambiguity Set Model for Uncertain Power Injections

The compact form of the DRO model is presented as:

$$\min_{\chi^{\mathrm{inv}},\chi^{\mathrm{opr}}} \left\{ \Theta^{\mathrm{inv}}(\chi^{\mathrm{inv}}) + \max_{\mathbb{P}\in\mathcal{U}} \mathbb{E}_{\mathbb{P}} \left(\Theta^{\mathrm{opr}}(\chi^{\mathrm{opr}}, \tilde{\mathbf{u}}) \right) \right\} \tag{5.4}$$

where $\Theta^{\mathrm{inv}}/\Theta^{\mathrm{opr}}$ are the the investment/operational objective functions and $\chi^{\mathrm{inv}}/\chi^{\mathrm{opr}}$ the vectors of investment/operational variables. $\tilde{\mathbf{u}}$ defines the vector of the uncertain variables while the ambiguity set $\mathcal{U}$ characterises the distribution of the uncertain power injections for the entire planning horizon and is obtained as a Cartesian product of the set at each time step and for all operating scenarios:

$$\mathcal{U} = \prod_{t\in T, o\in\mathcal{O}} \mathcal{U}_{to} \tag{5.5}$$

where

$$\mathcal{U}_{to} = \left\{ \mathbb{P}_{to} : \begin{array}{ll} \mathbb{E}_{\mathbb{P}_{to}}(\tilde{p}_{dto}) = p^{\mathrm{N}}_{dto}, & \forall d \\ \mathbb{E}_{\mathbb{P}_{to}}(\tilde{p}_{rto}) = p^{\mathrm{N}}_{rto}, & \forall r \\ \mathbb{P}_t \left\{ \begin{array}{l} \tilde{p}_{dto} \in \mathcal{V}_{to} \\ \tilde{p}_{rto} \in \mathcal{V}_{to} \end{array} \right\} = 1, & \end{array} \right\} \tag{5.6}$$

In (5.6) the first and second lines indicate that the mean of the uncertain injections is defined by their respective forecast values while the third line guarantees that all uncertain realisations are within the uncertainty set $\mathcal{V}_{to}$.

For this study, the polyhedral uncertainty set proposed in [134] is adopted, where a budget

of uncertainty Γ is used to control the conservatism, $\mathcal{V}_{to}$ is expressed by constraints:

$$\mathcal{V}_{to} = \left\{ \begin{array}{ll} \tilde{p}_{dto} = p^{\mathrm{N}}_{dto} + \hat{p}_{dto} - \check{p}_{dto}, & \forall d \\ \tilde{p}_{rto} = p^{\mathrm{N}}_{rto} + \hat{p}_{rto} - \check{p}_{rto}, & \forall r \\ 0 \leq \hat{p}_{dto} \leq \overline{\hat{p}}_{dto}, \quad 0 \leq \check{p}_{dto} \leq \overline{\check{p}}_{dto}, & \forall d \\ 0 \leq \hat{p}_{rto} \leq \overline{\hat{p}}_{rto}, \quad 0 \leq \check{p}_{rto} \leq \overline{\check{p}}_{rto}, & \forall r \\ 0 \leq \left(\sum\limits_{d \in \mathcal{D}} \left(\dfrac{\hat{p}_{dto}}{\overline{\hat{p}}_{dto}} + \dfrac{\check{p}_{dto}}{\overline{\check{p}}_{dto}} \right) + \sum\limits_{r \in \mathcal{R}} \left(\dfrac{\hat{p}_{rto}}{\overline{\hat{p}}_{rto}} + \dfrac{\check{p}_{rto}}{\overline{\check{p}}_{rto}} \right) \right) \leq \Gamma_{to} & \end{array} \right\} \tag{5.7}$$

5.2.3 Extended Formulation of the Planning Model

The proposed DRO planning model in (6.5.1.2) is expanded as follows:

Objective

The term $\Theta^{\mathrm{inv}}(\chi^{\mathrm{inv}})$ in the objective function is given by:

$$\Theta^{\mathrm{inv}} = \sum_{b \in \mathcal{B}} C_b \cdot z_b + \sum_{s \in \mathcal{S}} C_s \cdot z_s + \sum_{r \in \mathcal{R}} C_r \cdot z_r \tag{5.8a}$$

where $C_{b/s/r}$ are the investment costs of the associated units and $z_{b/s/r}$ are the binary variables indicating the investment status of a unit i.e. a value of 1/0 indicates installed/not-installed.

The total operational costs captured by $\Theta^{\mathrm{opr}}(\chi^{\mathrm{opr}})$ are defined as:

$$\Theta^{\mathrm{opr}} = \sum_{o \in \mathcal{O}} \sum_{t \in \mathcal{T}} \left(\sum_{s \in \mathcal{S}} C^{\mathrm{op}}_{s} \cdot p_{sto} + \sum_{r \in \mathcal{R}} C^{\mathrm{op}}_{r} \cdot p_{rto} + \sum_{d \in \mathcal{D}} C^{\mathrm{sh}}_{d} \cdot \tilde{p}_{dto} \cdot (1 - z_{dto}) + \sum_{i \in \mathcal{N}} \epsilon \cdot q^{\mathrm{aux}}_{ito} \right) \tag{5.8b}$$

here $C^{\mathrm{op}}_{s/r}$ are the marginal operational costs of each unit while C^{sh}_{d} are penalty costs associated with load shedding. Variable z_{dto} is used to indicate the connection status of a load i.e. a value of 1/0 indicates connected/not-connected. To ensure the nodal reactive power balance, a small cost ϵ has been applied to the magnitude of reactive power generation denoted by the auxiliary variable q^{aux}_{ito}, further clarifications to this are presented in the next section. In the following, a definition of the constraints applied to the model is presented.

Power Flow Constraints

A linearized version of the 'DistFlow' model [75] is used to formulate the power flow equations in (5.8c)-(5.8e) (see Section 3.2.3, Model 3), where v_{ito} denotes the square magnitude of voltage at each node $i \in \mathcal{N}$, time period $t \in \mathcal{T}$, and operating condition $o \in \mathcal{O}$:

$$\sum_{s\in\mathcal{S}^i} p_{sto} + \sum_{r\in\mathcal{R}^i} p_{rto} + \sum_{b\in\mathcal{B}^i}(p^{\text{dch}}_{bto} - p^{\text{ch}}_{bto}) + P_{i^+ito} - \sum_{i^-\in\mathcal{N}^{i^-}} P_{ii^-to} \geq \sum_{d\in\mathcal{D}^i} \tilde{p}_{dto}\cdot z_{dto}, \qquad \forall i,t,o \qquad (5.8c)$$

$$\sum_{s\in\mathcal{S}^i} q_{sto} + \sum_{r\in\mathcal{R}^i} q_{rto} + Q_{i^+ito} - \sum_{i^{\text{dn}}\in\mathcal{N}^{i^-}} Q_{ii^-to} \geq \sum_{d\in\mathcal{D}^i} \tilde{q}_{dto}\cdot z_{dto}, \qquad \forall i,t,o \qquad (5.8d)$$

$$v_{i^+to} = v_{ito} + 2\left(r_{i^{\text{up}}i}\cdot P_{i^+ito} + x_{i^{\text{up}}i}\cdot Q_{i^+ito}\right), \qquad \forall i,t,o \qquad (5.8e)$$

$$-q^{\text{aux}}_{ito} \leq \sum_{s\in\mathcal{S}^i} q_{sto} + \sum_{r\in\mathcal{R}^i} q_{rto} \leq q^{\text{aux}}_{ito}, \qquad \forall i,t,o \qquad (5.8f)$$

$$q^{\text{aux}}_{ito} \geq 0, \qquad \forall i,t,o \qquad (5.8g)$$

where superscript "$^{\text{ch}}/_{\text{dch}}$" indicate the charge and discharge powers of the battery units.

The different generators in the network have the capability to inject as well as absorb reactive power i.e. operate in both inductive and capacitative modes. It is required that the nodal reactive power balance given the mode of operation i.e., injection/absorption is respected. This is ensured when equality exists between the left-hand-side and right-hand-side of (5.8d). This requirement is met using the non-negative auxiliary variable q^{aux}_{ito} in (5.8f) to which a small cost is applied in the objective function such that equality in (5.8d) is maintained.

Dispatchable Generation Constraints

Conventional units are fully dispatchable while renewable units are assumed to be dispatchable-down within their capacity limits. The limitations on the power injections from both types of units are denoted as:

$$0 \leq p_{sto} \leq \overline{p}_s\cdot z_s, \qquad -\overline{q}_s\cdot z_s \leq q_{sto} \leq \overline{q}_s\cdot z_s, \qquad \forall s,t,o \qquad (5.8h)$$

$$-\text{rp}^{\text{dn}}_s \leq p_{sto} - p_{s(t-1)o} \leq \text{rp}^{\text{up}}_s, \qquad \forall s,t,o \qquad (5.8i)$$

$$0 \leq p_{rto} \leq \tilde{p}_{rto}\cdot z_r, \qquad \forall r,t,o \qquad (5.8j)$$

$$-\tan\overline{\phi}_r\cdot\tilde{p}_{rto}\cdot z_r \leq q_{rto} \leq \tan\overline{\phi}_r\cdot\tilde{p}_{rto}\cdot z_r, \qquad \forall r,t,o \qquad (5.8k)$$

Binary variable z_s/z_r indicates the investment status of the conventional/renewable unit limited by their maximum active /reactive power capacities denoted by $\overline{p}_{s/r}/\overline{q}_{s/r}$. With respect to the renewable units, maximum capacity at a given time is based on the forecast value denoting the available usable power of the unit. This can be less than its nominal design capacity. The maximum ramp up/down limits $\mathrm{rp}_s^{\mathrm{up}}/\mathrm{rp}_s^{\mathrm{dn}}$ of the diesel generators are defined in (5.8i).

BES dynamics and Constraints

Constraint (5.8l) limits the charging/discharging power of battery units within their charge/discharge capacities while (5.8m) prevents simultaneous charging z_{bto}^{ch} and discharging z_{bto}^{dch} of the battery given its investment status z_b. The battery State-of-Charge (SoC) at each hour is limited by the maximum/minimum energy limit $\overline{e}_b/\underline{e}_b$ in (5.8n), while the initial (e_{bo}^{ini}) and final SOC are set by constraint (5.8o), given charging/discharging efficiency $\xi_b^{\mathrm{ch}}/\xi_b^{\mathrm{dch}}$.

$$0 \leq p_{bto}^{\mathrm{dch}} \leq \overline{p}_b^{\mathrm{dch}} \cdot z_{bto}^{\mathrm{dch}}, \qquad 0 \leq p_{bto}^{\mathrm{ch}} \leq \overline{p}_b^{\mathrm{ch}} \cdot z_{bto}^{\mathrm{ch}}, \qquad \forall b,t,o \tag{5.8l}$$

$$z_{bto}^{\mathrm{dch}} + z_{bto}^{\mathrm{ch}} = z_b, \qquad \forall b,t,o \tag{5.8m}$$

$$\underline{e}_b \cdot z_b \leq e_{bo}^{\mathrm{ini}} + \sum_{\tau=1}^{t} \left(\xi_b^{\mathrm{ch}} \cdot p_{b\tau o}^{\mathrm{ch}} - \frac{1}{\xi_b^{\mathrm{dch}}} \cdot p_{b\tau o}^{\mathrm{dch}} \right) \leq \overline{e}_b \cdot z_b, \qquad \forall b,t,o \tag{5.8n}$$

$$\sum_{t \in \mathcal{T}} \left(\xi_b^{\mathrm{ch}} \cdot p_{bto}^{\mathrm{ch}} - \frac{1}{\xi_b^{\mathrm{dch}}} \cdot p_{bto}^{\mathrm{dch}} \right) = 0, \qquad \forall b,o \tag{5.8o}$$

Thermal Loading and Voltage Constraints

Quadratic constraint (5.8p) denotes the secure line loading limits, this is linearized using a piece-wise linear approximation approach defined in [82] (see Model 3 Section 3.2.3), while (5.8q) defines the limits on nodal voltages.

$$(P_{i^{\mathrm{up}}ito})^2 + (Q_{i^{\mathrm{up}}ito})^2 \leq (S_{i^{\mathrm{up}}i})^2, \qquad \forall i,t,o \tag{5.8p}$$

$$\underline{v} \leq v_{ito} \leq \overline{v}, \qquad v_{to|i=0} = 1, \qquad \forall i,t,o \tag{5.8q}$$

5.2.4 Compact Matrix Formulation

For a clearer presentation, the overall formulation in (5.8a)-(5.8q) can be presented as a compact matrix expressed as:

$$\min \left\{ \Theta^{\text{inv}}(\chi^{\text{inv}}) + \max_{\mathbb{P}\in\mathcal{U}} \mathbb{E}_{\mathbb{P}} \left(\Theta^{\text{opr}}(\chi^{\text{opr}}, \tilde{\boldsymbol{u}})\right) \right\} \tag{5.9a}$$

$$\text{s.t. } \boldsymbol{A}\chi^{\text{inv}} + \boldsymbol{B}\boldsymbol{h}(\chi^{\text{opr}}, \tilde{\boldsymbol{u}}) \leq \boldsymbol{w} + \boldsymbol{W}\tilde{\boldsymbol{u}}, \quad \forall \tilde{\boldsymbol{u}} \in \mathcal{V} \tag{5.9b}$$

Constraints (5.8c)-(5.8q) are generalised into (5.9b) where function $h(\chi^{\text{opr}}, \tilde{\boldsymbol{u}})$ is associated with the effect of the uncertain variables on the decision variables during system operation, while $\boldsymbol{A}$, $\boldsymbol{B}$, $\boldsymbol{w}$ and $\boldsymbol{W}$ are constant matrices. Set $\mathcal{V}$ is the uncertainty set defined in (5.7).

5.2.5 Transformation of the Worst-Case Expectation

Based on the definition of the ambiguity set $\mathcal{U}$ in (5.6), the worst-case expectation in objective of the operation problem in (5.9a) can be explicitly represented as:

$$\max_{\mathbb{P}\in\mathcal{U}} \mathbb{E}_{\mathbb{P}} \left(\Theta^{\text{opr}}(\chi^{\text{opr}}, \tilde{\boldsymbol{u}})\right) = \max \int_{\mathcal{V}} \Theta^{\text{opr}}(\chi^{\text{opr}}, \tilde{\boldsymbol{u}}) \, \mathrm{d}P(\tilde{\boldsymbol{u}}) \tag{5.10a}$$

$$\text{s.t} \int_{\mathcal{V}} \tilde{\boldsymbol{u}} \, \mathrm{d}P(\tilde{\boldsymbol{u}}) = \boldsymbol{u}^{\text{N}} \qquad (\text{dual } \boldsymbol{\eta}) \tag{5.10b}$$

$$\int_{\mathcal{V}} \mathrm{d}P(\tilde{\boldsymbol{u}}) = 1 \qquad (\text{dual } \boldsymbol{\beta}) \tag{5.10c}$$

$$\mathrm{d}P(\tilde{\boldsymbol{u}}) \geq 0, \qquad \forall \tilde{\boldsymbol{u}} \in \mathcal{V} \tag{5.10d}$$

where the decision variable $P(\tilde{\boldsymbol{u}})$ is the probability distribution function; while $\boldsymbol{\eta}$ and $\boldsymbol{\beta}$ are vectors of dual variables associated with constraints (5.10b) and (5.10c), respectively. Using the duality theory [135], the formulation in (5.10) can be transformed into a minimisation problem as indicated below:

$$\max_{\mathbb{P}\in\mathcal{U}} \mathbb{E}_{\mathbb{P}} \left(\Theta^{\text{opr}}\right) = \min \left(\boldsymbol{\beta} + \boldsymbol{\eta}'\boldsymbol{u}^{\text{N}}\right) \tag{5.11a}$$

$$\text{s.t. } \boldsymbol{\beta} + \boldsymbol{\eta}'\tilde{\boldsymbol{u}} \geq \Theta^{\text{opr}}(\chi^{\text{opr}}, \tilde{\boldsymbol{u}}), \ \forall \tilde{\boldsymbol{u}} \in \mathcal{V} \tag{5.11b}$$

The model can now be represented as:

$$\min \left(\Theta^{\text{inv}} + \boldsymbol{\beta} + \boldsymbol{\eta}'\boldsymbol{u}^{\text{N}}\right) \tag{5.12a}$$

$$\text{s.t. } \boldsymbol{\beta} + \boldsymbol{\eta}'\tilde{\boldsymbol{u}} \geq \Theta^{\text{opr}}(\chi^{\text{opr}}, \tilde{\boldsymbol{u}}) \qquad \forall \tilde{\boldsymbol{u}} \in \mathcal{V} \tag{5.12b}$$

$$\boldsymbol{A}\chi^{\text{inv}} + \boldsymbol{B}\boldsymbol{h}(\chi^{\text{opr}}, \tilde{\boldsymbol{u}}) \leq \boldsymbol{w} + \boldsymbol{W}\tilde{\boldsymbol{u}} \qquad \forall \tilde{\boldsymbol{u}} \in \mathcal{V} \tag{5.12c}$$

The model indicated in (5.12) contains a bilinear term $\boldsymbol{\eta}'\tilde{\boldsymbol{u}}$ resulting in a non-convex formulation that is NP hard. Additionally, (5.12) is intractable due to its infinite-dimensional nature i.e., it should be feasible for any realisation of the uncertain parameters whose coverage is defined by the ambiguity set in (5.6). One approach to obtain a tractable formulation of the min-max problem can be based on decomposition algorithms [12, 91, 136, 137] where the problem is decomposed into one master problem and several sub-problems and solved iteratively. A Big-M transformation that recasts the bilinear terms into linear ones has also been adopted for the work in [138]. In this work, decision rules and duality theory are used to recast the problem to its robust counterpart. This approach eliminates the use of multi-stage strategies that can face convergence issues.

5.3 Solution Approach

In the following, a three-step procedure to derive the tractable, convex, robust counterpart of the problem that can be easily solved by available off-the-shelf solvers is presented.

5.3.1 Defining the Decision Rules

LDRs restrict the recourse decisions/actions to affine functions of the uncertain injections [139]. Note that by its nature, the decision-making process involves multiple stages i.e., the decisions made at each time step are dependant on the decisions made at the previous time steps. Disregarding this dependency in the decision rule at each time step could violate the nonanticipativity constraints present in the model. In this work, these constraints relate to the inter-temporal constraints on the ramping limits of the generators (5.8i) and battery state-of-charge at the end of planning horizon (5.8n)-(5.8o).

As a first step, a nonanticipative LDR is formulated for the independent variables, i.e. hourly active and reactive power injection/absorption of the conventional, renewable, and BES units. The voltage levels, current and power flows depend on the power injection/absorption hence do not require explicit LDR definition. The active and reactive

power policies for the injection from each unit $n \in \mathcal{S} \cup \mathcal{R} \cup \mathcal{B}$ is thus defined as:

$$p_{nto} = p^{\mathrm{N}}_{nto} + \sum_{k=1}^{t} \left(\sum_{d \in \mathcal{D}} \hat{p}^{\mathrm{AD}}_{ndkto} \cdot \hat{p}_{dko} - \check{p}^{\mathrm{AD}}_{ndkto} \cdot \check{p}_{dko} + \sum_{r \in \mathcal{R}} -\hat{p}^{\mathrm{AR}}_{nrkto} \cdot \hat{p}_{rko} + \check{p}^{\mathrm{AR}}_{nrkto} \cdot \check{p}_{rko} \right) \tag{5.13a}$$

$$q_{nto} = q^{\mathrm{N}}_{nto} + \sum_{k=1}^{t} \left(\sum_{d \in \mathcal{D}} \left(\hat{q}^{\mathrm{AD}}_{ndkto} \cdot \hat{p}_{dko} - \check{q}^{\mathrm{AD}}_{ndkto} \cdot \check{p}_{dko} \right) \cdot \tan\theta_{dko} + \sum_{r \in \mathcal{R}} \left(- \hat{q}^{\mathrm{AD}}_{nrkto} \cdot \hat{p}_{rko} + \check{q}^{\mathrm{AD}}_{nrkto} \cdot \check{p}_{rko} \right) \cdot \tan\overline{\phi} \right) \tag{5.13b}$$

Superscripts "D" and "R" relate to variables associated with demand-related and renewable-related uncertainty, respectively. The rule definitions in (5.13) expressing the effect of the uncertain parameters can be compactly represented as:

$$h(\chi^{\mathrm{opr}}, \tilde{\boldsymbol{u}}) = \chi^{\mathrm{opr,N}} + \sum_{k \in K} (\chi^{\mathrm{opr,A}}_k)' \Delta \tilde{\boldsymbol{u}}_k \tag{5.14}$$

where K is a set of all dependant decisions at each stage for all hours of the planning horizon. The vector $\tilde{\boldsymbol{u}}$ at time t includes all uncertain parameters from hour 1 to t. Variable $\chi^{\mathrm{opr,A}}_k$ is normally referred to as the participation factor of a generating unit towards mitigation of power imbalance in real-time operation resulting from unplanned power deviations.

5.3.2 Problem Reformulation with linear decision rules

In this second step, the problem is reformulated based on the LDR defined in (5.14). The rule defined is then applied to the model as follows:

$$\min \ \Theta^{\mathrm{inv}} + \boldsymbol{\beta} + \boldsymbol{\eta}' \boldsymbol{u}^{\mathrm{N}} \tag{5.15a}$$

subject to

$$\boldsymbol{\beta} \geq \boldsymbol{C}\chi^{\mathrm{opr,N}} + \sum_{k \in K} \boldsymbol{C}(\chi^{\mathrm{opr,A}}_k)' \Delta \tilde{\boldsymbol{u}}_k - \boldsymbol{\eta}' \tilde{\boldsymbol{u}}, \qquad \forall \tilde{\boldsymbol{u}} \in \mathcal{V} \tag{5.15b}$$

$$\boldsymbol{A}\chi^{\mathrm{inv}} + \boldsymbol{B}\chi^{\mathrm{opr,N}} - \boldsymbol{w} \leq \boldsymbol{W}\tilde{\boldsymbol{u}} - \sum_{k \in K} \boldsymbol{B}(\chi^{\mathrm{opr,A}}_k)' \Delta \tilde{\boldsymbol{u}}_k, \qquad \forall \tilde{\boldsymbol{u}} \in \mathcal{V} \tag{5.15c}$$

where the operation cost function $\Theta^{\mathrm{opr}}(\chi^{\mathrm{opr}}, \tilde{\boldsymbol{u}})$ has been reformulated as $\Theta^{\mathrm{opr}}(\chi^{\mathrm{opr}}, \tilde{\boldsymbol{u}}) = \boldsymbol{C}\chi^{\mathrm{opr,N}} + \boldsymbol{C}(\chi^{\mathrm{opr,A}})' \Delta \tilde{\boldsymbol{u}}$. The incorporation of the LDRs eliminates the infinite-dimensional

constraints due to the uncertain variables.

However, the optimisation problem (5.15) is still intractable due to the universal quantifier over the vector uncertain parameters (i.e., $\forall \tilde{\boldsymbol{u}} \in \mathcal{V}$). To obtain a robust solution against any realisation of uncertain parameters, a worst-case reformulation is introduced in this work using the protection functions $\Phi^1(\tilde{\boldsymbol{u}})$ and $\Phi^2(\tilde{\boldsymbol{u}})$ as given below:

$$\min \ \Theta^{\text{inv}} + \boldsymbol{\beta} + \boldsymbol{\eta'} \boldsymbol{u}^{\text{N}} \tag{5.16a}$$

$$\text{s.t. } \boldsymbol{\beta} - \boldsymbol{C}\chi^{\text{opr,N}} \geq \underbrace{\max_{\tilde{\boldsymbol{u}} \in \mathcal{V}} \Big(\sum_{k \in K} \boldsymbol{C} \chi_k^{\text{opr,A}} \Delta \tilde{\boldsymbol{u}}_k - \boldsymbol{\eta'} \tilde{\boldsymbol{u}} \Big)}_{\Phi^1(\tilde{\boldsymbol{u}})} \tag{5.16b}$$

$$\begin{aligned} &\boldsymbol{A}\chi^{\text{inv}} + \boldsymbol{B}\chi^{\text{opr,N}} - \boldsymbol{w} \\ &\qquad \leq \underbrace{\max_{\tilde{\boldsymbol{u}} \in \mathcal{V}} \big(\boldsymbol{W}\tilde{\boldsymbol{u}} - \sum_{k \in K} \boldsymbol{B} (\chi_k^{\text{opr,A}})' \Delta \tilde{\boldsymbol{u}}_k \big)}_{\Phi^2(\tilde{\boldsymbol{u}})} \end{aligned} \tag{5.16c}$$

The protection functions $\Phi^1(\tilde{\boldsymbol{u}})$ and $\Phi^2(\tilde{\boldsymbol{u}})$ for constraints (5.16b) and (5.16c) depend on the polyhedral uncertainty set $\mathcal{V}$ defined in (5.7), they can be rewritten as:

$$\begin{aligned} \Phi^1(\tilde{\boldsymbol{u}}) = \max_{\tilde{\boldsymbol{u}} \in \mathcal{V}} \Bigg(&\Big(\sum_{k \in K} \boldsymbol{C} (\chi_k^{\text{opr,A}})' \hat{\boldsymbol{u}}_k - \boldsymbol{\eta'} \hat{\boldsymbol{u}} \Big) \\ &- \Big(\sum_{k \in K} \boldsymbol{C} (\chi_k^{\text{opr,A}})' \check{\boldsymbol{u}}_k - \boldsymbol{\eta'} \check{\boldsymbol{u}} \Big) - \boldsymbol{\eta'} \boldsymbol{u}^{\text{N}} \Bigg) \end{aligned} \tag{5.17a}$$

$$\begin{aligned} \Phi^2(\tilde{\boldsymbol{u}}) = \max_{\tilde{\boldsymbol{u}} \in \mathcal{V}} \Bigg(&\Big(\boldsymbol{W}\hat{\boldsymbol{u}} - \sum_{k \in K} \boldsymbol{B} (\chi_k^{\text{opr,A}})' \hat{\boldsymbol{u}}_k \Big) \\ &- \Big(\boldsymbol{W}\check{\boldsymbol{u}} - \sum_{k \in K} \boldsymbol{B} (\chi_k^{\text{opr,A}})' \check{\boldsymbol{u}}_k \Big) + \boldsymbol{W}\boldsymbol{u}^{\text{A}} \Bigg) \end{aligned} \tag{5.17b}$$

$$\text{s.t.} \quad 0 \leq \hat{\boldsymbol{u}} \leq \overline{\hat{\boldsymbol{u}}} \qquad \text{(dual } \boldsymbol{\lambda}\text{)} \tag{5.17c}$$

$$0 \leq \check{\boldsymbol{u}} \leq \overline{\check{\boldsymbol{u}}} \qquad \text{(dual } \boldsymbol{\pi}\text{)} \tag{5.17d}$$

$$\hat{\boldsymbol{u}} \big/ \overline{\hat{\boldsymbol{u}}} + \check{\boldsymbol{u}} \big/ \overline{\check{\boldsymbol{u}}} = \boldsymbol{\Gamma} \qquad \text{(dual } \boldsymbol{\psi}\text{)} \tag{5.17e}$$

where $\boldsymbol{\lambda}$, $\boldsymbol{\pi}$ and $\boldsymbol{\psi}$ are vectors of the dual variables associated with constraints (5.17c)-(5.17e).

5.3.3 Applying Duality Theory

Finally, in the third step, the duality theory is utilised to obtain a tractable reformulation of the problem. The maximisation problem in (5.17a) can be recast into a minimisation problem using the duality theory as follows:

$$\Phi^1(\tilde{\boldsymbol{u}}) = \min \left(\sum_{k\in K} \left(\overline{\hat{\boldsymbol{u}}}' \boldsymbol{\lambda}_k^1 + \overline{\breve{\boldsymbol{u}}}' \boldsymbol{\pi}_k^1 + \boldsymbol{\Gamma}' \boldsymbol{\psi}_k^1 \right) - \boldsymbol{\eta}' \boldsymbol{u}^{\mathrm{N}} \right) \tag{5.18a}$$

$$\text{s.t.} \quad \boldsymbol{\lambda}_k^1 + \left(1 \big/ \overline{\hat{\boldsymbol{u}}} \right)' \boldsymbol{\psi}_k^1 \geq \left(\boldsymbol{C}(\chi_k^{\mathrm{opr,A}}) - \boldsymbol{\eta}_{|k=t} \right) \qquad \forall k \in K \tag{5.18b}$$

$$\boldsymbol{\pi}_k^1 + \left(1 \big/ \overline{\breve{\boldsymbol{u}}} \right)' \boldsymbol{\psi}_k^1 \geq -\left(\boldsymbol{C}(\chi_k^{\mathrm{opr,A}}) - \boldsymbol{\eta}_{|k=t} \right) \qquad \forall k \in K \tag{5.18c}$$

The dual of the maximisation problem in (5.17b) is a minimisation problem of the form:

$$\Phi^2(\tilde{\boldsymbol{u}}) = \min \left(\sum_{k\in K} \left(\overline{\hat{\boldsymbol{u}}}' \boldsymbol{\lambda}_k^2 + \overline{\breve{\boldsymbol{u}}}' \boldsymbol{\pi}_k^2 + \boldsymbol{\Gamma}' \boldsymbol{\psi}_k^2 \right) + \boldsymbol{W} \boldsymbol{u}^{\mathrm{A}} \right) \tag{5.19a}$$

$$\text{s.t.} \quad \boldsymbol{\lambda}_k^2 + \left(1 \big/ \overline{\hat{\boldsymbol{u}}} \right)' \boldsymbol{\psi}_k^2 \geq \left(\boldsymbol{W} - \boldsymbol{B}(\chi_k^{\mathrm{opr,A}}) \right) \qquad \forall k \in K \tag{5.19b}$$

$$\boldsymbol{\pi}_k^2 + \left(1 \big/ \overline{\breve{\boldsymbol{u}}} \right)' \boldsymbol{\psi}_k^2 \geq -\left(\boldsymbol{W} - \boldsymbol{B}(\chi_k^{\mathrm{opr,A}}) \right) \qquad \forall k \in K \tag{5.19c}$$

The superscripts "1" and "2" are utilised to distinguish between the dual variables in (5.18) and (5.19), respectively. The overall problem is therefore reformulated as:

$$\min \ \Theta^{\mathrm{inv}} + \boldsymbol{\beta} + \boldsymbol{\eta}' \boldsymbol{u}^{\mathrm{N}} \tag{5.20a}$$

$$\text{s.t.} \ \boldsymbol{\beta} - \boldsymbol{C} \chi^{\mathrm{opr,N}} \geq \sum_{k\in K} \left(\overline{\hat{\boldsymbol{u}}}' \boldsymbol{\lambda}_k + \overline{\breve{\boldsymbol{u}}}' \boldsymbol{\pi}_k + \boldsymbol{\Gamma}' \boldsymbol{\psi}_k \right) - \boldsymbol{\eta}' \boldsymbol{u}^{\mathrm{N}} \qquad \forall k \in K \tag{5.20b}$$

$$\boldsymbol{A} \chi^{\mathrm{inv}} + \boldsymbol{B} \chi^{\mathrm{opr,N}} - \boldsymbol{w} \leq \sum_{k\in K} \left(\overline{\hat{\boldsymbol{u}}}' \boldsymbol{\lambda}_k + \overline{\breve{\boldsymbol{u}}}' \boldsymbol{\pi}_k + \boldsymbol{\Gamma}' \boldsymbol{\psi}_k \right) + \boldsymbol{W} \boldsymbol{u}^{\mathrm{A}} \qquad \forall k \in K \tag{5.20c}$$

$$\boldsymbol{\lambda}_k^1 + \left(1 \big/ \overline{\hat{\boldsymbol{u}}} \right)' \boldsymbol{\psi}_k^1 \geq \left(\boldsymbol{C}(\chi_k^{\mathrm{opr,A}}) - \boldsymbol{\eta}_{|k=t} \right) \qquad \forall k \in K \tag{5.20d}$$

$$\boldsymbol{\pi}_k^1 + \left(1 \big/ \overline{\breve{\boldsymbol{u}}} \right)' \boldsymbol{\psi}_k^1 \geq -\left(\boldsymbol{C}(\chi_k^{\mathrm{opr,A}}) - \boldsymbol{\eta}_{|k=t} \right) \qquad \forall k \in K \tag{5.20e}$$

$$\boldsymbol{\lambda}_k^2 + \left(1 \big/ \overline{\hat{\boldsymbol{u}}} \right)' \boldsymbol{\psi}_k^2 \geq \left(\boldsymbol{W} - \boldsymbol{B}(\chi_k^{\mathrm{opr,A}}) \right) \qquad \forall k \in K \tag{5.20f}$$

$$\boldsymbol{\pi}_k^2 + \left(1 \big/ \overline{\breve{\boldsymbol{u}}} \right)' \boldsymbol{\psi}_k^2 \geq -\left(\boldsymbol{W} - \boldsymbol{B}(\chi_k^{\mathrm{opr,A}}) \right) \qquad \forall k \in K \tag{5.20g}$$

$$\boldsymbol{\lambda}^1 \geq 0,\ \boldsymbol{\pi}^1 \geq 0,\ \boldsymbol{\lambda}^2 \geq 0,\ \boldsymbol{\pi}^2 \geq 0 \tag{5.20h}$$

The problem formulation in (5.20) is a single-level MILP problem that can tractably be solved by various available off-shelf solvers. To further provide clarification on the solution approach, the reformulation of constraint (5.12b) is illustrated in (5.21) and (5.22).

Step 1 and 2: Formulation and application of the LDRs

$$\begin{aligned}
&\beta_{to} + \sum_{d\in\mathcal{D}} \eta_{dto}\cdot(p^{\mathrm{N}}_{dto} + \hat{p}_{dto} - \check{p}_{dto}) + \sum_{r\in\mathcal{R}} \mu_{rto}\cdot(p^{\mathrm{N}}_{rto} + \hat{p}_{rto} - \check{p}_{rto}) \\
&\quad \geq \sum_{s\in\mathcal{S}} C^{\mathrm{op}}_s \cdot \Bigg[p^{\mathrm{N}}_{sto} + \sum_{k=1}^{t}\Bigg(\sum_{d\in\mathcal{D}} \hat{p}^{\mathrm{AD}^1}_{dsko}\cdot\hat{p}_{dko} - \check{p}^{\mathrm{AD}^1}_{dsko}\cdot\check{p}_{dko} \\
&\qquad\qquad + \sum_{r\in\mathcal{R}} -\hat{p}^{\mathrm{AR}^1}_{rsko}\cdot\hat{p}_{rko} + \check{p}^{\mathrm{AR}^1}_{rsko}\cdot\check{p}_{rko}\Bigg)\Bigg] \\
&\quad + \sum_{r'\in\mathcal{R}} C^{\mathrm{op}}_{r'} \cdot \Bigg[p^{\mathrm{N}}_{r'to} + \sum_{k=1}^{t}\Bigg(\sum_{d} \hat{p}^{\mathrm{AD}^1}_{dr'ko}\cdot\hat{p}_{dko} - \check{p}^{\mathrm{AD}^1}_{dr'ko}\cdot\check{p}_{dko} \\
&\qquad\qquad + \sum_{r\in\mathcal{R}} -\hat{p}^{\mathrm{AR}^1}_{rr'ko}\cdot\hat{p}_{rto} + \check{p}^{\mathrm{AR}^1}_{rr'ko}\cdot\check{p}_{rto}\Bigg)\Bigg] \\
&\quad + \sum_{d\in\mathcal{D}} C^{\mathrm{op}}_d \cdot ((p^{\mathrm{N}}_{dto} + \hat{p}_{dto} - \check{p}_{dto}))\cdot(1 - z_{dto}) + \sum_{i\in\mathcal{N}} \epsilon\cdot q^{\mathrm{aux}}_{ito},
\end{aligned} \qquad \forall t, o \tag{5.21}$$

Step 3: Reformulation using duality theory

$$\begin{aligned}
&\beta_{to} + \sum_{d\in\mathcal{D}} \Big(\eta_{dto}\cdot p^{\mathrm{N}}_{dto} - C^{\mathrm{op}}_d\cdot p^{\mathrm{N}}_{dto}\cdot(1 - z_{dto})\Big) + \sum_{r\in\mathcal{R}} \Big(\mu_{rto}\cdot p^{\mathrm{N}}_{rto}\Big) \\
&\quad - \sum_{r'\in\mathcal{R}} C^{\mathrm{op}}_{r'}\cdot p^{\mathrm{N}}_{r'to} - \sum_{s\in\mathcal{S}} C^{\mathrm{op}}_s\cdot p^{\mathrm{N}}_{sto} - \sum_{i\in\mathcal{N}} \epsilon\cdot q^{\mathrm{aux}}_{ito} \qquad \forall t, o \\
&\quad \geq \sum_{k=1}^{t}\Bigg(\sum_{d\in\mathcal{D}} (\lambda^{\mathrm{D}^1}_{dkto} + \pi^{\mathrm{D}^1}_{dkto})\cdot\overline{p}^{*}_{dko} + \sum_{r\in\mathcal{R}^\infty} (\lambda^{\mathrm{R}^1}_{rkto} + \pi^{\mathrm{R}^1}_{rko})\cdot\overline{p}^{*}_{rkto} + \Gamma_{ko}\cdot\psi^1_{ko}\Bigg),
\end{aligned} \tag{5.22a}$$

$$\begin{aligned}
&\lambda^{\mathrm{D1}}_{dkto} + \psi^1_{kto}\cdot\frac{1}{\overline{\hat{p}}_{dkto}} \\
&\quad \geq -\eta_{do|k=t} + \sum_{s\in\mathcal{S}} C^{\mathrm{op}}_s\cdot\hat{p}^{\mathrm{AD}^1}_{dskto} + \sum_{r'\in\mathcal{R}} C^{\mathrm{op}}_{r'}\cdot\hat{p}^{\mathrm{AD}^1}_{dr'kto} + C^{\mathrm{op}}_d\cdot(1 - z_{do|k=t}),
\end{aligned} \qquad \forall(k\in t), d, t, o \tag{5.22b}$$

$$\begin{aligned}
&\pi^{\mathrm{D}^1}_{dkto} + \psi^1_{kto}\cdot\frac{1}{\overline{\check{p}}_{dko}} \\
&\quad \geq \eta_{do|k=t} - \sum_{s\in\mathcal{S}} C^{\mathrm{op}}_s\cdot\check{p}^{\mathrm{AD}^1}_{dskto} - \sum_{r'\in\mathcal{R}} C^{\mathrm{op}}_{r'}\cdot\check{p}^{\mathrm{AD}^1}_{dr'kto} - C^{\mathrm{op}}_d\cdot(1 - z_{do|k=t}),
\end{aligned} \qquad \forall(k\in t), d, t, o \tag{5.22c}$$

$$\lambda^{\mathrm{R}^1}_{rkto} + \psi^1_{kto} \cdot \frac{1}{\hat{\bar{p}}_{rkto}} \geq -\mu_{ro|k=t} - \sum_{s\in\mathcal{S}} C^{\mathrm{op}}_s \cdot \hat{p}^{\mathrm{AR}^1}_{rskto} - \sum_{r'\in\mathcal{R}} C^{\mathrm{op}}_{r'} \cdot \hat{p}^{\mathrm{AR}^1}_{rr'kto}, \qquad \forall(k\in t), r, t, o \tag{5.22d}$$

$$\pi^{\mathrm{R}^1}_{rkto} + \psi^1_{kto} \cdot \frac{1}{\check{\bar{p}}_{rkto}} \geq \mu_{ro|k=t} + \sum_{s\in\mathcal{S}} C^{\mathrm{op}}_s \cdot \check{p}^{\mathrm{AR}^1}_{rskto} + \sum_{r'\in\mathcal{R}} C^{\mathrm{op}}_{r'} \cdot \check{p}^{\mathrm{AR}^1}_{rr'kto}, \qquad \forall(k\in t), r, t, o \tag{5.22e}$$

5.4 Case Studies

5.4.1 Test System Setup

The data-driven DRO-based planning model described above is tested on a modified European CIGRE low voltage network [140] sketched in Fig. 5.1 and load and line parameters defined in Appendix A.3. It is assumed that the network is operated in the islanded mode with no connection to the grid. One SG unit is already installed at node 1. The investment candidates include three Photo-Voltaic (PV) units PV_1 and PV_2 and PV_3; three Energy Storage (ES) units denoted ES_1 and ES_2 and ES_3; three diesel generators i.e., SG units SG_1 and SG_2 and SG_3, with the capacity of each set at 0.55 MW. Candidate units with subscripts "$_1$", "$_2$" and "$_3$" are located at nodes 11, 17 and 18, respectively. The investment and operational costs are shown in Table. 5.1. The load profiles and renewable generation profiles have been obtained from [141] using UK values in 2019. A single year planning period is considered including a varying number of representative days with a planning horizon of 24 hours for each representative day. The

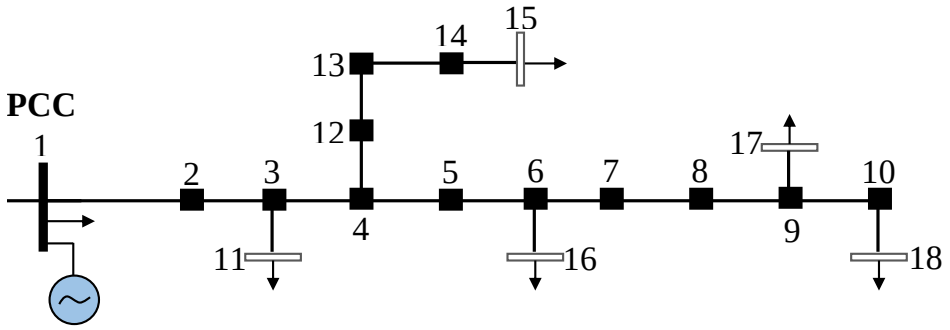

Figure 5.1: Modified European CIGRE low voltage network.

Table 5.1: Investment costs of different technologies

Technology	Battery (ES)	Solar (PV)	Diesel (SG)
Investment Cost [M£/MW]	0.98	0.84	0.54
Annualized Investment Cost [£/MW]	96040	56280	36180
Operation Cost [£/MW/h]	-	0	150

Table 5.2: Variation of investment costs, decisions, and operating costs with the budget of uncertainty

			Investment Decisions			
Budget [Γ]	Investment Cost [M£]	Operation Cost [M£]	PV	ES	SG	Comp. Time [s]
0	0.0310	0.1283	PV_3	-	-	108
1	0.0929	0.1607	PV_1, PV_2, PV_3	-	-	222
2	0.0929	0.3361	PV_1, PV_2, PV_3	-	-	342
3	0.0929	0.4986	PV_1, PV_2, PV_3	-	-	452
4	0.0929	0.5404	PV_1, PV_2, PV_3	-	-	571
5	0.1102	0.5715	PV_1, PV_2, PV_3	-	SG_3	683
6	0.1102	0.5848	PV_1, PV_2, PV_3	-	SG_3	804
7	0.1102	0.5848	PV_1, PV_2, PV_3	-	SG_3	919
8	0.1102	0.5848	PV_1, PV_2, PV_3	-	SG_3	1040

simulation was performed in Python using Pyomo [85] to model the optimisation problem and Gurobi [86] employed as a solver.

5.4.2 Optimal Solution Versus Budget of Uncertainty

The robustness and thus conservatism of the model can be varied by the budget of uncertainty. A higher budget of uncertainty corresponds to the widening of the uncertainty spectrum captured in the model parameters. In the study network, a maximum value of eight includes the forecast errors of both the loads (five) and renewable generations (three) available. In Table 5.2, the effect of an increase in the budget of uncertainty to the investment decisions and operating costs is presented considering two representative days. It should be noted that the case of zero budget of uncertainty is similar to the stochastic solution of the problem. Both the total investment and operational costs are seen to increase with the former reaching a plateau at a value of four while the latter becomes constant at a value of six. At zero, a total cost of 0.1503 M£ is recorded compared to a value of 0.695 M£ at the maximum budget of uncertainty. While the maximum value of the budget of uncertainty captures all potential forecast errors within the ambiguity set, it can be rather conservative.

5.4.3 Optimal Solution Versus Number of Representative days

By increasing the number of representative days in the ambiguity set of a DRO problem, the distributional nature of the uncertainty is better captured. In Fig. 5.2, the result of

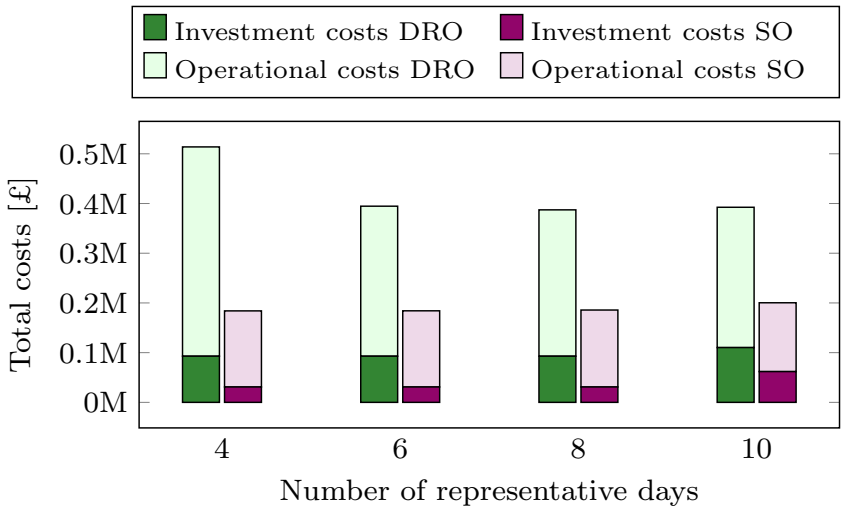

Figure 5.2: Total costs under different number of representative days for DRO and SO models.

variation of the number of representative days is presented for both the proposed DRO model and the SO model. The budget of uncertainty for the DRO model is set to four in this case study. The total costs in the proposed DRO model are shown to reduce with an increase in the number of representative days with total costs recorded at 0.5139 M£ at four representative days compared to 0.3924 M£ at ten representative days. While the investment costs increase with more representative days, the operational costs indicate a decline.

Table 5.3 presents the investment decisions taken under DRO and SO uncertainty handling. With more representative days, the available usable power from the renewable sources is better represented and thus more usable. Additionally, the variations in forecast load profiles are better represented with the increased operational scenarios i.e., representative days. The load variations require flexibility in available generation. This flexibility requirement is fulfilled by the installation of the SG unit in the case of ten representative days preventing any load curtailment. The overall result indicates a lower cost and less conservative optimal solution with more representative days. On the other hand, both investment and operational costs in the case of SO are shown to increase with an increase in the representative days. Nonetheless, the total costs in the case of DRO are higher than that with SO as the latter provides a more optimistic solution while the former presents a more robust solution. Table 5.3 presents the investment decisions taken under DRO and SO uncertainty handling.

Table 5.3: Investment decisions under DRO and SO models for increasing representative days and $\Gamma = 4$.

	DRO		SO	
Rep. Days	Decision	Comp. Time [s]	Decision	Comp. Time [s]
4	PV_1, PV_2, PV_3	109	PV_1	44
6	PV_1, PV_2, PV_3	333	PV_1	118
8	PV_1, PV_2, PV_3	682	PV_1	217
10	PV_1, PV_2, PV_3, SG_3	1175	PV_1, PV_2	476

5.4.4 Computational Performance

In Table 5.2, it is indicated that an increase in the budget of uncertainty results in the exponential increment of simulation time of the DRO problem. A similar result is obtained in Table 5.3 with more representative days considered in the analysis. Both increments are due to the widening of the uncertainty spectrum captured in the model parameters, i.e., the applied budget of uncertainty, and in the available data, i.e., the representative operation scenarios. However, as compared to the SO model (see Table 5.3), the computational time in the case of the DRO is much greater. A compromise between the data captured and the model parameters must be made to minimise the computational effort.

5.5 Conclusion

In practice, electrification of remote and islanded communities with no connection to the main grid is entangled with many techno-economic issues. The intermittency in power supply from the renewable energy generation in addition to the load demand variations leads to further complexities during system modelling. In this chapter, a DRO-based MILP planning model for the design of islanded MGs has been presented. A moment-based ambiguity is utilised to represent the inherent uncertainty in load and renewable power generation. A three-step approach to reformulate the model into a tractable optimisation problem using LDRs and duality theory is proposed. The model has been applied to a low-voltage CIGRE network and planning decisions are analysed against the budget of uncertainty, available distributional information modelled by various representative days and additionally compared to the SO model.

Chapters 4 and 5 have presented techniques that enhance the modelling accuracy of optimisation problems for the secure analysis of the MG operation. The robustness of the DRO technique with the flexibility to incorporate as much probabilistic information as possible renders it imperative to the analysis of HILP events. This ensures that

adequate power generation and potentially control support are present in the network given the occurrence of an emergency event. This is especially beneficial due to the lack of statistical information on the nature of injections in power networks, especially during potential destructive events. However, its conservatism and computational inefficiency can be a deterrent to its adoption. Moreover, as the accuracy of the SO model increase with available data, this simultaneously significantly increases the number of variables and constraints, and the problem may become intractable. Both network modelling accuracy and uncertainty handling are vital to the security and resilience of the network however the system operator should take into consideration aspects such as the required accuracy, robustness of the solution, and the computational efficiency. In the next chapters, the MG planning problem is further enhanced to consider not only steady-state but additionally dynamic security in system analysis.

Part III

Transients-Aware Planning Methodologies

Chapter 6

Inertia-Aware Investment and Operational Planning Models for Microgrids

In previous chapters, the basic models for planning in active distribution methods and Microgrids (MGs) have been presented. Convexification techniques have been applied to approximate the power flows to ensure tractability of the model as well as stochastic and robust methods to handle uncertainty. Thus far, only steady-state security constraints have been applied to planning models for the microgrids studied. In this chapter, an approach to include dynamic or transient frequency security constraints based on frequency trajectories in the transition mode between grid-connected and islanding during emergency events into the planning problem is proposed. A microgrid is able to transition to an islanded state in case of major faults occurring in the main grid. This process ensures service continuity to critical customers, however, such a transition can include large excursions in the transient state. The frequency response during transition is described by a set on non-linear equations that would result in a non-linear planning model directly applied to the planning problem. This chapter proposes an iterative algorithm that incorporates transient inertia constraints in a planning problem and ensures both static and transient security during microgrid planning. The work in this chapter is presented in publication [C4] and [J2].

6.1 Introduction and Related Work

The islanding capability of a MG is critical in enhancing resilience by ensuring continuity and mitigating interruptions of energy supply to consumers in the event of extreme weather conditions or significant faults in the bulk transmission grid [142, 143]. The successful island creation, especially following disastrous events, is subject to the secure transient performance of DERs, thus ensuring the survivability of the MG. However, unlike traditional bulk grids, MGs are inherently faced with a lack of rotational inertia and damping capability affecting their security in the event of significant power imbalance [12, 144]. A MG is considered secure if all equipment (e.g., lines and generators) operate within their technical limits and tolerances avoiding subsequent network disconnections and associated risk of cascading failures [145]. Thus, it is vital to design a resilient and reliable MG able to withstand both High-Impact-Low-Frequency (HILF) and Low-Impact-High-Frequency (LIHF) uncertainties, under static and transient operational constraints. On the one hand, static islanding constraints ensure the MG's operational adequacy in supplying the forecasted electricity demand. On the other hand, transient islanding constraints ensure the MG's operational security by adhering to a dynamic response within the defined regulatory limits and, consequently, avoiding the operation of protective devices that would result in DER disconnections.

Related Work

Different planning tools including stochastic [102], robust [33, 108–110], and distributionally robust [146] approaches have been previously presented in the literature for optimal investment in distribution networks and MGs aiming at enhancing system resilience to extreme contingencies. In [102], a stochastic model has been proposed for optimal investment in distribution networks under different disastrous events characterized by a set of scenarios. In [108], a robust resilience-constrained MG planning model is introduced under the uncertainty of loads and power generation of Renewable Energy Sources (RESs), with islanding from the main grid considered as another source of uncertainty. In [109], a robust defender-attacker-defender model is presented for optimal hardening planning in resilient distribution networks, considering topology reconfiguration and islanding formation. Besides, in [33], a robust model is proposed for hardening and investment planning in distribution networks based on a multi-stage and multi-zone uncertainty modeling of spatial and temporal characteristics of natural disasters. Additionally, a distributionally robust resilience-constrained investment planning model under natural disasters is introduced in [146], where a moment-based ambiguity set characterizes extreme events. These

however neglect both static and transient frequency metrics in their formulations.

In [147], static frequency security for primary, secondary, and tertiary control levels in MGs has been studied, however, transient frequency security was not considered. The inclusion of transient frequency constraints is complex due to the large number of equations required to represent the frequency trajectories based on the type characteristic generator type and distinct dynamic response they exhibit [42]. Such high-order models can result in intractability when applied to an optimisation problem. The multi-machine frequency model is reduced to a one-machine model using the concept of single-machine equivalent (SME) to obtain a system equivalent [42, 148]. An adaptive load frequency sensitivity index has been derived in [149] to ensure sufficient frequency regulating reserve is available to aid the fast return of the system frequency to normal limits in case of contingency. In [150] a transient stability-constrained Optimal Power Flow (OPF) is proposed where limits on rotor angle deviations estimated using a one-machine infinite-bus equivalent, are applied to facilitate secure frequency response. A discretized transient response is embedded in the OPF problem in [151] to ensure a secure transient frequency response.

In [152] and [153] a simplification of the SME Centre of Inertia (CoI) to a single linear first-order differential equation is adopted. In [152], an analytical formulation is presented to limit the Rate-of-Change-of-Frequency (RoCoF), while [153] uses the first model of transient frequency metrics to analyse the post-fault response. Such simplified frequency response models tend to describe system dynamics inaccurately and cannot quantify the support provided by different units. Additionally, this model considers a system with only converter interfaced generators. A reduced second-order model is used in [154] to determine sufficient synthetic inertia and droop slopes for a collection of traditional and inverter-interfaced generators that satisfy both steady-state and dynamic frequency requirements. Moreover, in [155] and [1], the unit commitment problem is solved under frequency-related constraints for traditional and low-inertia grids, where frequency-related constraints are derived based on a low-order non-linear frequency response model [43]. The low-order model in [43] ignores small time constants providing a model that approximates the system frequency performance while including the essential behavior of speed governing and turbine response.

Even though the literature offers several operational planning models for traditional bulk grids under dynamic security constraints [1, 150–155], previous resilience-constrained investment planning models for MGs [108, 156], and even active distribution networks [33, 102, 108, 109], have only considered static operational constraints rather than dynamic. Nevertheless, all aforementioned studies have certain drawbacks, as they are based on ei-

ther simplified dynamic models [152–154], linearized frequency-related constraints [155], or make *ex-ante* bound extractions on the relevant variables [1] to simplify the planning model. Furthermore, the simplifications therein represent the characteristic properties of transmission networks rather than active distribution networks and MGs. Accordingly, it is vital to present a resilience-oriented MG planning tool, including both static and transient constraints, based on a detailed dynamic model to ensure satisfactory operation given the abrupt main grid disconnection in the event of extreme contingencies.

Contributions

The contribution of this chapter is threefold.

First, a min-max-min, stochastic-robust, investment and operational planning model, to design a resilient MG under both HILF and LIHF uncertainties is proposed. The HILF uncertainty pertains to the unscheduled islanding of the MG from the main grid while the LIHF uncertainties relate to correlated load and RES generation. For the latter, the k-means clustering technique is used to obtain a sufficient number of scenarios (i.e., representative days) characterising different realisations of LIHF uncertainties. The stochastic approach obtains an optimal solution over all LIHF scenarios while the robust approach immunises each scenario (i.e., every hour of each representative day) against the power loss associated with the unscheduled islanding of the MG (i.e., HILF scenario) at an optimized cost.

Second, an inclusion of both static and transient islanding constraints (i.e., the maximum RoCoF and the frequency nadir as transient-state criteria, and the frequency deviation as a quasi steady-state criterion) in the proposed model to ensure resilience under HILF and LIHF uncertainties. The transient constraints are analytically derived based on the Center-of-Inertia (CoI) frequency response model of the system.

Third, a tractable three-stage solution approach is proposed to solve the model as the developed min-max-min, hybrid, stochastic-robust investment problem with a non-linear frequency response cannot be solved directly.

The rest of the chapter is organised as follows. Section 6.2 presents the modelling assumptions and notation adopted throughout the chapter while Section 6.3 presents the frequency response model used to derive the analytical transient frequency metrics. In Section 6.4, the planning model is described in a compact form together with the main modelling preliminaries. Section 6.5 presents the detailed problem formulation under static and transient islanding constraints. Section 6.6 describes the test network and

input data applied, whereas Section 6.7 discusses the application of the proposed investment planning model on the CIGRE 18-node distribution network in order to design a resilient MG under different operating conditions. Finally, Section 6.8 concludes this chapter.

6.2 Modelling Preliminaries

In this chapter, the uncertainty pertaining to the unscheduled islanding of the MG from the main grid is considered as HILF due to its severe impact on the MG brought about by the loss of a large power in/outfeed from/to the main grid and its low probability of occurrence. In addition, uncertainties pertaining to load and renewable generation are considered as LIHF due to their low impact but high probability of occurrence. For instance, the load of the MG at each hour of a single day is a continuous uncertain parameter, and this uncertain parameter can be repeated $24 \times 365 = 8760$ times per year. On the contrary, a MG may face only a few unscheduled islandings per year. Therefore, the former is a high-frequency uncertainty while the later is a low-frequency one.

Both types of uncertainties have been considered in the proposed stochastic-robust model to enhance the resilience of the MG. In general, a stochastic approach finds a solution that is optimal on average for a set of scenarios characterising uncertain parameters, while a robust approach finds a solution that is optimal for the worst-case realisation of uncertain parameters. In this study, a stochastic approach is utilised to characterise the uncertainty of load and renewable generation by a set of scenarios, named as representative days. In addition, a robust approach is utilised to characterise the uncertainty of unscheduled islanding from the main grid. The proposed approach considers the possibility of an islanding event for all hours of each representative day. Hence, it is robust against a disruptive event at all hours of each representative day.

The main modelling preliminaries in the proposed investment planning model are:

- Without loss of generality, a single-year planning horizon is considered rather than a multi-year one to reach a compromise between accuracy and tractability of the proposed model.
- To capture interday/intraday variation/ramping of uncertain loads and power generation of RESs, a sufficient number of representative days (i.e., *scenarios*) is considered, obtained by the k-means clustering technique [157].

- A single scheduling period of each representative day is considered to be *one hour* both in grid-connected and islanded modes.
- The MG is assumed to have a radial network topology, as such, a linearised version of the DistFlow model is used for the power flow formulation to obtain a linear optimisation problem [158,159]. Additionally, the quadratic line flow expressions are linearised using a piecewise linear approximation [160]. Finally, a constant marginal cost is utilised to eliminate the non-linearity of quadratic cost functions [157].
- It is assumed that an unscheduled islanding event might happen at *each* period of the representative days considered.
- After an islanding, a single period of islanded operation is assumed and the probability of further contingencies in the islanded mode is not considered.

Furthermore, all indices, parameters, sets, and variables used in this chapter are presented in the nomenclature.

Nomenclature

Functions

$\Theta^{\mathbf{gm,opr}}$	Total operational costs in grid-connected mode [$].
$\Theta_{to}^{\mathbf{im,opr}}$	Total penalty costs of disconnecting loads from MG at hour t in representative day o in islanded mode [$].
$\breve{\Theta}^{\mathbf{im,opr}}$	Vector-valued function of total penalty costs of disconnecting loads from MG in islanded mode [$].
$\Theta^{\mathbf{inv}}$	Total investment costs [$].

Indices

g	Index of generators, $g \in \{c, d, i, v\}$.
i	Index of nodes, i^+/i^- being a node before/after node i.
o	Index of representative days.
t	Index of hours.
ψ	Index of iterations.
l	Index of lines, l^{i^+}/l^{i^-} being the line connecting upstream/downstream of node i.

Parameters

c_{go}	Daily capacity factor of generator g in representative day o.

$d_{ito}^{\mathrm{p_c/q_c}}$	Constant part of active/reactive load power [kW/kVAr].
e_{io}	Flexible energy demand of node i in representative day o [kWh].
$e_{to}^{\mathrm{b/s}}$	Buying/selling price of electricity from/to the main grid at hour t in representative day o [$/kWh].
e_g^{FR}	Minimum reserve energy capacity for transient frequency response of generator g [kWh].
fc_i	Penalty cost of shifting demand at node i [$/kWh].
ic_g	Annualised investment cost of generator g [$].
ic_l	Annualised investment/reinforcement cost of a line l [$].
mc_g	Marginal cost of generator g [$/kWh].
pc_i	Penalty cost of disconnecting demand at node i [$/kWh].
p_{gto}^{AV}	Maximum available power for CIG unit g at hour t in representative day o [kW].
p_g^{FR}	Minimum reserve power capacity for transient frequency response of generator g [kW].
p_g^{nom}	Nominal capacity of CIG and SG g [kW].
$r_g^{\mathrm{dn/up}}$	Ramp-down/ramp-up limit of generator g [kW/h].
$r_{l^{i^-}}$	Resistance of the line l connecting nodes (i, i^-) [Ω].
$x_{l^{i^-}}$	Reactance of the line l connecting nodes (i, i^-) [Ω].
$\overline{S}_{l^{i^-}}$	Capacity of the line l connecting nodes (i, i^-) [kVA].
$z_{l^{i^-}}^0$	Initial status of a line l connecting nodes (i, i^-) (i.e., 1/0: built/not-built).
α	Scaling factor.
ζ	Damping ratio.
ω_n	Natural frequency [Hz].
τ_o	Weighting factor of representative day o.
ϵ	Corrective power deviation tolerance [kW].

Sets

$\mathcal{C}$	Set of CIGs, $\mathcal{C}^i$ being the set of generators connected to node i.
$\mathcal{C}^{d/v}$	Set of CIGs with droop/VSM control scheme.
$\Omega^{\mathrm{gm,opr}}$	Feasible space of operational variables in grid-connected mode.
$\Omega^{\mathrm{im,opr}}$	Feasible space of operational variables in islanded mode.
Ω^{inv}	Feasible space of investment-related variables.
$\mathcal{L}$	Set of lines connecting neighbouring nodes.
Ω^{MG}	Feasible space of the MG planning problem.

$\mathcal{N}$ Set of nodes, $\mathcal{N}^i$ being the set of nodes after and connected to node i.

$\mathcal{O}$ Set of representative days.

$\mathcal{S}$ Set of SGs, $\mathcal{S}^i$ being the set of generators connected to node i.

$\mathcal{T}$ Set of hours in a representative day.

Symbols

$\hat{\bullet}/\check{\bullet}$ Upward/downward deviations of the quantity $\bullet$ in the islanded mode from its value in the grid-connected mode (i.e., $\hat{d}^{\mathrm{pf}}_{ito}$, $\check{d}^{\mathrm{pf}}_{ito}$ and $\hat{d}^{\mathrm{qf}}_{ito}$, $\check{d}^{\mathrm{qf}}_{ito}$).

$|\bullet|$ Cardinality of the set $\bullet$.

$\underline{\bullet}/\overline{\bullet}$ Lower/upper bounds of the quantity $\bullet$.

Variables

$d^{\mathrm{p/q}}_{ito}$ Active/reactive load power at node i, hour t, and representative day o [kW/kVAr].

$d^{\mathrm{pf/qf}}_{ito}$ Flexible part of active/reactive load power at node i, hour t, and representative day o [kW/kVAr].

p/q_{gto} Active/reactive power generation of generator g at hour t and representative day o [kW/kVAr].

$p/q^{\mathrm{b/s}}_{to}$ Active/reactive power bought/sold to the main grid at hour t and representative day o [kW/kVAr].

$P_{l^{i^-}to}$ Active power flow of a line connecting nodes (i, i^-) at hour t and representative day o [kW].

$Q_{l^{i^-}to}$ Reactive power flow of a line connecting nodes (i, i^-) at hour t and representative day o [kVAr].

v_{ito} Voltage magnitude at node i, hour t, and representative day o [V].

y_{ito} Binary variable indicating the connection status of load at node i, hour t, and representative day o (i.e., 1/0: connected/disconnected).

z_g Binary variable indicating the investment status of generator g (i.e., 1/0: built/not-built).

$z_{l^{i^-}}$ Binary variable indicating the investment/reinforcement status of a line connecting nodes (i, i^-) (i.e., 1/0: built/not-built).

Vectors

χ Vector of all investment and operational variables.

$\chi^{\mathrm{gm,opr}}$ Vector of "wait-and-see" operational variables in grid-connected mode.

$\chi^{\mathrm{im,opr}}$ Vector of "wait-and-see" operational variables in islanded mode.

χ^{inv}	Vector of "here-and-now" investment variables.

6.3 Analytic Formulation of the Transient Frequency Metrics

The frequency response model adopted in this chapter is based on the uniform representation of frequency transients initially presented in [43] for a system of only SGs and modified in [1, 161] for a low-inertia system. The dynamic model illustrated by the block diagram in Fig. 6.1 comprises of both traditional SGs (indexed by $i \in \mathcal{S}$) and CIGs (indexed by $c \in \mathcal{C}$). The impact of *grid-supporting* CIGs providing frequency support via droop ($d \in \mathcal{C}^d \subseteq \mathcal{C}$) and Virtual Synchronous Machine (VSM) ($v \in \mathcal{C}^v \subseteq \mathcal{C}$) control is also included, as these are the two most common control approaches in the literature [46, 162].

By analysis of the block diagram in Fig. 6.1, the transfer function $G(s)$ between the active power change $\Delta P_e(s)$, where positive values corresponding to a net load decrease, and the CoI frequency deviation $\Delta f(s)$ can be derived as:

$$G(s) = \frac{\Delta f(s)}{\Delta P_e(s)} = \Bigg(\underbrace{(sM_s + D_s)}_{\text{SGs swing dynamics}} + \underbrace{\sum_{i \in \mathcal{S}} \frac{K_i(1 + sF_iT_i)}{R_i(1 + sT_i)}}_{\text{SGs turbine \& governor response}} + \underbrace{\sum_{d \in \mathcal{C}^d} \frac{K_d}{R_d(1 + sT_d)}}_{\text{droop-based CIGs}} + \underbrace{\sum_{v \in \mathcal{C}^v} \frac{sM_v + D_v}{1 + sT_v}}_{\text{VSM-based CIGs}} \Bigg)^{-1}. \tag{6.1}$$

where M_s and D_s denote the aggregated normalised inertia and damping of SGs respectively, while K_i, F_i, T_i and R_i refer to the mechanical gain factor, fraction of total power generated by the SG turbine, turbine time constant and droop of SG i, respectively. Parameters K_d, R_d and T_d define the power gain factor, droop and and time constant of the droop-based CIG d, respectively, and M_v, D_v and T_v denote the virtual inertia constant, virtual damping constant and time constant of of the VSM-based CIGs v.

It is noteworthy to mention that while different generators can have slightly distinct transient frequency response, the dynamics described by the CoI swing equation with aggregate inertia M_s and damping D_s has been shown to adequately capture the system behaviour [43, 161]. Also, droop-based CIGs consider only the damping capability of the

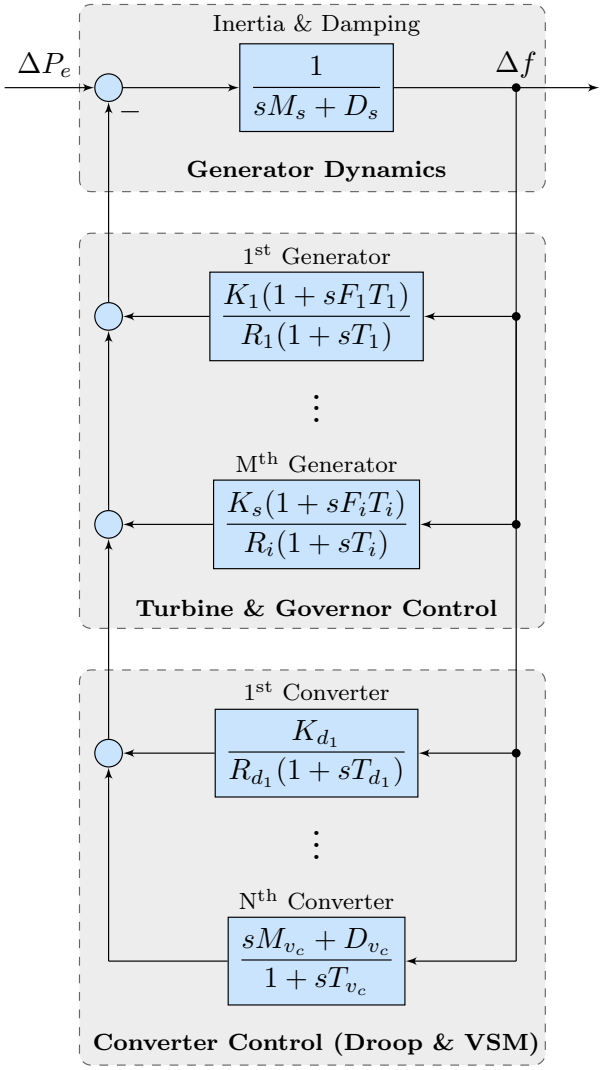

Figure 6.1: Uniform system frequency dynamics model [1]

converter (i.e., $D = 1/R_d$) while the VSM-based CIGs consider both the damping and the "inertia" capability of the converter (i.e., D_v and M_v, respectively) [161]

Assuming that the time constants ($T_i \approx T$) of all SGs are orders of magnitude higher than the ones of converters [163], one can approximate $T \gg T_{d,v} \approx 0$, which transforms (6.1) into:

$$G(s) = \frac{1}{MT} \frac{1 + sT}{s^2 + 2\zeta\omega_n s + \omega_n^2}, \tag{6.2}$$

where $\omega_n = \sqrt{\frac{D+R_s}{MT}}$ and $\zeta = \frac{M+T(D+F_s)}{2\sqrt{MT(D+R_s)}}$. The parameters are calculated as follows:

$$M_s = \sum_{i \in \mathcal{S}} M_i \frac{P_i}{P_{b_s}}, \qquad D_s = \sum_{i \in \mathcal{S}} D_i \frac{P_i}{P_{b_s}}, \tag{6.3a}$$

$$R_s = \sum_{i \in \mathcal{S}} \frac{K_i}{R_i} \frac{P_i}{P_{b_s}}, \qquad F_s = \sum_{i \in \mathcal{S}} \frac{K_i F_i}{R_i} \frac{P_i}{P_{b_s}}, \tag{6.3b}$$

$$M_c = \sum_{v \in \mathcal{C}^v} M_v \frac{P_{c_v}}{P_{b_c}}, \qquad D_c = \sum_{v \in \mathcal{C}^v} D_v \frac{P_{c_v}}{P_{b_c}}, \tag{6.3c}$$

$$R_c = \sum_{d \in \mathcal{C}^d} R_d \frac{P_{c_d}}{P_{b_c}}, \tag{6.3d}$$

$$M = \frac{M_s P_{b_s} + M_c P_{b_c}}{P_{b_g} + P_{b_c}}, \tag{6.3e}$$

$$D = \frac{D_s P_{b_s} + D_c P_{b_c} + R_c P_{b_c}}{P_{b_s} + P_{b_c}}. \tag{6.3f}$$

Parameter P_i and P_c denotes the active power capacity of the SG and CIG, respectively, scaled over their respective sums of active power capacity of all connected SGs and CIGs, P_{b_s} and P_{b_c}.

Following a disturbance, the dynamic frequency response is characterized by the instantaneous RoCoF ($\dot{f}_{\max}$) and frequency nadir ($\Delta f_{\max}$), whereas the steady-state response is governed by the constant frequency deviation from a pre-disturbance equilibrium (Δf_{ss}). Assuming a step-wise disturbance in the active power $\Delta P_e(s) = -\Delta P/s$, where ΔP is the net power change, the time-domain expression for frequency deviation ($\omega(t) \equiv \Delta f(t)$) can be derived as follows:

$$\omega(t) = -\frac{\Delta P}{M}\left(\frac{1}{T\omega_n^2} + \frac{1}{\omega_d} e^{-\zeta\omega_n t}\left(\sin\omega_d t - \frac{1}{\omega_n t}\sin\omega_d t + \phi\right)\right), \tag{6.4}$$

where $\omega_d = \omega_n\sqrt{1-\zeta^2}$ and $\phi = \sin^{-1}\left(\sqrt{1-\zeta^2}\right)$.

The maximum RoCoF occurs at $t_r = 0^+$, the instance of the disturbance i.e., $\dot{\omega}_{max} = \dot{\omega}(t_r)$. The time-domain expression for RoCoF can be therefore obtained by solving $\dot{\omega}(t_r)$ and is derived as:

$$\dot{f}_{\max} = \dot{f}(t_0^+) = -\frac{\Delta P}{M}, \tag{6.5}$$

The frequency nadir described in (6.6) occurs at the time instance t_m when $\dot{\omega}(t_m) = 0$,

this is derived as:

$$\Delta f_{\max} = -\frac{\Delta P}{D + R_s}\left(1 + \sqrt{\frac{T(R_s - F_s)}{M}}e^{-\zeta\omega_n t_m}\right), \tag{6.6}$$

with $t_m = \left({}^{1}/_{\omega_d}\right)\tan^{-1}\left({}^{\omega_d}/_{(\omega_n\zeta - T^{-1})}\right)$.

Finally, the quasi steady-state frequency given in (6.7) is derived from (6.4) for $t \to \infty$ as:

$$\Delta f_{\text{ss}} = -\frac{\Delta P}{D + R_s}, \tag{6.7}$$

It is clear that the aggregate system parameters such as M, D, R_g and F_g have a direct impact on frequency performance. In particular, RoCoF and steady-state deviation are explicitly affected by M and (D, R_g), respectively, while frequency nadir has a non-linear dependency on all four system factors. With the increasing penetration of CIGs and subsequent decommissioning of conventional SGs, these parameters are drastically reduced and can compromise the overall frequency performance. To prevent the accidental activation of load-shedding, under/over frequency and RoCoF protection relays, the proposed three-stage solution algorithm, described in the following, imposes limits on the aforementioned frequency metrics to account for low levels of inertia and damping and their impact on the frequency response after a MG islanding. The analytical model and closed-form expressions defining the different metrics have been verified and studied in [164], [148] and [165].

6.4 Problem Description

6.4.1 Compact Formulation under Static Constraints

The proposed min-max-min investment and operational planning model under static operational constraints in grid-connected and islanded mode can be presented in compact form as:

$$\min_{\chi \in \Omega^{\text{MG}}} \ \Theta^{\text{inv}}(\chi^{\text{inv}}) + \Theta^{\text{gm,opr}}(\chi^{\text{inv}}, \chi^{\text{gm,opr}}) + ||\breve{\Theta}^{\text{im,opr}}(\chi^{\text{inv}}, \chi^{\text{gm,opr}}, \chi^{\text{im,opr}})||_{\infty}, \tag{6.8}$$

where $\Omega^{\text{MG}} = \{\chi = [\chi^{\text{inv}}, \chi^{\text{gm,opr}}, \chi^{\text{im,opr}}] \,|\, \chi^{\text{inv}} \in \Omega^{\text{inv}}\,;\, \chi^{\text{gm,opr}} \in \Omega^{\text{gm,opr}}\,;\, \chi^{\text{im,opr}} \in \Omega^{\text{im,opr}}\}$, $\breve{\Theta}^{\text{im,opr}} = [\min\, \Theta^{\text{im,opr}}_{11}, ..., \min\, \Theta^{\text{im,opr}}_{n^{\text{T}},n^{\text{O}}}]$, $n^{\text{T}} = |\mathcal{T}|$, and $n^{\text{O}} = |\mathcal{O}|$. Thus,

$||\breve{\Theta}^{\text{im,opr}}||_\infty = \max(\min_{\forall t,\forall o} \Theta_{to}^{\text{im,opr}})$. Hence, the objective function (6.8) minimizes the total investment costs (Θ^{inv}), the *"expected"* total operation costs in grid-connected mode for all hours of all representative days ($\Theta^{\text{gm,opr}}$), and the *"worst-case"* total penalty costs of disconnecting loads from MG in islanded mode for all hours in all representative days ($\Theta^{\text{im,opr}}$).

The min-max-min objective function (6.8) can be rewritten as a single minimisation problem by using the auxiliary variable γ:

$$\min_{\chi \in \Omega^{\text{MG}}} \ \Theta^{\text{inv}}(\chi^{\text{inv}}) + \Theta^{\text{gm,opr}}(\chi^{\text{inv}}, \chi^{\text{gm,opr}}) + \gamma \tag{6.9a}$$

$$\text{s.t.} \quad \gamma \geq \Theta_{to}^{\text{im,opr}}(\chi^{\text{inv}}, \chi^{\text{gm,opr}}, \chi^{\text{im,opr}}), \ \forall t \in \mathcal{T}, o \in \mathcal{O}, \tag{6.9b}$$

The optimisation problem (6.9) is a Mixed-Integer Linear Programming (MILP) problem, and as such can be solved by available software packages to obtain optimal investment and operation decisions in grid-connected and islanded mode.

However, the operation decisions may violate transient islanding constraints. To remedy such limitation and ensure MG resilience before and after an islanding event, a non-linear model for evaluation of the transient frequency response of a MG after islanding can be incorporated. The resulting problem becomes a Mixed-Integer Non Linear Programming (MINLP) problem that is intractable for practical applications. A three-stage methodology that incorporates the transient frequency constraints through sequential linearization and iterative tightening of power bounds is thus proposed.

6.4.2 Three-Stage Solution Algorithm

The proposed three-stage approach proposed for solving the problem (6.9) with the inclusion of static and transient security constraints is illustrated in Fig. 6.2 and can be summarised as follows:

6.4.2.1 Stage 1: Solving the Static Investment Planning Problem

At each iteration ψ, the investment planning model (6.9) is first solved under static security constraints in both grid-connected and islanded mode. In the case that transient frequency security is desired to ensure MG survivability during abrupt islanding, the process flow to Stages 2 and 3 can be adopted. Otherwise, the process flow terminates at Stage 1 where only grid-connected and static islanding requirements are met. A detailed formulation is provided in Section 6.5.1.

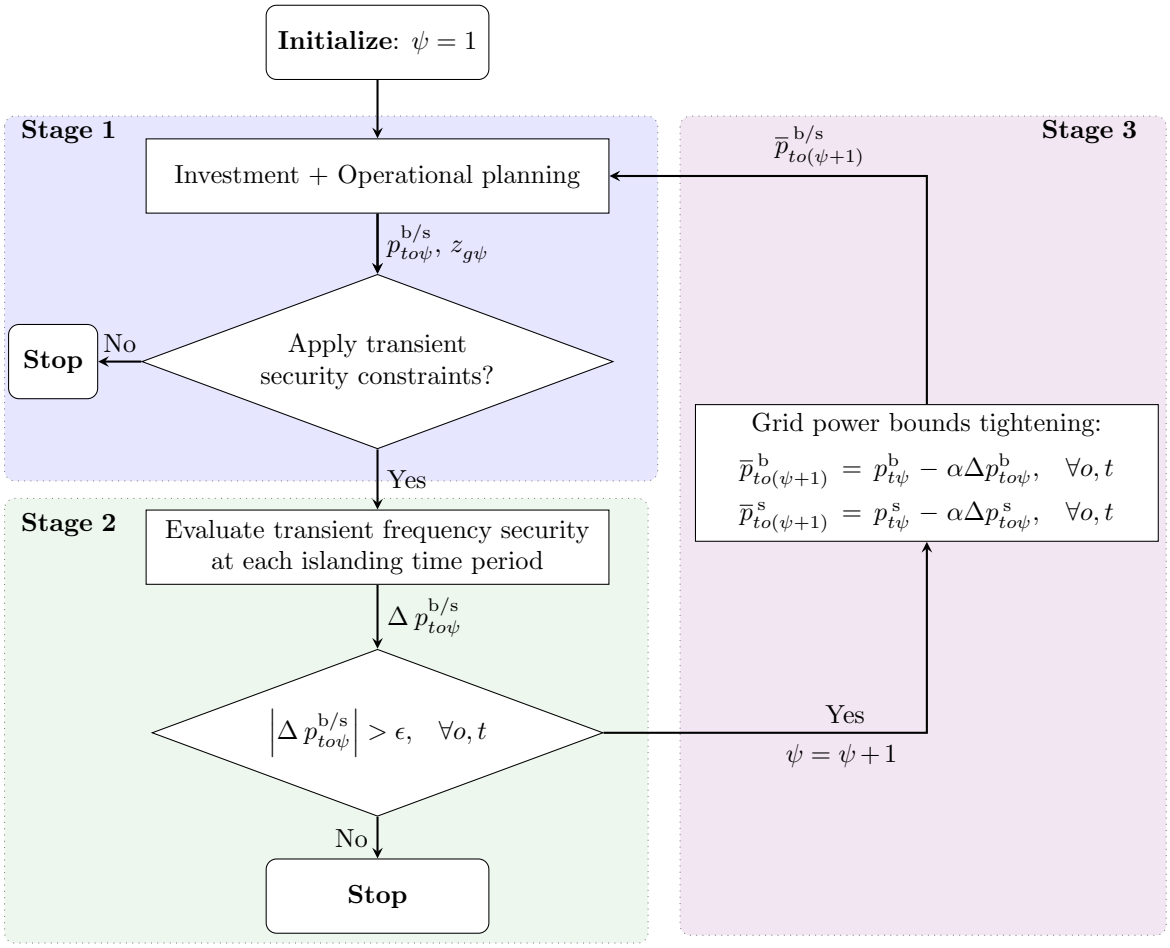

Figure 6.2: Proposed three-stage inertia-aware MG planning algorithm.

6.4.2.2 stage 2: Evaluating Transient Frequency Security

The unscheduled loss of power exchange with the main grid may result in large frequency transients within the MG. Following the discussion from Section 6.3, the transient frequency response is characterised by the magnitude of the abrupt active power loss (ΔP) and the aggregate control parameters of all MG generators (M, D, R_g, and F_g). Therefore, the magnitude of the potential disturbance at each hour of every representative day during the planning horizon is set equal to the power exchange with the main grid scheduled at the time of the disconnection (i.e., $\Delta P = p^{\text{b/s}}_{to\psi}$). At the same time, the control parameters depend on the built/not-built status of generators in the MG at each iteration ($z_{g\psi}$). Consequently, at each iteration ψ, this stage of the algorithm uses the variables $p^{\text{b/s}}_{to\psi}$ and $z_{g\psi}$ obtained from the first stage to evaluate the solution feasibility under transient security constraints in (6.5), (6.6) and (6.7) described in detail in Section 6.5.2.

The solution of the second stage provides the minimum amount of corrective deviation ($\Delta p^{\text{b/s}}_{to\psi}$) from the scheduled power exchange with the main grid ($p^{\text{b/s}}_{to\psi}$) to meet the transient security criteria. If this value is zero or less than a small tolerance (ϵ), the op-

timal investment and operational solution obtained from the first-stage problem ensures frequency security in islanded mode, and the algorithm is terminated. Otherwise, the algorithm proceeds to the third stage.

6.4.2.3 Stage 3: Tightening Power Exchange with the Main Grid

The third stage of the algorithm employs the non-zero solution obtained from the previous stage to tighten the limits imposed on the power exchange with the main grid at each hour of every representative day throughout the planning horizon. Once the bounds have been altered, the algorithm proceeds to the next iteration $(\psi + 1)$. The modified limits may lead either to a change in the power exchange with the main grid (through operational decisions), a change in the investment decisions, or both.

6.5 Extended Formulation under Static and Transient Frequency Constraints

In this section, the extended formulation of the proposed planning tool under static and transient constraints is presented. The iteration index ψ is omitted for better legibility and brevity.

6.5.1 Extended Formulation under Static Constraints (Stage 1)

The optimisation problem in the first stage corresponds to the compact formulation (6.9), including investment limitations and static operational constraints in grid-connected and islanded mode. The extended terms in the objective function and the constraints are outlined in the following.

6.5.1.1 Investment

The term $\Theta^{\text{inv}}(\chi^{\text{inv}})$ in the objective function of the proposed planning problem is given by:

$$\min_{\chi^{\text{inv}}} \ \Theta^{\text{inv}} = \sum_{g \in \{\mathcal{S},\mathcal{C}\}} (ic_g \cdot z_g) + \sum_{l \in \mathcal{L}} (ic_l \cdot z_l)\,, \tag{6.10}$$

and includes the total investment/reinforcement costs of generators/lines throughout the planning horizon. The optimisation variables $\chi^{\text{inv}} = \{z_g, z_l\}, \forall g \in \{\mathcal{S},\mathcal{C}\} \wedge \forall l \in \mathcal{L}$ are *here-and-now* decisions (i.e. not a function of uncertain parameters, and thus, non-adjustable) [166].

6.5.1.2 Grid-Connected Operation

The function $\Theta^{\text{gm,opr}}$ capturing the operational cost in grid-connected mode is given by:

$$\begin{aligned}\min_{\chi^{\text{gm,opr}}} \quad \Theta^{\text{gm,opr}} = &\sum_{o\in\mathcal{O}}\sum_{t\in\mathcal{T}}\left(\tau_o\cdot\left(e^{\text{b}}_{to}\cdot p^{\text{b}}_{to} - e^{\text{s}}_{to}\cdot p^{\text{s}}_{to}\right)\right)\\ &+\sum_{o\in\mathcal{O}}\sum_{t\in\mathcal{T}}\sum_{g\in\{\mathcal{S},\mathcal{C}\}}\left(\tau_o\cdot mc_g\cdot p_{gto}\right)+\sum_{o\in\mathcal{O}}\sum_{t\in\mathcal{T}}\sum_{i\in\mathcal{N}}\left(\tau_o\cdot fc_i\cdot d^{\text{p}_f}_{ito}\right)\end{aligned} \tag{6.11a}$$

The objective function minimises the total operation costs, including the total costs of power exchange with the main grid, the total operation costs of generators, and the total penalty costs of shifting loads away from the periods preferred by consumers. The constraints that need to be taken into account to reflect operational limitations in grid-connected mode are:

Constraints on active and reactive power flows: The power flows based on the linearized version of the DistFlow model [158, 159], denoted as Model 3 in Chapter 3.

$$P_{l^{i^+}to} + p^{\text{b}}_{to|i=1} - p^{\text{s}}_{to|i=1} + \sum_{g\in\{\mathcal{S}^i,\mathcal{C}^i\}} p_{gto} = \sum_{i^-\in\mathcal{N}^i} P_{l^{i^-}to} + d^{\text{p}}_{ito}, \qquad \forall i,t,o, \tag{6.11b}$$

$$Q_{l^{i^+}to} + q^{\text{b}}_{to|i=1} - q^{\text{s}}_{to|i=1} + \sum_{g\in\{\mathcal{S}^i,\mathcal{C}^i\}} q_{gto} = \sum_{i^-\in\mathcal{N}^i} Q_{l^{i^-}to} + d^{\text{q}}_{ito}, \qquad \forall i,t,o, \tag{6.11c}$$

$$v_{i^+to} - v_{ito} = \left(r_{l^{i^+}}\cdot P_{l^{i^+}to} + x_{l^{i^+}}\cdot Q_{l^{i^+}to}\right), \qquad \forall i,t,o, \tag{6.11d}$$

Constraints on power exchange with the main grid: Equations (6.11e)-(6.11f) ensure the non-negativity and impose the upper limits on the power exchange with the main grid.

$$0 \le p^{\text{b}}_{to} \le \overline{p}^{\text{b}}_{to}, \qquad 0 \le p^{\text{s}}_{to} \le \overline{p}^{\text{s}}_{to}, \qquad \forall t,o, \tag{6.11e}$$

$$0 \le q^{\text{b}}_{to} \le \overline{q}^{\text{b}}_{to}, \qquad 0 \le q^{\text{s}}_{to} \le \overline{q}^{\text{s}}_{to}, \qquad \forall t,o, \tag{6.11f}$$

Note that $p^{\text{b/s}}_{to}$ and $q^{\text{b/s}}_{to}$ in (6.11b) and (6.11c) are included only at the Point-of-Common Coupling (PCC) node denoted by $n = 1$.

Constraints on constant and flexible load: The limitations in (6.11g)-(6.11j) reflect the power balance of constant and flexible loads as well as the limitations of flexible loads at each node and at every hour of each representative day. For the flexible loads, (6.11k) ensures that their required daily energy consumption is maintained for each representative day.

$$d^{\text{p}}_{ito} = d^{\text{p}_\text{c}}_{ito} + d^{\text{p}_\text{f}}_{ito}, \qquad \forall i,t,o, \tag{6.11g}$$

$$d^{\mathrm{q}}_{ito} = d^{\mathrm{q_c}}_{ito} + d^{\mathrm{q_f}}_{ito}, \qquad \forall i,t,o, \tag{6.11h}$$

$$\underline{d}^{\mathrm{p_f}}_{ito} \leq d^{\mathrm{p_f}}_{ito} \leq \overline{d}^{\mathrm{p_f}}_{ito}, \qquad \forall i,t,o, \tag{6.11i}$$

$$\underline{d}^{\mathrm{q_f}}_{ito} \leq d^{\mathrm{q_f}}_{ito} \leq \overline{d}^{\mathrm{q_f}}_{ito}, \qquad \forall i,t,o, \tag{6.11j}$$

$$\sum_{t\in\mathcal{T}} d^{\mathrm{p}}_{ito} = e_{io}, \qquad \forall i,o, \tag{6.11k}$$

Constraints on power generation of the DERs: The capacity, reserve and ramp-rate limits of the distributed generators are described in constraints (6.11l)-(6.11p) at each hour of every representative day.

$$0 \leq p_{gto} \leq \overline{p}_{gto} \cdot z_g, \qquad \forall g \in \{\mathcal{S},\mathcal{C}\},t,o, \tag{6.11l}$$

$$\overline{p}_{gto} = p^{\mathrm{nom}}_g - p^{\mathrm{FR}}_g, \qquad \forall g \in \{\mathcal{S}\},t,o, \tag{6.11m}$$

$$\overline{p}_{gto} = \min(p^{\mathrm{nom}}_g - p^{\mathrm{FR}}_g, p^{\mathrm{AV}}_{gto}), \qquad \forall g \in \{\mathcal{C}\},t,o, \tag{6.11n}$$

$$\underline{q}_{gto} \cdot z_g \leq q_{gto} \leq \overline{q}_{gto} \cdot z_g, \qquad \forall g \in \{\mathcal{C},\mathcal{S}\},t,o, \tag{6.11o}$$

$$-r^{\mathrm{dn}}_g \leq p_{gto} - p_{g(t-1)o} \leq r^{\mathrm{up}}_g, \qquad \forall g \in \mathcal{S},t,o, \tag{6.11p}$$

$$\sum_{t\in\mathcal{T}} p_{gto} + e^{\mathrm{FR}}_g \leq c_{go} \cdot \sum_{t\in\mathcal{T}} \overline{p}_{gto}, \qquad \forall g \in \mathcal{S},o, \tag{6.11q}$$

Parameter p^{FR}_g in (6.11l) and (6.11n) relates to the minimum active power reserve capacity of each generator allocated to transient frequency control. This requirement can be predefined by the grid code [38] or calculated as:

$$p^{\mathrm{FR}}_g = \left(M_g \dot{f}_{\mathrm{lim}} + (D_g + R_g)\Delta f_{\mathrm{lim}}\right)$$

with $\dot{f}_{\mathrm{lim}}$, and Δf_{lim} denoting the maximum acceptable RoCoF, and frequency deviation prior to under-frequency load shedding, respectively. The energy adequacy for transient performance, defined by parameter e^{FR}_g, is calculated as
$e^{\mathrm{FR}}_g = \left(M_g \dot{f}_{\mathrm{lim}} T^{\mathrm{FC^I}} + (D_g + R_g)\Delta f_{\mathrm{lim}} T^{\mathrm{FC^P}}\right)$ where $T^{\mathrm{FC^I}}$ and $T^{\mathrm{FC^P}}$ define the delivery periods for inertia and primary frequency response, respectively. It should be noted here that delivery periods $T^{\mathrm{FC^I}}$ and $T^{\mathrm{FC^P}}$ include all hours considered in the planning horizon of each representative day.

Energy reserves (e^{FR}_g) for transient frequency control in CIGs are commonly provided by three different approaches, i.e. can be provided by the converter-side DC-link capacitor energy storage [167], by a battery energy storage attached to the CIG [168], or by decreasing the CIG output from the maximum power point to allow for upward regulation. In

this work, it is assumed that the energy and power reserves for transient frequency control of CIG units are provided by the DC-side capacitor as detailed in [167]. Furthermore, (6.11l)-(6.11n) limit the SG and CIG output power to accommodate for the necessary power reserves (p_g^{FR}). For the synchronous units the maximum available power $\bar{p}_{gto}$ is given by the unit's power capacity reduced in order to account for the frequency reserves required (6.11m). On the other hand, for CIG units the power output at any time period is dependent on the weather conditions and as such its maximum power point at each hour p_g^{AV} will further limit the available power that can be dispatched (6.11n). Moreover, the reactive power limits of CIGs are based on the maximum generated active power, i.e., $\overline{q}_{gto} = \tan\phi \cdot \overline{p}_{gto}$, where $\cos\phi$ is the maximum power factor of a unit defined by the grid code. Constraint (6.11q) defines the daily capacity factor of SGs in each representative day of the planning horizon [169].

Constraints on line thermal limits: Constraint (6.11r) imposes the thermal loading limits of each line. This quadratic constraint is linearised by means of a convex polygon, defined by inner approximations of the thermal loading circle [160], this is illustrated in Model 3 in Section 3.2.3.

$$P_{lto}^2 + Q_{lto}^2 \leq \left(\overline{S}_l^0\right)^2 \cdot z_l^0 + \left(\overline{S}_l\right)^2 \cdot z_l, \qquad \forall l, t, o, \tag{6.11r}$$

$$z_l^0 + z_l = 1, \qquad \forall l, \tag{6.11s}$$

The initial status of the line is represented by $z_l^0 = 1$ if there is no requirement for investment at loading capacity $\overline{S}_l^0$. If however the line loading limits are violated, a new line with higher loading capacity $\overline{S}_l$ can be utilised.

Constraints on nodal voltage magnitudes: The limits on the nodal voltage magnitudes throughout the planning horizon are ensured as:

$$\underline{v} \leq v_{ito} \leq \overline{v}, \qquad v_{to|i=1} = 1, \qquad \forall i, t, o, \tag{6.11t}$$

During grid-connected operation the vector of *wait-and-see* decision variables (i.e. a function of uncertain parameters, and thus, adjustable) [166] is given by $\chi^{\mathrm{gm,opr}} = \{d_{ito}^{\mathrm{p/q}}, d_{ito}^{\mathrm{pf/qf}}, p_{gto}, P_{lto}, p_{to}^{\mathrm{b/s}}, q_{gto}, Q_{lto}, q_{to}^{\mathrm{b/s}}, v_{ito}\}$.

6.5.1.3 Islanded Operation

It is assumed that at every hour of each representative day, the MG should be able to withstand an unscheduled islanding event. The operation planning problem of a MG in

islanded mode is aimed at ensuring survivability and self-sufficiency, where priority is given to critical loads. It is worthwhile to note that, in this study, the self-sufficiency is ensured for one period (i.e., one hour) after disconnection from the main grid. However, the islanded operation period can be straightforwardly extended to multiple periods based on the required resilience. Hereafter, the superscript "im" denotes operational variables in islanded mode. The function $\Theta_{to}^{\text{im,opr}}$ capturing the operational cost in islanded mode is given by:

$$\min_{\chi_{to}^{\text{im,opr}}} \quad \Theta_{to}^{\text{im,opr}} = \sum_{i \in \mathcal{N}} \left(pc_i \left((1 - y_{ito})\, d_{ito}^{\text{p}_\text{c}} + \check{d}_{ito}^{\text{p}_\text{f}} \right) \right) \tag{6.12a}$$

The objective function (6.12a) minimizes the total unserved load and ensures an adequate supply of at least the critical MG loads. It should be noted that pc_n describes the priority level of the load at a specific node, with higher values suggesting more critical loads, and the amount of unserved flexible load is denoted by $\check{d}_{nto}^{\text{p}_\text{f}}$.

The constraints that need to be taken into account to reflect operational limitations in islanded mode are:

Constraints on the active and reactive power flows:

$$P_{l^{i+}to}^{\text{im}} + \sum_{g \in \{\mathcal{S}^i, \mathcal{C}^i\}} p_{gto}^{\text{im}} = \sum_{i^- \in \mathcal{N}^i} P_{l^{i-}to}^{\text{im}} + \left(y_{ito} \cdot d_{ito}^{\text{p}_\text{c}} + d_{ito}^{\text{im,p}_\text{f}} \right), \qquad \forall i, t, o, \tag{6.12b}$$

$$Q_{l^{i+}to}^{\text{im}} + \sum_{g \in \{\mathcal{S}^i, \mathcal{C}^i\}} q_{gto}^{\text{im}} = \sum_{i^- \in \mathcal{N}^i} Q_{l^{i-}to}^{\text{im}} + \left(y_{ito} \cdot d_{ito}^{\text{q}_\text{c}} + d_{ito}^{\text{im,q}_\text{f}} \right), \qquad \forall i, t, o, \tag{6.12c}$$

$$v_{i^+to}^{\text{im}} - v_{ito}^{\text{im}} = \left(r_{l^{i+}} \cdot P_{l^{i+}to}^{\text{im}} + x_{l^{i+}} \cdot Q_{l^{i+}to}^{\text{im}} \right), \qquad \forall i, t, o, \tag{6.12d}$$

Constraints on the constant and flexible load:

$$d_{ito}^{\text{im,p}_\text{f}} = d_{ito}^{\text{p}_\text{f}} + \hat{d}_{ito}^{\text{p}_\text{f}^+} - \hat{d}_{ito}^{\text{p}_\text{f}^-}, \qquad \forall i, t, o, \tag{6.12e}$$

$$d_{ito}^{\text{im,q}_\text{f}} = d_{ito}^{\text{q}_\text{f}} + \hat{d}_{ito}^{\text{q}_\text{f}^+} - \hat{d}_{ito}^{\text{q}_\text{f}^-}, \qquad \forall i, t, o, \tag{6.12f}$$

$$0 \leq \hat{d}_{ito}^{\text{p}_\text{f}^+}, \hat{d}_{ito}^{\text{q}_\text{f}^+}, \hat{d}_{ito}^{\text{p}_\text{f}^-}, \hat{d}_{ito}^{\text{q}_\text{f}^-}, \qquad \forall i, t, o, \tag{6.12g}$$

$$\underline{d}_{ito}^{\text{p}_\text{f}} \leq d_{ito}^{\text{im,p}_\text{f}} \leq \overline{d}_{ito}^{\text{p}_\text{f}}, \qquad \forall i, t, o, \tag{6.12h}$$

$$\underline{d}_{ito}^{\text{q}_\text{f}} \leq d_{ito}^{\text{im,q}_\text{f}} \leq \overline{d}_{ito}^{\text{q}_\text{f}}, \qquad \forall i, t, o, \tag{6.12i}$$

$$d_{ito}^{\text{im,p}} \leq e_{io} - \sum_{t'=1}^{t-1} d_{it'o}^{\text{p}}, \qquad \forall i, t, o, \tag{6.12j}$$

Constraints on power generation of different units:

$$0 \leq p^{\text{im}}_{gto} \leq \overline{p}_{gto} \cdot z_g, \qquad \forall g \in \{\mathcal{C}, \mathcal{S}\}, t, o, \qquad (6.12k)$$

$$\underline{q}_{gto} \cdot z_g \leq q^{\text{im}}_{gto} \leq \overline{q}_{gto} \cdot z_g, \qquad \forall g \in \{\mathcal{C}, \mathcal{S}\}, t, o, \qquad (6.12l)$$

$$-r^{\text{dn}}_g \leq p^{\text{im}}_{gto} - p_{gto} \leq r^{\text{up}}_g, \qquad \forall g \in \mathcal{S}, t, o, \qquad (6.12m)$$

$$p^{\text{im}}_{gto} \leq c_{go} \cdot \sum_{t \in \mathcal{T}} \overline{p}_{gto} - \sum_{t'=1}^{t-1} p_{gto}, \qquad \forall g \in \mathcal{S}, t, o, \qquad (6.12n)$$

Constraints on line thermal limits:

$$P^{\text{im}^2}_{lto} + Q^{\text{im}^2}_{lto} \leq S^2_{lto} \cdot \left(z^0_l + z_l\right), \qquad \forall l, t, o, \qquad (6.12o)$$

Constraints on nodal voltage magnitudes:

$$\underline{v} \leq v^{\text{im}}_{ito} \leq \overline{v}, \; v^{\text{im}}_{to|i=1} = 1, \qquad \forall i, t, o, \qquad (6.12p)$$

where, similarly to the previous operation planning problem in grid-connected mode, all operation variables $\chi^{\text{im,opr}}_{to} = \{\hat{d}^{\text{p}_\text{f}/\text{q}_\text{f}}_{ito}, d^{\text{im,p}_\text{f}/\text{im,q}_\text{f}}_{ito}, \hat{p}_{gto}, p^{\text{im}}_{gto}, P^{\text{im}}_{lto}, \hat{q}_{gto}, q^{\text{im}}_{gto}, Q^{\text{im}}_{lto}, v^{\text{im}}_{ito}\}$ are *wait-and-see* decisions.

Constraints (6.12b)-(6.12d) enforce the post-islanding power flow balance, whereas the deviations between the amount of flexible load served in grid-connected and islanded mode are given by (6.12e)-(6.12f) and used to determine the fraction of served and unserved flexible loads in islanded mode. Moreover, (6.12h)-(6.12i) enforce the limitations of flexible loads in islanded mode, and (6.12j) restricts the supply of flexible loads in terms of respective demand already served before the current time instance affected by a disconnection from the main grid. Constraints (6.12k)-(6.12l) denote capacity limits of generators, (6.12m)-(6.12n) indicate that re-scheduling actions of SGs in islanded mode are subject to their ramp rate and daily capacity factor limitations as well as their scheduling actions before the current time step. Furthermore, similar to the formulation in grid-connected mode, (6.12o) defines the thermal loading limit of each line and (6.12p) limit the nodal voltage magnitudes. In the grid-connected mode the voltage at the PCC is maintained by the stiff grid, while in the islanded mode it is controlled by the DERs.

The final optimization problem is a MILP problem in the first stage of the algorithm, and its solution is subsequently used in the feasibility check in the second stage.

6.5.2 Formulation of the Transient Security Problem (Stage 2)

The feasibility of the planning solution under transient security constraints is necessary to guarantee the secure islanding of a MG. According to the metrics described in (6.5), (6.6), (6.7) and the discussions in Section 6.4.2, the transient frequency response in the event of islanding depends on the amount of power exchange with the main grid at the time of the event (i.e., $\Delta P = p_{to\psi}^{\text{b/s}}$) and the control parameters of the online generators in the MG (i.e., $M(z_{g\psi})$, $D(z_{g\psi})$, $F_g(z_{g\psi})$ and $R_g(z_{g\psi})$). Note however that, with respect to decision variables, (6.5) and (6.7) are linear while (6.6) is highly non-linear. Given the optimal values of decision variables obtained from the first stage ($p_{to\psi}^{\text{b/s}}$ and $z_{g\psi}$), the non-linear term in (6.6) can be defined as a constant at each iteration. Consequently, at each iteration ψ, the feasibility check can be formulated as a linear programming problem of the form:

$$\Theta_{to}^{\text{dyn}} = \min_{\Delta p_{to\psi}^{\text{b/s}}} \left| \Delta p_{to\psi}^{\text{b/s}} \right| \tag{6.13a}$$

The constraints that need to be taken into account to ensure transient security feasibility are:

$$\left| \frac{p_{to\psi}^{\text{b/s}} + \Delta p_{to\psi}^{\text{b/s}}}{M} \right| \leq \dot{f}_{\text{lim}}, \tag{6.13b}$$

$$\left| \frac{p_{to\psi}^{\text{b/s}} + \Delta p_{to\psi}^{\text{b/s}}}{D + R_g} \cdot \left(1 + \sqrt{\frac{T(R_g - F_g)}{M}} e^{-\zeta \omega_n t_m} \right) \right| \leq \Delta f_{\text{lim}}, \tag{6.13c}$$

$$\left| \frac{p_{to\psi}^{\text{b/s}} + \Delta p_{to\psi}^{\text{b/s}}}{D + R_g} \right| \leq \Delta f_{\text{ss,lim}}. \tag{6.13d}$$

The feasibility checking problem (6.13) is solved independently for each hour t of every representative day o. Constraints (6.13b)-(6.13d) enforce permissible frequency response limits pertaining to RoCoF, frequency nadir, and quasi-steady-state frequency deviation [38], respectively, whereas slack variables $\Delta p_{to\psi}^{\text{b/s}}$ are used to identify the violations of transient security limits at a specific hour and iteration. Accordingly, (6.13a) provides the minimum change needed in the scheduled power exchange with the main grid from the first stage to ensure frequency security.

6.5.3 Bound Tightening (Stage 3)

After solving (6.13) for each considered time step at each iteration ψ, the value of $\Delta p^{\mathrm{b/s}}_{to\psi}$ is used to modify and tighten the power exchange limits with the main grid at the next iteration $(\psi+1)$:

$$\overline{p}^{\mathrm{b}}_{to(\psi+1)} = p^{\mathrm{b}}_{to\psi} - \alpha \Delta p^{\mathrm{b}}_{to\psi}, \qquad \forall t, o, \tag{6.14a}$$

$$\overline{p}^{\mathrm{s}}_{to(\psi+1)} = p^{\mathrm{s}}_{to\psi} - \alpha \Delta p^{\mathrm{s}}_{to\psi}, \qquad \forall t, o. \tag{6.14b}$$

The scaling factor α is used to apply a less conservative bound modification to account for intertemporal power shifting and investment candidates with frequency support. Furthermore, α prevents the emergence of oscillatory non-convergence that might occur due to the multi-stage nature of the solution algorithm. In this work, a value of $\alpha \in [0.5, 0.7]$ was adopted, calculated through a heuristic approach. Alternatively, a line-search approach could be implemented in the algorithm, allowing to select the maximum α that satisfies the requirements while minimizing the computational time.

The proposed algorithm (see Fig. 6.2) can be summarised as:

Stage 1: Investment and operational planning with static security, (6.10)-(6.12);

Stage 2: Transient security evaluation at all hours, (6.13);

Stage 3: Grid power bounds tightening, (6.14).

6.6 Description of Study Network

A modified CIGRE residential low-voltage network [140], illustrated in Fig. 6.3, is used to analyze the performance of the proposed planning tool. The network parameters are defined in Appendix A.3. It is assumed that one SG is already preset at PCC (SG_1) and the investment candidates comprise one SG (SG_2) and three PV CIGs (i.e., PV_1 and PV_2 interfaced via *grid-supporting* converters, and PV_3 operating in *grid-feeding* mode

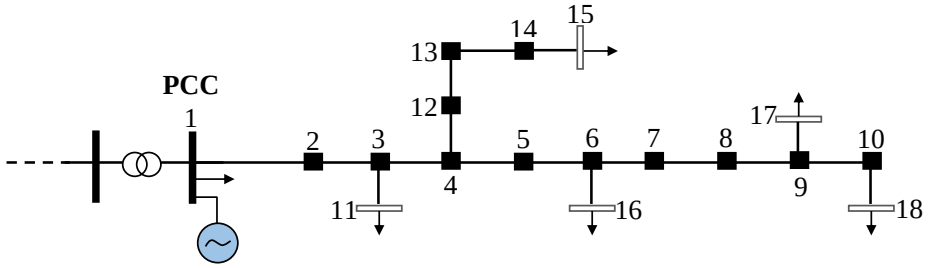

Figure 6.3: Modified CIGRE European low voltage network.

Table 6.1: Generator Control Parameters and Investment Costs

	SG_1	SG_2	PV_1	PV_2	PV_3
Annualized investment cost ($)	-	40 000	70 000	65 000	60 000
Capacity (kW)	280	350	350	350	350
Node	1	15	17	11	18
M (s)	14	14	14	-	-
D (p.u.)	0.9	0.9	0.9	-	-
K (p.u.)	1	1	1	1	-
R (p.u.)	0.03	0.03	-	0.05	-
F (p.u.)	0.35	0.35	-	-	-

Existing generator

Candidate generators

with fixed power output).

The fundamental control parameters obtained from [1] and investment costs (derived from [108, 170]) of all generators are provided in Table 6.1, while system operation costs are given in Table 6.2. The fixed operational costs are included as a markup in the annualised investment costs while the variable operational costs are as defined in Table 6.2. The load parameters are defined in Table 6.3 where 50 % of nominal load connected at node 1 is shiftable, whereas high priority critical loads are connected at nodes 15 and 16. The patterns of loads and PV generation in Texas during 2016 [171] are used to obtain representative days through k-means clustering. The profiles of four representative days for load and PV power generation are depicted in Fig. 6.4.

The transient security constraints are enforced through thresholds imposed on RoCoF ($\dot{f}_{\text{lim}} = 2\,\text{Hz/s}$), frequency nadir ($\Delta f_{\text{lim}} = 0.8\,\text{Hz}$), and quasi-steady-state frequency deviation ($\Delta f_{\text{ss,lim}} = 0.2\,\text{Hz}$). Also, a value of $\epsilon = 10^{-2}$ is adopted.

The implementation was done in MATLAB, with the optimization model formulated in YALMIP [172] and solved by Gurobi [86].

Table 6.2: System Operation Costs

Import ($/kWh)	Export ($/kWh)	SG ($/kWh)	PV ($/kWh)	Demand shift penalty ($/kWh)	Demand disconnection penalty ($/kWh)
30	15	60	0	100	$(150 - 200)^*$

*Based on the level of demand criticality, only in islanded mode

Table 6.3: Load Parameters (F: Flexible, C: Constant)

Node	1	11	15	16	17	18
Type	F	C	C	C	C	C
Nominal Load [kVA]	200	15	52	210	35	47
Power factor	0.95	0.95	0.95	0.85	0.95	0.95

High priority load

Low priority load

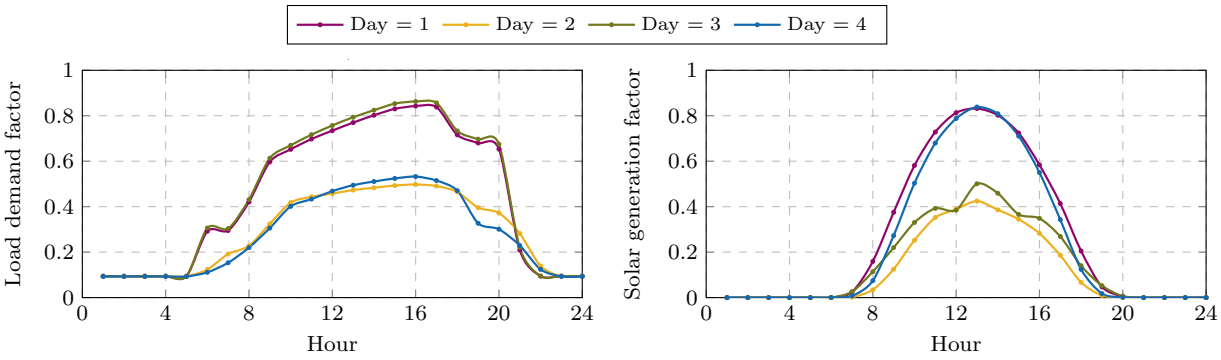

Figure 6.4: Demand and solar power generation patterns (four representative days).

6.7 Case studies

To analyze the performance of the proposed planning tool, three cases are considered:

Case 1: MG planning without robust islanding constraints (stochastic approach);

Case 2: MG planning only with robust static islanding constraints (stochastic-robust approach);

Case 3: MG planning with robust static and transient frequency islanding constraints (stochastic-robust approach).

Case 2 considers only Stage 1, while Case 3 considers all the stages of the proposed algorithm.

6.7.1 Analysis of Expected Investment and Operational Costs

In this analysis, the costs of the three aforementioned case studies are compared under the consideration of four representative days. Let us first study Case 1, with the respective costs under different capacity limits of the main feeder listed in Table 6.4. Initially for conciseness, the result obtained with four representative days and scenarios illustrated by the profiles in Fig. 6.4 is presented. Understandably, the MG mainly relies on more affordable power provided by the main grid instead of dispatching SG_1 installed at PCC. Under the unlimited import capacity from the main grid, investments in local generation are not economical due to the low cost of imported power. However, with the introduction of grid capacity limits (e.g., in instances of net load growth and faults experienced in the network), the operational costs increase as a result of the MG relying on the more expensive SG_1 at the PCC. Further, the reduction of grid capacity limits finally leads to the instalment of PV_3, which yields higher investment but lower operational costs compared to SG_2 and thus significantly reduces the overall costs.

The variation between investment and operational costs for Cases 2 and 3 is provided in Table 6.5, where the optimal solution at iteration $\psi = 1$ corresponds to the optimal costs of Case 2. The problem in Cases 2 and 3 is solved considering unlimited power import from the main grid. The MG requires higher reliability in Case 2 compared to Case 1 in order to minimise the loss of load under static security constraints during islanding. Whereas in Case 3 the survivability and resilience of the MG are also considered by including the transient security constraints. To ensure the MG resilience, higher investment and operational costs are enforced in both of these case studies compared to Case 1 due to inclusion of static and transient islanding constraints. Indeed, a 400 % cost increase for Case 2 is observed, with a further 10 % increase for Case 3. In both of these cases,

Table 6.4: Cost comparison with variation in main grid capacity for Case 1: MG Planning without Islanding Constraints

Main grid capacity (kW)	Investment costs & decisions ($)	Operational costs ($)	Total costs ($)	Installed capacity (kW)
Unlimited	0	56 394	56 394	280
250	0	77 795	77 795	280
150	60 000 (PV_3)	47 473	107 473	630

Table 6.5: Planning Costs for Case 2 (Final Cost in Blue) and Case 3 (Final Cost in Green) Including Four Representative Days.

ψ	Investment costs ($) & decisions	Operational costs ($)	Demand shift penalty ($)	Demand disconnection penalty ($)	Total costs ($)
1	128 000 (PV_2, PV_3 + Lines 1-2, 2-3, 3-11)	96 956	3 613	5 548	224 956
2	127 000 (PV_2, PV_3 + Lines 1-2, 2-3)	113 872	8 543	5 337	240 872
3	127 000 (PV_2, PV_3 + Lines 1-2, 2-3)	118 924	8 796	5 081	245 924
4	127 000 (PV_2, PV_3 + Lines 1-2, 2-3)	120 423	8 572	5 334	247 423
5	127 000 (PV_2, PV_3 + Lines 1-2, 2-3)	120 890	8 805	5 081	247 890

the installation of renewable DERs reduces the total costs despite the significantly higher underlying investment costs. More precisely, renewable DERs contribute to increased line flows and power export to the main grid, thus necessitating a greater network capacity indicated by the upgrade of the lines between nodes (1-2) and (2-3). However, in turn, the MG adequacy improves with installing renewable DERs, reflected in the reduction of lost load and ensuring that critical loads are supplied even during emergency islanding situations.

Focusing on Case 3, it is noticeable that operational costs increase at each iteration due to the use of expensive SGs and flexible loads to mitigate the feasibility violation. The use of flexible loads accrues a customer inconvenience penalty which would increase operational cost greatly, however, in this case, the flexible loads operate during instances of higher solar power generation thus averaging out the total operational cost. Nevertheless, when operational flexibility alone cannot guarantee security, more units are installed. Finally, it can be seen that tightening of the power exchange limits (and thus the power export) with the main grid alleviates some of the network investments (e.g., line 3-11 for iterations 1 and 2). Thus, the MG planner can be made aware of the enforced additional cost to ensure the resilience of the system through including transient security constraints in Case 3 as compared to Case 2.

In Fig. 6.5, a comparison of the total design costs considering either a deterministic/stochastic (Case 1) or deterministic/stochastic-robust (Case 2 & 3) model in all three

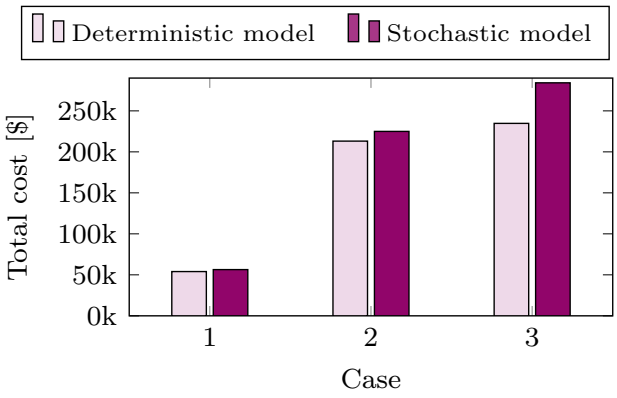

Figure 6.5: Total costs for deterministic and stochastic models in Cases 1, 2 and 3.

cases is presented. The deterministic model in Cases 1, 2, and 3 considers only one representative day (i.e., the expected average daily load and power generation patterns). As noticeable in Fig. 6.5, a deterministic model provides a rather optimistic solution that can lead to system vulnerabilities for both static and transient security. This risk is shown to grow with the inclusion of transient security (Case 3). Hence, increasing the number of scenarios provides a more accurate system representation, which ensures a more robust design. This is further analysed in Section 6.7.3.1.

6.7.2 Transient Security Analysis

In Case 3, the MG survivability is ensured by meeting the prescribed transient security criteria. In the second stage of the algorithm (see Fig. 6.2), the slack variable $\Delta p_{to}^{\mathrm{b/s}}$ is used to indicate the amount of adjustment needed in the scheduled power exchange with the main grid to satisfy the transient frequency requirements. Fig. 6.6 showcases the metrics describing the dynamic performance of the MG's CoI after islanding at each hour. The first iteration corresponds to the system response without transient security requirements (Case 2).

A significant improvement is recorded in the maximum RoCoF values, even within a single iteration (e.g., reduction from 8 Hz/s to 3.5 Hz/s after the first iteration). Furthermore, each successive iteration reduces the power exchange with the main grid during the hours when security limits are violated until all limits are satisfied. The amount of aggregated corrective power deviations ($\sum_{t\in\Omega^T} \Delta p_{to}^{\mathrm{b/s}}$) in Table 6.6 is monotonically decreased with each iteration until the transient security constraints are fulfilled. The aggregated power deviations indicate the power changes applied to the power exchange limits for the different violating hours. At each time instant grid capacity limits in successive iterations vary depending on the islanding dynamic performance. For representative days 2 and 3,

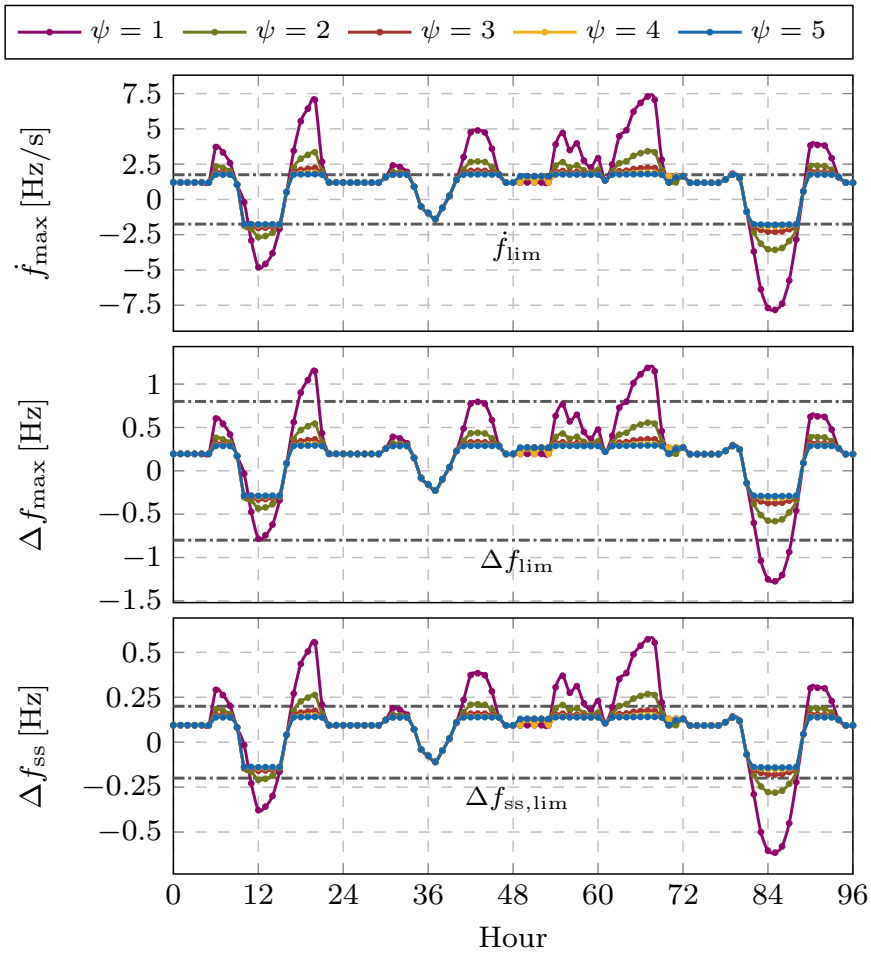

Figure 6.6: System performance in terms of the transient frequency metrics for different iterations of the proposed algorithm including four representative days.

no corrective power deviations are required for power export. This is also evident from Fig. 6.6 where no violations are recorded in the negative range (power export) for all metrics between hours 25 and 72 (range of hours for day 2 and 3) hence eliminating the need for bound tightening in this region. It is however noteworthy that these improvements in terms of security and resilience are achieved at the expense of higher operational costs by dispatching costly SG and flexible loads.

It is clear from Fig. 6.6 that the RoCoF threshold is the most limiting factor for secure transient operation. This is expected, since PV-based CIGs yield a more economic solution but do not provide the same level of inertia as SGs, thus degrading the transient performance. In particular, SG_1 and PV_1 provide both inertia and damping, PV_2 improves damping through droop control, and PV_3 offers no frequency support. Since the inertia and damping contribution of SG_1 and PV_2 do not lead to sufficient transient performance, the reduction in the power exchange with the main grid is needed to ensure a satisfactory response. This is achieved through power provision from PV_2 and PV_3 as

Table 6.6: Aggregated corrective power deviations at each iteration including four representative days in Case 3

	Representative Day							
	1	2	3	4	1	2	3	4
ψ	Aggregated import power deviations (kW)				Aggregated export power deviations (kW)			
1	751.00	467.70	1426.20	257.10	328.20	0.00	0.00	1102.80
2	225.30	140.30	427.85	77.15	98.45	0.00	0.00	330.85
3	67.60	42.10	128.35	23.15	29.55	0.00	0.00	99.25
4	20.30	12.65	38.50	6.95	8.85	0.00	0.00	29.80
5	6.10	3.80	11.30	2.10	2.65	0.00	0.00	8.95

well as higher activation of flexible loads.

The analytical result in Fig. 6.6 is validated through a time-domain simulation of the MG. In the time-domain simulation, the CIGs are modeled as detailed in [163] while the SGs are modeled by a 6^{th}-order model equipped with a reheat turbine speed governor [42] and an IEEE ACIA exciter [173]. The dynamic simulations were performed with PyRAMSES [60] software. The disconnection from the grid occurs at time = 1 s. As indicated in Fig. 6.7, neither Case 1 nor Case 2 ensures a secure transition to islanded state given an abrupt islanding event. However, the solution of Case 3 ensures the transient security, and thus, survivability of the MG during the transition to the islanded mode, as shown in Fig. 6.7.

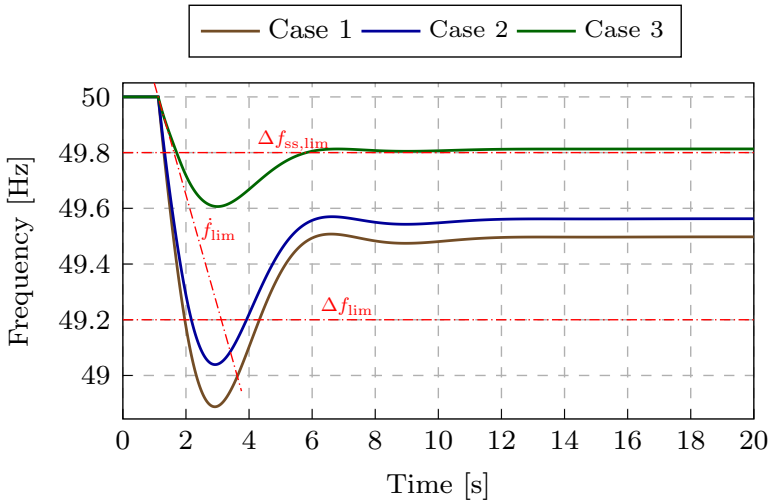

Figure 6.7: MG CoI frequency response after an abrupt islanding event at hour = 20 for each of the three cases studied.

6.7.3 Sensitivity Analysis

6.7.3.1 Representative Days

The stochasticity of both load and generation profiles affects the planning accuracy, usually resulting in under- or overestimation. As previously described in Section 6.6, the load and generation profiles are obtained by utilizing the k-means clustering for different representative days. Understandably, the number of considered representative days has a direct impact on the solution of the algorithm. This can be observed in Fig. 6.8, where the total investment and operational costs for Cases 2 and 3 increase with the number of representative days. In particular, employing more representative days provides a better representation of system operation, thus allowing for more accurate estimates of different costs. Additionally, an increase in the representative days results in a more robust design as more scenarios for an abrupt islanding event can be taken into account during system design. On the other hand, it also imposes a higher computational burden as this results in a significant increase in the solution space of the problem leading to the intractability of the optimization problem as further clarified in Section 6.7.5. In particular, the results in Fig. 6.8 indicate that the overall costs plateau for excessive number of representative days, suggesting that the case studies considering up to 16 representative provide a good trade-off between the accuracy of cost estimates and the needed computational effort. Furthermore, Table 6.7 provides the investment decisions for Cases 2 and 3. The additional units for the result of 16 and more representative days in Case 3, a consequence of the better representation of the operation scenarios further ensures that a more robust transient security solution is obtained.

6.7.3.2 Operational Flexibility

While flexible loads provide more degrees of freedom for operational planning, they are costly. In spite of their high operational costs, in this study they provide a more affordable option compared to investments in additional generators for improving system flexibility by reducing the peak power exchange with the main grid. Indeed, Table 6.5 shows a successive increase in the use of flexible loads for improving the transient frequency response. This is justified by the fact that flexible loads provide a peak shaving service vital for ensuring survivability during transients. In Case 2, as the number of representative days was increased, the use of flexible loads showed a correlation with the load adequacy in islanded mode. Results indicate lower load curtailment with the availability of flexible loads, as seen in Fig. 6.9.

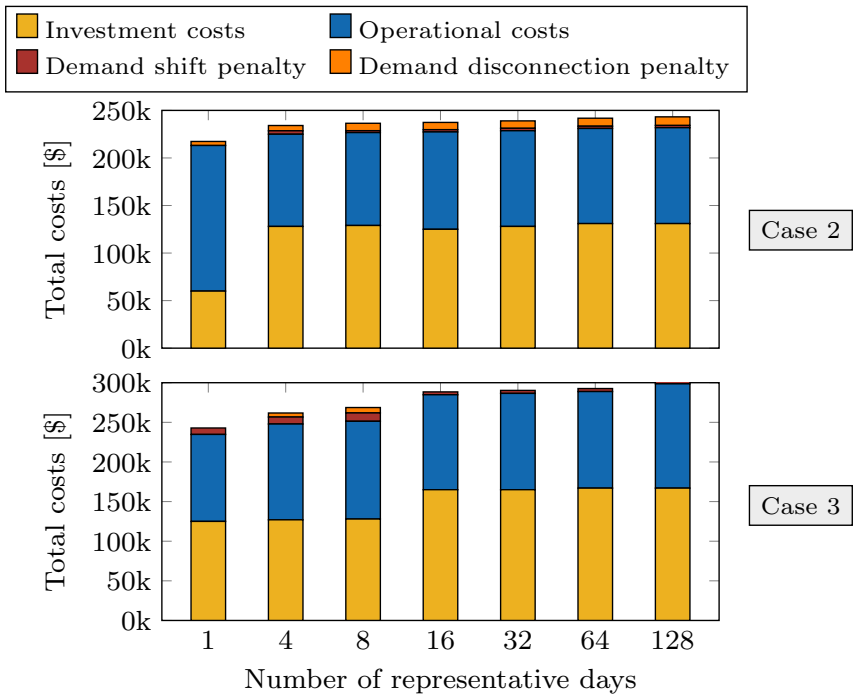

Figure 6.8: Total costs for different representative days in Cases 2 and 3.

Table 6.7: Investment costs and decisions considering Cases 2 and 3 for different representative days

Investment costs ($) and decisions		
Representative days	Case 2	Case 3
1	60000 (PV_3)	125000 (PV_2, PV_3)
4	128000 (PV_2, PV_3 + Line 1-2, 2-3, 3-11)	127000 (PV_2, PV_3 + Line 1-2, 2-3)
8	128000 (PV_2, PV_3 + Line 1-2, 2-3, 3-11)	127000 (PV_2, PV_3 + Line 1-2, 2-3)
16	128000 (PV_2, PV_3 + Line 1-2, 2-3, 3-11)	165000 (PV_2, PV_3, SG_2)
32	128000 (PV_2, PV_3 + Line 1-2, 2-3, 3-11)	165000 (PV_2, PV_3, SG_2)
64	130000 (PV_2, PV_3 + Line 1-2, 2-3, 3-4, 4-5, 5-6, 3-11)	167000 (PV_2, PV3, SG_2 + Line 4-5, 5-6)
128	130000 (PV_2, PV_3 + Line 1-2, 2-3, 3-4, 4-5, 5-6, 3-11)	167000 (PV_2, PV_3, SG_2 + Line 4-5, 5-6)

Case 3 was also studied with and without flexible loads to thoroughly analyze their impact. In the case of 1 and 16 representative days, the operational costs experience a marginal decrease under the use of flexible loads, whereas the investment costs remain intact, as depicted in Fig. 6.10. In contrast, for other representative periods the use of flexible loads leads to lower investment costs, as they alleviate the problems pertaining to adequate power supply. Moreover, in all four cases the total costs increase without the use of flexible loads, thus making their adoption vital for system flexibility and eco-

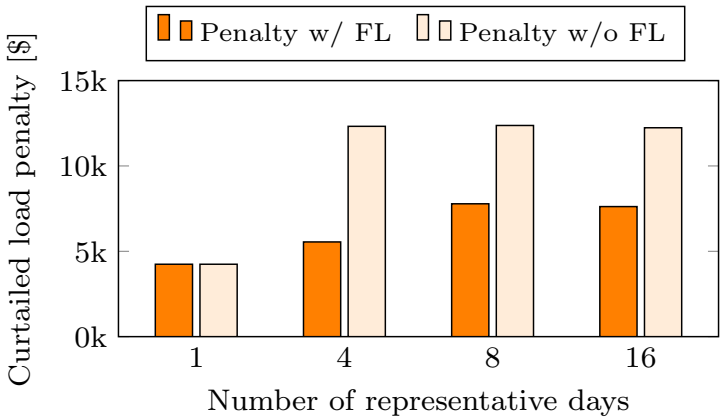

Figure 6.9: Sensitivity of curtailed load penalty to the presence of flexible loads for different representative days in Case 2.

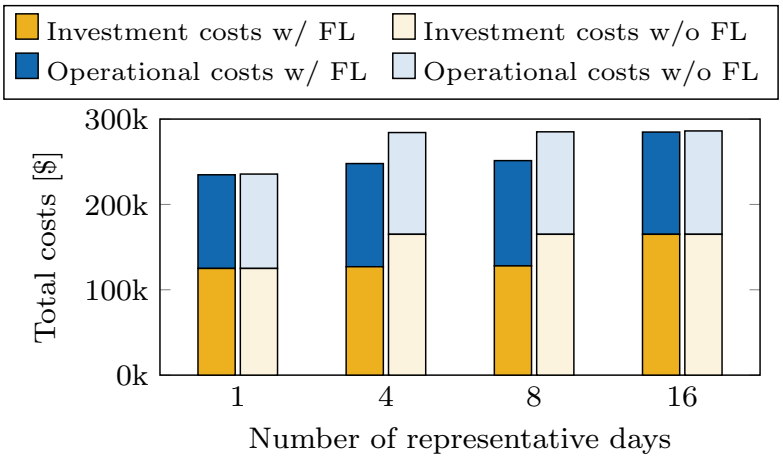

Figure 6.10: Sensitivity of investment and operational costs to the presence of flexible loads for different representative days in Case 3.

nomic operation. The latter aspect is primarily related to the presence of renewable PV units, which allow for the loads to be shifted to periods of higher solar generation. This differentiation is more prominent in cases with 4 and 8 representative days since the use of flexible loads allows to differ investment decisions.

Table 6.8: Comparison Between Out-of-Sample and In-Sample Total Operational Costs and Design Feasibility

	Operational costs	Demand shift penalty	Demand disconnection penalty	Transient feasibility
Case 2	9.7% ↑	0.0%	0.0%	78.6%
Case 3	7.3% ↓	5.4% ↓	0.0%	100%

6.7.4 Out-of-sample Performance

To evaluate the performance of the system design and its feasibility against different realisations of uncertain parameters, the full pattern of realistic 365 days as out-of-sample scenarios for load and PV generation is adopted. Using the optimal investment solution provided in for 16 representative days in both Case 2 and 3, an operational planning problem is run separately for each of the 365 days for out-of-sample analysis. The total operational costs and transient feasibility considering all 365 days is compared with the solution provided based on the representative day clusters. Table 6.8 presents a comparison between total operational costs of in-sample and out-of-sample scenarios. It is noteworthy to mention that in-sample scenarios are used within the proposed investment planning tool to obtain the optimal MG design, while the out-of-sample scenarios are used to evaluate the long-term performance of the optimal design under different realisations of uncertain loads and PV generations. Understandably, there is a slight increment in the total operational cost in Case 2 with only static security constraints. In other words, the stochastic approach may not be able to cover the entire spectrum of potential scenarios that may occur in system operation. However, the total costs with the inclusion of transient security constraints show a decrease indicating that the design remains robust to all different potential islanding scenarios in the year. Furthermore, Table 6.8 shows the transient feasibility percentage for the optimal solutions in Case 2 and Case 3. According to Table 6.8, the optimal MG design in Case 2 is not feasible in 21.4% of the out-of-sample scenarios. However, the optimal design remains 100.0% feasible when considering either only static security or both static and transient security for MG design in Case 3.

6.7.5 Computational Effort and Scalability

All case studies have been performed on a laptop with an Intel Core i5 processor at 1.8GHz with 8GB memory. The three stages of the proposed algorithm are solved as: Stage 1 - stochastic-robust MILP; Stage 2 - deterministic Linear Programming (LP); and Stage 3 - analytical problem. For Stages 2 and 3, the computing time is less than 1.5 s on average to obtain the solution of each individual hour. However, in Stage 1, the solution space of the problem is a function of the number of scenarios, i.e., number of representative days. In Table. 6.9, a comparison of the computational time for different numbers of representative days and different state-of-the-art optimization tools is presented. An increase in the number of representative days leads to a larger solution space with more decision variables, and consequently, a higher computational time. By adopting a suitable

Table 6.9: Computation Time for Different Representative Days

	Computation time [s]		
No. of representative days	GUROBI	CPLEX	MOSEK
1	25	26	28
4	63	108	274
8	156	230	689
16	354	465	2254
64	2787	6027	189658

solver, the computational time can be optimized. In Table. 6.9 GUROBI solver indicates the fastest response. Nonetheless, the exponential growth in solution time and increase in the solution space with the number of representative days can further increase the risk of intractability. Therefore, it is vital to compromise between accuracy and tractability of the proposed planning tool by choosing a sufficient number of representative days. In the same regard, a single-year planning model was utilized as opposed to a multi-year model. While the latter provides a higher accuracy, the number of variables and constraints increase significantly resulting in a higher risk of intractability.

6.8 Conclusion

This chapter proposes a MG investment and operational planning problem under both steady-state operational constraints in grid-connected and islanding modes in addition to transient frequency islanding constraints. By explicitly embedding the islanding constraints in the planning problem, the survivability of the system can be guaranteed while self-sufficiency is assessed as a function of the load supplied in islanded conditions. However, after the islanding event, the transient behaviour of the MG is dictated both by the non-linear dynamics and the investment and operation decisions, which poses many challenges concerning the problem formulation. The problem is addressed by proposing an iterative three-stage algorithm that resolves the underlying tractability issues and computational challenges, as well as shows excellent performance on the examined case studies. Furthermore, it has been highlighted that the presence of flexible loads and the control capability of the local generators is vital in improving the MG operational flexibility and robustness. It is clear though that not considering the transient behaviour of the MG right after the islanding event, can lead to optimistic investment and operational decisions and can endanger the survivability of the MG.

The next chapter covers additional aspects that are required to enhance opitmality and

computational efficiency. More specifically, the impact of information exchange between different layers of the algorithm on the solution optimality and rate of convergence is assessed further.

Chapter 7

A Decomposition Strategy for Inertia-aware Planning Models

The integration of the frequency dynamic evolution into MG investment and operational planning problems is vital in improving the security of the system in the post-contingency states. The task of including transient security constraints in a planning problem is however non-trivial. This is due to the highly non-linear and non-convex nature of the analytical closed form of the frequency metrics and power flow constraints. Additionally, during system planning various integer variables originate from modelling of the physical components e.g operation of automatic devices such as tap changers, implementation of priority controls and from binary decisions such as whether or not to install new devices during the expansion planning problems. The resulting model, a Mixed Integer Nonlinear Programming (MINLP) problem, is intractable due to the enumerations required at all the discrete integer points in the feasible search space [174] and its non-convexity.

In Chapter 6, an iterative solution algorithm that uses a bound-tightening technique to solve inertia-aware MG investment and operational planning problems and mitigate any existing security violations is presented. However, the algorithm proposed therein sequentially uses the solution at each stage to inform the next with no information exchange on the impact of current or previous solutions between stages. As such, it does not allow for exchange of sensitivity information between the solutions provided at the different stages, leading to conservative and sub-optimal solutions. In this chapter, a decomposition-based solution strategy is proposed to solve the same problem. This algorithm ensures information exchange between the different stages by using dual-cutting planes. Moreover,

the highly non-linear expression of the frequency nadir is approximated with a first-order Taylor expansion. The performance of the algorithm is tested under different operational scenarios generated using a clustering technique and the results are compared with the bounds-tightening technique presented in Chapter 6.

7.1 Introduction

Related Works

As discussed in Chapter 6, the application of dynamic constraints on the frequency security problem to an optimisation problem is no trivial task. This is due to the high order nonlinear expressions defining the dynamic frequency response resulting in a high computational burden. In [42], the time evolution of system frequency deviation has been described by a first-order ordinary differential equation. This dynamic model is adopted in [153] to formulate expressions for frequency nadir, RoCoF, and quasi-steady-state frequency to apply to a stochastic scheduling problem. Whilst the RoCoF and nadir constraints are convex, the non-linear nadir expression has been approximated by a bi-linear constraint with further sufficient conditions on the approximation defined by mixed-integer linear constraints.

Sufficient conditions derived from a pre-determined frequency trajectory are applied to the linearized frequency nadir constraints in [175] for unit commitment and economic dispatch of power generators. In [176], a two-step linearisation technique defined by an inner approximation utilising overestimating planes and the standard big-M technique is employed to linearise the nadir expression. While the work in [177] transforms the frequency nadir constraints into the capacity reserve constraints using a series of linear frequency security margin constraints formulated by piece-wise linearisation fitting of the non-linear expression. Similarly [155] tackles this problem by approximating the nadir expression using a Piece-Wise Linearisation (PWL) technique. In the linearised form, the expression is suitably integrated into a security-constrained unit commitment problem with frequency limits applied.

In [164], a low order time-domain frequency response model and the analytical expressions for the transient frequency security metrics were derived considering only SG units and enhanced in [165] to include the support from CIG units. The work in [1] uses ex-ante bound extractions on the variables in the nadir expression using potential dispatch conditions that are then applied to the optimisation problem replacing the non-linear nadir expression.

Differing from the techniques proposed in the above literature, a sequential linearisation using an iterative technique was proposed in Chapter 6 using the frequency model in [165]. The first stage of the problem ensures optimality of the planning solution while the second stage is a feasibility checking problem against the transient security problem. In the third stage, new tighter bounds are formulated for the first stage problem if violations exist. This approach does not require any approximation of the transient frequency constraints when applied to the optimisation problem. However, it provided a rather conservative solution. In addition, similar to the previous literature, the effect of the composite generator parameters on the planning solution and security limits is not adequately studied.

In this chapter, an iterative two-level solution based on dual-cutting planes is proposed to solve the model presented in Chapter 6. The dual-cutting planes ensure that the effect of parameter changes in the second-level feasibility-checking problem is captured by the first-level planning solution. The approach, therefore, allows for the decoupling of frequency services where emphasis can be applied on single or multiple services provision. This ensures the optimal sizing and provision of frequency services by a network.

Contributions

The contribution of this chapter is therefore twofold.

First, two, three-stage decomposition strategies that tractably incorporate the non-linear transient frequency security constraints in an investment and operational planning problem for MGs are proposed. The decomposition approach proposed utilises dual cutting planes to ensure bi-directional information exchange between the stages of the planning problem. In addition, a Taylor series expansion is utilised to convexify the non-linear constraints resulting in a tractable solution approach.

Second, the functionality of the proposed decomposition-based algorithms is compared against the bounds-tightening approach presented in Chapter 6 under different operational scenarios characterised by representative days generated by the k-means clustering method. Metrics utilised include the transient performance, planning costs and computational efficiency of the three models. The performance is verified on the 18-bus CIGRE European LV network and a 30-bus medium voltage distribution network.

The remainder of the chapter is organised as follows: Section 7.2 reviews different decomposition techniques used in dealing with mixed-integer nonlinear problems. Section 7.3 presents a recollection of the frequency response algorithm and formulation of the

planning problem while Section 7.4 describes the proposed decomposition strategy for the inertia-aware planning model. The case study results are presented in Section 7.5 and finally conclusions are drawn in Section 7.6.

7.2 Dealing with Mixed Integer Nonlinear Programming Problems Using Decomposition Techniques

A general formulation of a Mixed Integer Nonlinear Programming (MINLP) problem can be described as:

$$\phi = \min \quad f(x, y) \tag{7.1a}$$

$$\text{s.t.} \quad g_j(x, y) \leq 0, \quad \forall j = 1, \ldots, m \tag{7.1b}$$

$$x \in \mathbb{R}, y \in \mathbb{Z}, \tag{7.1c}$$

where x and y denote continuous and integer variable respectively while m represent the number of constraints. ϕ is the optimal solution to the problem while the variables take on values (x^*, y^*) at optimality.

Decomposition methods exploit the problem structure by decomposing the large problem into smaller problems that can be solved in parallel or sequentially. The operations common to the different methods for solving MINLPs using such techniques involve two main iterative steps i.e., first, the relaxation of the problem and second constraint enforcement and search of the solution space [178]. For an optimisation problem $\{\min f(x, y) : (x, y) \in \Psi\}$, the problem $\{\min f_{\mathrm{R}}(x, y) : (x, y) \in \Psi_{\mathrm{R}}\}$ is a relaxation if $\Psi \subseteq \Psi_{\mathrm{R}}$ and $f(x, y) \leq f_{\mathrm{R}}(x, y)$. Relaxation provides a lower bound ϕ_{L} for the solution of (7.1a). A relaxation can be performed in various ways including relaxing the integer variables to a continuous form with upper and lower limits or relaxing them using convex constraints defined by a set of supporting hyperplanes [178], e.t.c.
Constraint enforcement includes all search procedures aimed at excluding solutions infeasible to the original (un-relaxed) problem through 'branching' or tightening of the relaxation. The goal is that the algorithm can eventually converge to a solution that satisfies all constraints to the problem. Branching is a process where the relaxation is divided into two or more separate problems, while tightening involves the addition of further inequalities to the problem by adding new constraints that satisfy all feasible solutions but exclude a given infeasible solution. This second step usually provides an

upper bound ϕ_U to the original problem. An optimal solution (convergence) is obtained on termination of the iteration when the lower bound from the relaxation is equal or larger than the upper bound or as close as possible.

Before providing a brief description of the main algorithms adopted in research, a few key concepts are described:

Cutting plane methods

The goal with cutting plane methods is to find if a certain point in the relaxation space Ψ_R belongs to the feasible set of the un-relaxed problem Ψ. If the solution to the relaxation (denoted here as (x_R^*, y_R^*)) lies in the feasible space this is the optimal solution ($x_R^* = x^*$, $y_R^* = y^*$). Otherwise, a *valid inequality* is generated in form of a separating hyperplane which separates the region where all feasible solutions lie excluding (x_R^*, y_R^*). If the valid inequality successfully excludes the infeasible solution, it is referred to as a *cut*. The separating hyperplane can then be added as an inequality to the relaxation to further narrow down (tighten) the search space. Figure 7.1 illustrates the concept of cutting planes.

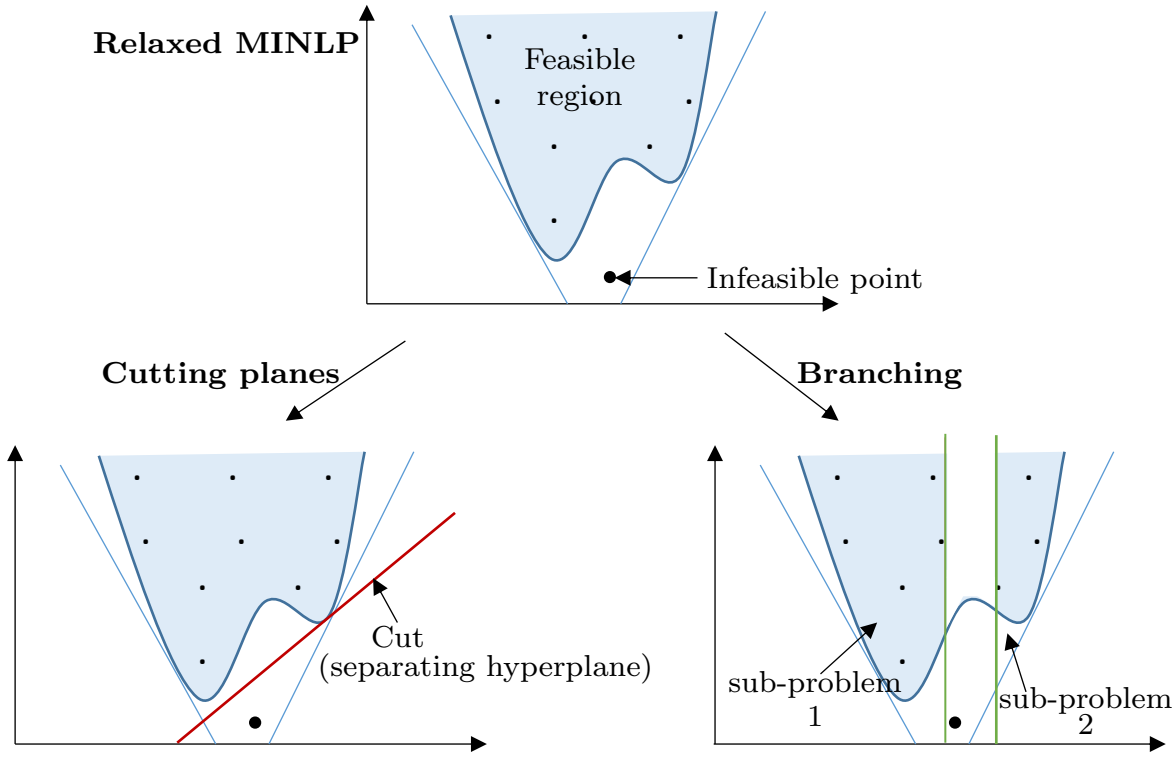

Figure 7.1: Illustration of the cutting planes and branching concepts.

Branching

Branching partitions the problem into sub problems based on the value (or range of values) of the integer variables in the feasible region. Based on an infeasible solution obtained from the relaxation, branching can create, for example, two sub-problems based on constraints of the form: ($y \leq \lceil y_{\mathrm{R}} \rceil$) and ($y \leq \lfloor y_{\mathrm{R}} \rfloor$), as illustrated in Fig. 7.1. These sub-problems represent the branching decisions and the solutions to the MINLP can lie in either of the sub-problems. The sub-problems are each recursively solved by the same procedure. The result is a search-tree of sub-problems (nodes) and constraints (edges) which can be utilised to manage all sub-problems that need to be solved.

7.2.1 Primal decomposition/Cuts

A non-separable problem of the form given in (7.2), with the variable y in this case being a coupling (complicating) variable can be complex to solve. Variable y is considered a complicating variable or coupling variable given that when it is fixed the problem is separable in x_1 and x_2. This can be seen as a case of a MINLPs where the integer constraints can complicate the solution to a given problem.

$$\min_{x_1, x_2, y} \quad f(x_1, y) + f(x_2, y) \tag{7.2}$$

In primal decomposition, to make the problem separable, the value of y is fixed to y^k for a given scenario k creating two sub-problems i.e.

$$\text{sub-problem 1:} \quad \Phi_1(y) = \min_{x_1} \quad f_1(x_1, y^k) \tag{7.3a}$$

$$\text{sub-problem 2:} \quad \Phi_2(y) = \min_{x_2} \quad f_1(x_2, y^k) \tag{7.3b}$$

The original problem in (7.2) is then transformed into the master problem denoted as:

$$\min_{y} \quad \Phi_1(y) + \Phi_2(y) \tag{7.4}$$

At each iteration, the two sub-problems are solved in parallel to obtain optimal values of x_1 and x_2 which are then used to update the value of y in the master problem until convergence is achieved.

7.2.2 Dual Decomposition/Cuts

Dual cuts deal with the coupling integer variable in (7.2) by introducing new variables y_1 and y_2, as well as a new constraint $y_1 = y_2$. A dual problem of the original problem is formulated using the Lagrangian as:

$$\mathcal{L}(x_1, x_2, y_1, y_2) = f_1(x_1, y_1) + f_2(x_2, y_2) + \lambda(y_1 - y_2) \tag{7.5}$$

where λ is the Lagrangian multiplier also known as the the dual variable associated with the new constraint $\{y_1 = y_2\}$.

Equation (7.5) is separable and can be decomposed into sub-problems of the form:

$$\text{sub-problem 1:} \quad \Phi_1(\lambda) = \min_{x_1, y_1} \quad f_1(x_1, y_1) + \lambda^T y_1 \tag{7.6a}$$

$$\text{sub-problem 2:} \quad \Phi_2(\lambda) = \min_{x_2, y_2} \quad f_1(x_2, y_2) + \lambda^T y_2 \tag{7.6b}$$

The master problem in this case is the dual problem of the form:

$$\min_{\lambda} \quad \Phi_1(\lambda) + \Phi_2(\lambda) \tag{7.7}$$

The dual sub-problems (7.6) can be solved in parallel or sequentially to update the dual variable λ which is used by the master problem to obtain an upper bound solution to a given problem. Optimality is attained when convergence between the master and sub-problems is achieved.

7.2.3 Decomposition Techniques

The most widely adopted decomposition algorithms for solving MINLP with a separable structure problems include Branch-and-bound (BB), Outer Approximation (OA) and Bender's Decomposition (BD) [174, 179].

BB [180] adopts the branching concept as a first step to partition the feasible region into sub-regions or sub-problems and thus obtain lower bounds to the optimal solution. These are then removed from further consideration i.e. pruned if: (i) the sub-problem is infeasible; (ii) the lower bound obtained is higher than the current upper bound obtained so far and (iii) the solution to the sub-problem is feasible i.e. the integer variables take on discrete values in which case these provide the upper bound to the original problem. The algorithm is terminated when no nodes are left to explore and the solution returned is proven to be optimal. The BB algorithm is usually only applied in cases where the

sub-problems are few or relatively inexpensive to solve [71, 181].

The OA algorithm proposed in [182, 183] uses primal information to linearise the objective and constraints around a given point. Based on the linearisations, the problem is decomposed into Non-Linear Programming (NLP) sub-problems with continuous variables and a Mixed Integer Linear Programming (MILP) master problem containing the integer variables.

BD [91, 184] utilises a similar procedure to OA but with the difference stemming from the nature in which the master MILP problem is defined. Unlike OA that is based on primal cuts of the MINLP, BD eliminates the continuous variables by projecting the MINLP in a reduced space consisting of only the complicating variables using dual cuts.

Fixing the complicating variable $y = y^k$, the NLP problem is formulated as:

$$
\begin{aligned}
f(x_k, y_k) = \min_{x,y} \quad & f(x, y) && && \text{(7.8a)}\\
\text{s.t.} \quad & g_j(x, y) \leq 0, \quad \forall j = 1, \ldots, m && && \text{(7.8b)}\\
& y = y^k, && (\textit{dual}\ \lambda^k) && \text{(7.8c)}\\
& x \in X, \quad y \in Y && && \text{(7.8d)}
\end{aligned}
$$

The solution of the problem above provides values for the non-complicating variable, x, and the dual variable λ^k associated with the constraint (7.8c) that fixes the complicating variables to a given value.

The Benders master problem, solved at iteration k, is defined as:

$$
\begin{aligned}
\min_{y,\alpha} \quad & \alpha && && \text{(7.9a)}\\
\text{s.t.} \quad & \alpha \geq f(x^k, y^k) + \lambda^k (y - y^k), && \forall k = 1, \ldots, K && \text{(7.9b)}\\
& y \in Y && && \text{(7.9c)}
\end{aligned}
$$

While BD on average requires more iterations than the OA method, the former has a smaller master problem that considers only the integer variables and the single constraint (7.9b) used to combine the effect of constraints in the sub-problems hence it is more tractable [185].

The structure of an inertia-aware planning problem is comparable to a separable MINLP problem. If the investment decision and/or operational dispatch decisions are fixed, the transient security relations can be evaluated to ensure feasibility of the solution. The

upper bounds are provided by the transient security problems while the lower bounds are obtained during the dispatch problem. Convergence, and therefore optimality, is achieved when the upper and lower bounds are equal or within a defined tolerance. In the subsequent sections, the formulation of the decomposition based problem is presented in more detail.

7.3 Preliminaries

7.3.1 Frequency Response Model

Recalling from Section 6.3, the frequency metrics namely frequency nadir $\Delta f_{\max}$, RoCoF $\dot{f}_{\max}$ and quasi steady-state deviation Δf_{ss} can be obtained analytically as follows:

$$\dot{f}_{\max} = \dot{f}(t_0^+) = -\frac{\Delta P}{M}, \tag{7.10a}$$

$$\Delta f_{\max} = -\frac{\Delta P}{D+R_s}\left(1+\sqrt{\frac{T(R_s-F_s)}{M}}e^{-\zeta\omega_n t_m}\right), \tag{7.10b}$$

$$\Delta f_{\text{ss}} = -\frac{\Delta P}{D+R_s}, \tag{7.10c}$$

where $\omega_n = \sqrt{\frac{D+R_s}{MT}}$ and $\zeta = \frac{M+T(D+F_s)}{2\sqrt{MT(D+R_s)}}$. Time t_m denoting the time instance of frequency nadir is defined as:

$$t_m = \left({}^{1}\!/_{\omega_d}\right)\tan^{-1}\left({}^{\omega_d}\!/_{(\omega_n\zeta - T^{-1})}\right) \tag{7.11}$$

where variable ω_d defined as $\omega_d = \omega_n\sqrt{1-\zeta^2}$. Further parameters in (7.10) are calculated as:

$$M_s = \sum_{i\in\mathcal{S}} M_i \frac{P_i}{P_s^{\text{base}}}, \qquad D_s = \sum_{i\in\mathcal{S}} D_i \frac{P_i}{P_s^{\text{base}}}, \tag{7.12a}$$

$$R_s = \sum_{i\in\mathcal{S}} \frac{K_i}{R_i}\frac{P_i}{P_s^{\text{base}}}, \qquad F_s = \sum_{i\in\mathcal{S}} \frac{K_i F_i}{R_i}\frac{P_i}{P_s^{\text{base}}}, \tag{7.12b}$$

$$M_c = \sum_{v\in\mathcal{C}^v} M_v \frac{P_{c_v}}{P_c^{\text{base}}}, \qquad D_c = \sum_{v\in\mathcal{C}^v} D_v \frac{P_{c_v}}{P_c^{\text{base}}}, \tag{7.12c}$$

$$R_c = \sum_{d\in\mathcal{C}^d} R_d \frac{P_{c_d}}{P_c^{\text{base}}}, \tag{7.12d}$$

$$M = \frac{M_s P_s^{\text{base}} + M_c P_c^{\text{base}}}{P_g^{\text{base}} + P_{b_c}^{\text{base}}}, \tag{7.12e}$$

$$D = \frac{D_s P_s^{\text{base}} + D_c P_c^{\text{base}} + R_c P_c^{\text{base}}}{P_s^{\text{base}} + P_c^{\text{base}}}. \tag{7.12f}$$

where M_s, D_s, F_s and R_s are associated with the weighted averages of the inertia constants for the CoI, damping constants, fractions of the total power generated by the turbines and droop, respectively, for all SGs. While parameters M_c, D_c and R_c represent the weighted average of inertia of all CIGs, the weighted average of all virtual damping constant of Virtual Synchronous Machine (VSM) based CIGs and weighted average droop of all CIGs respectively. M and D denote the normalised inertia constant and damping, respectively, of all SGs and CIGs.

Parameters P_i and P_c are associated with the active power capacity of the SG and CIG, respectively, while P_s^{base} and P_s^{base} denote respective base power of all connected SGs and CIGs described by: $P_s^{\text{base}} = \sum_{i \in \mathcal{S}} P_i$ and $P_c^{\text{base}} = \sum_{c \in \mathcal{C}} P_c$.

It is clearly seen that the aggregate system control parameters M, D, R_g and F_g have a direct impact on frequency performance. In particular, RoCoF and steady-state deviation are explicitly affected by M and (D, R_g), respectively, while frequency nadir has a highly non-linear dependency on all four system parameters.

7.3.2 Compact Formulation

The inertia-aware expansion planning problem for a MG can be compactly represented as:

$$\min_{\chi \in \Omega^{\text{MG}}} \ \Theta^{\text{inv}}(\chi^{\text{inv}}) + \Theta^{\text{gm,opr}}(\chi^{\text{inv}}, \chi^{\text{gm,opr}}) + \gamma \tag{7.13a}$$

$$\text{s.t.} \quad \gamma \geq \Theta_{to}^{\text{im,opr}}(\chi^{\text{inv}}, \chi^{\text{gm,opr}}, \chi^{\text{im,opr}}), \qquad \forall t \in \mathcal{T}, o \in \mathcal{O}, \tag{7.13b}$$

$$\Phi(\chi^{\text{inv}}, \chi^{\text{gm,opr}}) = 0, \tag{7.13c}$$

$$\Lambda(\chi^{\text{inv}}, \chi^{\text{gm,opr}}) \leq 0, \tag{7.13d}$$

$$\dot{f}_{to}^{\max} \leq \overline{\dot{f}}^{\max}, \qquad \forall t \in \mathcal{T}, o \in \mathcal{O}, \tag{7.13e}$$

$$\Delta f_{to}^{\max} \leq \overline{\Delta f}^{\max}, \qquad \forall t \in \mathcal{T}, o \in \mathcal{O}, \tag{7.13f}$$

$$\underline{\Delta f}^{\text{ss}} \leq \Delta f_{to}^{\text{ss}} \leq \overline{\Delta f}^{\text{ss}}, \qquad \forall t \in \mathcal{T}, o \in \mathcal{O} \tag{7.13g}$$

where set Ω^{MG} includes all decision variables χ relating to the investment χ^{inv}, grid-connected operation $\chi^{\text{gm,opr}}$ and islanded operation $\chi^{\text{im,opr}}$ of the MG i.e., $\Omega^{\text{MG}} = \{\chi = [\chi^{\text{inv}}, \chi^{\text{gm,opr}}, \chi^{\text{im,opr}}] \,|\, \chi^{\text{inv}} \in \Omega^{\text{inv}} \,;\, \chi^{\text{gm,opr}} \in \Omega^{\text{gm,opr}} \,;\, \chi^{\text{im,opr}} \in \Omega^{\text{im,opr}}\}$.

The objective function (7.13a) minimises the total investment costs (Θ^{inv}), the *"ex-*

pected" total operation costs in grid-connected mode for all hours of all representative days ($\Theta^{\text{gm,opr}}$), and the *"worst-case"* total penalty costs of disconnecting loads from MG in islanded mode for each hours in all representative days ($\Theta^{\text{im,opr}}$). The auxiliary variable γ is used to minimise the costs at each hour rather than the aggregated costs for all hours and all representative days. Constraints (7.13c) and (7.13d) relate to the static investment and operational constraints in grid-connected and islanded modes described in Section 6.5.1. The transient frequency security constraints are applied using constraints (7.13e)-(7.13g). In this study, the transient response in (7.10) depends on the amount of power exchange with the main grid at the time of islanding of the MG i.e., $\Delta P = \boldsymbol{p}_{to}^{\text{grid}} = \{p_{to}^{\text{b}}, p_{to}^{\text{s}}\}$.

The formulation in (7.13) is an inertia-aware planning problem subjected to the transient frequency security constraints (7.13e), (7.13f) and (7.13g) under various operational scenarios. This ensures that both the operational feasibility and adequacy of operating reserves for frequency support are satisfied by the planning solution obtained.

The planning problem (7.13) is an MINLP including the integer variables of the investment status of the candidate generators and the non-linear, non-convex transient security constraints. It should be emphasised that the support provided by a generator g given its availability or investment status z_g is based on its control parameters i.e., $M(z_g)$, $D(z_g)$, $F_g(z_g)$ and $R_g(z_g)$. This problem is NP-hard and can be intractable.

To tackle the issue of intractability, first the problem is decomposed into a master problem and sub-problems where the sub-problems include relaxations of the integer variables. Secondly, the non-linear transient constraints here mainly relating to the nadir constraint (7.13f) are convexified. The final multi-stage model is tractable and includes MILP master problems and LP sub-problems as described in the following section.

7.4 A Decomposition Strategy for Inertia-Aware MG Planning based on Dual Cutting Planes

In this section, two algorithms outlining a computationally efficient approach to solve the problem using dual-cutting planes are proposed. The solution approach utilises the Bender's decomposition algorithm to decompose and solve the MINLP problem based on a four-step iterative procedure. Unlike the approach presented in Section 6.5, where the effect of the Stage 1 solutions to the Stage 2 outcome is not captured, the dual cutting planes applied in this chapter capture the sensitivity of the relaxed master-problem

variables to the solution of the sub-problem. The sensitivities are then used in the computation of the master problem at the next iteration therefore capturing the impact of master problem solutions to the sub-problem outcome.

7.4.1 Algorithm 1

In Algorithm 1 (A1), the complicating variables are associated with power exchange with the grid $\boldsymbol{p}^{\text{grid},\kappa}$ and the total of the inertia constants for the CoI, damping constants, fractions of the total power generated by the turbines and droop of the connected DERs. These are denoted as $\breve{M}_s$, $\breve{D}_s$, $\breve{F}_s$ and $\breve{R}_s$ associated with the total of the inertia constants for the CoI, damping constants, fractions of the total power generated by the turbines and droop, respectively, for all SGs. The accent $\breve{\bullet}$ is used to differentiate a non-normalised parameter from its normalised counterpart. In addition, $\breve{M}_c$, $\breve{D}_c$ and $\breve{R}_c$ are the total available inertia of all CIGs, virtual damping constant of VSM-based CIGs and droop of all CIGs, respectively. While $\breve{M}$ and $\breve{D}$ denote the total inertia constant and damping, respectively, of all SGs and CIGs. The tasks involved at each iteration are detailed as follows:

Step 1: Initial Formulation of the Master Problem

Initially, at iteration $\kappa = 1$, the master problem, which is a relaxation of (7.13), is solved to obtain feasible values of the complicating variables. It is formulated as follows:

$$\min_{\chi \in \Omega^{\text{MG}}} \ \Theta^{\text{inv}}(\chi^{\text{inv}}) + \Theta^{\text{gm,opr}}(\chi^{\text{inv}}, \chi^{\text{gm,opr}}) + \gamma \tag{7.14a}$$

$$\text{s.t. } \gamma \geq \Theta^{\text{im,opr}}_{to}(\chi^{\text{inv}}, \chi^{\text{gm,opr}}, \chi^{\text{im,opr}}), \qquad \forall t \in \mathcal{T}, o \in \mathcal{O}, \tag{7.14b}$$

$$\Phi(\chi^{\text{inv}}, \chi^{\text{gm,opr}}) = 0, \tag{7.14c}$$

$$\Lambda(\chi^{\text{inv}}, \chi^{\text{gm,opr}}) \leq 0, \tag{7.14d}$$

$$\breve{M}_s = \sum_{i \in \mathcal{S}} M_i P_i \cdot z_i, \qquad \breve{D}_s = \sum_{i \in \mathcal{S}} D_i P_i \cdot z_i, \tag{7.14e}$$

$$\breve{R}_s = \sum_{i \in \mathcal{S}} \frac{K_i}{R_i} P_i \cdot z_i, \qquad \breve{F}_s = \sum_{i \in \mathcal{S}} \frac{K_i F_i}{R_i} P_i \cdot z_i, \tag{7.14f}$$

$$\breve{M}_c = \sum_{v \in \mathcal{C}^v} M_v P_{c_v} \cdot z_v, \qquad \breve{D}_c = \sum_{v \in \mathcal{C}^v} D_v P_{c_v} \cdot z_v, \tag{7.14g}$$

$$\breve{R}_c = \sum_{d \in \mathcal{C}^d} R_d P_{c_d} \cdot z_d, \tag{7.14h}$$

$$\breve{M} = \breve{M}_s + \breve{M}_c, \tag{7.14i}$$

$$\breve{D} = \breve{D}_s + \breve{D}_c + \breve{R}_c, \tag{7.14j}$$

$$P^{\text{base}} = P_s^{\text{base}} + P_c^{\text{base}} = \sum_{i \in \mathcal{S}} P_i + \sum_{c \in \mathcal{C}} P_c. \tag{7.14k}$$

The master problem (7.14) for A1 is an MILP problem.

Step 2: Linearisation at each operating point

For strong duality to hold the sub-problems in Bender's decomposition should be convex in nature [186, 187]. The nadir constraint (7.13f) defined in (7.10b) is highly non-linear, before its application to the sub-problem, it is linearised around the operating point at each hour of every representative day. Taylor's expansion is utilised to linearise this constraint at each iteration based on the investment status of the different DERs. The nadir expression is therefore reformulated as:

$$\Delta \boldsymbol{f}_{\kappa}^{\max} = \boldsymbol{p}_{\kappa}^{\text{grid}} \cdot \underbrace{\frac{1}{D + R_s}\left(1 + \sqrt{\frac{T(R_s - F_s)}{M}} e^{-\zeta \omega_n t_m}\right)}_{h(D, R_s, F_s, M)} \tag{7.15a}$$

$$\begin{aligned} \approx \boldsymbol{p}_{\kappa}^{\text{grid}} \cdot \Bigg(h_{\kappa} + \frac{\partial h_{\kappa}}{\partial D}\Big(D - D_{\kappa}\Big) + \frac{\partial h_{\kappa}}{\partial R_s}\Big(R_s - R_{s,\kappa}\Big) + \frac{\partial h_{\kappa}}{\partial F_s}\Big(F_s - F_{s,\kappa}\Big) \\ + \frac{\partial h_{\kappa}}{\partial M}\Big(M - M_{\kappa}\Big)\Bigg) \end{aligned} \tag{7.15b}$$

The Taylor expansion introduces an approximation error that lowers the accuracy of the expression. The proximity between the true and approximate expressions is computed using the absolute error i.e., $\epsilon(\Delta \boldsymbol{f}_{\kappa}^{\max}) = \left|\left(\Delta \boldsymbol{f}_{\kappa}^{\max}\right)_{\text{exact}} - \left(\Delta \boldsymbol{f}_{\kappa}^{\max}\right)_{\text{approx}}\right|$, and the relative error i.e., $\frac{\epsilon(\Delta \boldsymbol{f}_{\kappa}^{\max})}{\left(\Delta \boldsymbol{f}_{\kappa}^{\max}\right)_{\text{exact}}}$. Application of these metrics to the above approximation for 1000 scenarios indicated an average absolute error of 4.7878×10^{-4} and a relative error of 0.2734%. Higher order approximations can be adopted for higher accuracy, however, this can result in the non-convexity of the optimisation problem and further complexity. Moreover, dynamic simulation indicated in the preceding sections further provide guarantees on the efficacy of the first order approximation.

Step 3: Formulation of the sub-problem

To check the whether the transient security constraints (7.13e)-(7.13g) are satisfied based on the solution of the master problem ($z_{c,s}^{\kappa} \in \{\mathcal{S}, \mathcal{C}\}, \boldsymbol{p}_{\kappa}^{\text{grid}}$) at iteration κ, feasibility sub-problems are formulated for each hour of every representative day. A slack vector

$\Delta \boldsymbol{p}^{\text{grid},\kappa}$ is introduced and the sub-problems formulated as follows:

$$\min_{\Delta \boldsymbol{p}_\kappa^{\text{grid}}} |\Delta \boldsymbol{p}_\kappa^{\text{grid}}| \tag{7.16a}$$

s.t.

$$\underline{f}^{\max} \leq \frac{\left(\boldsymbol{p}^{\text{grid}} + \Delta \boldsymbol{p}_\kappa^{\text{grid}}\right)}{\breve{M}\big/P_\kappa^{\text{base}}} \leq \overline{f}^{\max}, \tag{7.16b}$$

$$\underline{\Delta f}^{\text{ss}} \leq \frac{\left(\boldsymbol{p}^{\text{grid}} + \Delta \boldsymbol{p}^{\text{grid}}\right)}{\breve{D}\big/P_\kappa^{\text{base}} + \breve{R}_s\big/P_{\kappa,s}^{\text{base}}} \leq \overline{\Delta f}^{\text{ss}} \tag{7.16c}$$

$$\begin{aligned}\underline{\Delta f}^{\max} \leq \left(\boldsymbol{p}^{\text{grid}} + \Delta \boldsymbol{p}_\kappa^{\text{grid}}\right) \cdot \Bigg(& h_\kappa + \frac{\partial h_\kappa}{\partial D}\frac{\left(D - \breve{D}_\kappa\right)}{P_\kappa^{\text{base}}} + \frac{\partial h_\kappa}{\partial R_s}\frac{\left(R_s - \breve{R}_{s,\kappa}\right)}{P_{\kappa,s}^{\text{base}}} \\ & + \frac{\partial h^\kappa}{\partial F_s}\frac{\left(F_s - \breve{F}_{s,\kappa}\right)}{P_{\kappa,s}^{\text{base}}} + \frac{\partial h^\kappa}{\partial M}\frac{\left(M - \breve{M}_\kappa\right)}{P_\kappa^{\text{base}}}\Bigg) \leq \overline{\Delta f}^{\max},\end{aligned} \tag{7.16d}$$

$$\boldsymbol{p}^{\text{grid}} = \boldsymbol{p}_\kappa^{\text{grid}} \qquad (\text{dual } \boldsymbol{\lambda}_\kappa) \tag{7.16e}$$

$$M = \breve{M}_\kappa \qquad (\text{dual } \boldsymbol{\alpha}_\kappa) \tag{7.16f}$$

$$D = \breve{D}_\kappa \qquad (\text{dual } \boldsymbol{\pi}^\kappa) \tag{7.16g}$$

$$R_s = \breve{R}_{s,\kappa} \qquad (\text{dual } \boldsymbol{\mu}_\kappa) \tag{7.16h}$$

$$F_s = \breve{F}_{s,\kappa} \qquad (\text{dual } \boldsymbol{\sigma}_\kappa) \tag{7.16i}$$

where $\boldsymbol{\lambda}_\kappa$, $\boldsymbol{\alpha}_\kappa$, $\boldsymbol{\pi}_\kappa$, $\boldsymbol{\mu}_\kappa$ and $\boldsymbol{\sigma}_\kappa$ are dual variables associated to the constraints that fix the grid power exchange, aggregated inertia, damping, droop and turbine power fraction, respectively, in the sub-problems. These provide the sensitivity of the respective values of complicating variables to the solution obtained from the sub-problem. The sub-problem (7.16) is a Linear Programming (LP) problem.

If the solution to (7.16) is such that the slack variable are equal to zero i.e., $\Delta \boldsymbol{p}_\kappa^{\text{grid}} = 0$, this implies feasibility of the master problem. In this case the algorithm is terminated and the optimal solution is defined by the solution of the master problem.

If, on the other hand, the solution to (7.16) is such that the slack variables are greater than zero i.e., $|\Delta \boldsymbol{p}_\kappa^{\text{grid}}| > 0$, this implies the infeasibility of the sub-problem given the

values of the complicating variables. Physically, this is associated with violations of transient security constraints. In order to eliminate these violations, feasibility cuts are added to the master problem. This ensures that the infeasible solution is removed from the solution space using the dual cutting planes.

Step 4: Formulation of Resilience Feasibility Cut

The master problem in (7.14) is updated with the dual cutting planes applied for every hour of each representative day defined as follows:

$$\begin{aligned}\Delta \boldsymbol{p}_{\nu}^{\text{grid}} + \boldsymbol{\lambda}_{\nu}(\boldsymbol{p}_{\kappa+1}^{\text{grid}} - \boldsymbol{p}_{\nu}^{\text{grid}}) + \boldsymbol{\alpha}_{\nu}(M_{\kappa+1} - M_{\nu}) + \boldsymbol{\pi}_{\nu}(D_{\kappa+1} - D_{\nu}) \\ + \boldsymbol{\mu}_{\nu}(R_{s,\kappa+1} - R_{s,\nu}) + \boldsymbol{\sigma}^{\nu}(F_{s,\kappa+1} - F_{s,\nu}) \leq 0, \qquad \forall \nu = 1, \ldots, \kappa\end{aligned} \tag{7.17}$$

Algorithm 1 has dual cutting planes associated with the grid power exchange and the unit control parameters i.e. inertia and damping constant. This implies that the sufficiency of frequency support is examined based on the power exchange with the grid at each hour $\boldsymbol{p}^{\text{grid}}$, in addition to the aggregated levels of inertia M, damping D and droop support R_s of committed generators and to the turbine power fraction F_s of SG units.

7.4.2 Algorithm 2

Differing from A1, the complicating variables in Algorithm 2 (A2) are defined by the investment status of the different DERs and power exchange with the grid i.e., $z_{c,s}^{\kappa} \in \{\mathcal{S}, \mathcal{C}\}$ and $\boldsymbol{p}^{\text{grid},\kappa}$, respectively. The steps taken to find an optimal solution based on A2 are defined as follows:

Step 1: Formulation of the Master Problem

At iteration $\kappa = 1$, feasible values of the complicating variables are obtained from the MILP master problem, a relaxation of (7.13), formulated as follows:

$$\min_{\chi \in \Omega^{\text{MG}}} \Theta^{\text{inv}}(\chi^{\text{inv}}) + \Theta^{\text{gm,opr}}(\chi^{\text{inv}}, \chi^{\text{gm,opr}}) + \gamma \tag{7.18a}$$

$$\text{s.t. } \gamma \geq \Theta_{to}^{\text{im,opr}}(\chi^{\text{inv}}, \chi^{\text{gm,opr}}, \chi^{\text{im,opr}}), \qquad \forall t \in \mathcal{T}, o \in \mathcal{O}, \tag{7.18b}$$

$$\Phi(\chi^{\text{inv}}, \chi^{\text{gm,opr}}) = 0, \tag{7.18c}$$

$$\Lambda(\chi^{\text{inv}}, \chi^{\text{gm,opr}}) \leq 0, \tag{7.18d}$$

$$P^{\text{base}} = P_s^{\text{base}} + P_c^{\text{base}} = \sum_{i \in \mathcal{S}} P_i + \sum_{c \in \mathcal{C}} P_c. \tag{7.18e}$$

Step 2: Linearisation

The linearisation step is as undertaken in a similar manner to A1 and the result applied to the sub-problem.

Step 3: Formulation of the sub-problem

The feasibility of the master problem defined in (7.18) is evaluated using the sub-problems described as follows:

$$\min_{\Delta \boldsymbol{p}_\kappa^{\text{grid}}} \ |\Delta \boldsymbol{p}_\kappa^{\text{grid}}| \tag{7.19a}$$

s.t.

$$\underline{f}^{\max} \leq \frac{\left(\boldsymbol{p}^{\text{grid}} + \Delta \boldsymbol{p}_\kappa^{\text{grid}}\right)}{M} \leq \overline{f}^{\max}, \tag{7.19b}$$

$$\underline{\Delta f}^{\text{ss}} \leq \frac{\left(\boldsymbol{p}^{\text{grid}} + \Delta \boldsymbol{p}_\kappa^{\text{grid}}\right)}{D + R_s} \leq \overline{\Delta f}^{\text{ss}} \tag{7.19c}$$

$$\begin{aligned}\underline{\Delta f}^{\max} \leq \left(\boldsymbol{p}^{\text{grid}} + \Delta \boldsymbol{p}_\kappa^{\text{grid}}\right) \cdot \Bigg(h_\kappa + \frac{\partial h_\kappa}{\partial D}\Big(D - D_\kappa\Big) + \frac{\partial h_\kappa}{\partial R_s}\Big(R_s - R_{s,\kappa}\Big) \\ + \frac{\partial h_\kappa}{\partial F_s}\Big(F_s - F_{s,\kappa}\Big) + \frac{\partial h_\kappa}{\partial M}\Big(M - M_\kappa\Big)\Bigg) \leq \overline{\Delta f}^{\max},\end{aligned} \tag{7.19d}$$

$$M_s = \sum_{i \in \mathcal{S}} M_i \frac{P_i}{P_{s,\kappa}^{\text{base}}} \cdot z_i, \qquad D_s = \sum_{i \in \mathcal{S}} D_i \frac{P_i}{P_{s,\kappa}^{\text{base}}} \cdot z_i, \tag{7.19e}$$

$$R_s = \sum_{i \in \mathcal{S}} \frac{K_i}{R_i} \frac{P_i}{P_{s,\kappa}^{\text{base}}} \cdot z_i, \qquad F_s = \sum_{i \in \mathcal{S}} \frac{K_i F_i}{R_i} \frac{P_i}{P_{s,\kappa}^{\text{base}}} \cdot z_i, \tag{7.19f}$$

$$M_c = \sum_{v \in \mathcal{C}^v} M_v \frac{P_{c_v}}{P_{c,\kappa}^{\text{base}}} \cdot z_c, \quad D_c = \sum_{v \in \mathcal{C}^v} D_v \frac{P_{c_v}}{P_{c,\kappa}^{\text{base}}} \cdot z_c, \tag{7.19g}$$

$$R_c = \sum_{d \in \mathcal{C}^d} R_d \frac{P_{c_d}}{P_{c,\kappa}^{\text{base}}} \cdot z_c, \tag{7.19h}$$

$$M = \frac{M_s P_{s,\kappa}^{\text{base}} + M_c P_{c,\kappa}^{\text{base}}}{P_{g,\kappa}^{\text{base}} + P_{c,\kappa}^{\text{base}}}, \tag{7.19i}$$

$$D = \frac{D_s P_{s,\kappa}^{\text{base}} + D_c P_{c,\kappa}^{\text{base}} + R_c P_{c,\kappa}^{\text{base}}}{P_{s,\kappa}^{\text{base}} + P_{c,\kappa}^{\text{base}}} \tag{7.19j}$$

$$\boldsymbol{p}^{\text{grid}} = \boldsymbol{p}_\kappa^{\text{grid}} \qquad (\text{dual } \boldsymbol{\lambda}_\kappa) \tag{7.19k}$$

$$\boldsymbol{z}_s = \boldsymbol{z}_{s,\kappa} \qquad (\text{dual } \boldsymbol{\alpha}_{s,\kappa}) \tag{7.19l}$$

$$\boldsymbol{z}_c = \boldsymbol{z}_{c,\kappa} \qquad (\text{dual } \boldsymbol{\pi}_{c,\kappa}) \tag{7.19m}$$

where $\boldsymbol{\lambda}_\kappa$, $\boldsymbol{\alpha}_{s,\kappa}$, and $\boldsymbol{\pi}_{c,\kappa}$, are dual variables associated to the constraints that fix the grid power exchange, SG and CIG investment status, respectively, in the sub-problems.

Step 4: Formulation of Resilience Feasibility Cut

The master problem in (7.18) is updated with the dual cutting planes in case of infeasibility of any of the sub-problems (7.19) i.e., $|\Delta \boldsymbol{p}^{\text{grid},\kappa}| > 0$. The cutting planes are defined as follows:

$$\begin{aligned} \Delta \boldsymbol{p}_{\nu}^{\text{grid}} + \boldsymbol{\lambda}_{\nu}(\boldsymbol{p}_{\kappa+1}^{\text{grid}} - \boldsymbol{p}_{\nu}^{\text{grid}}) + \sum_{s\in\mathcal{S}} \boldsymbol{\alpha}_{\nu,s}(z_{s,\kappa+1} - z_{s,\nu}) \\ + \sum_{c\in\mathcal{C}} \boldsymbol{\pi}_{\nu,c}(z_{c,\kappa+1} - z_{c,\nu}) \leq 0, \qquad \forall \nu = 1,\ldots,\kappa \end{aligned} \tag{7.20}$$

The dual cutting planes in A2 are associated with the grid power exchange and the integer variables relating to the investment status of the different units. The feasibility and thus sufficiency of the frequency support will thus depend on the grid power p^{grid} at each hour and the level of support offered by the different invested DERs.

In both Algorithm 1 and 2, the master problem is an MILP while the sub-problems are LP. These are tractable reformulations of the MINLP problem in (7.13) and can be easily solved with available off-the-shelf optimisation solvers. Figure 7.2 summarises the proposed algorithms.

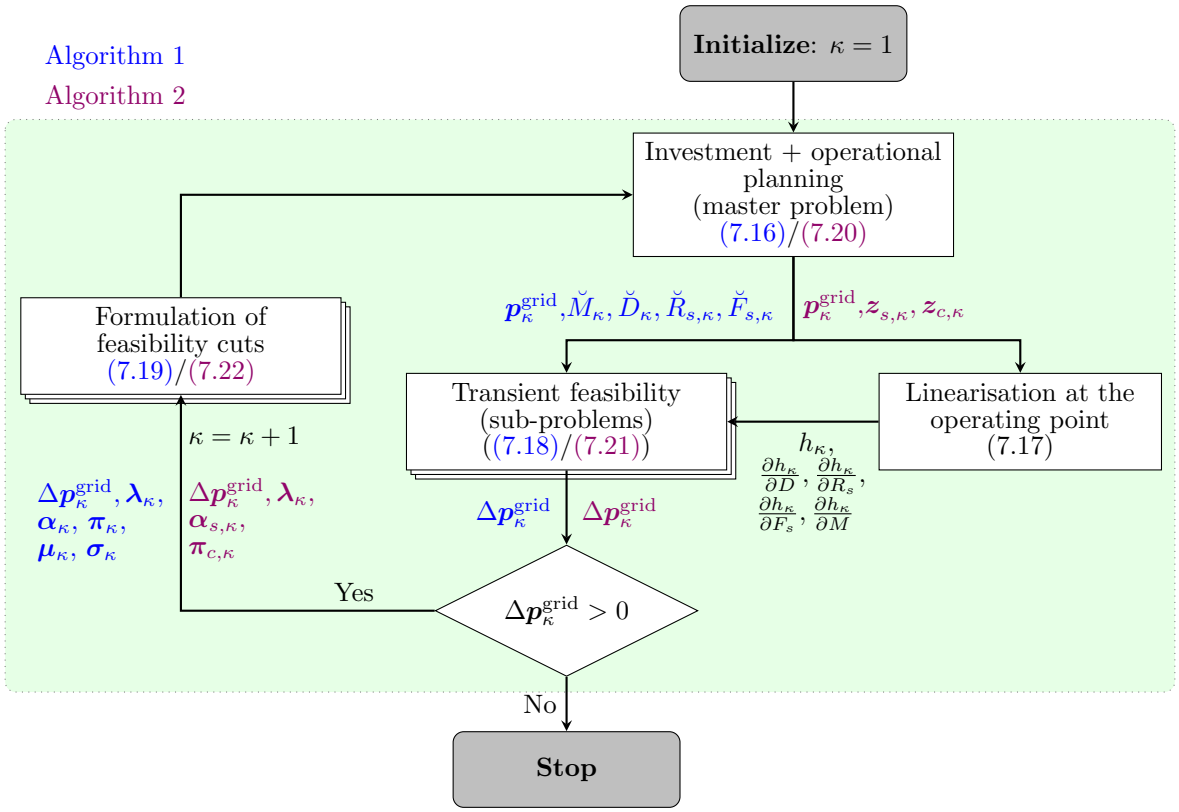

Figure 7.2: Proposed decomposition algorithm for inertia-aware MG planning (where variables are differentiated with A1(blue), A2(purple), and both A1 and A2(black))

7.5 Case Study Results

The algorithms are applied to the European CIGRE low-voltage study network [140] presented in Section 6.6. Recalling from Section 6.6, the 18-bus network has one SG unit already present and the investment candidates comprise of one SG (SG_2) and three PV CIGs i.e., PV_1 and PV_2 interfaced via *grid-supporting* converters, and PV_3 operating in *grid-feeding* mode with fixed power output. Candidates PV_1 and PV_2 provide VSM control and droop control, respectively. The generator parameters are as described in Table 6.1 of Section 6.6. The transient security constraints are enforced through thresholds imposed on RoCoF ($\dot{f}_{\text{lim}} = 2\,\text{Hz/s}$), frequency nadir ($\Delta f_{\text{lim}} = 0.6\,\text{Hz}$), and quasi-steady-state frequency deviation ($\Delta f_{\text{ss,lim}} = 0.2\,\text{Hz}$). The implementation was done in MATLAB, with the optimisation model formulated in YALMIP [172] and solved by Gurobi [86].

In the following, the performance of the decomposition-based A1 and A2 is compared with the grid-bounds tightening algorithm presented in Chapter 6, Section 6.4.2 herein referred to as Algorithm 0 (A0). Additionally, the Base case is used to denote the model with investment and operational planning under grid connected and islanding operational scenarios but with no transient frequency security constraints.

7.5.1 Planning Costs

The costs and planning decisions considering four representative days are compared with each of the three algorithms A1, A2 and A3 as indicated in Table 7.1. With all techniques, there exists an increment in total costs as compared to the Base case. For A0, a 10% increment in total costs is obtained as compared to an 8.8% increment with A1 and A2. The total investment costs are lowest with A0 as compared to A1 and A2. On the other hand, the solution for A0 results in the highest operational costs.

When transient security constraints are applied to the problem, it is essential that the algorithm minimises costs while ensuring that the level of frequency support in the network is adequate to eliminate existing violations. A0 selects an additional droop-based CIG while a VSM-based CIG is adopted in the case of A1 and A2. Recall that the transient security constraints depend on the aggregated levels of parameters M, D, R_s and F_s provided by the installed units (see (7.12e) and (7.12f)). While the total power capacity installed is similar for algorithms A0, A1 and A2, the support offered by the specific CIG units varies. A0 selects the lower-cost, grid-supporting converter PV_2 which only contributes to only the aggregated damping levels D while A1 and A2 both select PV_1

contributing to the both aggregated damping and inertia levels (see (7.12e) and (7.12f)). Droop-based CIGs contribute to frequency support only in the PFC region and not the IR region (see fig. 2.1 in Section 2.3.2). Therefore A0 resorts to more expensive operational measures such as increment of power generation from the operationally costly SG unit and use of flexible loads to reduce the power exchanged with the grid as indicated by the higher operation costs and demand shift penalty in Table 7.1.

As more frequency support is available from the units selected by A1 and A2, the preventive operational actions undertaken to reduce the frequency security violations are minimised. The solution with A0 considered the least cost investment unit while A1 and A2 installed the unit with the most frequency support. Unlike A0, the decomposition approach used in A1 and A2 provides sensitivity information from the second-stage problems to the first-stage problem resulting in a solution that is not only optimal in cost but as well ensures optimal frequency support available in the network. Additionally, as the total installed capacity of generation is available in both cases, the adequacy levels in the islanded operation are similar thus resulting in the same demand disconnection penalties.

7.5.2 Dynamic Performance

Based on the units installed by each algorithm, the total aggregated level of M and D are 7.84 s and 18 p.u for A0 as compared to 17.64 s and 1.13 p.u for A1 and A2. Figure

Table 7.1: Comparison of optimal costs and decisions, inertia support and computational performance for each algorithm for four representative days.

	Base	**Algorithm 0**	**Algorithm 1**	**Algorithm 2**
Costs and decisions				
Total cost ($)	223390	244780	242740	242740
Investment cost ($)	61000	126000	131000	131000
Investment decisions	PV_3	PV_2, PV_3	PV_1, PV_3	PV_1, PV_3
Operational cost ($)	162390	118780	111740	111740
Demand shift penalty	3675	8468	7787	7787
Demand disconnection penalty	14536	5337	5337	5337
Computational performance				
Number of iterations	-	6	4	4
Computation time (s)	612	4540	3438	3386
Inertia support				
M (s)	7.84	7.84	17.64	17.64
D (p.u)	0.50	18.00	1.13	1.13

7.3 presents a box plot that indicates the variations in the measured values for each of the frequency security metrics for the 96 hours in four representative days. The security threshold in each case is indicated by the dotted red line.

In the case of the RoCoF values indicated in Fig. 7.3a, an average of 1.59 Hz/s is obtained for A0 as compared to 0.79 Hz/s for A1 and A2. RoCoF is mainly dependant on the total inertia level (M) present in the network (see (7.10a)). The solution provided by A0 provides inertia levels of 7.84 s, provided mainly by the pre-installed SG. The result with A1 and A2 includes the additional installation of VSM-based unit PV_1 resulting in an inertia level of 17.64 s and therefore better performance level as compared to A0.

On the other hand, the quasi steady-state frequency is dependant on aggregated D and R_s parameters as indicated in (7.10c). Averages of 49.89 Hz and 49.87 Hz are obtained for A0 and A1/A2 respectively as indicated in Fig. 7.3c. The aggregated damping levels are higher with the units installed by the solution to A0 hence it provides a better performance in this case. Finally, the frequency nadir has a nonlinear dependency on control parameters M, D, R_s and M_s (see (7.10b)). A0 indicates a better performance as compared to A1 and A2 (see Fig. 7.3b) with average values at 49.7 Hz as compared to a 49.5 Hz average in the Base case.

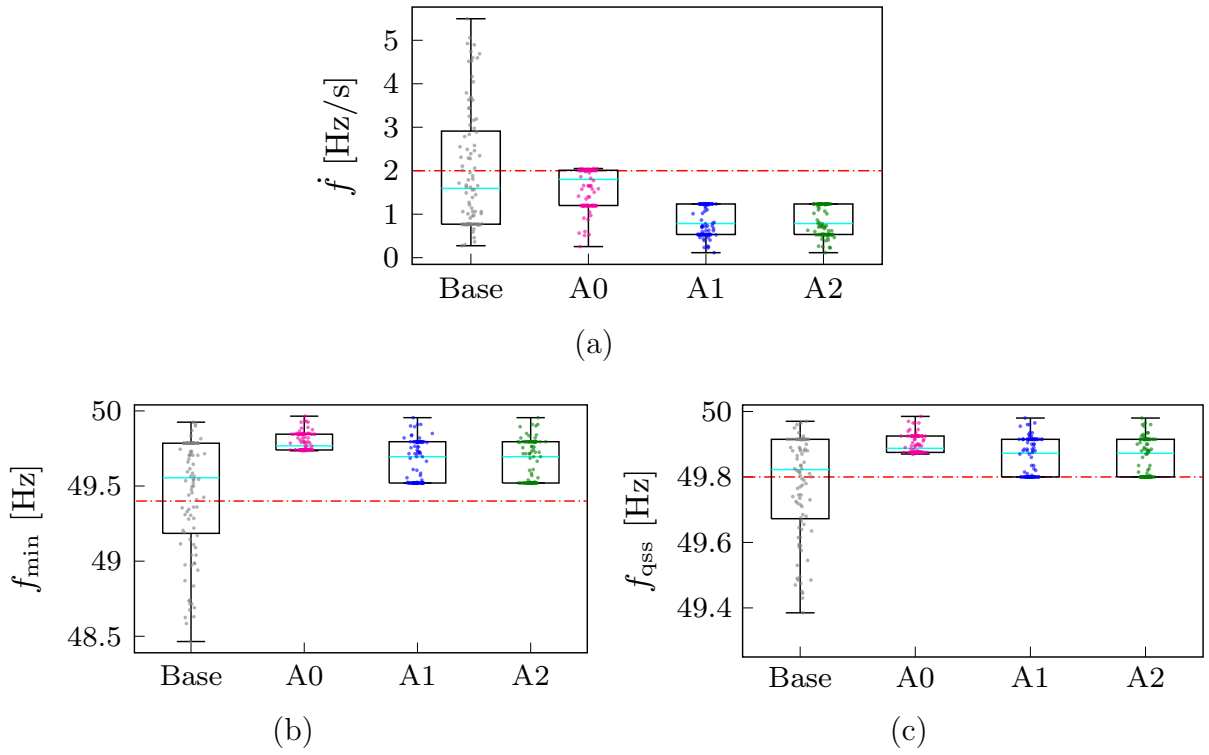

Figure 7.3: Metric variation in each algorithm with respect to the (a) RoCoF, (b) nadir and (c) quasi steady-state frequency considering all hours in four representative days.

The impact of the inclusion of transient constraints on the active power exchange with the grid is shown in Fig. 7.4. All the algorithms provide a solution that is robust to the loss of power exchange with the main grid at every operation scenario. For the MG, this is usually the largest power injection resulting in large frequency excursions. A0 explicitly restricts the bounds on the grid power exchange at each hour while A1 and A2 vary the dispatch based on the sensitivities to both the power loss and available inertia. The result of A0 is shown to be more conservative as compared to A1 and A2. This is especially due to the lack of the bidirectional information exchange between the problems at each stage. A0 only restricts power exchange based on feasibility of the sub-problems problem without knowledge of the effect of the other parameters that define the frequency problem. It is noteworthy to mention that during instances of power import disconnection from the grid can result potential under-frequency, while for power export, over-frequencies can be recorded where sufficient support is unavailable.

The analytical performance, shown in Fig. 7.3, is further validated using a time-domain simulation to ensure practicability. Figure 7.5 indicates the frequency trajectories for the operational scenario at hour 68 given the optimal solution provided by A0 and A1. Note from Fig. 7.4 that this hour presents the highest power exchange from the grid and thus the worst-case mismatch in power if the MG is disconnected from the main grid. In the time-domain simulation, the grid disconnection occurs at time = 1 s and the dotted red lines have been used to indicate the maximum security bounds. The superiority of A1 over A0 is further validated in Fig. 7.5 which compares the frequency trajectories of each technique. While in this scenario, all metrics of A1 show a better performance than A0, this may however not always be the case as indicated Fig. 7.3. The frequency evolution is dependent on both the level of power mismatch at the instant of disconnection dictated by the hourly power exchange and the control support available. Note further that approximation errors existing from the analytical approximation are mitigated in the time-domain simulation which provides the true nature of system performance.

7.5.3 Computational Performance

The computation time for each of the methods is indicated in Table 7.1. The solution with A0 is obtained after six iterations between the main and sub-problems as compared to only four iterations required for A1 and A2. With A1 and A2, the dual cutting planes from all complicating variables ensure faster elimination of the infeasible regions as opposed to only the grid bounds with A0. Therefore, the convergence of A1 and A2 is shown to be much faster as compared with A0. Furthermore, a 25% decrease in computing time is

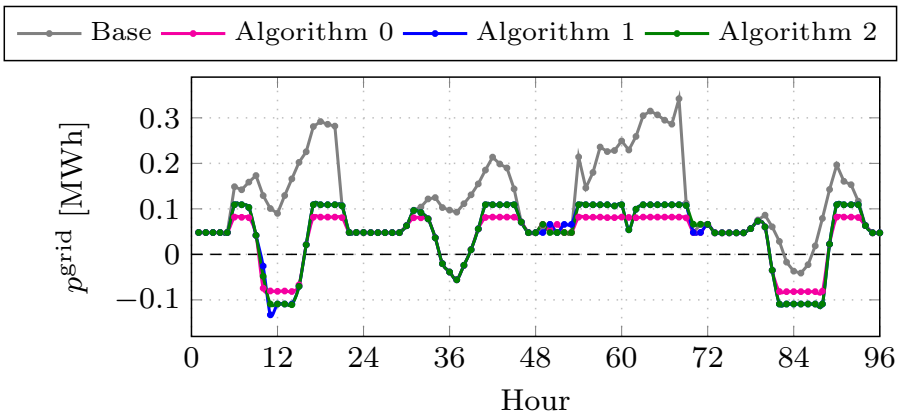

Figure 7.4: Impact of the transient frequency constraints on active power exchange with the grid for the different algorithms (-/+ indicate power export/import).

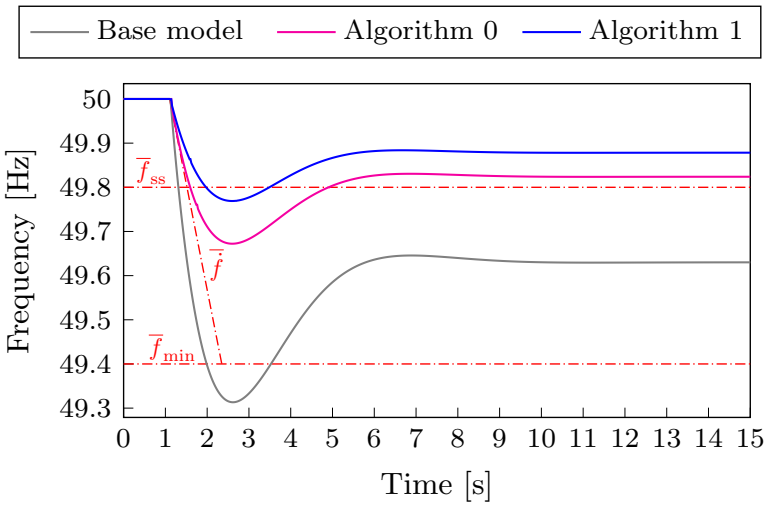

Figure 7.5: Evolution of the CoI frequency for the different algorithms for 15 seconds after the grid disconnection at hour 68.

recorded with the application of A1 and A2. While A1 and A2 provided similar optimal solutions in this case study, A2 is shown to obtain the solution faster as compared to A1 and is therefore more computationally efficient.

7.5.4 Sensitivity to Variation in Security Thresholds

Tightening the thresholds i.e. reducing the upper bounds and increasing the lower bounds, increases the system requirement on power reserves necessary for frequency support from the system. Three case studies are defined to analyse the effect of threshold variations i.e.

(i) Case A: denotes to the initially applied thresholds

(ii) Case B: denotes to the tightening of *only* the RoCoF threshold

(iii) Case C: denotes to tightening of *only* the quasi-steady-state frequency

The higher support requirements can be met by, one, further leveraging high-cost preventive actions. If however the current the system configuration fails to meet the security requirement, two, new units can be installed to increase support levels. Furthermore, as shown in (7.10), the different metrics are dependant on either one or a combination of different control parameters. Hence, commitment of a generator will depend on its suitability to enhance performance. The effect of threshold variation to the aggregated damping and inertia magnitudes is presented in Fig. 7.6 while the sensitivity of the planning solutions to threshold variations is presented in Tables 7.2 and Table 7.3.

In Case B, the RoCoF thresholds are reduced from 2 Hz/s to 0.5 Hz/s. From (7.10), RoCoF is more dependant on aggregated inertia M. Figure 7.6 indicates an increase in inertia levels for all the algorithms. A significant increment to 34.66 s with A1/A2 as compared to 17.64 s in Case A is shown while a lower increment of 22.28 s is obtained with A0. While all algorithms present the need to install an additional unit as indicated in Table 7.2, units installed with A0 include a droop-based generator that has a no contribution to aggregated system inertia. As such, algorithm A0 resorts to more expensive preventative actions to further eliminate violations increasing total costs.

For Case C, the quasi steady-state frequency deviation bound is reduced from 0.2 Hz to 0.1 Hz. The quasi steady-state frequency is dependant on the magnitude of control

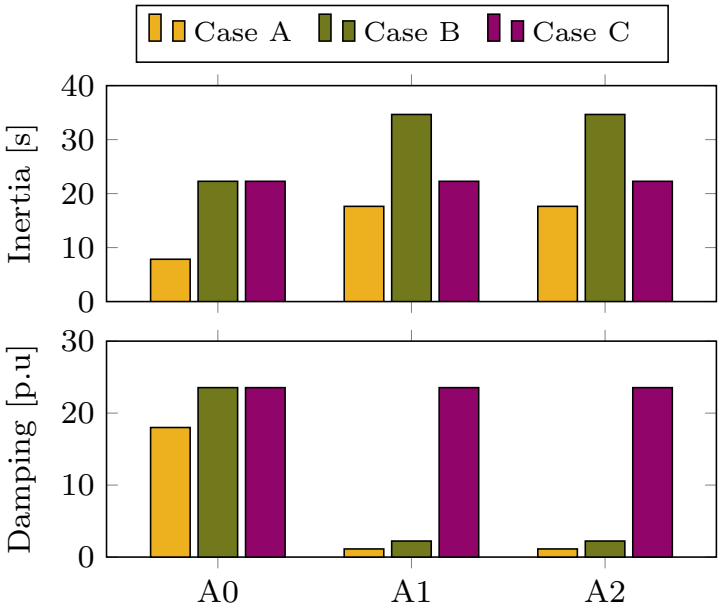

Figure 7.6: Variation of the normalised aggregated inertia and damping constants for different threshold levels of the frequency security metrics.

Table 7.2: Planning costs and decisions with tighter transient security bounds on RoCoF (Case B: Tightening RoCoF to 0.5 Hz/s).

	Algorithm 0	**Algorithm 1**	**Algorithm 2**
Costs and decisions			
Total cost ($)	302790	295303	295319
Investment cost ($)	166000	170000	170000
Investment decisions	PV_2, PV_3, SG_2	PV_1, PV_3, SG_2	PV_1, PV_3, SG_2
Operational cost ($)	136790	125303	125319
Demand shift penalty ($)	15765	6437	6437
Demand disconnection penalty ($)	0	0	0
Computational performance			
No. of iterations	6	4	4
Computation time (s)	3484	2453	2300

Table 7.3: Planning costs and decisions with tighter transient security bounds on quasi steady-state frequency (Case C: Tightening quasi steady-state frequency deviation limit to 0.1 Hz).

	Algorithm 0	**Algorithm 1**	**Algorithm 2**
Costs and decisions			
Total cost ($)	296734	296665	296665
Investment cost ($)	166000	166000	166000
Investment decisions	PV_2, PV_3, SG_2	PV_2, PV_3, SG_2	PV_2, PV_3, SG_2
Operational cost ($)	130734	130665	130665
Demand shift penalty ($)	14786	14756	14756
Demand disconnection penalty ($)	0	0	0
Computational performance			
No. of iterations	7	3	3
Computation time	3787	1956	1947

parameters for damping and droop (see (7.10)). In Fig. 7.6, damping levels for Case C with A1/A2 are shown to increase from 1.13 p.u in Case A to 23.54 p.u in Case C. Note that in this case, the units installed with A1/A2 include a droop-based CIG PV_2 instead of VSM-based PV_1 (see Table 7.3) as in Case A and B. This is due to the higher requirement for damping support with Case C as compared to Case A necessitating the

adoption of units that result in better performance. Total damping levels are shown to increase from 1.13 p.u in Case A to 23.54 p.u in Case C for A1/A2.

The results presented in Tables 7.2 and 7.3 as well as Fig. 7.6 further indicate the need for sensitivity information exchange between the two stages of the algorithm i.e. master- and sub-problems. This simultaneously optimises both frequency support and system costs as highlighted by the superiority of the solution obtained with A1 and A2 as compared to A0.

7.5.5 Scalability

The algorithm is tested on the 30-bus, MV distribution network shown in Fig. 7.7. The network consists of one pre-installed SG unit at node one. A further seven candidate generators are considered for investment at nodes $=\{3, 6, 12, 18, 24, 27\}$, these include: 1×SG, 2×PV_1 VSM-based CIGs, 2×PV_2 droop-based CIGs and 2×PV_3 fixed power output CIGs. The network topology and line parameters were obtained from [188] and defined in Appendix A.4.

The results indicated in Table 7.4 are obtained for the optimal solution of the 30-bus network with varying RoCoF threshold. It is observed that while A1 and A2 still indicate the same investment solutions, the former provides lower total costs in each case. However, in both cases, A2 is observed to be more computationally efficient as compared to A1. The choice between A1 and A2 therefore will depend on the choice between computational efficiency and optimality of the final solution.

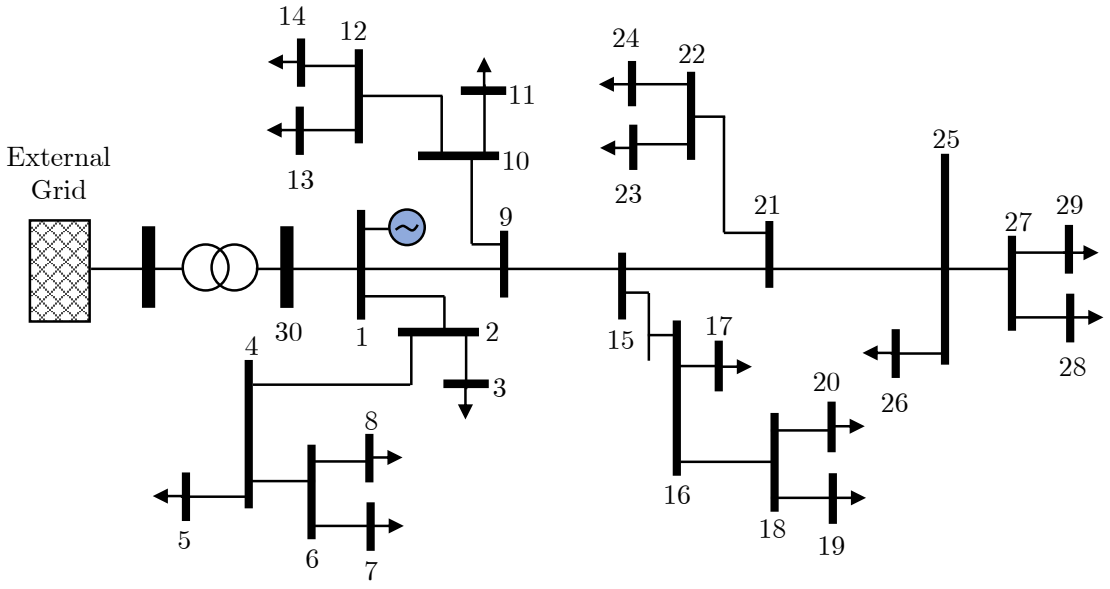

Figure 7.7: Medium voltage 30-bus test network.

Table 7.4: Planning solutions for the 30-bus network with varying RoCoF thresholds.

(a) Case A: RoCoF limit = 2 Hz/s

	Algorithm 0	**Algorithm 1**	**Algorithm 2**
Costs and decisions			
Total cost ($)	3045089	2881913	2960361
Investment decision	2×PV_3, 2×SG	2×PV_2, 2×SG	2×PV_2, 2×SG
Inertia support			
M (s)	15.60	15.60	15.60
D (p.u)	1.17	34.50	34.50
Computational performance			
Computation time (s)	7255	4599	4377

(b) Case B: RoCoF limit = 1 Hz/s

	Algorithm 0	**Algorithm 1**	**Algorithm 2**
Costs and decisions			
Total cost ($)	3760089	3131387	3140962
Investment decision	2×PV_3, 1×PV_3, 2×SG	1×PV_1, 1×PV_3, 2×SG	1×PV_1, 1×PV_3, 2×SG
Inertia support			
M (s)	15.60	22.60	22.60
D (p.u)	17.84	1.47	1.47
Computational performance			
Computation time (s)	6745	5048	4585

7.6 Conclusion

The frequency of HILF events in the power networks requires that systems are designed to be resilient. Moreover, both static and dynamic security need be considered to ensure survivability of the network given the occurrence of such events. Embedding the real-time dynamic security constraints is however not straightforward and attention to ensure model tractability is key.

In Chapter 6, a bounds-tightening algorithm that sequentially checked the dynamic constraints formulated as linear constraints was proposed. This model provided conservative grid limits and was not optimal with regards to the dynamic support provided. In this

chapter, two, tractable algorithms that decompose the problem into multiple levels while ensuring information exchange between levels using dual-cutting planes are proposed. The approach not only provides a faster rate of convergence, but solutions that are more sensitive to inertia support provided by each unit. The superiority of the improved algorithms is highlighted under various operational scenarios and security threshold levels.

The techniques presented in Chapters 6 and 7 rely on an approximated analytical representation of the frequency metrics in the optimisation problem. This can present inaccuracies in the analysis of the dynamic security of the network. Moreover, the work in both chapters ignores voltage security and associated metrics. In the next chapter, a technique that aims at alleviating the inaccuracy while considering both the frequency and voltage security of the microgrid is presented.

Chapter 8

Resilient Microgrid Scheduling with Steady-State and Transient Frequency and Voltage Security

The resilient operation of a microgrid (MGs) relies strongly on their ability to operate in islanded mode, autonomously from the bulk grid, whilst adhering to secure operation requirements. Catastrophic events in the transmission grid can lead to abrupt MG islanding accommodated by large frequency and voltage excursions due to power imbalances within the MG. It is vital that MG scheduling algorithms incorporate both static and transient security metrics to ensure a secure transition during islanding, immunised against the transient phenomena. Chapters 6 and 7 presented techniques for dealing with inertia-aware investment and operational planning problems. However, neglecting the effects to the voltage transient security can result in insecure results where voltage violations exist. In this chapter, both frequency- and voltage-related security constraints are incoporated in a MG operational planning problem to ensure robust operation against abrupt islanding events. An iterative dynamic optimisation approach, based on the sensitivities of active and reactive power injections to the system security frequency and voltage metrics, to incorporate transient and static security constraints in the planning problem is employed. Due to their non-linear and intractable nature, the transient security constraints are reformulated as linear sequential resilience cuts resulting in a computationally efficient problem. The performance of the algorithm is shown on a 30-bus, 20 kV, distribution network, subject to a 24 hour variation in load and renewable generation. The work in

this chapter is presented in publication [C3] and [J1].

8.1 Introduction

In the event of HILF events, the capability of MGs to successfully move from grid-connected to islanded mode and ensure supply continuity is critical in enhancing the system resilience. The islanding process might fail due to inadequacy in power supply capacity, loss of synchronisation for grid-connected converters, and the action of generator protections resulting in unit disconnections. Notably, the large transient excursions in the MG voltage and frequency during the abrupt transition can affect the MG's operational integrity [11, 12]. If not adequately addressed, the transient phenomena can lead to cascading failures and destabilise the MG.

However, with the increasing integration of Converter-Interfaced Generators (CIGs) it becomes more demanding to ensure system security. While the fast-acting CIGs have numerous advantages, the replacement of Synchronous Generators (SGs) results in a radical transformation of the dynamic response and operational characteristics of the system; affecting both voltage and frequency security during fault conditions [10]. Therefore, it is necessary that DERs must provide grid-supporting services, including frequency control, inertia support, reactive power support, and voltage control, to ensure operational stability and security during emergency conditions.

Related Works

Traditionally, operational planning problems for MGs in grid-connected and islanded modes have focused on the network behaviour in pre- and post-contingency steady states [63, 189, 190]. This approach ensures self-sufficiency and steady-state stability but neglects the transient security during system transition. The works in [191, 192] have analysed the frequency and voltage security in steady-state but neglect the transient response. More recently studies have introduced "transient-aware" planning approaches aiming to provide preventive-control solutions and mitigate the effects of large transient excursions during HILF events. The approaches taken in the literature take two forms:

1. Solving a single optimisation problem with the inclusion of dynamic metrics based on analytical formulations or derived security indices [153–155, 193]; and,
2. Solving iterative multi-stage algorithms that feed information on the system dynamic nature into the planning problem based on external analyses [194–196].

The first group uses simplified low-order, dynamic response models, to formulate the analytical formulations of dynamic metrics that can then be incorporated into the optimisation problem. This approach results in a lower computational effort but inherits approximation errors from simplifications made. The second group analyses the system dynamics separately and the results are used to formulate constraints for the optimisation problem. This approach benefits from a more accurate representation of the system through the use of the full non-linear dynamic model or time-domain simulations.

With regard to frequency transients, in [153–155, 193], analytical formulations of the frequency security metrics have been developed based on a reduced-order single machine equivalent Centre-of-Inertia (CoI) frequency model. In [153, 155], unit commitment and economic dispatch problems are proposed for networks with only conventional generators, incorporating security constraints based on linearised analytical formulations of frequency metrics. Enhanced models incorporating frequency support from both SG and CIGs are used for the unit commitment and dispatch problems formulated in [154, 193]. The solution approach in chapters 6 and 7 presented in][J2] and [C4] proposes an iterative multi-level approach that includes non-linear frequency constraints into a MG operational planning problem.

With regards to voltage security, in [197], the Differential-Algebraic-Discrete (DAD) equations describing the system dynamic response are discretised and applied to the security dispatch problem to limit voltage dips and system instability. While a sensitivity-based preventive control approach has been used in [195] to limit voltages within the secure loading margins in post-contingency states. Reference [198] presents a strategy that uses trajectory sensitivities on the system voltage stability margins to determine generator re-scheduling and shunt compensation required to ensure system response is maintained within the defined bounds given load uncertainties. In [199], security constraints for post-fault operation based on sensitivities of the voltage stability margin to the shunt reactive power compensation are added to the model predictive control algorithm to prevent voltage collapse of the system.

The control vector parameterization approach is adopted in [200] to ensure the system does not violate the post-fault transient voltage dip criteria after an N-1 event by using the result of the system dynamics to evaluate the constraints of the optimisation problem. The objective in the study looks at the identification of optimum VAr support to mitigate slow voltage recovery problems and short-term insecurity. The under-frequency/under-voltage load shedding scheme can also be applied to improve system transient security and stability in case of major grid faults thus preventing blackouts. Moreover, the model

proposed in [201] adds constraints based on trajectory sensitivities of margin indices for transient voltage and frequency deviation security, and transient angle stability of the system, to simultaneously minimise emergency load-shedding as well as ensure stability and security. Finally, in [202], the transient voltage dynamics model is discretised and embedded into the reactive power planning problem to immunise against fault-induced delayed voltage recovery based on trajectory sensitivities.

Existing literature has focused on either optimising frequency response or voltage response separately. However, excursions stemming from abrupt MG islanding involve both voltage and frequency; thus, neglecting one can provide an optimistic evaluation of the MG security and resilience. In addition the above literature on optimising voltage security focuses on bulk transmission systems and looks into either long-term voltage stability margins [195, 198, 202] or the post fault transient voltage recovery [199, 200] – neglecting the effect of FRT limitations. The effect of dynamic frequency and voltage security during MG operational planning has not been adequately studied. Furthermore, aforementioned literature analyses frequency with only active power reserves and voltage with only reactive power reserves neglecting the effect of both active and reactive power to voltage or frequency response.

Contributions

In this chapter, the limitations mentioned above are addressed by enhancing the MG operational planning problem taking into account transient and static constraints relating to both voltage and frequency variations during and after an event-triggered emergency islanding. Constraints on pre-contingency (grid-connected), post-contingency (islanded), and transient (switching) states of the MG are included in the MG planning problem, enabling both supply adequacy and the confinement of transient trajectories within secure regions. A dynamic optimisation technique, based on sequential constraint transcription, to represent both the voltage and frequency security constraints is adopted.

Consequently, the main contributions of this chapter are:

- A multi-period, mixed-integer, second-order cone MG operational planning problem that considers grid-connected and islanded mode of operation with security constraints on both the frequency and voltage transient performance during abrupt disconnection.
- A multi-stage solution algorithm that uses the sensitivities derived from dynamic simulations to formulate transient security constraints transcribed onto the MG

operation problem through sequential resilience cuts.

- A case study analysing the effect of both active and reactive power reserves on MG voltage and frequency security.

The rest of the chapter is organised as follows. In Section 8.2, the transient frequency and voltage metrics and models adopted for MG support are presented. Section 8.3 presents the detailed problem formulation and proposed solution algorithm. Section 8.4 discusses the application of the algorithm to a 30-bus test system to highlight the benefit to enhancing MG operational security and resilience. Finally, the main conclusions of the chapter are summarised in Section 8.5.

8.2 Frequency and Voltage Security Criteria

As previously discussed in Chapter 2, current grid codes are continually being modified with Fault Ride-Through (FRT) Requirements for Generators (RfG) to remain connected and supportive during transient grid faults [38]. For various levels of grid frequency and voltage drop/rise, the FRT RfG show the time-frequency/time-voltage profiles for which the DERs should remain connected and support the grid by active/reactive power injection/absorption. The FRT is aimed at immunising against generation loss and where frequency or/and voltage support is provided, reduce the levels of degradation in the network.

Recalling from Section 2.3.2, Fig. 8.1 shows the profiles and support regions for frequency and voltage response after major fault. Times t_0, t_c and t_r relate to time instance of fault occurrence, fault clearance and recovery period (quasi-steady state), respectively. In Fig. 8.1a the frequency deviation following a large disturbance is sketched highlighting the Inertial Response (IR) and Primary Frequency Response (PFR) regions for emergency frequency support. The main performance metrics used in resilience analysis include the maximum Rate-of-change of Frequency (RoCoF), $\left(\dot{f}(t)\right)$, the frequency nadir, $(\pm\Delta f_{max})$, and the post-fault steady-state frequency deviation, (Δf_{ss}).

Similarly, Fig. 8.1b shows the Low/High Voltage Ride-Through (L/HVRT) regions and the quasi-steady state regions for voltage support. The metrics for resilience analysis are defined by the security bounds on Low Voltage Ride-Through (LVRT), $V_{\min}$, High Voltage Ride-Through (HVRT), $V_{\max}$ and upper/lower post-fault recovery voltages, $\overline{V}_{\text{rec}}/\underline{V}_{\text{rec}}$. A unit will be tripped to avoid damage when these technical limits are exceeded, thus increasing the risk of further disconnections and cascading network failures.

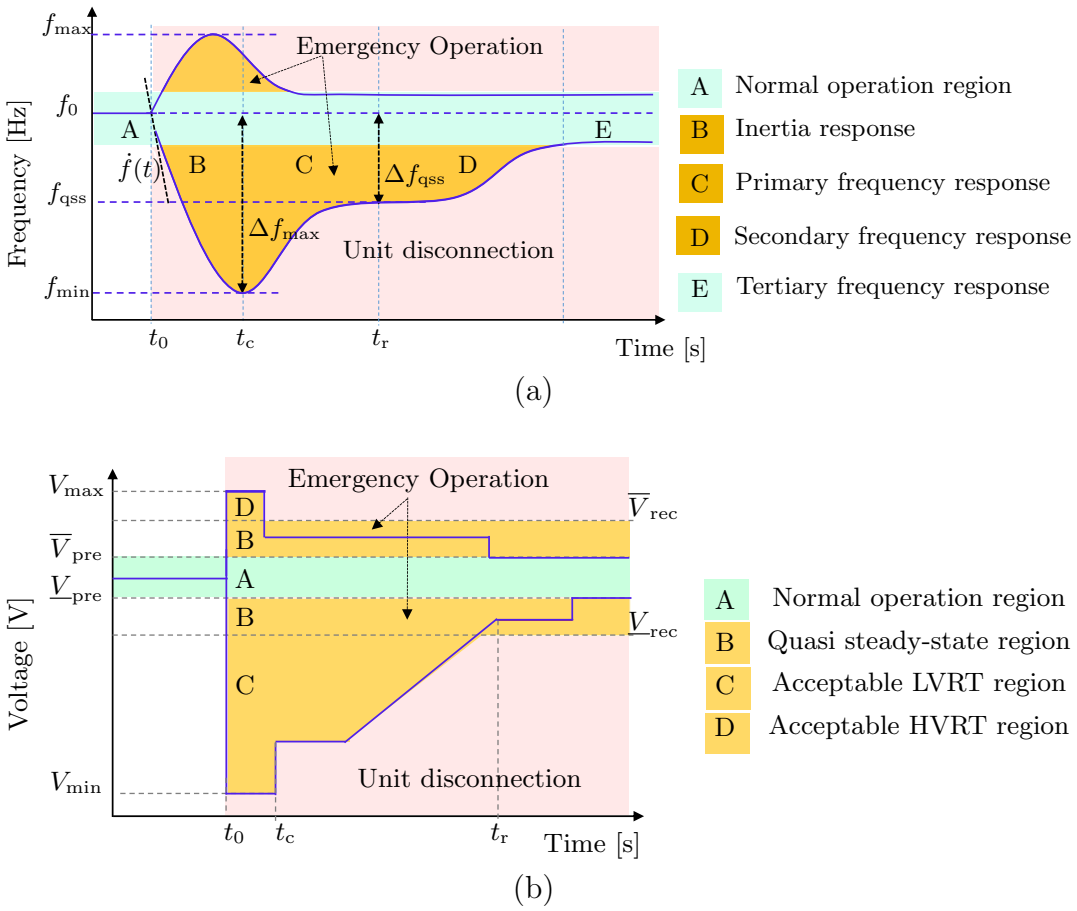

Figure 8.1: DER frequency (a) and voltage (b) FRT profile and support regions with grid fault occurring at time t_0.

In this chapter, it is assume that the MG should be able to withstand the islanding transients at each planning instance $t \in \mathcal{T}$ without violating the FRT and L/HVRT criterion described in this section. The frequency and voltage support models described in Sections 2.3.3 and 2.3.4, respectively, are adopted for the CIG and SG units.

8.3 Problem Formulation

8.3.1 Preliminaries

Bold letters are used to indicate vectors while entries of vectors are denoted by regular letters. This work considers a radial balanced network represented by a connected graph $\mathcal{G}(\mathcal{N}, \mathcal{L})$, with $\mathcal{N} := \{0, 1, \ldots, N\}$ denoting the set of network nodes including the substation node 0, and $\mathcal{L} \subseteq \mathcal{N} \times \mathcal{N}$ designating the set of network branches. The distribution network hosts a number of producers/consumers, where $\mathcal{S} \subseteq \mathcal{N}$ indicates the subset of nodes with SGs, $\mathcal{C} \subseteq \mathcal{N}$ the subset of nodes with CIGs, $\mathcal{D} \subseteq \mathcal{N}$ the subset of nodes with loads and $\mathcal{D}^{\text{v}} \subseteq \mathcal{D} \subseteq \mathcal{N}$ is the subset of nodes with Flexible Loads (FLs). The set of

nodes with generators is thus obtained by the following set union $\mathcal{M} \coloneqq \mathcal{S} \cup \mathcal{C}$. The set of respective units at node $i \in \mathcal{N}$ are given by $\mathcal{S}^i \subseteq \mathcal{S}$, $\mathcal{C}^i \subseteq \mathcal{C}$, and $\mathcal{D}^i \subseteq \mathcal{D}$. Cardinallity of the previously defined sets is denoted by: $n_d \coloneqq |\mathcal{D}|$, $n_s \coloneqq |\mathcal{S}|$, $n_l \coloneqq |\mathcal{L}|$, and $n_c \coloneqq |\mathcal{C}|$, respectively. Indices s, c and d are associated with synchronous generators, RESs and load demand while index $g \in \mathcal{M}$ is associated with all generating units.

The active and reactive power injections at each bus i are defined by $s_i = p_i + \mathbf{j}q_i$. The power injections are derived from the bulk grid s^{grid} where s^{imp} (s^{exp}) denotes import (export), DERs s_g, and loads s_d. Each branch $l \in \mathcal{L}$ is represented by a Π model connected by two adjacent nodes $\eta(l^+) = i$ (upstream) and $\eta(l^-) = j$ (downstream) with the upstream (sending) and downstream (receiving) ends denoted by l^+ and l^-, respectively. Variable $S_{l^+} = P_{l^+} + \mathbf{j}Q_{l^+}$ ($S_{l^-} = P_{l^-} + \mathbf{j}Q_{l^-}$) defines the apparent power flows into a line at the sending (receiving) while $f_{l^{+/-}}$ is the square of current flowing into the line from sending/receiving nodes. The square of voltage magnitude at each node is denoted by v_i. y_l^s is the series admittance given by $y_l^s = 1/(r_l + \mathbf{j}x_l) = 1/z_l$ while $y_{l^+}^{sh} = \mathbf{j}b_{l^+}^{sh}$ and $y_{l^-}^{sh} = \mathbf{j}b_{l^+}^{sh}$ are the shunt admittances at the sending and receiving ends, respectively ($y_{l^+}^{sh} = y_{l^-}^{sh} = \mathbf{j}b_l^{sh}/2$). Lines connected downstream to a node are included in set $\mathcal{L}^{\eta(l^+)}$ while those connected upstream to a node are included in set $\mathcal{L}^{\eta(l^-)}$. The interface between the MG and the bulk grid is located at the Point-of-Common-Coupling (PCC).

For the proposed MG planning algorithm, the optimization problem is formulated to include three sets of operational constraints relating to: pre-emergency steady-state operation (grid-connected mode); post-emergency steady-state operation (islanded mode); and transient state operation (islanding mode). The problem formulation for grid connected operation is defined over a planning horizon $\mathcal{T}$. Without loss of generality, hourly planning periods are considered. For each hour $t \in \mathcal{T}$, a potential emergency islanding event in the MG is assumed. Once the MG is islanded, only one hour of islanded operation is taken into consideration.

The response of the system in the event of large disturbances, such as fault triggered islanding, is governed by the behaviour of the loads, generators, and network, described by differential-algebraic equations. In addition, a change in control configuration can be triggered based on a measured value of a system state. This adds discrete states to the existing continuous states resulting in a system governed by a set of Differential-Algebraic-Discrete (DAD) equations. The model of a dynamically constrained planning

problem can be represented as shown in (8.1).

$$\min_{\boldsymbol{u}} f(\boldsymbol{y}, \boldsymbol{u}) \tag{8.1a}$$

s.t.

$$\boldsymbol{g}(\boldsymbol{y}, \boldsymbol{u}) = \boldsymbol{0} \tag{8.1b}$$

$$\boldsymbol{h}(\boldsymbol{y}, \boldsymbol{u}) \leq \boldsymbol{0} \tag{8.1c}$$

$$\boldsymbol{m}(\dot{\boldsymbol{x}}, \boldsymbol{x}, \boldsymbol{y}, \boldsymbol{u}) = \boldsymbol{0} \tag{8.1d}$$

$$\boldsymbol{n}(\boldsymbol{x}, \boldsymbol{y}, \boldsymbol{u}) \leq \boldsymbol{0} \tag{8.1e}$$

$$\underline{\boldsymbol{y}} \leq \boldsymbol{y} \leq \overline{\boldsymbol{y}}, \quad \underline{\boldsymbol{x}} \leq \boldsymbol{x} \leq \overline{\boldsymbol{x}}, \quad \underline{\boldsymbol{u}} \leq \boldsymbol{u} \leq \overline{\boldsymbol{u}} \tag{8.1f}$$

where $\boldsymbol{y}$ represents the steady-state operational variables (nodal voltages, power flows in the distribution lines and power consumption by load in the network) while $\boldsymbol{u}$ denote the control variables, these include the active and reactive power injections by the different generation units and the power exchange with the grid. Equation (8.1b) corresponds to the AC power flow network constraints in steady-state operation, while (8.1c) includes the different techno-economic operational constraints applied to the network such as line loading constraints, voltage constraints and generation limits on the different units. The system dynamics after MG islanding are represented by the set of differential-algebraic equations in (8.1d), where variables $\boldsymbol{x}$ denote the differential state variables. The transient response trajectory constraints (see Fig. 8.1) are defined in (8.1e), while (8.1f) ensure the security bounds on variables. The goal is to find optimal values of the control variables $\boldsymbol{u}^*$ such that the cost function (8.1a) is minimised, all constraints are satisfied, and that will drive the system response to a feasible post-islanding transient trajectory $\boldsymbol{x}^*$. The problem in (8.1) is difficult to solve due to its infinite dimensions and highly nonlinear nature [203].

Different approaches have been proposed in power systems to solve problems with a similar structure as (8.1), including dynamic optimisation techniques, analytical methods based on the Single-Machine Equivalent (SME), and computational intelligence methods such as machine learning techniques [204–206]. Obtaining a true analytical solution to the closed form model describing the system dynamic response using the SME method is not a straight forward operation when considering both voltage and frequency response in the network. More so in CIG-dominated networks the disjoint nature of control support, as described in (2.4) and (2.8), along with unit saturation and limit cycles that can occur especially during emergency states.

On the other hand, full discretization of (8.1d)-(8.1e) by embedding numerical integration methods, as described in [197], ensures that steady-state and dynamic equations are simultaneously satisfied. However, each step of the discretization introduces a new set of optimisation states with inter-temporal coupling between them. It is quite evident that this process can quickly expand the solution space of the optimisation problem making it intractable.

Finally, the direct sequential method adopted in this chapter is a technique for solving dynamically constrained problems where only the control states are discretized and approximated based on a basis function in each section of the discretized time window [204]. The basis functions at each time stage can be piece-wise constant, linear, quadratic, or polynomial functions [203]. This allows for the decoupling of the model (8.1) where the control variables can be estimated in the time-domain simulation of the DAD model (8.1d)-(8.1e) and trajectories of the state variables in the optimization problem estimated based on their gradients w.r.t the control variables in the time-domain simulation.

In this work, piece-wise constant functions are ussed to approximate control variables. Thus, the control variables vector $\boldsymbol{u}$ is approximated as:

$$\boldsymbol{u} = \boldsymbol{u}_k, \qquad k = 1, \ldots, n \tag{8.2}$$

where k is the iterative stage. At the same time, the performance metrics $\boldsymbol{\mu}$, presented in Section 8.2 and illustrated on Fig. 8.1, can be approximated as:

$$\boldsymbol{\mu}_k = \boldsymbol{\mu}_{k-1} + \boldsymbol{\delta}^u_{\mu,k}(\boldsymbol{u}_k - \boldsymbol{u}_{k-1}), \qquad k = 1, \ldots, n \tag{8.3}$$

where $\delta^u_{\mu,k}$ is the gradient (i.e. sensitivity) of the performance metric μ w.r.t the control variable u at iteration k.

Therefore, (8.3) replaces (8.1d)-(8.1e) transforming the model (8.1) for the k-th iteration to:

$$\min_{\boldsymbol{u}_k} f(\boldsymbol{y}_k, \boldsymbol{u}_k) \tag{8.4a}$$

s.t.

$$g(\boldsymbol{y}_k, \boldsymbol{u}_k) = \boldsymbol{0} \tag{8.4b}$$

$$h(\boldsymbol{y}_k, \boldsymbol{u}_k) \leq \boldsymbol{0} \tag{8.4c}$$

$$\boldsymbol{\mu}_k = \boldsymbol{\mu}_{k-1} + \boldsymbol{\delta}^u_{\mu,k}(\boldsymbol{u}_k - \boldsymbol{u}_{k-1}) \tag{8.4d}$$

$$\underline{\boldsymbol{y}} \leq \boldsymbol{y}_k \leq \overline{\boldsymbol{y}}, \quad \underline{\boldsymbol{\mu}} \leq \boldsymbol{\mu}_k \leq \overline{\boldsymbol{\mu}}, \quad \underline{\boldsymbol{u}} \leq \boldsymbol{u}_k \leq \overline{\boldsymbol{u}} \tag{8.4e}$$

where the time-domain-related variables and constraints have been replaced by the performance metrics extracted from the time-domain simulations.

The resulting problem in (8.4) is a finite-dimensional problem that can be easily solved by off-the-shelf optimisation tools. Using the direct sequential method, an iteration between the optimisation problem and a time-domain simulation continues until both optimality and feasibility, based on the defined stopping criteria, are obtained.

Therefore, shifting from the solution approaches presented in Chapters 6 and 7, the approach proposed in this chapter externally couples the optimisation problem with a time-domain simulation. The transient security constraints are derived utilising the result of the time-domain simulation as opposed to the closed-form analytical expressions used in the previous chapter. Moreover, the sensitivities embedded into the optimisation problem are based on the effect of variation of control states to system trajectories providing better insight into the system response to state variation. In the following, the detailed design of the constraints and overall model formulation is presented.

8.3.2 Design of the Transient Security Constraints

The performance metrics $\boldsymbol{\mu}$ of concern are defined in Fig. 8.1, relating to the values of frequency and voltages during the emergency response of the different generation units. The control states relate to the active and reactive power injections of both the grid and the DERs prior to emergency islanding. Therefore at each iteration, the path constraints in (8.4d) take the form described below.

8.3.2.1 Frequency Transient Constraints

The CoI frequency response is utilised to model the frequency transient response. While the CoI model shows slight variations as compared to the local frequency oscillations of the generating units, it provides a smoother overall frequency that aids provision of better control from CIGs [144, 207]. The path constraints on frequency response from (8.4d)-(8.4e) at the k-th iteration take the form:

$$\begin{aligned}\boldsymbol{\omega}^{\mathrm{cr}}_{(k+1)} \leq \boldsymbol{\omega}^{\mathrm{cr}}_{\gamma} + \boldsymbol{\delta}^{p^{\mathrm{grid}}}_{\boldsymbol{\omega}^{\mathrm{cr}},\gamma} \cdot (\boldsymbol{p}^{\mathrm{grid}}_{(k+1)} - \boldsymbol{p}^{\mathrm{grid}}_{\gamma}) \\ + \boldsymbol{\delta}^{q^{\mathrm{grid}}}_{\omega^{\mathrm{cr}},\gamma} \cdot (\boldsymbol{q}^{\mathrm{grid}}_{(k+1)} - \boldsymbol{q}^{\mathrm{grid}}_{\gamma}) + \Delta\boldsymbol{\omega}^{\mathrm{cr}}_{\mathrm{slk}}, \ \forall \gamma = 1, \ldots, k\end{aligned} \tag{8.5a}$$

$$\boldsymbol{\omega}^{\min}_{k+1} \geq \underline{\boldsymbol{\omega}}^{\min}, \qquad \boldsymbol{\omega}^{\max}_{k+1} \leq \overline{\boldsymbol{\omega}}^{\max} \tag{8.5b}$$

$$\underline{\dot{\boldsymbol{\omega}}} \leq \dot{\boldsymbol{\omega}}_{k+1} \leq \overline{\dot{\boldsymbol{\omega}}} \tag{8.5c}$$

$$\underline{\boldsymbol{\omega}}^{\text{qss}} \leq \boldsymbol{\omega}_{k+1}^{\text{qss}} \leq \overline{\boldsymbol{\omega}}^{\text{qss}} \tag{8.5d}$$

where superscript $^{\text{cr}} \in \{\text{RoCoF, min, max, qss}\}$ correspond to the magnitudes of RoCoF, frequency nadir, frequency zenith and quasi-steady state frequency, respectively. $\Delta\omega_{\text{slk}}^{\text{cr}}$ is a slack variable added to prevent infeasibility of the problem. The control states are characterised by active (p^{grid}) and reactive (q^{grid}) power exported or imported from the grid at each hour prior to emergency islanding. Constraints (8.5b)-(8.5d) are applied to restrict the frequency states within the technical boundaries illustrated in Fig. 8.1 where units remain connected to the network.

The equality sign in (8.5a) has been replaced with an inequality, to ensure satisfaction of the path constraint at all previous iterations. This transformation adds multiple constraints with the aim of tightening the feasible state space and restricting trajectories within the secure regions defined in Fig. 8.1. It also enhances the convergence rate of the solution algorithm.

8.3.2.2 Voltage Transient Constraints

Due to the very local nature of voltage evolution, the transient voltage metrics are formulated at the terminal node of each generator unit. For generator $g \in \{\mathcal{S}, \mathcal{C}\}$, the transient voltage constraints are formulated as:

$$\begin{aligned}\boldsymbol{V}_{(k+1)}^{\text{cr}} \leq \boldsymbol{V}_{\gamma}^{\text{cr}} + \sum_{g\in\{\mathcal{S},\mathcal{C}\}} \Big(& \boldsymbol{\delta}_{V_g^{\text{cr}},\gamma}^{p_g} \cdot (\boldsymbol{p}_{g,(k+1)} - \boldsymbol{p}_{g,\gamma}) \\ & + \boldsymbol{\delta}_{V_g^{\text{cr}},\gamma}^{q_g} \cdot \big(\boldsymbol{q}_{g,(k+1)} - \boldsymbol{q}_{g,\gamma}\big)\Big) + \Delta\boldsymbol{V}_{\text{slk}}^{\text{cr}},\ \forall\gamma = 1,\ldots,k\end{aligned} \tag{8.6a}$$

$$\boldsymbol{V}_{k+1}^{\text{LVRT}} \geq \underline{\boldsymbol{V}}_{\min}, \qquad \boldsymbol{V}_{k+1}^{\text{HVRT}} \leq \overline{\boldsymbol{V}}_{\max} \tag{8.6b}$$

$$\underline{\boldsymbol{V}}_{\text{rec}} \leq \boldsymbol{V}_{k+1}^{\text{rec}} \leq \overline{\boldsymbol{V}}_{\text{rec}} \tag{8.6c}$$

where superscript $^{\text{cr}} \in \{\text{LVRT, HVRT, rec}\}$ correspond to the voltage magnitudes at LVRT, HVRT and post-fault recovery voltage, respectively. For the voltage resilience metrics in (8.6a), the effect of the post-emergency voltage levels at the terminals of each generator to the pre-emergency active and reactive power injections at all generators in the network is considered when formulating the linearized path constraint. Hence, the control states are the characterised by active (p_g) and reactive (q_g) power injected by the all generators. The slack variable $\Delta V_{\text{slk}}^{\text{cr}}$ immunises against infeasibility of the problem while constraints (8.6b)-(8.6c) ensure voltages at each generator are not in the region

where unit disconnection occurs. The use of the slack variables is vital given the high probability of conflicting constraints when both frequency and voltage constraints are applied. These are heavily penalised in the objective function.

Constraints (8.5) and (8.6) define the transient islanding constraints applied at each hour of the planning horizon. These ensure system states are maintained within the acceptable emergency operation regions illustrated in Fig. 8.1.

8.3.3 Static Operation Constraints

The steady-state operation constraints are designed to provide a snap-shot of system performance at each hour of the planning horizon. These include constraints on the grid-connected and islanded operation of the MG associated to (8.4b)-(8.4c) and defined in extended form as:

Constraints on Power Flow and Power Balance

The constraints on active and reactive power flows in the network have been formulated using a Second-Order Cone Programming (SOCP) model [73], presented in 3.2 denoted as Model 4, which extends the DistFlow power model to include the line charging:

$$s_{it} = \sum_{d\in\mathcal{D}^i} s_{dt} - s^{\text{imp}}_{t|i=\text{PCC}} + s^{\text{exp}}_{t|i=\text{PCC}} - \sum_{g\in\{\mathcal{S}^i,\mathcal{C}^i\}} s_{gt}, \qquad \forall i\in\mathcal{N},\ t\in\mathcal{T} \quad (8.7a)$$

$$s_{it} = \sum_{\eta(l^+)=i} S_{l^+} + \sum_{\eta(l^-)=i} S_{l^-} \qquad \forall i\in\mathcal{N},\ t\in\mathcal{T} \quad (8.7b)$$

$$f_{tl^+} v_{t\eta(l^+)} \geq |S_{tl^+}|^2 \ \text{ or } \ f_{tl^-} v_{t\eta(l^-)} \geq |S_{tl^-}|^2, \qquad \forall l\in\mathcal{L},\ t\in\mathcal{T} \quad (8.7c)$$

$$|\alpha_{l^+}|^2 v_{t\eta(l^+)} - v_{t\eta(l^-)} = 2\,\text{Re}(\alpha_{l^+} z_l^* S_{tl^+}) - |z_l|^2 f_{tl^+}, \qquad \forall l\in\mathcal{L},\ t\in\mathcal{T} \quad (8.7d)$$

$$|\alpha_{l^-}|^2 v_{t\eta(l^-)} - v_{t\eta(l^+)} = 2\,\text{Re}(\alpha_{l^-} z_l^* S_{tl^-}) - |z_l|^2 f_{tl^-}, \qquad \forall l\in\mathcal{L},\ t\in\mathcal{T} \quad (8.7e)$$

$$\alpha^*_{l^+} v_{t\eta(l^+)} - z_l^* S_{tl^+} = \left(\alpha^*_{l^-} v_{t\eta(l^-)} - z_l^* S_{tl^-}\right)^*, \qquad \forall l\in\mathcal{L},\ t\in\mathcal{T} \quad (8.7f)$$

Constraint (8.7a) ensures the power balance at each node. Power import/export from the grid is only defined at the PCC node ($i = 0$). In islanded mode, the power import and export to the grid is set to zero. Equations (8.7b)-(8.7f) describe the power flow equations with parameter $\alpha_{l^+} = 1 + z_l y^{sh}_{l^+}$. The equality in constraint (8.7c) has been relaxed to an inequality to transform the power flow equation from a non-linear to SOCP model to improve tractability and global optimality.

Constraints on Grid Power Exchange

Defined only for the grid-connected mode, the bounds on power imports and exports to the grid take the form:

$$\begin{aligned} &0 \leq p_t^{\text{imp}} \leq \overline{p}_t^{\text{imp}} \cdot z_t^{\text{P}}, \quad 0 \leq p_t^{\text{exp}} \leq \overline{p}_t^{\text{exp}} \cdot (1 - z_t^{\text{P}}), \\ &0 \leq q_t^{\text{imp}} \leq \overline{q}_t^{\text{imp}} \cdot z_t^{\text{Q}}, \quad 0 \leq q_t^{\text{exp}} \leq \overline{q}_t^{\text{exp}} \cdot (1 - z_t^{\text{Q}}), \end{aligned} \quad \forall t \in \mathcal{T} \tag{8.8}$$

where the binary variables $z_t^{\text{P}}/z_t^{\text{Q}}$ prevent the simultaneous import and export of active/reactive power.

Constraints on Loads

Power consumption of load at each node can be fixed (s_{dt}^{f}) or variable (s_{dt}^{v}) i.e. flexible load, the limitations applied to the load variations over the planning horizon include:

$$[p/q]_{dt} = ([p/q]_{dt}^{\text{f}} + [p/q]_{dt}^{\text{v}}) \cdot z_{dt}, \qquad \forall d \in \mathcal{D},\ t \in \mathcal{T} \tag{8.9a}$$

$$0 \leq p_{dt} \leq \overline{p}_d, \quad 0 \leq q_{dt} \leq \overline{q}_d, \qquad \forall d \in \mathcal{D},\ t \in \mathcal{T} \tag{8.9b}$$

$$\sum_{t \in \mathcal{T}} p_{dt}^{\text{d}} = E_d, \qquad \forall d \in \mathcal{D} \tag{8.9c}$$

$$p_{dt} \leq E_d - \sum_{\tau=1}^{t-1} p_{d\tau}, \qquad \forall d \in \mathcal{D},\ t \in \mathcal{T} \tag{8.9d}$$

where the binary variable z_{dt} indicates the connection status of the load. In grid connected mode, this value is forced to one i.e. all load should be served in its entirety. On the contrary, in islanded mode, z_{dt} can take on a value of one $\Longrightarrow$ load-connected or zero $\Longrightarrow$ load-curtailed. Constraint (8.9b) ensures the total load does not exceed the peak load defined at a given node, this is defined based on the maximum consumption at a node. Note that flexible loads relate to large consumers that are able to upwardly/downwardly adjust consumption when required within their maximum consumption limits. In grid connected mode, constraint (8.9c) ensures that the defined energy consumption E_d for the day is met. During islanded operation, (8.9d) ensures that only un-served load consumption is met. The fraction of un-served load at any hour given the daily requirement is defined by the right-hand side of (8.9d).

Constraints on power production from SGs

$$0 \leq p_{st} \leq \overline{p}_{st}, \quad \underline{q}_s \leq q_{st} \leq \overline{q}_s, \qquad \forall s \in \mathcal{S}, t \in \mathcal{T} \tag{8.10a}$$

$$-rd_s \leq p_{st} - p_{s(t-1)} \leq ru_s, \qquad \forall s \in \mathcal{S}, t \in \mathcal{T} \tag{8.10b}$$

The limits to power output of the SG units are defined in (8.10a) while their inter-hour ramp-up ru_s and ramp-down rd_s limits ensured in (8.10b).

Constraints on power production from CIGs

In line with current grid code, operation of renewable energy units at power factor less than one is allowed, thus the limits on power production from CIG units are defined as:

$$0 \leq p_{ct} \leq \overline{p}_{ct}, \quad 0 \leq q_{ct} \leq \tan(\overline{\phi}) \cdot \overline{p}_{ct}, \quad \forall c \in \mathcal{C}, t \in \mathcal{T}, \tag{8.11}$$

here $\cos(\overline{\phi})$ is the minimum acceptable power factor of the CIG defined by the grid code.

Constraints on Steady-Stage Voltage

Voltage levels at each node in steady-state operation should be maintained within the normal operation region illustrated in Fig. 8.1b. In both grid-connected and islanded mode, this is ensured by:

$$\underline{v} \leq v_{it} \leq \overline{v}, \quad v_{t|i=\text{PCC}} = 1 \text{ pu}, \qquad \forall i \in \mathcal{N},\ t \in \mathcal{T} \tag{8.12}$$

Constraints on Line Loading

The transmission capacity of each line is maintained within secure bounds as:

$$0 \leq f_{l^+} \leq (\overline{f}_l), \quad 0 \leq f_{l^-} \leq (\overline{f}_l), \quad \forall l \in \mathcal{L},\ t \in \mathcal{T} \tag{8.13}$$

Objective Function

The objective is a min-max function that contains a minimisation of the grid-connected mode operational costs, $\Theta^{\text{gm}}(\boldsymbol{u}^{\text{gm}})$ under the worst case islanding penalties at each hour $\Theta_t^{\text{im}}(\boldsymbol{u}^{\text{im}})$ defined as a single minimisation problem by utilising auxiliary variable α:

$$\min_{\boldsymbol{u}} \ \Theta^{\text{gm}}(\boldsymbol{u}^{\text{gm}}) + \alpha \tag{8.14a}$$

s.t.

$$\alpha \geq \Theta_t^{\text{im}}(\boldsymbol{u}^{\text{im}}), \qquad \forall t \in \mathcal{T}, \tag{8.14b}$$

$$\Theta^{\mathrm{gm}}(\boldsymbol{u}^{\mathrm{gm}}) = \sum_{t\in\mathcal{T}} \Bigg(\Big(C^{\mathrm{imp^P}} \cdot p_t^{\mathrm{imp}} - C^{\mathrm{exp^P}} \cdot p_t^{\mathrm{exp}} \Big) + \Big(C^{\mathrm{imp^Q}} \cdot q_t^{\mathrm{imp}} - C^{\mathrm{exp^Q}} \cdot q_t^{\mathrm{exp}} \Big) \Bigg) + \sum_{t\in\mathcal{T}} \sum_{g\in\{\mathcal{S},\mathcal{C}\}} \big(C_g^{\mathrm{P}} \cdot p_{gt} + C_g^{\mathrm{Q}} \cdot q_{gt} \big) + \sum_{t\in\mathcal{T}} \sum_{d\in\mathcal{D}^{\mathrm{v}}} \big(C_d^{\mathrm{v}} \cdot p_{dt}^{\mathrm{v}} \big) + \sum_{t\in\mathcal{T}} \sum_{\mathrm{cr}\in\mathrm{cr}^{\mathrm{CoI}}} \big(C_{\mathrm{slk}}^{\mathrm{cr}} \cdot \Delta\omega_{\mathrm{slk},t}^{\mathrm{cr}} \big) + \sum_{t\in\mathcal{T}} \sum_{g\in\{\mathcal{S},\mathcal{C}\}} \sum_{\mathrm{cr}\in\mathrm{cr}^{\mathrm{V}}} \big(C_{\mathrm{slk}}^{\mathrm{cr}} \cdot \Delta V_{\mathrm{slk},g,t}^{\mathrm{cr}} \big) \tag{8.14c}$$

$$\Theta_t^{\mathrm{im}}(\boldsymbol{u}^{\mathrm{im}}) = \sum_{d\in\mathcal{D}} \big(C_d \cdot (1 - z_{dt}) \big(p_{dt}^{\mathrm{f}} + p_{dt}^{\mathrm{v}} \big) \big) \tag{8.14d}$$

In grid connected mode, (8.14c), the active/reactive power is imported/exported from/to the grid at costs $C^{\mathrm{imp^{P/Q}}}/C^{\mathrm{exp^{P/Q}}}$ while the generation costs of the different generators are defined by $C_g^{\mathrm{P/Q}}$. Additionally, penalty costs C_d^{v} applied to the variable loads due the inconvenience of shifting demand away from the consumer preferred time. High penalty costs $C^{\mathrm{CoI,slk}}$ and $C_g^{\mathrm{cr,V}}$ are applied to the slack variables to ensure they are only utilised when absolutely necessary. The islanded operation costs in (8.14d) denote to the penalties C_d incurred when a load is curtailed during the emergency operation. The overall optimization problem is formulated as a Mixed-Integer Second Order Cone Programming (MISOCP) problem.

8.3.4 Solution Algorithm

The proposed solution approach iterates between an optimisation problem, a time-domain dynamic simulation, and an extraction stage as illustrated in Fig. 8.2. The tasks involved at each step are detailed as follows:

Step 1: Initially, setting iteration $k = 1$, the grid-connected and islanded mode MG scheduling problems, i.e. (8.7)-(8.14), are solved simultaneously to derive the output vectors $\boldsymbol{u}_{0,t}, \boldsymbol{y}_{0,t}$ of the optimised hourly operating points. Subscript "$_0$" is used to indicate the pre-contingency steady state (see Fig. 8.1) value of the respective control and state variables. The grid-connected mode problem is solved for the entire planning horizon $\mathcal{T}$ together, while a one-hour islanded operation problem is solved at each hour $t \in \mathcal{T}$. The optimisation problem (8.7)-(8.14) ensures both static security and system adequacy in the pre- and post-islanded MG operation. The problem is robust to abrupt islanding at each hour defined by the loss of power from the grid.

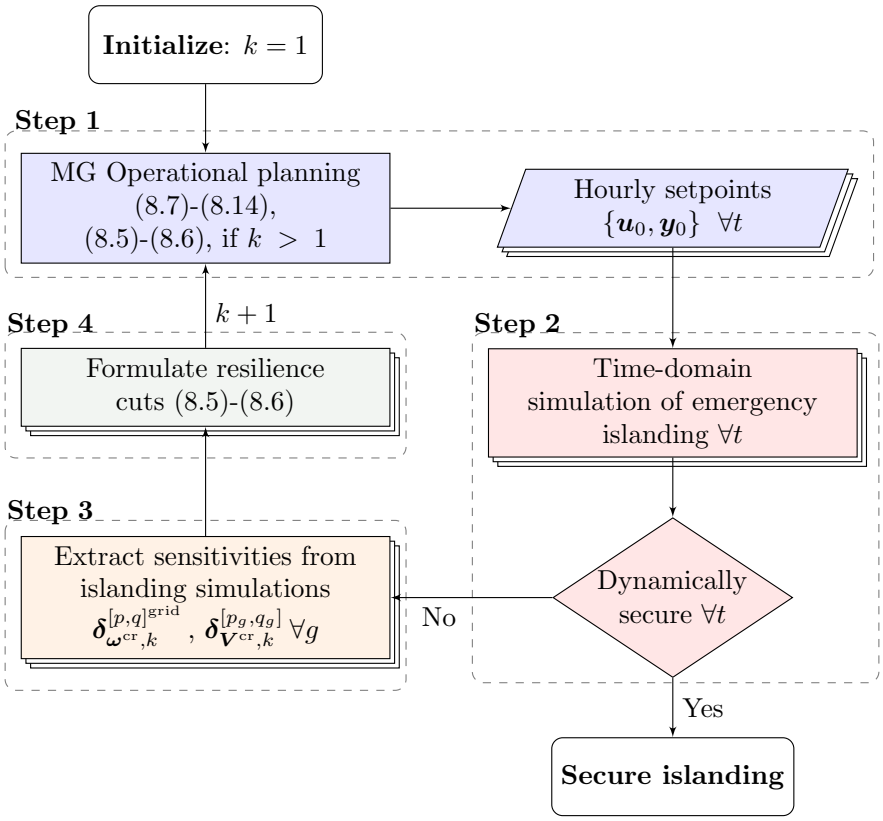

Figure 8.2: Proposed Algorithm for microgrid scheduling with transient frequency and voltage security constraints.

Step 2: In this step, the hourly operating points in grid-connected mode from Step 1 are used to perform a time-domain dynamic simulation where an abrupt islanding scenario is induced to check that voltage and frequency trajectories remain within the secure regions. This is based on the metrics defined in Section 8.2. If all performance metrics are satisfied, a secure islanding is assumed. Otherwise, the algorithm formulates resilience cuts in Steps 3 and 4 to be added to the scheduling problem of Step 1.

Step 3: The value of each metric is derived from the measurements of the frequency and voltage states between times t_0 to t_r (see Fig. 8.1) during the MG transition to islanded state. Given any security violations at any hour of the planning horizon, the sensitivity coefficients ($\delta_{\omega^{\mathrm{cr}},kt}^{[P,Q]^{\mathrm{grid}}}$ and $\delta_{V^{\mathrm{cr}},kt}^{[P_g,Q_g]}$) of the frequency and voltage metrics to the respective control states (power injections) are obtained. The finite difference method is used to calculate the sensitivities and the calculations are based on multiple time-domain simulations of the emergency disconnections with small changes to the active or reactive power injections in the pre-contigency steady-state i.e.

$$\delta \begin{matrix} \big[P/Q\big]_{kt}^{[g/\mathrm{grid}]} \\ \big[V/\omega\big]_{kt}^{\mathrm{cr}} \end{matrix} = \frac{\partial \big[V/\omega\big]_{kt}^{\mathrm{cr}}}{\partial \big[P/Q\big]_{kt}^{[g/\mathrm{grid}]}} \tag{8.15}$$

$$= \frac{\left[V/\omega\right]_{kt}^{\text{cr}}\left(\left[P/Q\right]_{kt}^{0+}\right) - \left[V/\omega\right]_{kt}^{\text{cr}}\left(\left[P/Q\right]_{kt}^{0-}\right)}{2\Delta[P/Q]}$$

where $[P/Q]_{kt}^{0+} = [P/Q]_{kt}^{0} + \Delta[P/Q]$ and $[P/Q]_{kt}^{0-} = [P/Q]_{kt}^{0} - \Delta[P/Q]$, with $[P/Q]_{kt}^{0}$ the initial power exchange by the grid or generator computed in Step 1. That is, $[P/Q]_{kt}^{0+}$ (resp. $[P/Q]_{kt}^{0-}$) implies an increase (resp. decrease) in power flow "**from**" the MG "**to**" the main grid.

Step 4:

The feasibility resilience cuts at iteration k defined in (8.5)-(8.6) are formulated for each hour based on the values of the metrics and associated sensitivities. These are then applied to the grid-connected optimisation problem in Step 1. The problem in Step 1 is updated and re-solved including all resilience cuts from $\gamma = 1$ to k.

8.4 Simulation Results

8.4.1 System Setup

The proposed algorithm was evaluated on a 30-bus, 20 kV, distribution network shown in Fig. 8.3 with three CIGs and two SG units and a base power of 10 MVA. The network topology and line parameters were obtained from [188] and defined in Appendix A.4. It serves 12 loads modelled as constant current for active power and constant impedance for reactive power, in addition to three induction motors at buses 14, 20 and 28. In the steady-state optimization problem, all loads are modelled as constant power loads with peak load consumption at 15 MVA. The CIGs are modelled based on reference [56] with added VSM control for frequency support as in (2.4). For the SGs, a 6^{th}-order model equipped with the DEGOV1 speed governor and the IEEE AC1A exciter is adopted. The dynamic simulation was performed with PyRAMSES [60], while the optimization model was implemented in PYOMO [85] and GUROBI [86] employed as a solver. The load and solar profiles (shown in Fig. 8.4) are adopted from [208] and power import, export, and SG production costs were set to 15 \$/MW, 5 \$/MW and 40 \$/MW, respectively.

The dynamic response during emergency islanding is simulated after a three phase fault at the high-voltage bus occurring at $t_0 = 1$ s with t_c at 1.1 s and t_r set at 5 s after the fault occurrence (see Fig. 8.1). The MG performs an emergency islanding five cycles after clearing the fault by opening the interconnection at the PCC (node 30). From Fig. 8.1, the limits to the performance metrics have been set as: $\overline{\dot{f}(t)} = \pm 3$ Hz/s, $f_{max} = 50.8$ Hz,

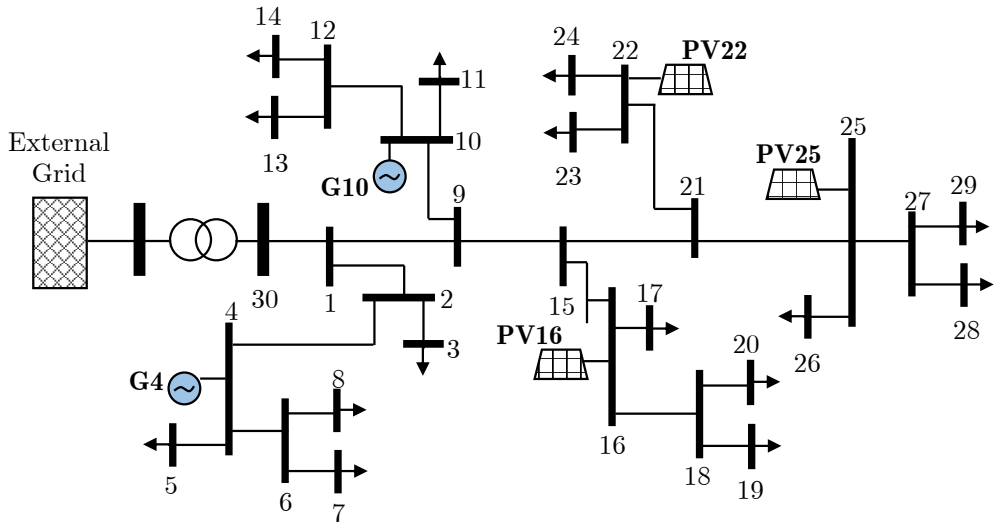

Figure 8.3: One-line diagram of test system.

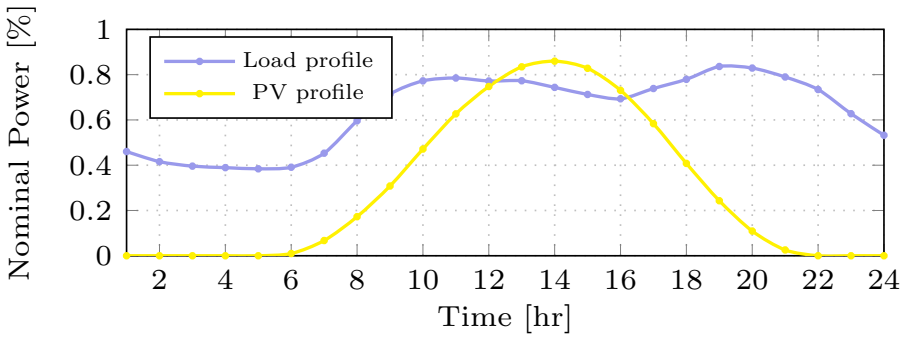

Figure 8.4: Solar power generation and load demand profiles.

$f_{min} = 49.6$ Hz, $f_{qss} = 49.8/50.2$ Hz, for the frequency response and $V_{min} = 0.45$ p.u., and $V_{max} = 1.2$ p.u., $\underline{V}_{\text{rec}} = 0.9$ p.u. and $\overline{V}_{\text{rec}} = 1.1$ p.u. for the voltage trajectories. The steady-state voltages in normal operation are set within bounds of $\underline{V}_{\text{pre}} = 0.95$ p.u. to $\overline{V}_{\text{pre}} = 1.05$ p.u. The value of the RoCoF is calculated based on the measured frequencies between t_c and t_r as:

$$\dot{f}(t) = \frac{f(t + \Delta t) - f(t)}{\Delta t} \tag{8.16}$$

The maximum RoCoF derived from the measurements no greater than 0.5s after MG disconnection from the grid.

To investigate the effect of transient-aware MG scheduling on system security, three different case studies are analysed in the operational planning problem:

- Base case: No transient security constraints. Only MG static islanding constraints
- Case 1: The constraints of the Base case plus transient frequency security constraints

- Case 2: The constraints of the Base case plus transient voltage security constraints
- Case 3: The constraints of the Base case plus both transient frequency and voltage security constraints.

8.4.2 Preventive Power Rescheduling

Cases 1, 2 and 3 result in both active and reactive power rescheduling to ensure the satisfaction of the transient security requirements. Figure 8.5 shows the scheduled power exchange with the grid for each of the cases. In Case 1 (see Fig. 8.5-green), the active power imported from the grid is shown to significantly reduce at hours 10, 19, 20, 21, compared to the Base Case. This is a result of the actions taken to ensure the secure frequency transient response in case of unplanned islanding. However, the effect to reactive power is less substantial. An average hourly power increase of 0.062 MVar is observed for reactive power in comparison to an average reduction of 0.521 MW in case active power for the entire planning horizon compared to the Base case. The sensitivities of active power to the frequency metrics are as expected more significant than to reactive power. The reduction in active power imported from the grid implies that more power has to be generated locally in the MG to improve the system frequency response in the case of un-intentional islanding.

With only voltage transient security considered in Case 2 (see Fig. 8.5-blue), an average hourly active power increase of 0.272 MW and a reactive power reduction of 0.473 MVar is observed compared to the Base case. Local reserves of reactive power are used to ensure non-violation of the voltage security metrics during islanding. These are mainly provided

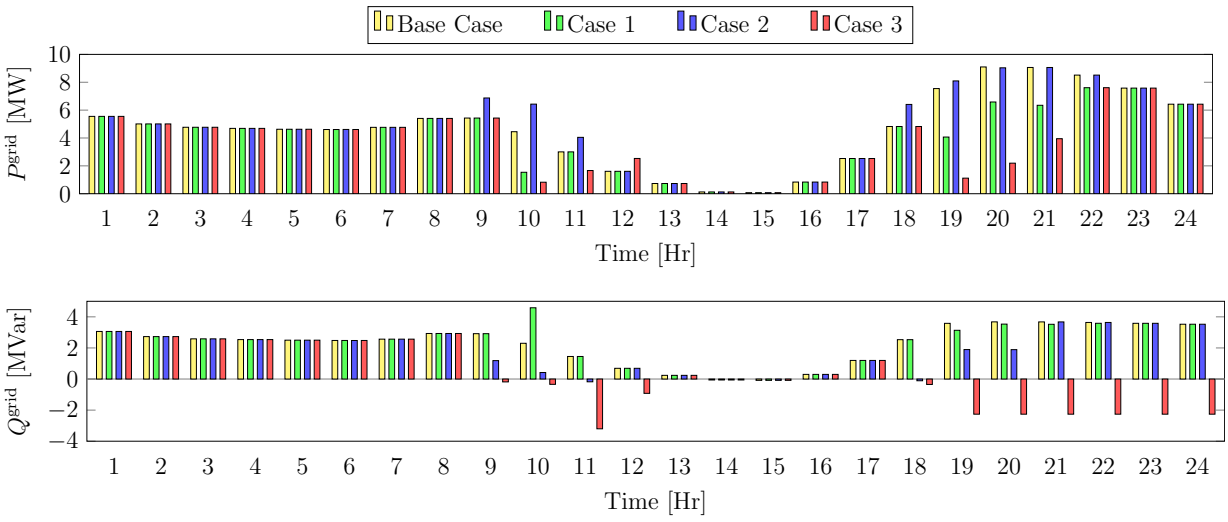

Figure 8.5: Scheduling of active and reactive power exchanged with the grid for the different planning cases ((+) indicates power import and (-) indicates power export).

by the SG units as the system will prioritise the cheap active power from the renewable units. In addition, power factor limitations on the CIG units can reduce their capability to provide reactive power. The increase in active power import aids in the improvement of the pre-contingency voltage levels which reduces the dynamic reactive power support necessary to maintain voltages during an event.

Case 3 (see Fig. 8.5-red), that includes both frequency and voltage transient constraints, indicates notable variations in both active and reactive power schedules. In this case, an hourly average of 0.975 MW active power and 2.089 MVar reactive power over the planning horizon is to be generated by the DERs in the MG to ensure a secure transient performance as compared to the Base case. However, the adherence to both frequency and voltage metrics is non-trivial especially given the competing requirements on the system power reserved by each of transient metrics. That is, both the frequency and voltage related metrics have sensitivity against both active and reactive power – thus, they might compete for resources. This is shown in Fig. 8.5 at hours 10, 11, 19 and 22 for active power and hours 10, 21 and 22 for reactive power when comparing Cases 1 and 2.

8.4.3 Transient Security Performance

The performance of the MG with respect to the transient security metrics (see Fig. 8.1) for frequency and voltage is presented in Figs. 8.6 and 8.7, respectively. The box and whisker

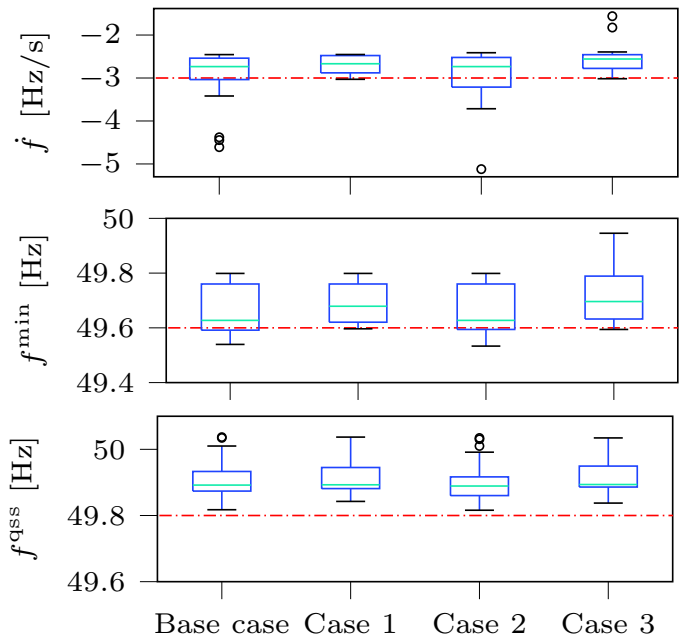

Figure 8.6: Box-Plots showing the distribution of the transient frequency security metrics for all hours based on the CoI frequency model.

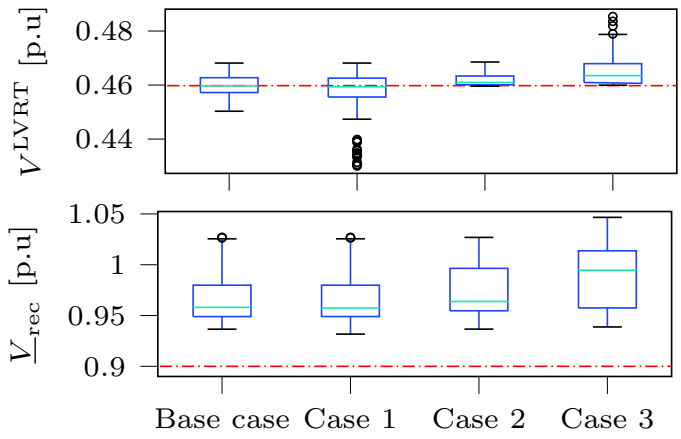

Figure 8.7: Box-Plots showing the distribution of the transient voltage security metrics at the local generators for all hours.

plot parameters have been set as: the box plot width is defined by the Interquartile range (IQR) i.e., the difference between 25th (Q1) and 75th (Q3) percentiles and the median while the whiskers are set by the minimum and maximum values in the dataset excluding outliers. These extend to Q1–1.5×IQR for the minimum and Q3+ 1.5×IQR for the maximum value. The dashed red line indicates the limit below which a violation, and thus unit disconnection, occurs during operation. In the Base case, violations exist at various hours in both the frequency and voltage metrics indicating the potential disconnection of the DERs during an abrupt islanding event of the MG. The Base case only takes into consideration the static security before and after MG islanding. For Case 1 in Fig. 8.6, it is observed that the optimal solution obtained after power rescheduling at all hours indicates no violations of the transient frequency metrics. However, with regards to the voltage metrics in Case 1 indicated in Fig. 8.7, the LVRT limits remain violated for several hours in the planning horizon. A similar trend is observed in Case 2 wherein while the voltage metrics remain within the defined limits, the RoCoF limit is violated at different hours of the operational schedule. The separate analysis of either frequency or voltage in the planning problem does not lead to a secure transition of the MG. Moreover, when only one type of the transient metrics is considered, Figs. 8.6 and Fig. 8.7 indicate further degradation in the system performance of the other metric type. Finally, the results for Case 3, indicate that both frequency and voltage transients are within the secure operation regions.

The power schedules computed for each hour are dynamically validated with the time-domain simulations (Step 2). Figures 8.8 and 8.9 show the frequency and voltage response respectively at hours 10, 19, 20, and 21 of the planning horizon with significant improvement in system performance for both metrics in Case 3. The preventive rescheduling of

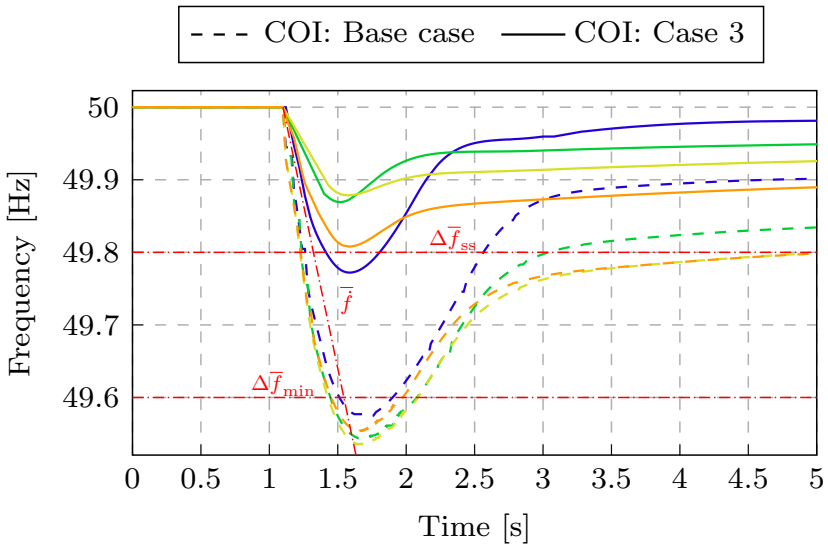

Figure 8.8: CoI frequency trajectories during operation in hours 10 (blue), 19 (green), 20 (yellow), and 21 (orange) for the Base case and Case 3 operation with a disconnection at time 1 s.

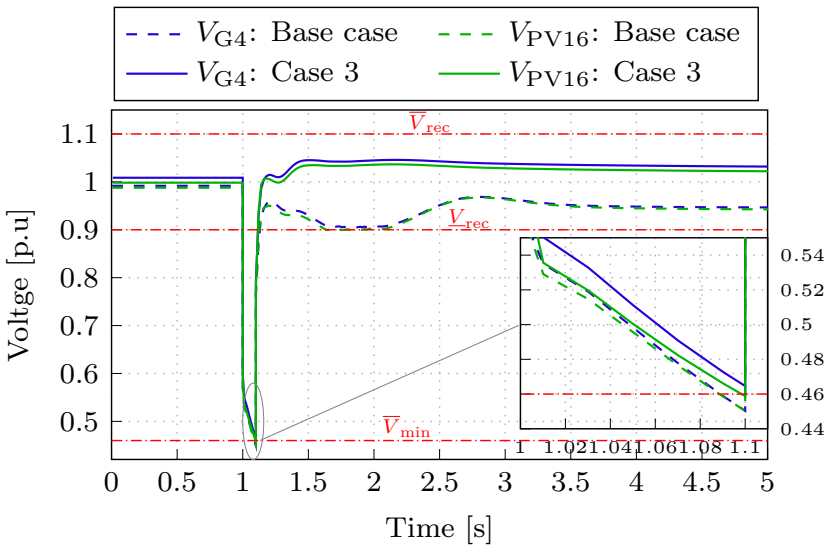

Figure 8.9: Voltage trajectories at the terminals of SG G4 and CIG PV16 at hour 19 for unintentional islanding at time 1 s.

power reserves greatly contributes to ensuring system degradation is minimised.

8.4.4 Effect to System Costs

The requirement for both static and dynamic security comes at a cost as indicated in Table 8.1 for the different case studies. In the Base case, the MG relies heavily on the cheaper power imported from the grid to ensure satisfaction of the different steady-state operational constraints. The requirement for transient security during islanding demands increased power generation from the local resources available in the MG. In Cases 1 and 2, increments of 2867 $ and 2706 $ are observed, respectively, in comparison with the Base

Table 8.1: Operational costs incurred the planning case studies

	Operation Cost [$]			
	Base	Case 1	Case 2	Case 3
Grid-connected	19203	22070	21909	38000
Islanded	0.0	0.0	0.0	0.0

case. In Case 1, higher priced active power is more utilised as compared to Case 2 that heavily relies on reactive power. As CIG units are already maximised due to their negligible operational costs, the SG units provide the power reserves necessary thus increasing the total operational costs. The extra cost incurred due to preventive rescheduling reflects the system security and resilience with respect to the islanding transients.

In Case 3, a significant extra cost of 18797 $ is observed. The active and reactive power scheduling requirements for the frequency and voltage metrics, shown to be competing in some hours and coherent in others (see Fig. 8.5), result in larger variations and higher costs. An overall increment of 15%, 14% and 98% is observed respectively for Cases 1, 2 and 3 as compared to the Base case to guarantee adherence to all transient security metrics.

8.4.5 Computational Performance

All case studies have been performed on a laptop with an Intel Core i7 processor at 2.5GHz with 32GB memory. The proposed approach is solved within four steps. Step 1 is solved using the PYOMO platform while the rest of the steps include a combination of numerical calculations performed with the python mathematical interface and time-domain simulations performed in PyRAMSES. In the 24-hour planning problem of Step 1, the solution is obtained in an average computation time of 6.15 s. Note that this time is dependent on the solution space of the problem. In PYOMO, for a simulation time set at 20 s, the average computation time for the operating point for a single hour is 0.792 s.

At each iteration, in Step 2 one simulation is carried out for each operating point (hour of operation) and dynamics checked to ensure no violations exist i.e., Sim^{0}_{kt}. If violations exist in the transient metrics at any hour, further simulations are carried out independently for each hour to calculate sensitivities to frequency and voltage metrics in Step 3 as follows:

- With respect to frequency dynamics: Only at the PCC bus, two simulations varying active power exchange above and below the value at Sim^{0}_{kt} i.e., $\text{Sim}^{0(\pm P)}_{kt|i=\text{PCC}}$ and two

simulations varying the reactive power exchange above and below the value at Sim^{0}_{kt} i.e., $\text{Sim}^{0(\pm Q)}_{kt|i=\text{PCC}}$ (see Equation (8.15)).

- With respect to voltage dynamics: At every generator bus, two simulations varying active power generation above and below the value at Sim^{0}_{kt} i.e., $\text{Sim}^{0(\pm P)}_{gkt}$ and two simulations varying the reactive power power generation above and below the value at Sim^{0}_{kt} i.e., $\text{Sim}^{0(\pm Q)}_{gkt}$ (see Equation (8.15)).

Therefore, the total the number of simulations performed at each hour of operation for Step 3 is equal to: $\big((4 \times \text{Sim}_g, \forall g) + (4 \times \text{Sim}_{i=\text{PCC}})\big)$. Similar to Step 1, the total computation time at Step 3 increases with the number of generators in the network and number of operating points i.e., hours, considered. Finally, note that as the algorithm iterates between the time domain simulation and optimisation problem convergence is guaranteed using the resilience cuts that reduce the feasible solution space at each iteration.

8.5 Conclusion

A MG can ensure the power supply continuity during emergency grid conditions through its islanded operation capabilities. Its survivability is however dependant on its operational states remaining within secure regions in the pre-islanding, post-islanding, and transition periods. This chapter proposes an algorithm to solve a transient-aware operational planning problem that ensure steady-state security and energy adequacy, as well as transient security during islanding. Linearised constraints related to the frequency and voltage security metrics are formulated (using time-domain simulations to derive sensitivity coefficients) and introduced as resilience cuts in the planning problem using an iterative approach. The performance of the proposed technique is demonstrated on a medium-voltage distribution network with results indicating that neglecting the voltage and frequency transient security constraints or considering only one of them provides an optimistic results with no security guarantees. Interactions between scheduling requirements for frequency and voltage metrics result in significant variations in active and reactive powers necessary to enhance system resilience and its associated costs. As a potential future direction for this work, the algorithm needs to be extended to handle the uncertainty in load demand and renewable resource variations discussed in Chapters 4 and 5. Moreover, the use of embedded trajectory sensitivities during time-domain simulation can provide more accurate values for the effect of active and reactive power to the transient metrics.

Chapter 9

Conclusions and Outlook

9.1 Summary of Work and Main Conclusions

The changing dynamics of the power system operation warrant a deeper analysis into the mechanisms that will ensure system preparedness in case of both internal and external disturbances more specifically those leading to an emergency state of operation. A microgrid (MG) in its different modes of operation, provides the operational flexibility required for ensuring that the system can survive uncertain and high-impact disturbances. This thesis has examined and analysed both steady-state and dynamic security aspects of MGs to ensure their resilient operation. The main conclusions and finding of this thesis are summarised as follows:

- The choice of the system model used in planning problems should consider the aspects of accuracy, tractability and scalability. Chapter 3 addressed the issue of system-level modelling using the Optimal Power Flow-based models. An analysis of the different formulations that can be adopted to ensure accurate modelling of the characteristics of MG networks was presented using different metrics. Moreover, it was showed that ignoring aspects of line charging in distribution networks with a high R/X ratio can lead to significant errors in applications dealing with voltage response of the system.

- Due to the uncertain nature of both load demand and renewable generation, it is vital that MG planning formulations apply probabilistic models to incorporate, study and analyse potential operational scenarios. Chapters 4 and 5 proposed stochastic and distributionally robust models, respectively, to tackle the uncertainties present

during system operation. While robust models provided better guarantees on the handling of all potential scenarios, the impact to system costs is much higher as compared to the stochastic models.

- MG islanding provided an effective solution to enhance resilience during emergency scenarios in the bulk grid. However, analysing only the post-islanding steady-state conditions is insufficient to ensure the survivability of the MG during the islanding transients. Chapters 6 and 7 proposed models to tackle transient frequency security while Chapter 8 dealt with both transient frequency and voltage security.
- Embedding the transient frequency and voltage dynamics model and the associated security metrics into a planning problem is a non-trivial task requiring careful scrutiny to the model's tractability. Chapter 6 tackles this challenge using an iterative bound-tightening approach while Chapter 7 adopts a decomposition-based approach. Moreover, Chapter 8 utilises linear resilience cuts based on sensitivities derived from a time-domain simulation rather than incorporating the full DAD model.
- In ensuring system security during transient operation, operational flexibility utilising demand response and re-scheduling of system power provided optimal solutions deferring the need to install additional generation units.
- Both active and reactive power reserves play a key role in ensuring transient security of the MG during the transition period to the islanded mode in emergency situations. Moreover, the support from CIGs if possible provides significant benefits to system performance in the transient state.
- There is a high cost associated to making the system more secure and resilient to islanding transients and operational uncertainties.

9.2 Outlook

While the thesis has proposed different methodologies for application to MG operation, there are various avenues for future work on the topics addressed. In the following, questions that remain unanswered and potential further investigations are summarised:

- The Distributionally Robust Optimisation algorithm presented in Chapter 5 provides better guarantees on handling uncertainty but can be impractical due to its conservativeness. This can be controlled by the type of increasing the statistical measure captured in the ambiguity set, investigating other types of support sets and

the consideration of a decomposition based two-stage algorithm to further reduce on the conservatism of the formulation.

- The work of this thesis has employed the Center-of-Inertia (CoI), which incorporates the contribution of each unit, to model the frequency trajectory during the transient state of the MG. However, with the increasing penetration of CIGs, greater variations are expected and it is necessary to determine whether this aggregated response model can accurately estimate the local frequency measured at the generator nodes. More so given that the concept of COI is based on the assumption of a system of coherent SG units. Moreover, generating units located nearer to the location of the point of the fault i.e. the MG Point-of-Common-Coupling may experience larger deviations as compared to those further away [209]. The different algorithms proposed to handle frequency transients should be improved to investigate the security of local frequency oscillations and their effect to system performance.

- The intermittent power generation of CIGs can present variations in the level of support available. In Chapters 6 and 7, it was assumed that active power reserves required for transient support were provide by a DC-link capacitor energy storage. However, it may be more practical to consider either reserves provided by a battery energy storage attached to the CIG or by reducing power output from the maximum power point by the reserve power requirement. The latter approach allows for upward power regulation to meet instantaneous active power requirement during emergency operation. This is similarly true in the case of reactive power provision for voltage support. However, this implies that the level of support at each operating scenario will vary based in the available power from the CIGs. The result is variability in level of frequency and voltage support available in the network. This uncertainty in support levels needs to be incorporated into the problem and further investigated to ensure robust operation.

- The studies in chapters 6-8 considered static control settings during the provision of frequency and voltage support to the MG. However, the settings of the controller parameters should be optimised to ensure the adaptability of support available to the varying operating scenarios. This notion has been presented in [154] utilising a second-order reduced frequency model. Further investigations into the dynamic modification of control actions and control settings following the dynamics during MG operation are necessary to ensure optimality of system response.

- The resilience of the MG has been defined based on the secure operation of the

system during both steady-state and transient operations. Conventional resilience metrics are defined based on static adequacy-related metrics ignoring the states and trajectories during the transient response of the network. Moreover, with the massive integration of CIGs and their variable nature, it presents the question of whether conventional metrics can still be sufficient for application in converter-dominated networks. The variation in system dynamics requires the re-evaluation of system analysis frameworks incorporating system preparedness, system survivability and system sufficiency/adequacy during emergency conditions in the power network.

Appendices

Appendix A

Network Parameters

A.1 Alderney Electricity Network

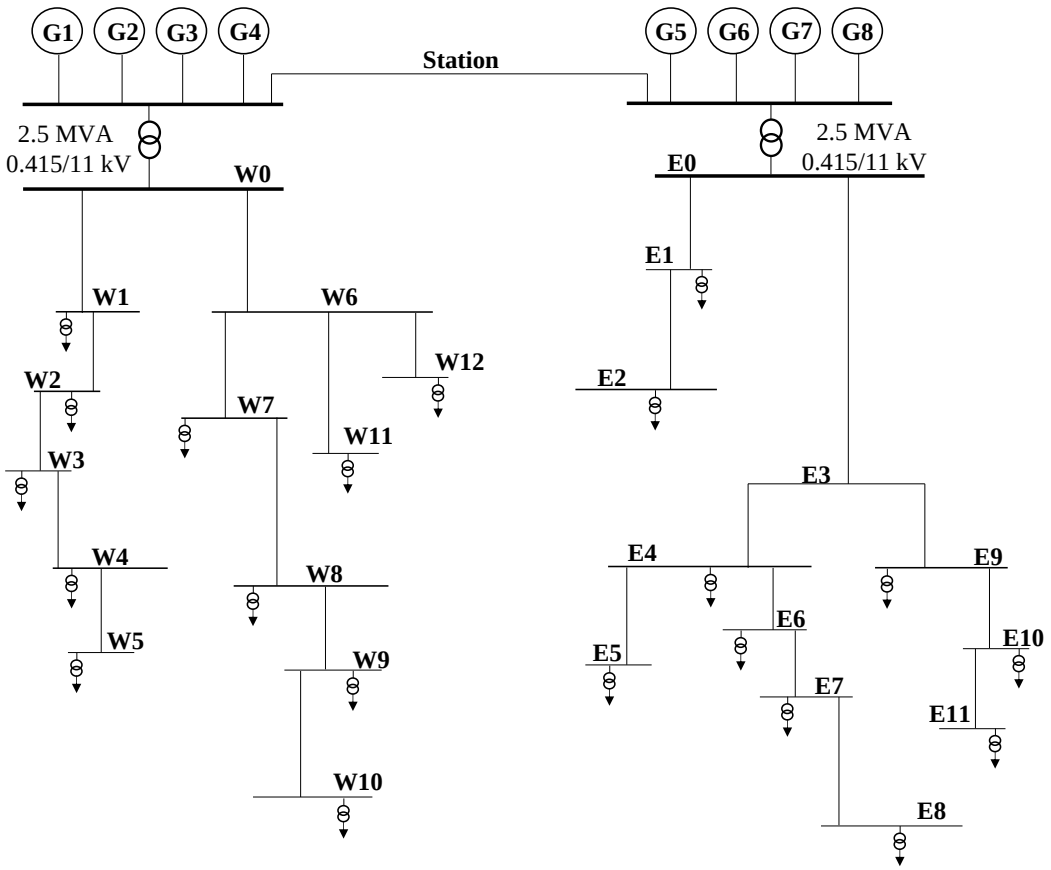

Figure A.1: The AEL network one-line diagram.

Table A.1: Alderney HV network connections and line parameters

Node from	**Node to**	**Size (mm^2)**	**Length (m)**	**R (Ω)**	**X (Ω)**	**B (μS)**
West						
W0	W1	25	630	0.5481	0.0674	71.251
W0	W6	70	630	0.2155	0.0693	57.199
W6	W11	16	572	0.8408	0.0807	32.346
W1	W2	70	1832	0.6265	0.2015	166.331
W2	W3	70	1105	0.3779	0.1216	100.325
W3	W4	70	485	0.1659	0.0533	44.034
W4	W5	70	534	0.1826	0.0587	48.483
W6	W7	70	527	0.1802	0.0580	47.847
W7	W8	70	100	0.0342	0.0110	9.079
W8	W9	16	205	0.3014	0.0289	11.593
W9	W10	16	225	0.3308	0.0317	12.724
East						
E0	E1	16	480	0.7056	0.0677	27.143
E1	E2	25	191	0.1827	0.0225	23.750
E0	E9	70	1000	0.3420	0.1100	90.792
E9	E10	70	475	0.1625	0.0523	43.126
E10	E11	70	400	0.1368	0.0440	36.317
E4	E6	70	260	0.0889	0.0286	23.606
E6	E7	70	246	0.0841	0.0271	22.335
E7	E8	70	1095	0.3745	0.1204	99.417

A.2 Modified IEEE 34-Bus Network

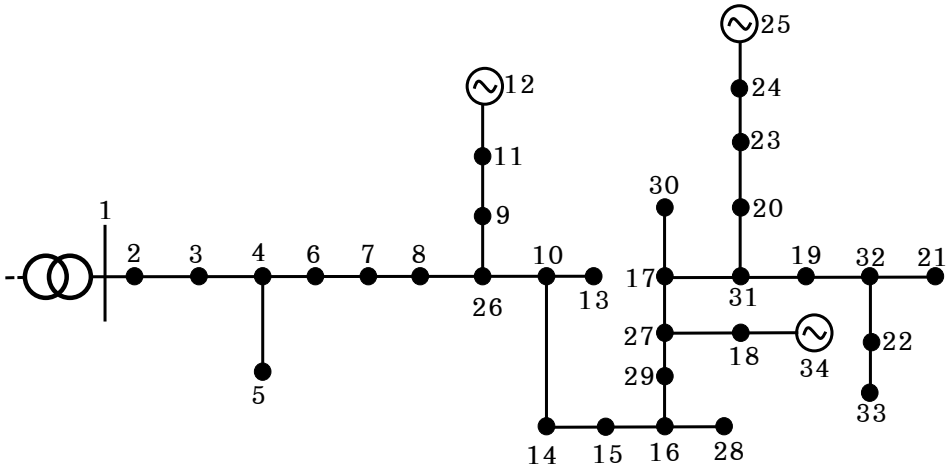

Figure A.2: One line diagram of the modified IEEE 34 bus network

Table A.2: Modified IEEE 34-Bus network connections and line parameters

Node from	**Node to**	**R** (Ω)	**X** (Ω)	**B** (μ**S**)
1	2	0.653208	0.651986	2.60687
2	3	0.438004	0.437185	1.748017
3	4	8.160034	8.144774	32.56567
4	5	3.077323	1.632921	4.6444
4	6	9.4943	9.476544	37.89055
6	7	7.527081	7.513004	30.03963
7	8	0.003655	0.002673	0.009698
26	9	0.906655	0.481099	1.368354
26	10	3.732057	2.729429	9.901941
9	11	25.52948	13.54672	38.52996
11	12	7.285049	3.865669	10.99484
10	13	1.606528	0.852473	2.424627
10	14	0.307045	0.224556	0.814655
14	15	7.471425	5.464205	19.82328
15	16	0.190075	0.139011	0.50431
27	17	1.791095	1.309912	4.752156
27	18	23.56038	50.59282	0
31	19	0.73837	0.540005	1.959052

31	20	0.102348	0.074852	0.271552
32	21	0.314355	0.229903	0.834052
32	22	0.102348	0.074852	0.271552
20	23	0.493465	0.360894	1.309267
23	24	1.330528	0.973078	3.530173
24	25	0.193731	0.141684	0.514009
8	26	0.113314	0.082872	0.300647
29	27	0.003655	0.002673	0.009698
16	28	12.36974	6.563759	18.66882
16	29	13.46246	9.845728	35.71875
17	30	0.858936	0.455778	1.296335
17	31	2.131038	1.558528	5.654095
19	32	0.979619	0.716442	2.599138
22	33	1.768834	1.308147	4.01658
18	34	2.673595	2.668595	10.66998

Table A.3: Modified IEEE 34-Bus load parameters

Node	**P [kW]**	**Q [kVar]**
1	0	0
2	0	0
3	30	15
4	0	0
5	16	8
6	0	0
7	0	0
8	0	0
9	0	0
10	5	2
11	34	17
12	135	70
13	40	20
14	4	2
15	17	8
16	0	0

17	7	3
18	0	0
19	36	24
20	0	0
21	27	16
22	0	0
23	144	110
24	25	12
25	43	27
26	0	0
27	0	0
28	4	2
29	0	0
30	2	1
31	4	2
32	30	15
33	28	14
34	150	75

A.3 Modified CIGRE 18-Bus European Low Voltage Network

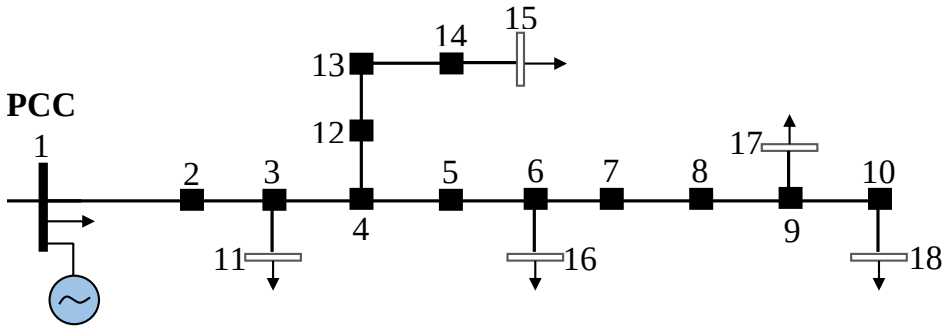

Figure A.3: One line diagram of the modified European CIGRE low voltage network.

Table A.4: Modified CIGRE 18-bus network line parameters

Node from	**Node to**	**Resistance (Ω/km)**	**Reactance (Ω/km)**	Length (m)
1	2	0.278	0.167	35
2	3	0.278	0.167	35
3	4	0.278	0.167	35
4	5	0.278	0.167	35
5	6	0.278	0.167	35
6	7	0.278	0.167	35
7	8	0.278	0.167	35
8	9	0.278	0.167	35
9	10	0.278	0.167	35
3	11	1.152	0.458	30
4	12	1.152	0.458	35
12	13	1.152	0.458	35
13	14	1.152	0.458	35
14	15	1.152	0.458	30
6	16	1.152	0.458	30/90
9	17	1.152	0.458	30
10	18	1.152	0.458	30

Table A.5: Modified CIGRE 18-bus network load parameters

Node	Load [kVA]	Power factor
1	200	0.95
11	15	0.95
15	52	0.95
16	55/210	0.95/0.85
17	35	0.95
18	47	0.95

A.4 30-Bus Medium Voltage Network

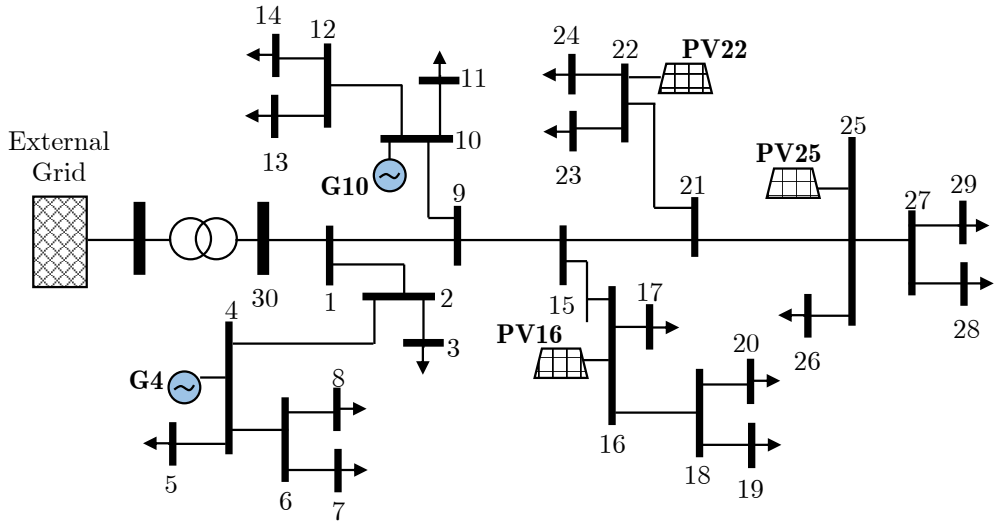

Figure A.4: One-line diagram of the 30-bus test system.

Table A.6: 30-Bus test network connections and line parameters

Node from	**Node to**	**Resistance (Ω)**	**Reactance (Ω)**
30	1	0.1464	0.4116
1	2	0.122	0.343
2	3	0.1342	0.3773
2	4	0.1708	0.4802
4	5	0.122	0.343
4	6	0.122	0.343
6	7	0.1342	0.3773
7	8	0.1464	0.4116
1	9	0.1464	0.4116
9	10	0.1464	0.4116
10	11	0.122	0.343
10	12	0.122	0.343
12	13	0.122	0.343
13	14	0.122	0.343
9	15	0.1342	0.3773
15	16	0.1342	0.3773
16	17	0.122	0.343

16	18	0.1586	0.4459
18	19	0.1342	0.3773
19	20	0.122	0.343
15	21	0.1464	0.4116
21	22	0.1464	0.4116
22	23	0.1342	0.3773
22	24	0.122	0.343
21	25	0.1586	0.4459
25	26	0.1464	0.4116
25	27	0.1464	0.4116
27	28	0.1586	0.4459
27	29	0.1342	0.3773

Table A.7: 30-Bus test network load parameters

Node	**P [MW]**	**Q [MVar]**
0	0	0
1	0	0
2	0	0
3	0.85	0.52
4	0	0
5	0.7	0.21
6	0	0
7	0.22	0.09
8	0.33	0.11
9	0	0
10	0	0
11	0.9	0.45
12	0	0
13	0.35	0.15
14	1.26	0.64
15	0	0
16	0	0
17	0.76	0.43
18	0	0

19	1.22	0.46
20	0.95	0.43
21	0	0
22	0	0
23	0.4	0.17
24	0.44	0.205
25	0	0
26	0.9	0.45
27	0	0
28	1.05	0.625
29	0.68	0.31

Bibliography

[1] M. Paturet, U. Markovic, S. Delikaraoglou, E. Vrettos, P. Aristidou, and G. Hug, "Stochastic unit commitment in low-inertia grids," *IEEE Trans. Power Syst.*, pp. 1–1, 2020.

[2] M. Panteli, D. N. Trakas, P. Mancarella, and N. D. Hatziargyriou, "Power systems resilience assessment: Hardening and smart operational enhancement strategies," *Proceedings of the IEEE*, vol. 105, no. 7, pp. 1202–1213, July 2017.

[3] R. Arghandeh, A. von Meier, L. Mehrmanesh, and L. Mili, "On the definition of cyber-physical resilience in power systems," *Renewable & Sustainable Energy Reviews*, vol. 58, pp. 1060 – 1069, 2016.

[4] Z. Li, M. Shahidehpour, F. Aminifar, A. Alabdulwahab, and Y. Al-Turki, "Networked microgrids for enhancing the power system resilience," *Proceedings of the IEEE*, vol. 105, no. 7, pp. 1289–1310, July 2017.

[5] M. Chaudry, P. Ekins, K. Ramachandran, A. Shakoor, J. Skea, G. Strbac, X. Wang, and J. Whitaker, "Building a resilient UK energy system," 2009, working paper.

[6] IEEE, "Ieee standard for the specification of microgrid controllers," *IEEE Std 2030.7-2017*, pp. 1–43, 2018.

[7] M. Panteli, D. N. Trakas, P. Mancarella, and N. D. Hatziargyriou, "Boosting the power grid resilience to extreme weather events using defensive islanding," *IEEE Trans. on Smart Grid*, vol. 7, no. 6, pp. 2913–2922, 2016.

[8] A. Hussain, V.-H. Bui, and H.-M. Kim, "Microgrids as a resilience resource and strategies used by microgrids for enhancing resilience," *Applied Energy*, vol. 240, pp. 56–72, 2019.

[9] M. Panteli and P. Mancarella, "The grid: Stronger, bigger, smarter?: Presenting a conceptual framework of power system resilience," *IEEE Power and Energy Magazine*, vol. 13, no. 3, pp. 58–66, 2015.

[10] S. Eftekharnejad, V. Vittal, G. T. Heydt, B. Keel, and J. Loehr, "Impact of increased penetration of photovoltaic generation on power systems," *IEEE Trans. on Pow. Sys.*, vol. 28, no. 2, pp. 893–901, 2013.

[11] A. H. Kasem Alaboudy, H. H. Zeineldin, and J. Kirtley, "Microgrid stability characterization subsequent to fault-triggered islanding incidents," *IEEE Trans. on Pow. Delivery*, vol. 27, no. 2, pp. 658–669, 2012.

[12] W. Zheng, P. Crossley, B. Xu, and H. Qi, "Transient stability of a distribution subsystem during fault-initiated switching to islanded operation," *Int. Journal of Elec. Pow. & Energy Sys.*, vol. 97, pp. 418–427, 2018.

[13] D. E. Olivares, A. Mehrizi-Sani, A. H. Etemadi, C. A. Cañizares, R. Iravani, M. Kazerani, A. H. Hajimiragha, O. Gomis-Bellmunt, M. Saeedifard, R. Palma-Behnke, G. A. Jiménez-Estévez, and N. D. Hatziargyriou, "Trends in microgrid control," *IEEE Transactions on Smart Grid*, vol. 5, no. 4, pp. 1905–1919, July 2014.

[14] T. L. Vandoorn, J. C. Vasquez, J. De Kooning, J. M. Guerrero, and L. Vandevelde, "Microgrids: Hierarchical control and an overview of the control and reserve management strategies," *IEEE Industrial Electronics Magazine*, vol. 7, no. 4, pp. 42–55, Dec 2013.

[15] J. Schiffer, D. Zonetti, R. Ortega, A. M. Stanković, T. Sezi, and J. Raisch, "A survey on modeling of microgrids—from fundamental physics to phasors and voltage sources," *Automatica*, vol. 74, pp. 135 – 150, 2016.

[16] R. Lee, M. Assante, and T. Conway, *Analysis of the Cyber Attack on the Ukrainian Power Grid, Electricity Information Sharing and Analysis Center.* http://www.nerc.com/pa/CI/ESISAC/Documents, 2015.

[17] C. Chen, J. Wang, F. Qiu, and D. Zhao, "Resilient distribution system by microgrids formation after natural disasters," *IEEE Transactions on Smart Grid*, vol. 7, no. 2, pp. 958–966, March 2016.

[18] P. Kundur, J. Paserba, and S. Vitet, "Overview on definition and classification of power system stability," in *CIGRE/IEEE PES International Symposium Quality*

and Security of Electric Power Delivery Systems, 2003. CIGRE/PES 2003., 2003, pp. 1–4.

[19] R. Arghandeh, M. Brown, A. Del Rosso, G. Ghatikar, E. Stewart, A. Vojdani, and A. von Meier, "The local team: Leveraging distributed resources to improve resilience," *IEEE Power and Energy Magazine*, vol. 12, no. 5, pp. 76–83, Sep. 2014.

[20] H. Farzin, M. Fotuhi-Firuzabad, and M. Moeini-Aghtaie, "Enhancing power system resilience through hierarchical outage management in multi-microgrids," *IEEE Transactions on Smart Grid*, vol. 7, no. 6, pp. 2869–2879, Nov 2016.

[21] H. Asano, N. Hatziargyriou, R. Iravani, and C. Marnay, "Microgrids: An overview of ongoing research, development, and demonstration projects," *IEEE Power Energy Magazine*, pp. 78–94, 01 2007.

[22] C. Yuen, A. Oudalov, and A. Timbus, "The provision of frequency control reserves from multiple microgrids," *IEEE Transactions on Industrial Electronics*, vol. 58, no. 1, pp. 173–183, Jan 2011.

[23] F. D. Moya, G. D. M. Jannuzzi, and L. C. P. Da Silva, "Distributed generation for the provision of operating reserves," in *2008 IEEE/PES Transmission and Distribution Conference and Exposition: Latin America*, Aug 2008, pp. 1–7.

[24] F. O. Resende, N. J. Gil, and J. A. P. Lopes, "Service restoration on distribution systems using multi-microgrids," *European Transactions on Electrical Power*, vol. 21, no. 2, pp. 1327–1342, 2011.

[25] J. Machowski, J. Bialek, and D. J. Bumby, *Power System Dynamics: Stability and Control, 2nd Edition*. Wiley - IEEE Press, 2008.

[26] F. Capitanescu, J. M. Ramos, P. Panciatici, D. Kirschen, A. M. Marcolini, L. Platbrood, and L. Wehenkel, "State-of-the-art, challenges, and future trends in security constrained optimal power flow," *Electric Power Systems Research*, vol. 81, no. 8, pp. 1731 – 1741, 2011.

[27] D. K. Molzahn and I. A. Hiskens, *A Survey of Relaxations and Approximations of the Power Flow Equations*. Foundations and Trends® in Electric Energy System, 2019, vol. 4, no. 1-2.

[28] C. V. Thierry van Cutsem, *Voltage Stability of Electric Power Systems*. Part of the The Springer International Series in Engineering and Computer Science book series (PEPS), 1998.

[29] S. Mat Zali and J. V. Milanović, "Generic model of active distribution network for large power system stability studies," *IEEE Transactions on Power Systems*, vol. 28, no. 3, pp. 3126–3133, Aug 2013.

[30] S. Ma, L. Su, Z. Wang, F. Qiu, and G. Guo, "Resilience enhancement of distribution grids against extreme weather events," *IEEE Transactions on Power Systems*, vol. 33, no. 5, pp. 4842–4853, Sep. 2018.

[31] H. Nagarajan, E. Yamangil, R. Bent, P. Van Hentenryck, and S. Backhaus, "Optimal resilient transmission grid design," in *2016 Power Systems Computation Conference (PSCC)*, June 2016, pp. 1–7.

[32] S. Ma, B. Chen, and Z. Wang, "Resilience enhancement strategy for distribution systems under extreme weather events," *IEEE Transactions on Smart Grid*, vol. 9, no. 2, pp. 1442–1451, March 2018.

[33] W. Yuan, J. Wang, F. Qiu, C. Chen, C. Kang, and B. Zeng, "Robust optimization-based resilient distribution network planning against natural disasters," *IEEE Trans. Smart Grid*, vol. 7, no. 6, pp. 2817–2826, 2016.

[34] Y. Xu, C. Liu, K. P. Schneider, F. K. Tuffner, and D. T. Ton, "Microgrids for service restoration to critical load in a resilient distribution system," *IEEE Transactions on Smart Grid*, vol. 9, no. 1, pp. 426–437, Jan 2018.

[35] A. Barnes, H. Nagarajan, E. Yamangil, R. Bent, and S. Backhaus, "Tools for improving resilience of electric distribution systems with networked microgrids," *arXiv e-prints*, p. arXiv:1705.08229, May 2017.

[36] Y. Xu, C. Liu, K. P. Schneider, and D. T. Ton, "Placement of remote-controlled switches to enhance distribution system restoration capability," *IEEE Transactions on Power Systems*, vol. 31, no. 2, pp. 1139–1150, March 2016.

[37] J. Q. Tortós and V. Terzija, "Controlled islanding strategy considering power system restoration constraints," in *2012 IEEE Power and Energy Society General Meeting*, July 2012, pp. 1–8.

[38] European Commission, "Commission regulation (EU) 2016/631 of 14 april 2016 establishing a network code on requirements for grid connection of generators (RfG)," *Official Journal of the European Union*, 2016.

[39] IEEE, "Ieee standard for interconnection and interoperability of distributed energy resources with associated electric power systems interfaces," *IEEE Std 1547-2018 (Revision of IEEE Std 1547-2003)*, pp. 1–138, 2018.

[40] ——, "IEEE Standard for Interconnecting Distributed Resources with Electric Power Systems," *IEEE Std 1547-2003*, pp. 1–28, 2003.

[41] Wind Generation Task Force, "The Technical Basis for the New WECC Voltage Ride-Though (VRT) Standard," A White Paper Developed by the Wind Generation Task Force, Tech. Rep., June 2007.

[42] Kundur, P, Neal J. Balu, and Mark G. Lauby, *Power system stability and control*. New York: McGraw-Hill, 1994.

[43] P. M. Anderson and M. Mirheydar, "A low-order system frequency response model," *IEEE Trans. Power Syst.*, vol. 5, no. 3, pp. 720–729, Aug 1990.

[44] K. Yeager and J. Willis, "Modeling of emergency diesel generators in an 800 megawatt nuclear power plant," *IEEE Transactions on Energy Conversion*, vol. 8, no. 3, pp. 433–441, 1993.

[45] Turbine-governor models: Standard dynamic turbine-governor systems in neplan power system analysis tool. [Online]. Available: https://www.neplan.ch/wp-content/uploads/2015/08/Nep_TURBINES_GOV.pdf

[46] J. Rocabert, A. Luna, F. Blaabjerg, and P. Rodríguez, "Control of power converters in AC microgrids," *IEEE Trans. Power Electron.*, vol. 27, no. 11, pp. 4734–4749, Nov 2012.

[47] Q.-C. Zhong and G. Weiss, "Synchronverters: Inverters that mimic synchronous generators," *IEEE Transactions on Industrial Electronics*, vol. 58, no. 4, pp. 1259–1267, 2011.

[48] Q.-C. Zhong, P.-L. Nguyen, Z. Ma, and W. Sheng, "Self-synchronized synchronverters: Inverters without a dedicated synchronization unit," *IEEE Transactions on Power Electronics*, vol. 29, no. 2, pp. 617–630, 2014.

[49] S. D'Arco, J. A. Suul, and O. B. Fosso, "A virtual synchronous machine implementation for distributed control of power converters in smartgrids," *Electric Power Systems Research*, vol. 122, pp. 180–197, 2015.

[50] J. M. Guerrero, L. G. de Vicuna, J. Matas, M. Castilla, and J. Miret, "A wireless controller to enhance dynamic performance of parallel inverters in distributed

generation systems," *IEEE Transactions on Power Electronics*, vol. 19, no. 5, pp. 1205–1213, Sep 2004.

[51] N. Soni, S. Doolla, and M. C. Chandorkar, "Improvement of transient response in microgrids using virtual inertia," *IEEE Transactions on Power Delivery*, vol. 28, no. 3, pp. 1830–1838, July 2013.

[52] T. Ise and H. Bevrani, "Virtual synchronous generators and their applications in microgrids," in *Integration of Distributed Energy Resources in Power Systems*, T. Funabashi, Ed. Academic Press, 2016, pp. 282 – 294.

[53] P. Kotsampopoulos, N. Hatziargyriou, B. Bletterie, and G. Lauss, "Review, analysis and recommendations on recent guidelines for the provision of ancillary services by distributed generation," in *2013 IEEE International Workshop on Inteligent Energy Systems (IWIES)*, Nov 2013, pp. 185–190.

[54] IEEE, "Ieee recommended practice for excitation system models for power system stability studies," *IEEE Std 421.5-2016 (Revision of IEEE Std 421.5-2005)*, pp. 1–207, 2016.

[55] Y. Bae, T.-K. Vu, and R.-Y. Kim, "Implemental control strategy for grid stabilization of grid-connected pv system based on german grid code in symmetrical low-to-medium voltage network," *IEEE Transactions on Energy Conversion*, vol. 28, no. 3, pp. 619–631, 2013.

[56] G. Chaspierre, P. Panciatici, and T. Van Cutsem, "Dynamic equivalent of a distribution grid hosting dispersed photovoltaic units," in *Proc. 10th Bulk Power Syst. Dyn. & Control Symp. (IREP)*, 2017, pp. 1–12.

[57] K. Kawabe, Y. Ota, A. Yokoyama, and K. Tanaka, "Novel dynamic voltage support capability of photovoltaic systems for improvement of short-term voltage stability in power systems," *IEEE Trans. on Power Sys.*, vol. 32, no. 3, pp. 1796–1804, 2017.

[58] B. Weise, "Impact of k-factor and active current reduction during fault-ride-through of generating units connected via voltage-sourced converters on power system stability," *IET Renewable Power Generation*, vol. 9, no. 1, pp. 25–36, 2015.

[59] G. Chaspierre, "Reduced-order modelling of active distribution networks for large-disturbance simulations," Ph.D. dissertation, University of Liege, 2020.

[60] P. Aristidou, S. Lebeau, and T. Van Cutsem, "Power system dynamic simulations using a parallel two-level schur-complement decomposition," *IEEE Trans. on Power Sys.*, vol. 31, no. 5, pp. 3984–3995, 2016.

[61] H. Guo, C. Zheng, H. H.-C. Iu, and T. Fernando, "A critical review of cascading failure analysis and modeling of power system," *Renewable and Sustainable Energy Reviews*, vol. 80, pp. 9 – 22, 2017. [Online]. Available: http://www.sciencedirect.com/science/article/pii/S1364032117308432

[62] J. Carpentier, "Contribution to the economic dispatch problem," *Bull. Soc. Fr. Electr*, vol. 3, no. 8, 1962.

[63] A. Khodaei, "Microgrid optimal scheduling with multi-period islanding constraints," *IEEE Transactions on Power Systems*, vol. 29, no. 3, pp. 1383–1392, 2014.

[64] A. Venzke, S. Chatzivasileiadis, and D. K. Molzahn, "Inexact convex relaxations for ac optimal power flow: Towards ac feasibility," *Electric Power Systems Research*, vol. 187, p. 106480, 2020.

[65] J. Lavaei and S. H. Low, "Zero duality gap in optimal power flow problem," *IEEE Transactions on Power Systems*, vol. 27, no. 1, pp. 92–107, 2012.

[66] S. Toune, H. Fudo, T. Genji, Y. Fukuyama, and Y. Nakanishi, "Comparative study of modern heuristic algorithms to service restoration in distribution systems," *IEEE Transactions on Power Delivery*, vol. 17, no. 1, pp. 173–181, Jan 2002.

[67] C. Gamarra and J. M. Guerrero, "Computational optimization techniques applied to microgrids planning: A review," *Renewable and Sustainable Energy Reviews*, vol. 48, pp. 413 – 424, 2015. [Online]. Available: http://www.sciencedirect.com/science/article/pii/S1364032115002956

[68] P. S. Georgilakis and N. D. Hatziargyriou, "A review of power distribution planning in the modern power systems era: Models, methods and future research," *Electric Power Systems Research*, vol. 121, pp. 89 – 100, 2015. [Online]. Available: http://www.sciencedirect.com/science/article/pii/S0378779614004490

[69] H. Hijazi and S. Thiébaux, "Optimal distribution systems reconfiguration for radial and meshed grids," *International Journal of Electrical Power & Energy Systems*, vol. 72, pp. 136 – 143, 2015, the Special Issue for

18th Power Systems Computation Conference. [Online]. Available: http://www.sciencedirect.com/science/article/pii/S014206151500109X

[70] R. Anand, D. Aggarwal, and V. Kumar, "A comparative analysis of optimization solvers," *Journal of Statistics and Management Systems*, vol. 20, no. 4, pp. 623–635, 2017. [Online]. Available: https://doi.org/10.1080/09720510.2017.1395182

[71] P. Panciatici, M. C. Campi, S. Garatti, S. H. Low, D. K. Molzahn, A. X. Sun, and L. Wehenkel, "Advanced optimization methods for power systems," in *2014 Power Sys. Compn. Conf.*, 2014, pp. 1–18.

[72] K. Christakou, D.-C. Tomozei, J.-Y. Le Boudec, and M. Paolone, "Ac opf in radial distribution networks – part i: On the limits of the branch flow convexification and the alternating direction method of multipliers," *Electric Power Systems Research*, vol. 143, pp. 438–450, 2017.

[73] F. Zhou and S. H. Low, "A note on branch flow models with line shunts," *IEEE Transactions on Power Systems*, vol. 36, no. 1, pp. 537–540, 2021.

[74] M. Nick, R. Cherkaoui, J. L. Boudec, and M. Paolone, "An exact convex formulation of the optimal power flow in radial distribution networks including transverse components," *IEEE Trans. on Automatic Control*, vol. 63, no. 3, pp. 682–697, 2018.

[75] M. Baran and F. Wu, "Network reconfiguration in distribution systems for loss reduction and load balancing," *IEEE Transactions on Power Delivery*, vol. 4, no. 2, pp. 1401–1407, 1989.

[76] M. Farivar and S. H. Low, "Branch flow model: Relaxations and convexification—part i," *IEEE Trans. on Power Sys.*, vol. 28, no. 3, pp. 2554–2564, 2013.

[77] S. H. Low, "Convex relaxation of optimal power flow—part ii: Exactness," *IEEE Trans. on Control of Net. Sys.*, vol. 1, no. 2, pp. 177–189, 2014.

[78] S. Huang, Q. Wu, J. Wang, and H. Zhao, "A sufficient condition on convex relaxation of ac optimal power flow in distribution networks," *IEEE Transactions on Power Systems*, vol. 32, no. 2, pp. 1359–1368, March 2017.

[79] L. Gan, N. Li, U. Topcu, and S. H. Low, "Exact convex relaxation of optimal power flow in radial networks," *IEEE Transactions on Automatic Control*, vol. 60, no. 1, pp. 72–87, Jan 2015.

[80] R. Madani, S. Sojoudi, and J. Lavaei, "Convex relaxation for optimal power flow problem: Mesh networks," *IEEE Transactions on Power Systems*, vol. 30, no. 1, pp. 199–211, Jan 2015.

[81] P. Fortenbacher and T. Demiray, "Linear/quadratic programming-based optimal power flow using linear power flow and absolute loss approximations," *International Journal of Electrical Power & Energy Systems*, vol. 107, pp. 680 – 689, 2019.

[82] Z. Yang, H. Zhong, A. Bose, T. Zheng, Q. Xia, and C. Kang, "A linearized opf model with reactive power and voltage magnitude: A pathway to improve the mw-only dc opf," *IEEE Transactions on Power Systems*, vol. 33, no. 2, pp. 1734–1745, 2018.

[83] W. H. Kersting, "Radial distribution test feeders," in *2001 IEEE Pow. Eng. Soc. Winter Meeting. Conf. Proc. (Cat. No.01CH37194)*, vol. 2, 2001, pp. 908–912 vol.2.

[84] N. Blair, N. DiOrio, J. Freeman, P. Gilman, S. Janzou, T. Neises, and M. Wagner, "System Advisor Model (SAM) General Description (Version 2017.9.5)," National Renewable Energy Laboratory, Golden, CO, Tech. Rep. NREL/ TP-6A20-70414, May 2018.

[85] W. E. Hart, J.-P. Watson, and D. L. Woodruff, "Pyomo: modeling and solving mathematical programs in python," *Mathematical Programming Computation*, vol. 3, no. 3, pp. 219–260, 2011.

[86] Gurobi Optimization, LLC, "Gurobi optimizer reference manual," 2020. [Online]. Available: http://www.gurobi.com

[87] A. Wächter and L. T. Biegler, "On the implementation of an interior-point filter line-search algorithm for large-scale nonlinear programming." *Math. Program.*, vol. 106, p. 25–57, 2007.

[88] D. E. Olivares, A. Mehrizi-Sani, A. H. Etemadi, C. A. Cañizares, R. Iravani, M. Kazerani, A. H. Hajimiragha, O. Gomis-Bellmunt, M. Saeedifard, R. Palma-Behnke, G. A. Jiménez-Estévez, and N. D. Hatziargyriou, "Trends in microgrid control," *IEEE Trans. Smart Grid*, vol. 5, no. 4, pp. 1905–1919, July 2014.

[89] L. Roald and G. Andersson, "Chance-constrained ac optimal power flow: Reformulations and efficient algorithms," *IEEE Transactions on Power Systems*, vol. 33, no. 3, pp. 2906–2918, May 2018.

[90] E. Delage and D. A. Iancu, *Robust Multistage Decision Making*. Institute for Operations Research and the Management Sciences (INFORMS), 2015, ch. 2, pp. 20–46. [Online]. Available: https://pubsonline.informs.org/doi/abs/10.1287/educ.2015.0139

[91] D. Bertsimas, E. Litvinov, X. A. Sun, J. Zhao, and T. Zheng, "Adaptive robust optimization for the security constrained unit commitment problem," *IEEE Transactions on Power Systems*, vol. 28, no. 1, pp. 52–63, 2013.

[92] P. Panciatici, Y. Hassaine, S. Fliscounakis, L. Platbrood, M. Ortega-Vazquez, J. L. Martinez-Ramos, and L. Wehenkel, "Security management under uncertainty: From day-ahead planning to intraday operation," in *2010 IREP Symposium Bulk Power System Dynamics and Control - VIII (IREP)*, Aug 2010, pp. 1–8.

[93] A. Ben-Tal, L. E. Ghaoui, and A. Nemirovski, *Robust Optimization*. Princeton Series in Applied Mathematics. Princeton Univ. Press, Oct. 2009.

[94] H. Rahimian and S. Mehrotra, "Distributionally robust optimization: a review," *arXiv preprint*, Aug. 2019.

[95] W. Wiesemann, D. Kuhn, and M. Sim, "Distributionally robust convex optimization," *Operations Research*, vol. 62, no. 6, pp. 1358–1376, 2014.

[96] E. Delage and Y. Ye, "Distributionally robust optimization under moment uncertainty with application to data-driven problems," *Operations Research*, vol. 58, pp. 595–612, 06 2010.

[97] A. Khodaei, "Provisional microgrid planning," *IEEE Trans. Smart Grid*, vol. 8, no. 3, pp. 1096–1104, May 2017.

[98] G. Muñoz-Delgado, J. Contreras, and J. M. Arroyo, "Multistage generation and network expansion planning in distribution systems considering uncertainty and reliability," *IEEE Transactions on Power Systems*, vol. 31, no. 5, pp. 3715–3728, 2016.

[99] M. Asensio, P. Meneses de Quevedo, G. Muñoz-Delgado, and J. Contreras, "Joint distribution network and renewable energy expansion planning considering demand response and energy storage—part i: Stochastic programming model," *IEEE Transactions on Smart Grid*, vol. 9, no. 2, pp. 655–666, 2018.

[100] E. Hajipour, M. Bozorg, and M. Fotuhi-Firuzabad, "Stochastic capacity expansion planning of remote microgrids with wind farms and energy storage," *IEEE Transactions on Sustainable Energy*, vol. 6, no. 2, pp. 491–498, 2015.

[101] A. Khayatian, M. Barati, and G. J. Lim, "Integrated microgrid expansion planning in electricity market with uncertainty," *IEEE Transactions on Power Systems*, vol. 33, no. 4, pp. 3634–3643, 2018.

[102] E. Yamangil, R. Bent, and S. Backhaus, "Resilient upgrade of electrical distribution grids," in *29th AAAI Conf. on Artificial Intelligence*, 2015.

[103] A. Khodaei, S. Bahramirad, and M. Shahidehpour, "Microgrid planning under uncertainty," *IEEE Trans. Power Syst.*, vol. 30, no. 5, pp. 2417–2425, Sep. 2015.

[104] A. Khayatian, M. Barati, and G. J. Lim, "Integrated microgrid expansion planning in electricity market with uncertainty," *IEEE Trans. Power Syst.*, vol. 33, no. 4, pp. 3634–3643, July 2018.

[105] N. Amjady, A. Attarha, S. Dehghan, and A. J. Conejo, "Adaptive robust expansion planning for a distribution network with DERs," *IEEE Trans. Power Syst.*, vol. 33, no. 2, pp. 1698–1715, 2017.

[106] A. Khodaei, "Provisional microgrid planning," *IEEE Transactions on Smart Grid*, vol. 8, no. 3, pp. 1096–1104, 2017.

[107] S. Dehghan, N. Amjady, and A. Kazemi, "Two-stage robust generation expansion planning: A mixed integer linear programming model," *IEEE Transactions on Power Systems*, vol. 29, no. 2, pp. 584–597, 2014.

[108] A. Khodaei, S. Bahramirad, and M. Shahidehpour, "Microgrid planning under uncertainty," *IEEE Transactions on Power Systems*, vol. 30, no. 5, pp. 2417–2425, 2015.

[109] Y. Lin and Z. Bie, "Tri-level optimal hardening plan for a resilient distribution system considering reconfiguration and dg islanding," *Applied Energy*, vol. 210, pp. 1266 – 1279, 2018.

[110] S. Geng and M. Vrakopoulou and I. A. Hiskens, "Optimal Capacity Design and Operation of Energy Hub Systems," *Proceedings of the IEEE*, 2020.

[111] F. S. Gazijahani and J. Salehi, "Robust design of microgrids with reconfigurable topology under severe uncertainty," *IEEE Transactions on Sustainable Energy*, vol. 9, no. 2, pp. 559–569, 2018.

[112] S. Mohamed, M. F. Shaaban, M. Ismail, E. Serpedin, and K. A. Qaraqe, "An efficient planning algorithm for hybrid remote microgrids," *IEEE Transactions on Sustainable Energy*, vol. 10, no. 1, pp. 257–267, 2019.

[113] M. V. Kirthiga, S. A. Daniel, and S. Gurunathan, "A methodology for transforming an existing distribution network into a sustainable autonomous micro-grid," *IEEE Transactions on Sustainable Energy*, vol. 4, no. 1, pp. 31–41, 2013.

[114] A. Narayan and K. Ponnambalam, "Risk-averse stochastic programming approach for microgrid planning under uncertainty," *Renewable Energy*, vol. 101, pp. 399–408, 2017.

[115] A. K. Jain, M. N. Murty, and P. J. Flynn, "Data clustering: A review," *ACM Comput. Surv.*, vol. 31, no. 3, p. 264–323, Sep. 1999.

[116] A. Bouguettaya, Q. Yu, X. Liu, X. Zhou, and A. Song, "Efficient agglomerative hierarchical clustering," *Expert Systems with Applications*, vol. 42, no. 5, pp. 2785–2797, 2015.

[117] S. Dehghan, N. Amjady, and A. J. Conejo, "Reliability-constrained robust power system expansion planning," *IEEE Trans. Power Syst.*, vol. 31, no. 3, pp. 2383–2392, 2015.

[118] *METEOBLUE AG*, 2020 (accessed February 3, 2020). [Online]. Available: http://www.meteoblue.com

[119] P. Denholm and R. Margolis, "Regional per capita solar electric footprint for the United States," National Renewable Energy Lab.(NREL), Golden, CO (United States), Tech. Rep., 2007.

[120] "Alderney electricity Ltd," http://www.alderney-elec.com), May 2020.

[121] S. Dehghan, A. M. Nakiganda, and P. Aristidou, "Pyeplan: A python-based energy planning tool," 11 2021. [Online]. Available: https://doi.org/10.5281/zenodo.5701072

[122] Committee on Climate Change, "Reducing UK emissions," 2019 Progress Report to Parliament), Tech. Rep., July 2019.

[123] Z. Wang, B. Chen, J. Wang, J. Kim, and M. M. Begovic, "Robust optimization based optimal dg placement in microgrids," *IEEE Transactions on Smart Grid*, vol. 5, no. 5, pp. 2173–2182, 2014.

[124] Z. Liang, H. Chen, X. Wang, S. Chen, and C. Zhang, "Risk-based uncertainty set optimization method for energy management of hybrid ac/dc microgrids with uncertain renewable generation," *IEEE Transactions on Smart Grid*, vol. 11, no. 2, pp. 1526–1542, 2020.

[125] D. E. Olivares, J. D. Lara, C. A. Cañizares, and M. Kazerani, "Stochastic-predictive energy management system for isolated microgrids," *IEEE Transactions on Smart Grid*, vol. 6, no. 6, pp. 2681–2693, 2015.

[126] Z. Shi, H. Liang, S. Huang, and V. Dinavahi, "Distributionally robust chance-constrained energy management for islanded microgrids," *IEEE Transactions on Smart Grid*, vol. 10, no. 2, pp. 2234–2244, 2019.

[127] F. Pourahmadi, J. Kazempour, C. Ordoudis, P. Pinson, and S. H. Hosseini, "Distributionally robust chance-constrained generation expansion planning," *IEEE Transactions on Power Systems*, vol. 35, no. 4, pp. 2888–2903, 2020.

[128] P. Xiong and C. Singh, "Distributionally robust optimization for energy and reserve toward a low-carbon electricity market," *Electric Power Systems Research*, vol. 149, pp. 137–145, 2017.

[129] W. Wei, F. Liu, and S. Mei, "Distributionally robust co-optimization of energy and reserve dispatch," *IEEE Transactions on Sustainable Energy*, vol. 7, no. 1, pp. 289–300, 2016.

[130] Y. Shui, H. Gao, L. Wang, Z. Wei, and J. Liu, "A data-driven distributionally robust coordinated dispatch model for integrated power and heating systems considering wind power uncertainties," *International Journal of Electrical Power & Energy Systems*, vol. 104, pp. 255–258, 2019.

[131] C. Duan, L. Jiang, W. Fang, and J. Liu, "Data-driven affinely adjustable distributionally robust unit commitment," *IEEE Transactions on Power Systems*, vol. 33, no. 2, pp. 1385–1398, 2018.

[132] P. M. Esfahani and D. Kuhn, "Data-driven distributionally robust optimization using the wasserstein metric: performance guarantees and tractable reformulations," *Mathematical Programming*, vol. 171, pp. 115–166, 2018.

[133] R. Mieth and Y. Dvorkin, "Data-driven distributionally robust optimal power flow for distribution systems," *IEEE Control Sys. Letters*, vol. 2, no. 3, pp. 363–368, 2018.

[134] D. Bertsimas and M. Sim, "The price of robustness," *Operations Research*, vol. 52, pp. 35–53, 02 2004.

[135] A. Shapiro, "On duality theory of conic linear problems," in *in Semi-Infinite Programming*. Kluwer Academic Publishers, 2000, pp. 135–165.

[136] P. Xiong and C. Singh, "A distributional interpretation of uncertainty sets in unit commitment under uncertain wind power," *IEEE Transactions on Sustainable Energy*, vol. 10, no. 1, pp. 149–157, 2019.

[137] C. Zhao and R. Jiang, "Distributionally robust contingency-constrained unit commitment," *IEEE Transactions on Power Systems*, vol. 33, no. 1, pp. 94–102, 2018.

[138] M. Zugno and A. J. Conejo, "A robust optimization approach to energy and reserve dispatch in electricity markets," *European Journal of Operational Research*, vol. 247, no. 2, pp. 659–671, 2015.

[139] D. Kuhn, W. Wiesemann, and A. Georghiou, "Primal and dual linear decision rules in stochastic and robust optimization," *Mathematical Programming*, vol. 130, pp. 177–209, 11 2009.

[140] K. Strunz, E. Abbasi, R. Fletcher, N. Hatziargyriou, R. Iravani, and G. Joos, "Benchmark systems for network integration of renewable and distributed energy resources," *CIGRE Task Force C6.04.02*, 04 2014.

[141] Open Power System Data. Data Package Time series. Version 2020-10-06. [Online]. Available: https://doi.org/10.25832/time_series/2020-10-06

[142] X. Liu, M. Shahidehpour, Z. Li, X. Liu, Y. Cao, and Z. Bie, "Microgrids for enhancing the power grid resilience in extreme conditions," *IEEE Trans. Smart Grid*, vol. 8, no. 2, pp. 589–597, March 2017.

[143] Y. Zhou, M. Panteli, R. Moreno, and P. Mancarella, "System-level assessment of reliability and resilience provision from microgrids," *Applied Energy*, vol. 230, pp. 374 – 392, 2018.

[144] F. Milano, F. Dörfler, G. Hug, D. J. Hill, and G. Verbič, "Foundations and challenges of low-inertia systems (invited paper)," in *2018 Power Systems Computation Conference (PSCC)*, 2018, pp. 1–25.

[145] P. Kundur, J. Paserba, V. Ajjarapu, G. Andersson, A. Bose, C. Canizares, N. Hatziargyriou, D. Hill, A. Stankovic, C. Taylor, T. Van Cutsem, and V. Vittal, "Definition and classification of power system stability ieee/cigre joint task

force on stability terms and definitions," *IEEE Transactions on Power Systems*, vol. 19, no. 3, pp. 1387–1401, 2004.

[146] S. Babaei, C. Zhao, and T. Ding, "Allocating distributed generators for resilient distribution system under uncertain probability distribution of natural disasters," in *2017 IEEE PES GM*, July 2017.

[147] M. Mazidi, N. Rezaei, F. J. Ardakani, M. Mohiti, and J. M. Guerrero, "A hierarchical energy management system for islanded multi-microgrid clusters considering frequency security constraints," *Int. Journal of Elec. Power & Energy Sys.*, vol. 121, p. 106134, 2020.

[148] D. L. H. Aik, "A general-order system frequency response model incorporating load shedding: analytic modeling and applications," *IEEE Trans. on Pow. Sys.*, vol. 21, no. 2, pp. 709–717, 2006.

[149] G. W. Chang, C.-S. Chuang, T.-K. Lu, and C.-C. Wu, "Frequency-regulating reserve constrained unit commitment for an isolated power system," *IEEE Transactions on Power Systems*, vol. 28, no. 2, pp. 578–586, 2013.

[150] R. Zarate-Minano, T. Van Cutsem, F. Milano, and A. J. Conejo, "Securing transient stability using time-domain simulations within an optimal power flow," *IEEE Transactions on Power Systems*, vol. 25, no. 1, pp. 243–253, 2010.

[151] D. Gan, R. J. Thomas, and R. D. Zimmerman, "Stability-constrained optimal power flow," *IEEE Trans. Power Syst.*, vol. 15, no. 2, pp. 535–540, May 2000.

[152] P. Daly, D. Flynn, and N. Cunniffe, "Inertia considerations within unit commitment and economic dispatch for systems with high non-synchronous penetrations," in *2015 IEEE Eindhoven PowerTech*, 2015, pp. 1–6.

[153] F. Teng, V. Trovato, and G. Strbac, "Stochastic scheduling with inertia-dependent fast frequency response requirements," *IEEE Transactions on Power Systems*, vol. 31, no. 2, pp. 1557–1566, 2016.

[154] S. S. Guggilam, C. Zhao, E. Dall'Anese, Y. C. Chen, and S. V. Dhople, "Optimizing der participation in inertial and primary-frequency response," *IEEE Transactions on Power Systems*, vol. 33, no. 5, pp. 5194–5205, 2018.

[155] H. Ahmadi and H. Ghasemi, "Security-constrained unit commitment with linearized system frequency limit constraints," *IEEE Transactions on Power Systems*, vol. 29, no. 4, pp. 1536–1545, 2014.

[156] X. Wu, Z. Wang, T. Ding, X. Wang, Z. Li, and F. Li, "Microgrid planning considering the resilience against contingencies," *IET Generation, Transmission Distribution*, vol. 13, no. 16, pp. 3534–3548, 2019.

[157] S. Dehghan, N. Amjady, and P. Aristidou, "A robust coordinated expansion planning model for wind farm-integrated power systems with flexibility sources using affine policies," *IEEE Systems Journal*, 2019.

[158] M. E. Baran and F. F. Wu, "Network reconfiguration in distribution systems for loss reduction and load balancing," *IEEE Trans. Power Del.*, vol. 4, no. 2, pp. 1401–1407, April 1989.

[159] Z. Wang, B. Chen, J. Wang, J. Kim, and M. M. Begovic, "Robust optimization based optimal dg placement in microgrids," *IEEE Trans. Smart Grid*, vol. 5, no. 5, pp. 2173–2182, Sep. 2014.

[160] Z. Yang, H. Zhong, A. Bose, T. Zheng, Q. Xia, and C. Kang, "A linearized opf model with reactive power and voltage magnitude: A pathway to improve the mw-only dc opf," *IEEE Trans. Power Syst.*, vol. 33, no. 2, pp. 1734–1745, March 2018.

[161] U. Markovic, Z. Chu, P. Aristidou, and G. Hug, "LQR-Based Adaptive Virtual Synchronous Machine for Power Systems with High Inverter Penetration," *IEEE Trans. Sustain. Energy*, vol. 10, no. 3, pp. 1501–1512, July 2019.

[162] U. Markovic, O. Stanojev, P. Aristidou, and G. Hug, "Partial grid forming concept for 100% inverter-based transmission systems," in *2018 IEEE PES GM*, Aug 2018.

[163] U. Markovic, O. Stanojev, E. Vrettos, P. Aristidou, D. Callaway, and G. Hug, "Understanding Stability of Low-Inertia Systems," *IEEE Trans. Power Syst.*, (under review). [Online]. Available: engrxiv.org/jwzrq

[164] P. M. Anderson and M. Mirheydar, "A low-order system frequency response model," *IEEE Trans. Power Syst.*, vol. 5, no. 3, pp. 720–729, Aug 1990.

[165] U. Markovic, Z. Chu, P. Aristidou, and G. Hug, "LQR-based adaptive virtual synchronous machine for power systems with high inverter penetration," *IEEE Trans. on Sustainable Energy*, vol. 10, no. 3, pp. 1501–1512, July 2019.

[166] R. J.-B. Wets, "Stochastic programming models: Wait-and-see versus here-and-now." in *Decision Making Under Uncertainty. The IMA Volumes in Mathematics and its Applications*, vol. 128, 2002.

[167] U. Markovic, V. Häberle, D. Shchetinin, G. Hug, D. Callaway, and E. Vrettos, "Optimal sizing and tuning of storage capacity for fast frequency control in low-inertia systems," in *2019 International Conference on Smart Energy Systems and Technologies (SEST)*, 2019, pp. 1–6.

[168] Y. Wen, W. Li, G. Huang, and X. Liu, "Frequency dynamics constrained unit commitment with battery energy storage," *IEEE Transactions on Power Systems*, vol. 31, no. 6, pp. 5115–5125, 2016.

[169] R. Turvey and D. Anderson, *Electricity economics: Essays and case studies*. Johns Hopkins University Press, Baltimore, 1977.

[170] U.S. Energy Information Administration, "Levelized costs of new generation resources in the annual energy outlook 2021," 2021. [Online]. Available: https://www.eia.gov/outlooks/aeo/pdf/electricity_generation.pdf

[171] Alliance for Sustainable Energy, Department of Energy , National Renewable Energy Laboratory, System Advisor Model, Version 2016.

[172] J. Löfberg, "Yalmip : A toolbox for modeling and optimization in matlab," in *2004 IEEE Intern. Conf. on Robotics and Automation*, 2004.

[173] IEEE, "IEEE recommended practice for excitation system models for power system stability studies," *IEEE Std 421.5-2005 (Revision of IEEE Std 421.5-1992)*, pp. 1–93, 2006.

[174] J. A. Taylor, *Convex Optimization of Power Systems*. Cambridge University Press, 2015.

[175] L. E. Sokoler, P. Vinter, R. Bærentsen, K. Edlund, and J. B. Jørgensen, "Contingency-constrained unit commitment in meshed isolated power systems," *IEEE Transactions on Power Systems*, vol. 31, no. 5, pp. 3516–3526, 2016.

[176] L. Badesa, F. Teng, and G. Strbac, "Simultaneous scheduling of multiple frequency services in stochastic unit commitment," *IEEE Transactions on Power Systems*, vol. 34, no. 5, pp. 3858–3868, 2019.

[177] Z. Zhang, E. Du, F. Teng, N. Zhang, and C. Kang, "Modeling frequency dynamics in unit commitment with a high share of renewable energy," *IEEE Transactions on Power Systems*, vol. 35, no. 6, pp. 4383–4395, 2020.

[178] P. Belotti, C. Kirches, S. Leyffer, J. Linderoth, J. Luedtke, and A. Mahajan, "Mixed-integer nonlinear optimization," *Acta Numerica*, vol. 22, p. 1–131, 2013.

[179] J. Lin, F. Magnago, and J. M. Alemany, "Chapter 1 - optimization methods applied to power systems: Current practices and challenges," in *Classical and Recent Aspects of Power System Optimization*, A. F. Zobaa, S. H. A. Aleem, and A. Y. Abdelaziz, Eds. Academic Press, 2018, pp. 1 – 18. [Online]. Available: http://www.sciencedirect.com/science/article/pii/B978012812441300001X

[180] I. Quesada and I. Grossmann, "An lp/nlp based branch and bound algorithm for convex minlp optimization problems," *Computers & Chemical Engineering*, vol. 16, no. 10, pp. 937 – 947, 1992, an International Journal of Computer Applications in Chemical Engineering. [Online]. Available: http://www.sciencedirect.com/science/article/pii/0098135492800288

[181] I. E. Grossmann, "Review of nonlinear mixed-integer and disjunctive programming techniques," *Optimization and Engineering*, vol. 3, no. 3, pp. 227–252, Sep 2002. [Online]. Available: https://doi.org/10.1023/A:1021039126272

[182] M. A. Duran and I. E. Grossmann, "An outer-approximation algorithm for a class of mixed-integer nonlinear programs," *Mathematical Programming*, vol. 36, no. 3, pp. 307–339, Oct 1986. [Online]. Available: https://doi.org/10.1007/BF02592064

[183] R. Fletcher and S. Leyffer, "Solving mixed integer nonlinear programs by outer approximation," *Mathematical Programming*, vol. 66, no. 1, pp. 327–349, Aug 1994. [Online]. Available: https://doi.org/10.1007/BF01581153

[184] A. M. Geoffrion, "Generalized benders decomposition," *Journal of Optimization Theory and Applications*, vol. 10, no. 4, pp. 237–260, Oct 1972. [Online]. Available: https://doi.org/10.1007/BF00934810

[185] C. D'Ambrosio and A. Lodi, "Mixed integer nonlinear programming tools: a practical overview," *4OR*, vol. 9, no. 4, pp. 329–349, Dec 2011. [Online]. Available: https://doi.org/10.1007/s10288-011-0181-9

[186] J. F. Benders, "Partitioning procedures for solving mixed-variables programming problems," *Numerische Mathematik*, vol. 4, no. 1, pp. 238–252, Dec 1962.

[187] A. Geoffrion, "Generalized benders decomposition." *Journal of Optimization Theory and Applications*, vol. 10, p. 237–260, 1972.

[188] E. Kägi-Kolisnyc, "Distribution Management System Including Dispersed Generation and Storage in a Liberalized Market Environment," Ph.D. dissertation, EPFL, Lausanne, Switzerland, 01 2009.

[189] C. Gouveia, J. Moreira, C. L. Moreira, and J. A. Peças Lopes, "Coordinating storage and demand response for microgrid emergency operation," *IEEE Transactions on Smart Grid*, vol. 4, no. 4, pp. 1898–1908, 2013.

[190] S. Karagiannopoulos, J. Gallmann, M. G. Vayá, P. Aristidou, and G. Hug, "Active distribution grids offering ancillary services in islanded and grid-connected mode," *IEEE Transactions on Smart Grid*, vol. 11, no. 1, pp. 623–633, 2020.

[191] I.-I. Avramidis, F. Capitanescu, S. Karagiannopoulos, and E. Vrettos, "A novel approximation of security-constrained optimal power flow with incorporation of generator frequency and voltage control response," *IEEE Transactions on Power Systems*, vol. 36, no. 3, pp. 2438–2447, 2021.

[192] Z. Chu and F. Teng, "Voltage stability constrained unit commitment in high ibg-penetrated power systems," 2021.

[193] M. Paturet, U. Markovic, S. Delikaraoglou, E. Vrettos, P. Aristidou, and G. Hug, "Stochastic unit commitment in low-inertia grids," *IEEE Trans. on Pow. Sys.*, vol. 35, no. 5, pp. 3448–3458, 2020.

[194] A. M. Nakiganda, S. Dehghan, and P. Aristidou, "Enhancing microgrid resilience and survivability under static and dynamic islanding constraints," in *2020 IEEE PES Innovative Smart Grid Technologies Europe (ISGT-Europe)*, 2020, pp. 539–543.

[195] F. Capitanescu and T. Van Cutsem, "Preventive control of voltage security margins: a multicontingency sensitivity-based approach," *IEEE Transactions on Power Systems*, vol. 17, no. 2, pp. 358–364, 2002.

[196] A. M. Nakiganda, T. Van Cutsem, and P. Aristidou, "Microgrid operational optimization with dynamic voltage security constraints," in *2021 IEEE Madrid PowerTech*, 2021, pp. 1–6.

[197] M. La Scala, M. Trovato, and C. Antonelli, "On-line dynamic preventive control: an algorithm for transient security dispatch," *IEEE Transactions on Power Systems*, vol. 13, no. 2, pp. 601–610, 1998.

[198] G. Hou and V. Vittal, "Trajectory sensitivity based preventive control of voltage instability considering load uncertainties," *IEEE Trans. on Pow. Sys.*, vol. 27, no. 4, pp. 2280–2288, 2012.

[199] L. Jin, R. Kumar, and N. Elia, "Security constrained emergency voltage stabilization: A model predictive control based approach," in *2008 47th IEEE Conf. on Decision and Control*, 2008, pp. 2469–2474.

[200] M. Paramasivam, A. Salloum, V. Ajjarapu, V. Vittal, N. B. Bhatt, and S. Liu, "Dynamic optimization based reactive power planning to mitigate slow voltage recovery and short term voltage instability," *IEEE Trans. on Pow. Sys.*, vol. 28, no. 4, pp. 3865–3873, 2013.

[201] X. Xu, H. Zhang, C. Li, Y. Liu, W. Li, and V. Terzija, "Optimization of the event-driven emergency load-shedding considering transient security and stability constraints," *IEEE Trans. on Power Sys.*, vol. 32, no. 4, pp. 2581–2592, 2017.

[202] H. Liu, V. Krishnan, J. D. McCalley, and A. Chowdhury, "Optimal planning of static and dynamic reactive power resources," *IET Gen., Transn. Dist.*, vol. 8, no. 12, pp. 1916–1927, 2014.

[203] W. F. Feehery and P. I. Barton, "Dynamic optimization with state variable path constraints," *Computers & Chemical Engineering*, vol. 22, no. 9, pp. 1241–1256, 1998.

[204] L. T. Biegler and I. E. Grossmann, "Retrospective on optimization," *Computers & Chemical Engineering*, vol. 28, no. 8, pp. 1169–1192, 2004.

[205] S. Abhyankar, G. Geng, M. Anitescu, X. Wang, and V. Dinavahi, "Solution techniques for transient stability-constrained optimal power flow – part i," *IET Generation, Transmission & Distribution*, vol. 11, no. 12, pp. 3177–3185, 2017.

[206] G. Geng, S. Abhyankar, X. Wang, V. Dinavahi, and I. P. T. F. on Interfacing Techniques for Solution Tools, "Solution techniques for transient stability-constrained optimal power flow – part ii," *IET Generation, Transmission & Distribution*, vol. 11, no. 12, pp. 3186–3193, 2017.

[207] A. Ortega and F. Milano, "Impact of frequency estimation for vsc-based devices with primary frequency control," in *2017 IEEE PES Innovative Smart Grid Technologies Conference Europe (ISGT-Europe)*, 2017, pp. 1–6.

[208] Open power system data. [Online]. Available: https://doi.org/10.25832/time_series/2020-10-06

[209] F. Milano and A. Ortega, "Frequency divider," *IEEE Transactions on Power Systems*, vol. 32, no. 2, pp. 1493–1501, 2017.